Integration of the Phosphorylation-Dependent Signaling in the DNA Damage Response Network: Implications for Cancer

by

Isaac Andrew Manke

B.A. Biology and Chemistry
Minnesota State University Moorhead, 2000

SUBMITTED TO THE DEPARTMENT OF BIOLOGY IN PARTIAL FULFILLMENT OF THE REQUIREMENTS FOR THE DEGREE OF

DOCTOR OF PHILOSOPHY IN BIOPHYSICAL CHEMISTRY AND MOLECULAR STRUCTURE AT THE MASSACHUSETTS INSTITUTE OF TECHNOLOGY

JUNE 2005

Signature of Author: _____

Department of Biology
May 17, 2005

Certified by: _____

Associate Professor of Biology
Michael B. Yaffe
Thesis Supervisor

Accepted by: _____

Professor of Biology
Stephen P. Bell
Chairman, Graduate Student Committee

Integration of the Phosphorylation-Dependent Signaling in the DNA Damage Response Network: Implications for Cancer

by

Isaac Andrew Manke

Submitted to the Department of Biology on May 17, 2005 in Partial Fulfillment of the Requirements for the Degree of Doctor of Philosophy in Biophysical Chemistry and Molecular Structure at the Massachusetts Institute of Technology

ABSTRACT

The cellular response to DNA damage is an evolutionarily conserved process mediated by Ser/Thr kinases that results in the formation of multiple protein-protein complexes designed to control the cell cycle. The assembly of those multi-protein complexes is often triggered by the phosphorylation of a protein generating a short phospho-motif that is subsequently recognized by a downstream phospho-binding domain. To gain a better understanding of the exact mechanisms by which kinases signal through their substrates to phospho-binding domains in the DNA damage signaling process, we used two complementary proteomic screening approaches to identify novel kinase substrates and new phospho-binding domains. First, to explore the p38/stress-activated protein kinase (SAPK) axis of DNA damage signaling, we determined the optimal phosphorylation motifs of mammalian p38/SAPK and MAPKAP Kinase-2. The optimal substrate phosphorylation motif for MAPKAP Kinase-2 closely matches the 14-3-3-binding site on CDC25B/C, and we show that MAPKAP Kinase-2 is directly responsible for CDC25B/C phosphorylation and 14-3-3-binding both in vitro and in response to UV-induced DNA damage within mammalian cells. Using RNA interference we demonstrate that down-regulation of MAPKAP Kinase-2 eliminates both the G2/M and intra S-phase checkpoints. We show that MAPKAP Kinase-2, more aptly named CHK3, is new member of the DNA damage checkpoint kinase family that functions in parallel with CHK1 and CHK2 to integrate DNA damage signaling responses and cell cycle arrest in mammalian cells. Second, to identify phospho-binding domains functioning downstream of the kinases ATM/ATR, we developed a high-throughput chemical proteomic screening approach to isolate phospho-binding domains that interact with the [Ser/Thr]-Gln motifs phosphorylated by ATM/ATR. We identified the tandem BRCA1 carboxy-terminal (BRCT) domains as novel phospho-specific binding domains regulating PTIP and BRCA1 function and show that the phospho-binding function of BRCA1 is lost in many BRCA1-BRCT mutations that predispose women to breast and ovarian cancer. Together with our 1.85Å X-ray crystal structure data of the phosphopeptide bound BRCA1 BRCT domains, we provide a molecular rational as to how these mutations disrupt some BRCA1 functions. In combination, our discoveries expand the molecular understanding as to how kinases signal to phospho-binding domains in the DNA damage response signaling network, provide insight into cancer development and as well as identify novel targets for the development of chemosensitizing therapeutic agents.

Thesis Supervisor: Michael B. Yaffe

Title: Associate Professor of Biology

Table of Contents

I.	**Signaling and Protein Phosphorylation in the DNA Damage Response Network**	6
	The DNA Damage Response Signaling Process	7
	Signaling and the Protein Kinase	9
	Signaling and the Phospho-Binding Domain	12
	DNA Repair Pathways and Cell Cycle Checkpoints	18
II.	**MAPKAP Kinase-2 is a Cell Cycle Checkpoint Kinase that Regulates the G2/M Transition and S-phase Progression in Response to UV Irradiation**	46
	Summary	47
	Introduction	48
	Results	51
	Discussion	65
	Experimental Procedures	69
	Figures	79
III.	**BRCT Repeats as Phosphopeptide-Binding Modules Involved in Protein Targeting**	94
	Summary	95
	Introduction	96
	Results	97
	Discussion	102
	Experimental Procedures	103
	Tables	110
	Figures	112
IV.	**Structure and Mechanism of BRCA1 BRCT Domain Recognition of Phosphorylated BACH1**	124
	Summary	125
	Introduction	126
	Results	129
	Discussion	137
	Experimental Procedures	139
	Table	144
	Figures	145
V.	**Future Directions**	155
	References	165
	Appendices	179

Manke IA, Nguyen A, Lim D, Stewart MQ, Elia AE, Yaffe MB. MAPKAP kinase-2 is a cell cycle checkpoint kinase that regulates the G2/M transition and S-phase progression in response to UV irradiation. Mol Cell. 2005 Jan 7;17(1):37-48.

Clapperton JA, Manke IA, Lowery DM, Ho T, Haire LF, Yaffe MB, Smerdon SJ. Structure and and mechanism of BRCA1 BRCT domain recognition of phosphorylated BACH1 with implications for cancer. Nat Struct Mol Biol. 2004 Jun;11(6):512-8. Epub 2004 May 9.

Manke IA, Lowery DM, Nguyen A, Yaffe MB. BRCT repeats as phosphopeptide-binding modules involved in protein targeting. Science. 2003 Oct 24;302 (5645): 636-9.

Acknowledgments

I would like to thank all members of the Yaffe lab. In particular I would like to thank Justine Stein and Erik Wilker for their help early on in my graduate career. Both Justine and Erik helped me learn new laboratory techniques and were helpful in my early training. I would also like to thank Katja Hoepker for her assistance with the phospho-binding screen. In addition to helping in the lab, Katja was and remains a good friend. Drew Lowery and Cokey Nguyen played instrumental roles in our successful completion of the BRCT domain work and meeting a tight deadline for publication. They too have not only been extremely helpful in lab but have also been great friends. Timmy Ho and Irma Rangel were extraordinary UROPs and I am confident they will meet great success in their graduate and professional careers. I want to thank Mary Stewart and Dan Lim for their experimental assistance in the MK2 project and I would also like to thank Mary for being an extremely supportive person. Sarah Bissonnette and Duaa Mohammad are excellent graduate students and I am very grateful for their friendship as well. I am extremely grateful to my advisor Michael Yaffe. He has been very encouraging and supportive during the stressful race to publish.

In addition to the Yaffe lab members, I would like to thank my friends outside the lab, know as LLUA, who have helped me survive graduate school. I have had great fun drinking and dominating athletic competitions. I would like to also thank my fiancée Jennifer Robbins for her help and support over the past four years, I could not have made it without her. In addition my parents Clarence and Ellen Manke have always provided infinite support and encouragement and have helped shaped the person that I am today. I would also like to thank my grandparents Ann Manke and Fred and Maltida Fielder.

Chapter 1

Signaling and Protein Phosphorylation in the DNA Damage Response Network

The DNA Damage Response Signaling Process

Most cancers exhibit genetic instability [1]. This instability occurs at both the nucleotide level and at the chromosome level [2]. In many cases, chromosomal instability results in the loss or gain of whole chromosomes [1]. While, the DNA damage signaling and repair pathway is necessary to maintain genomic integrity, we have only a skeletal understanding of how the DNA damage checkpoint functions to maintain genomic stability. Several types of DNA damage can trigger the different DNA damage checkpoints, which will temporarily halt cell division and allow for the repair of damaged DNA or, if the extent of damage is beyond the capacity of repair, the activation of apoptosis [2]. Protein complexes that recognize different types of DNA damage, such as lesions commonly caused by ionizing radiation (IR) and ultraviolet light (UV), initiate the activation of the kinases ataxia-telangiectasia mutated (ATM) and ataxia-telangiectasia- and RAD3-related (ATR) [1]. One protein complex thought to scan DNA for distortions and activate ATR is the Rad9/Rad1/Hus1 heterotrimeric checkpoint sliding clamp complex, which is similar to the proliferating cell nuclear antigen (PCNA) homotrimeric sliding clamp. Another protein complex, consisting of Mre11/Rad50/Nbs1, is thought to localize to sites of double stranded DNA breaks and subsequently increase the activation of ATM [2]. ATM and ATR transduce the signal of DNA damage that engages the DNA damage checkpoint and have overlapping functions as substrates common to both kinases have been identified. Activation of ATM and ATR leads to the phosphorylation and activation of several downstream substrates, including p53

and the Ser/Thr checkpoint kinases CHK1 and CHK2. One way in which both CHK1 and CHK2 regulate cell cycle progression is through their phosphorylation of the phosphatase CDC25B on Ser 309 and CDC25C on Ser 216. For the cell cycle to proceed to mitosis, CDC25B/C must translocate to the nucleus, where it activates Cdk1/cyclin B by reversing inhibitory phosphorylation events [3]. When CDC25B/C is phosphorylated on Ser 309 and Ser 216 respectively, it is bound by the phospho-specific binding protein 14-3-3, which sequesters CDC25B/C in the cytosol, thereby inhibiting the transition into mitosis [4, 5].

Simplistically, the DNA damage response signaling network can be thought of as a network comprised of sensors and tranducers. Sensors, such as the Rad17-RFC and 9-1-1, and Mre11-Rad50-Nbs1, are thought to directly associate with various forms of damaged DNA (and the damage repair complexes at those sites) to help serve as activation complexes that modulate, recruit, and localize specific signaling proteins such as kinases. Transducers include protein kinases that, when activated by the presence of sensor complexes and DNA damage, initiate a signal transduction cascade that propagates and amplifies the damage signal to ultimately cause cell cycle arrest or cell death.

There exists a need to identify additional kinase substrates of these DNA damage responsive kinases and to determine how kinase phosphorylation modulates these newly phosphorylated proteins. Therefore, the goals of my thesis are to identify new kinase substrates in the DNA damage response

pathway as well as identify new phospho-binding domains in the DNA damage response pathway that facilitate DNA damage signaling and repair.

Signaling and the Protein Kinase

Protein kinases are a fundamental component of almost all mammalian signaling pathways. Despite there fundamental roles, most kinases have relativity few, if any, identified substrates. Analysis of the human genome indicates that protein kinase catalytic domains are contained within ~1-2% of all potential open reading frames, and over 400 of these are thought to be either Ser/Thr or dual-specificity protein kinases [6]. In addition, 30% or more of all intracellular proteins are likely to be phosphorylated at some point in time during the lifetime of the cell. Protein phosphorylation often functions to regulate substrate binding and catalytic activity primarily by inducing allosteric changes in protein tertiary structure. However signal transduction by protein kinases also results in the directed assembly of multi-protein complexes at specific locations within the cell [7]. This process is particularly evident following DNA damage, where activation of DNA damage kinases results in the formation of protein-protein complexes at discrete foci within the nucleus [1]. In many cases, kinases directly control the formation of these multi-protein complexes by generating specific phosphorylated-motif sequences; modular binding domains then recognize these short phospho-motifs to mediate protein-protein interactions. Determining which protein kinases are responsible for phosphorylating particular protein substrates is critical for mapping signal transduction cascades that regulate the growth,

division, differentiation and death of a cell. To enhance our knowledge of the DNA damage signaling process, part of my thesis work focuses on the identification of additional kinase substrates in the DNA damage signaling network.

Determination of the optimal kinase phosphorylation motif by oriented peptide library screening

Oriented peptide library screening is a powerful method for the determination of the optimal kinase phosphorylation motif and for the identification of potential kinase substrates. Recent advances in mass spectrometry and the increasing use of phospho-motif-specific antibodies has now made it possible to experimentally identify phosphorylated substrates and simultaneously map the likely sites of phosphorylation [8, 9]. Despite the power of these approaches, however, both techniques have limited sensitivity for detecting phosphoproteins that are present at low levels within the cell. Many of these low abundance proteins include critical transcription factors and protein "control nodes" that lie near the top of signal amplification cacades. Thus additional approaches will be necessary to fully define kinase-dependent signaling networks. Oriented peptide library screening combined with bioinformatics-based searches of protein sequence databases offers an alternative strategy for identifying substrates – including low abundance substrates – of particular protein kinases, [10, 11].

In oriented peptide library screening, 10^7-10^{13} peptides are synthesized simultaneously by solid phase peptide synthesis, with all of the peptides containing either a single fixed Ser, Thr, or Tyr residue at an "orienting" position within the peptide sequence. The orienting residue in the peptides serves as the phospho-acceptor during an in vitro phosphorylation reaction with the protein kinase of interest and is flanked by a series of degenerate positions which contain a mixture of all possible amino acids. Only those peptides which contain favorable amino acids surrounding the fixed Ser, Thr, or Tyr residue will be preferentially phosphorylated by the kinase of interest. This subset of phosphorylated peptides can then be separated from the bulk of non-phosphorylated peptides using immobilized metal affinity chromatography (IMAC) [11, 12]. The recovered phosphopeptides, without any further separation, are sequenced in bulk by Edman degradation. By comparing the amount of each amino acid at each position flanking the fixed Ser, Thr, or Tyr in the phosphorylated peptides to the amount of each amino acid in the starting peptide library mixture, the affinity of the kinase for each amino acid in each position in the sequence is revealed [11]. The end result of this process is a matrix of selection values that describes, in quantitative terms, the relative importance of each amino acid at each position within the kinase substrate motif as well as the optimal peptide substrate sequence for that kinase. The matrix of kinase selectivity values can be used to search protein sequence databases and identify potential substrate proteins that contain the closest matches to the optimal protein kinase phosphorylation motif [10]. These putative substrates can then be

examined in vitro and in vivo to determine whether they are, in fact, kinase substrates after DNA damage. In addition, the optimal substrate peptide can be synthesized and used as a substrate to measure kinase activity in vitro, for example in an immunoprecipitation kinase assay to measure the change in kinase activity after DNA damage, or in a high-throughput screen for protein kinase inhibitors.

Signaling and the Phospho-Binding Domain

How does protein phosphorylation in response to DNA damage lead to DNA repair, cell cycle arrest, or cell death? In many cases, kinases control the orchestration of these complex cellular events that require the timely assembly of multi-molecular signaling or repair complexes at specific locations within the cell. The temporal and spatial control by these kinases is often achieved through phosphorylation-dependent binding and activation. Prior to the discovery of SH2 domains, protein phosphorylation was thought to regulate substrate binding and catalytic activity primarily by inducing allosteric changes in protein tertiary structure. A new view emerged with the observation that binding of SH2 domains to proteins occurred only when they carried a phosphotyrosine (pTyr) residue, introducing the idea that phosphorylation could function as a direct regulatory switch for protein-protein interactions. Because the first two phosphopeptide-binding modules that were recognized, SH2 and PTB domains, bound specificially to pTyr-containing sequences this view was not immediately applied to serine/threonine kinase signaling involved in cell cycle progression

[13-15]. However, the finding that 14-3-3 proteins recognize phosphorylated serine and threonine-based motifs on molecules involved in cell cycle progression started to support the idea that phospho-binding is more widespread. Recently, a number of additional modular domains that specifically recognize short pSer/pThr-containing sequences have been identified, including WW domains, FHA domains, the C-terminal domain of Polo-like kinases, and BRCT domains [16-20]. All of these pSer/pThr-binding domains participate in cell cycle regulation and the cellular response to genotoxic stress. These domains comprise a diverse structural group, and all recognize phosphoserine or phosphothreonine within a unique consensus motif directing specificity of ligand binding. The continued discovery of new domains has led to an increased appreciation of the role phosphopeptide recognition domains play in regulating the reversible assembly of multi-protein complexes. There most likely existsadditional phospho-binding domains that are involved in mediating protein-protein interactions in the DNA damage signaling process.

14-3-3 proteins

14-3-3 proteins are found in all eukaryotic cells and were the first family of pSer/pThr-binding molecules to be identified. Investigation of the optimal 14-3-3 binding motif by in vitro peptide library screening led to the identification of two optimal phosphoserine/threonine-containing motifs — RSX(pS/T)XP and RXXX(pS/T)XP — that are recognized by all seven 14-3-3 isotypes [21]. The 14-3-3 family of proteins play critical roles in several cellular processes [22-24],

including the DNA damage checkpoint response pathway. 14-3-3 proteins interact with phosphatases, apoptotic factors, transcription factors, cell surface receptors, ion channels, cytoskeletal proteins, and metabolic proteins to regulate the function of a ligand by increasing or decreasing the ligand's catalytic activity, facilitating or blocking molecular interactions between the ligand and other molecules, or regulating the subcellular localization of the bound protein [5, 25]. In one important example 14-3-3 proteins regulate subcellular localization by inducing the cytoplasmic sequestration of the CDC25 family of phosphatases upon phosphorylation by CHK1 or CHK2 in response to DNA damage [26, 27]. In this case, the cytoplasmic retention of the CDC25 phosphatases prevents the activation of CDC2-Cyclin B by CDC25 and thereby inhibits mitotic entry [28, 29].

FHA domains

FHA (Forkhead Associated) domains were originally identified through sequence profiling as a region of homology in forkhead transcription factors [30]. The phospho-binding function of FHA domains emerged from studies in *Arabidopsis* showing that a region encompassing the FHA domain of the protein KAPP (kinase-associated protein phosphatase) bound specifically to the phosphorylated form of the protein kinase RLK5 [31]. Oriented peptide library screening to determine the consensus motifs for phosphothreonine peptide binding has allowed a tentative grouping of FHA domains into discrete classes on the basis of specificity at the pThr+3 position (3 residues carboxy terminal to phosphothreonine) [32]. FHA domain-containing proteins have been most

extensively investigated in the context of cell cycle control and the cellular response to genotoxic damage. The mammalian kinase CHK2 contains a single FHA domain amino terminal to its kinase domain and mediates cell cycle arrest at multiple checkpoints in response to DNA damage. CHK2 causes cell cycle arrest by phosphorylating multiple substrates: the transcription factor p53 to induce G1 block, the phosphatase CDC25B/C whose phosphorylation results in 14-3-3 binding and G2/M arrest, and the G1 phosphatase family member CDC25A to trigger its degradation and cellular S-phase delay [33, 34]. One function of the FHA domain of CHK2 appears to be the regulation of the trans autophosphorylation of its kinase domain by mediating direct homo-dimerization through interaction with ATM-phosphorylated T68 of CHK2 [35, 36]. It is unclear how the FHA domain may target CHK2 to its substrates, and in some cases an additional surface is necessary, in conjunction with the phosphopeptide binding surface, for binding as with BRCA1 [37].

Identification of novel phospho-binding domains

To help elucidate the DNA damage signaling processes downstream of kinase activation, part of my thesis work focuses on the identification of additional phospho-binding domains that function to integrate the DNA damage signaling and repair process. Common screens to identify novel protein-protein interactions are often incapable of isolating interactions that require a post-translational modification, such as phosphorylation. The Yaffe lab recently designed a library versus library screen to identify new phospho-binding domains

downstream of cyclin-dependent kinases [18]. To perform this screen, proteins from a human brain cDNA library are in vitro translated (IVT) and labeled with [^{35}S]methionine then assayed for phospho-specific binding to oriented peptide libraries. Peptide libraries are synthesized as a biotin-tagged phospho and non-phospho peptides designed to represent the optimal phosphorylation motif of the kinase of interest, as determined by oriented peptide library screening discussed above. By using the biotin-tagged peptide library bound to streptavidin-conjugated agarose beads, proteins that bind to the phosphorylated form of this peptide, but not with the non-phosphorylated form, can be isolated, run on an SDS-PAGE gel and exposed to a phosphoimager plate for quantification. The ratio of phospho-specific binding to non-phospho binding can then be evaluated.

Part of my thesis project not only involves the identification of phospho-binding domains that interact with ATM and ATR substrates, but also involves improving upon the initial phospho-binding screen. The major drawback to the initial approach is the amount of time required to screen the cDNA library. The original cDNA library contained 26,000 clones that were translated in pools of ~100 cDNA clones per pool. Therefore 260 different IVT reactions and assays are required to screen the cDNA library. Furthermore, once a phospho-dependent interaction is discovered, the sub-fractionation of the cDNA pool to isolate the interaction is very time intensive and sometimes the initial observed interaction is never recovered. We therefore adapted the IVT screen to a 96 well format to greatly accelerate the screening process. Screening in 96 well format allowed a four fold larger library to be screened in ten rounds, with each round

requiring two days for completion followed by a two-week exposure to a phosphoimager plate. After identifying a pool that contains a phospho-dependent interaction, the cDNA from that pool is transformed into bacteria and plated on agar plates. Single colonies are then picked and their DNA isolated for re-screening. Performing the DNA mini-preps and re-screens in 96 well format allowes for a greater coverage of the cDNA pool, further decreasing the chance the positive clone will be lost.

Following isolation of the phospho-binding domain, the optimal phospho-binding motif can be determined using oriented peptide library screening [16]. In this approach the phospho-peptide library is incubated with a GST-phospho-binding domain fusion protein bound to GSH-agarose beads. After thorough washing, the bound peptides are eluted and sequenced, allowing for the determination of the optimal binding motif and the construction of a position specific scoring matrix [10]. After the construction of a matrix, Scansite <http://scansite.mit.edu> is used to search the entire human database for proteins containing the optimal binding motif [38]. Isothermal titration calorimetry is often used to confirm the results obtained from the peptide library screening and to determine the binding affinity of the optimal phosphopeptide to the phospho-binding domain. Common approaches to confirm the selection of the likely in vivo interacting proteins include pull-down assays and in vivo co-association studies.

The elucidation of undiscovered kinase substrates and phospho-binding domains in the DNA damage response pathway could provide molecular insight

into a number of DNA damage responsive cellular processes, examples of which are discussed below.

DNA Repair Pathways and Cell Cycle Checkpoints

The five major DNA repair pathways

The five major DNA repair pathways involved in maintaining genomic integrity are base excision repair (BER); homologous recombinational repair (HRR); mismatch repair (MMR); non-homologous end joining (NHEJ); and nucleotide excision repair (NER). Proteins associated with these types of DNA repair processes are well positioned to act as the first sensors of DNA damage, recruit the Rad17-RFC and 9-1-1 and Mre11-Rad50-Nbs1 complexes, activate the DNA damage checkpoint kinases, and trigger cell cycle arrest and apoptosis.

Base excision repair

BER is involved repairing single-base DNA damage caused by methylating and oxidizing agents, and the large number of spontaneous depurinations that occur (about 10,000 per cell per day) [39]. BER is activated through two different pathways depending on the type of DNA damage; one pathway involves single nucleotide BER and the other pathway involves long patch BER which removes 2-15 nucleotides. In BER, a DNA glycosylase binds the altered deoxynucleoside and catalyzes cleavage of the base-sugar bond to remove a damaged base [40]. Glycosylase activity generates an apurinic/apyrimidinic site (AP site). BER can also occur at a site of spontaneous

depurination. Ref-1, an AP endonuclease, then makes a 5' nick in the DNA backbone. This nicking is followed by poly(ADP-ribose) polymerase-1 (PARP-1) acting as a DNA nick surveillance protein by binding to the nicked DNA [41]. Repair patch synthesis and DNA ligation complete the BER process [39].

Ref-1 is gaining attention in the field because it has been shown to be elevated in a variety of cancers, indicating that during cancer progression enhanced BER may provide a growth advantage [41]. Ref-1 in addition to playing a role in BER, is also a regulator of cell cycle arrest and apoptosis [41].

PARP-1 is another protein gaining interest in the field. DNA damage increases the activity of PARP-1, which is activated by binding to single- or double-strand breaks in DNA. PARP-1 is also involved in long patch BER through the recruitment of DNA repair enzymes to the vicinity of a DNA lesion. PARP-1 catalyzes the synthesis of poly(ADP-ribose) onto substrate proteins in the vicinity of the damaged DNA [40]. The attachment of the negatively charged ADP-ribose polymers to proteins most likely creates a region of negative charge around the DNA break, thus further opening up the chromatin and allowing access of additional repair proteins to the site of DNA damage. Treatment of cells with PARP inhibitors can sensitize cells to apoptosis [40, 42]. Therefore at low levels of DNA damage, PARP activity may protect against apoptosis. In fact it has been suggested that, depletion of NAD+ and eventually ATP by PARP-1 utilization may provide a linkage between excessive DNA damage and the triggering of apoptosis [41]. Furthermore, p53 undergoes extensive poly(ADP) ribosylation in the apoptotic program suggesting that PARP-1 may activate p53

function in apoptosis. PARP-1 is also cleaved by caspase-3 suggesting that PARP-1 mediated BER is counterproductive once a cell is committed to apoptosis [40].

Homologous recombinational repair

HRR allows for the physical exchange of a DNA segment from a homologous intact DNA strand to restore DNA sequence information that is destroyed due to damage [43]. HHR is a preferred way to repair DNA double strand breaks because it is very accurate. However, because HHR requires a template daughter strand to assist in the repair process, it cannot be performed until after the damaged DNA strand has been replicated, and thus HHR is not possible in G1 and early S-phase [44, 45]. The major proteins involved in HHR are BRCA1, ATM, ATR, c-Abl, Werner syndrome gene (WRN), Bloom syndrome gene (BLM), p53, Rad51, and the breast cancer-associated gene 2 (BRCA2) [46, 47].

BRCA1 is involved in the assembly of the BRCA1-associated genome surveillance complex (BASC), which includes the proteins MSH2, MSH6, MLH1, ATM, BLM, and the RAD50-MRE11-NBS1 [48]. BASC is thought to act as a scaffold and sensor for DNA damage. The role for each protein in this complex or in the strand exchange reactions of HRR is not well understood [49]. BRCA1 interacts with Rad51 and participates with Rad51 in HRR of double-strand breaks and interstrand crosslinks caused by cisplatin [2, 46, 50, 51]. BRCA1, BRCA2 and RAD51 interact and co-localize in nuclear foci in the nucleus during S-phase

and mutations in BRCA2 give rise to phenotypic effects similar to those arising from mutations in BRCA1, suggesting that the proteins have related functions [51]. Despite the similarity in function of BRCA1 and BRCA2, the two genes are not related by sequence [51].

Mismatch repair

The post-replication correction of nucleotide mismatches involves a highly conserved set of MMR proteins including MLH1, PMS2, MSH2, MSH3, and MSH6 [52]. The MMR repair process involves the detection of the mismatch by the MSH2/MSH6 heterodimer, which leads to the recruitment of the MLH1/PMS2 heterodimer. The MSH2/MSH6 heterodimer is also part of the BASC complex and thus it may also be involved in HRR to correct base mismatches or other abnormalities that can arise from the strand exchange reactions of HRR [46, 48, 51].

Defects in the MMR process give rise to increased DNA mutations and a predisposition to cancer. Furthermore, mutations in MMR are implicated in the development of a wide variety of sporadic tumors [52]. The MMR system is involved in the cellular response to a variety of DNA damaging agents. MMR mutants defective in repair would be expected to exhibit increased cytotoxicity after treatment with DNA damaging agents, however these mutants are observed to be resistant to the normally cytotoxic effects of alkylating and methylating agents [52]. For example, MMR deficient cells are less sensitive to the induction of apoptosis by methylating agents which appears to be triggered by secondary

lesions, possibly double-strand breaks, caused by MMR processing. Methylating agents lead to p53 phosphorylation on several residues, and these phosphorylation events depend on the presence of functional MMR proteins [52]. This positions the MMR proteins as a proximal step of DNA damage signaling and in the activation of the DNA damage checkpoint.

Non-homologous end joining

HRR and NHEJ are two main processes for repairing double-strand breaks. Unlike HHR, NHEJ is regarded as largely inaccurate because it involves end-joining reactions with junctions containing deletions back to regions of semi-homology [53]. Despite this inaccuracy, recent data indicates that mammalian cells repair the majority of double-strand breaks by NHEJ, although there is emerging evidence that NHEJ may be coupled to HRR to generate accurate repair of double-strand breaks [46, 49]. Either way, the two pathways HRR and NHEJ can be thought of as complementary processes as double mutant cells defective in both HRR and NHEJ are profoundly more sensitive to IR than either mutant alone [46, 54]. The NHEJ processes are initiated by DNA-PK and DNA binding proteins Ku70 and Ku80. After binding to DNA ends of a double-strand break, Ku recruits the catalytic subunit of DNA-PK (often denoted as DNA-PKcs). DNA-PKcs is an inactive protein kinase which is activated upon association with Ku at DNA ends [42, 54]. The active complex of Ku and DNA-PK is able to position the ends of the double-strand break and allow their ligation by DNA ligase IV to complete NHEJ-mediated DNA repair [50].

Nucleotide excision repair

NER is responsible for the repair of DNA damage that contains large helix-distorting lesions. Common lesions repaired by NER include the UV-induced cyclobutane pyrimidine dimers and 6–4 photoproducts, as well as the adducts produced by chemotherapeutic agents like cisplatin [55, 56]. When DNA helix-distorting damage is produced by UV, the levels of p53 are increased to help activate NER. NER is a very complicated repair process though it has been reconstituted in vitro with purified components. The proteins involved in the NER process, including XPD, XPB, p53 and p33ING1b, are responsible for many steps of NER including the recognition of the DNA damage, the recruitment of repair complexes to the lesion, the modification of the DNA for helicases-mediated repair, the incision and release of the damage DNA in a single-strand fragment ranging from 24–32 nucleotides in length, the repair of the gap by DNA synthesis, and the DNA ligation to form the final phosphodiester bond [55, 56]. Like the BER pathway, the NER pathway consists of two subpathways: global genomic repair (GGR) and transcription coupled repair (TCR) [55, 57]. As expected, these pathways function differently, with GGR acting on damage in the non-transcribed regions of DNA and TCR acting on damage in actively transcribed DNA [40]. However, after activation, most enzymatic steps utilize the same enzymes and enzyme complexes [58].

The XPD helicase function is essential for NER, and mutations in XPD have been shown to alter stabilization and function of the transcription factor complex TFIIH. TFIIH is a nine-subunit complex that acts in NER. XPD and XPB

are members of this complex whose helicase activities are required for NER, as they allow the opening of DNA around the site of damage during the GGR subpathway of NER [59]. During the TCR subpathway of NER, it is thought that stalling of RNA pol II at a site of DNA damage recruits the TFIIH complex, with its XPD subunit, to participate in NER [55, 58]. When the XPD helicase function is lost due to alterations in its ATP hydrolysis region, neither the 5' to 3' incision around a DNA adduct can be detected. Various mutations in XPD display different defects in DNA repair, RNA transcription and apoptosis as well as cause diseases such as xeroderma pigmentosum, Cockayne's syndrome or trichothiodystrophy [40]. The XPB helicase also acts also within the TFIIH complex necessary for transcription and NER as well as for p53-dependent apoptosis [46, 59]. The few XPB mutations known each have different levels of deficiency with respect to repair of cyclobutane pyrimidine dimers and pyrimidine(6–4)pyrimidine dimmers [59, 60].

The induction of NER and apoptosis after UV damage in mouse fibroblasts is observed only in $p53^{+/+}$ and not in $p53^{-/-}$ cells, indicating that both stress response functions are dependent on wild-type p53 function [55, 59, 60]. Thus UV-induced apoptosis is not only dependent on XPB and XPD function, but also requires p53 function [46].

UV-induced DNA damage and the Rad17-RFC and 9-1-1 complex

Genetic screens to identify genes that affect sensitivity to genotoxins led to the identification of the Rad9, Hus1, and Rad1 orthologs. This complex is a

heterotrimeric ring composed of Rad9, Hus1, and Rad1, termed the 9-1-1 complex [61, 62]. These proteins are required for activation of checkpoint signaling pathways and interact in a stable complex in cells in a manner to the sliding DNA clamp PCNA [63]. The PCNA clamp serves as a sliding platform that tethers replication proteins and polymerases to the DNA. PCNA is loaded onto DNA by the ATPase replication factor C (RFC) complex [64]. In contrast, the 9-1-1 clamp interacts with and is loaded by a separate clamp loader that contains the checkpoint protein, Rad17. Rad17 interacts with four replication factor C subunits (Rfc2, Rfc3, Rfc4, Rfc5) to form a pentameric structure, referred to as the Rad17-RFC complex [64, 65]. These complexes of proteins are presumed to act in concert with one another. In a similar fashion to the loading of the PCNA sliding clamp complex, it is thought that during a checkpoint response the Rad17-RFC complex may recognize damage and load the 9-1-1 sliding clamp onto DNA [64]. Association of Rad17-RFC and the 9-1-1 heterotrimer has been identified in vitro, and each complex is inferred to bind to sites of DNA damage in vivo as the Rad17-RFC complex binds preferentially to DNA with primer-template-like structures; however loading of the 9-1-1 complex onto DNA by Rad17-RFC has not yet been shown in cells [2]. Once loaded, the 9-1-1 complex may serve to recruit DNA damage response proteins and enhance damage signaling to other checkpoint components [66].

For example, in response to genotoxic stresses such as DNA damage caused by alkylation or UV light the 9-1-1 complex is loaded onto chromatin to help activate the checkpoint signaling pathways [63]. The Rad17-RFC complex

together with the 9-1-1 complex is thought to help activate the ATR/CHK1 pathway and may recruit substrates of these kinases, including BRCA1 and its associated proteins, for phosphorylation by ATR [61]. Following DNA damage, ATR/ATRIP is recruited to chromatin in a reaction that does not require the 9-1-1 complex. Independently of ATR, the 9-1-1 clamp is loaded onto chromatin by the Rad17 clamp loader. The chromatin-bound 9-1-1 complex then facilitates the ATR-mediated phosphorylation and activation of CHK1. The ATR/ATRIP and Rad17-RFC clamp loader complexes are most likely not the actual sensors of DNA damage. After the replication fork encounters a lesion and stalls, extensive regions of single-stranded (ssDNA) are produced. ssDNA is also a common intermediate generated in the DNA repair process and it is a potential ATR/CHK1 pathway activator [63]. Exposed ssDNA is coated with the ssDNA-binding protein RPA, which is required for checkpoint activation. RPA-coated ssDNA directly recruits ATR/ATRIP and stimulates the Rad17-dependent loading of the 9-1-1 onto DNA. Studies in Xenopus egg extracts suggest that other intermediates also participate in the assembly of the ATR/ATRIP and 9-1-1 complexes onto chromatin at stalled replication forks [64]. Activated CHK1 plays critical roles in cellular checkpoint responses by stabilizing stalled replication forks, and blocking the firing of late origins of replication, and arresting cells in G2/M [67].

The 9-1-1 complex members are key participants in the Chk1 activation pathway. In this regard, studies have shown that Hus1$^{-/-}$ and Rad9$^{-/-}$ cells have CHK1 activation defects and disruption of Rad9, Hus1, or CHK1 produces a phenotypically similar response [46, 67]. Cells deficient for the 9-1-1 components

continue DNA replication after DNA damage, a phenomenon known as radioresistant DNA synthesis (RDS) that indicates defective checkpoint signaling during S-phase [65]. A major question is how the chromatin-bound 9-1-1 clamp complex promotes CHK1 activation. Recent work has shown that a unique feature of Rad9 is its "tail" that is required for this function. Unlike Hus1 and Rad1, Rad9 possesses an approximately 120-amino acid C-terminal tail region that is phosphorylated on several serine and threonine sites [60, 64]. The tail is not required for interaction with Hus1 and Rad1, interaction of the clamp with Rad17, or loading of the clamp onto chromatin, demonstrating that the tail is not required to form a functional clamp [64]. One of these phosphorylation sites is a consensus PIKK "SQ" site that is phosphorylated by ATR and ATM in response to DNA damage [2, 64]. It is unknown which kinases phosphorylate the other sites. Surprisingly, the PIKK consensus site is not required for CHK1 activation, instead as least one of the other sites is essential for Rad9 activation of CHK1 [2, 64, 68]. This data suggest an model where the phosphorylated Rad9 tail, in the chromatin-bound 9-1-1 complex, help recruits signaling proteins to the DNA lesions and facilitates the and activation of CHK1 [2, 64, 67].

IR-induced DNA damage and the Mre11-Rad50-Nbs1 complex

The Mre11-Rad50-Nbs1 (MRN) complex localizes to sites of double-strand breaks (DSB) in vivo and plays vital roles in DNA metabolism, including DSB repair, meiotic recombination, and telomere maintenance [69]. NBS1 (also termed nibrin) is the product of the gene mutated in the human chromosomal

instability disorder, Nijmegan breakage syndrome [70, 71]. The clinical features of NBS show considerable but not complete overlap with those features displayed by A-T patients. Treatment of cells with IR induces the rapid formation of nuclear foci containing the NBS1-Mre11-Rad50 complex and the foci assembly in close proximity to DNA DSB [72, 73]. Nbs1 contains an FHA domain and an adjacent BRCT domain, both of which are involved in targeting this complex to nuclear DNA damage foci [73, 74]. Cells deficient in Mre11 or Nbs1 continue DNA replication after IR, an RDS phenotype, and display errors in other cell cycle checkpoints [2, 75]. The overlapping clinical phenotypes of A-T and NBS prompted speculation that the two proteins might be functionally interconnected. This prediction was validated by reports that ATM phosphorylates NBS1 on up to three serine residues (Ser 343, Ser 397, and Ser 615), and that Ser to Ala substitutions at any one of these sites generates a mutant NBS1 protein that fails to complement the checkpoint defects in NBS cells [1, 75]. Exactly how the MRN complex signals through ATM in the checkpoint signaling process in not well understood though it appears to involve both protein localization and ATM kinase activation. [42].

Additional damage sensors: BRCA1

The breast-cancer susceptibility gene product, BRCA1, plays important roles in cell cycle control, transcriptional regulation, chromatin remodelling, and the response to DNA-damage [51, 76]. BRCA1 is a large, modular protein of 1863 amino-acid residues containing an N-terminal RING domain, a central

region rich in SQ/TQ dipeptide pairs, and tandem BRCT (Brca1 C-terminal) domains. BRCA1 appears to function in multiple points in checkpoint signaling perhaps by linking checkpoint arrest to DNA damage repair [76]. BRCA1 is thought to enhance cancer progression by allowing excessive DNA damage through insufficient DNA repair and loss of cell cycle arrest in the presence unrepaired DNA damage. Recent findings position ATM and ATR as critical upstream modulators of BRCA1. However, BRCA1 has also been sown to be required for ATM activation after DNA damage, placing BRCA1 both upstream and downstream of ATM [76]. Early in the DNA damage signaling response, BRCA1 becomes phosphorylated and initiates activation of checkpoint kinases and the localization of additional substrates for kinase phosphorylation [47, 77-79]. Once phosphorylated, BRCA1 may activate downstream protein kinase cascades, aiding in amplification of the damage signal by recruiting additional phosphorylation substrates [80]. BRCA1 also colocalizes with a number of proteins involved in DNA repair and/or replication, including Rad51, PCNA, Mre11-Rad50-Nbs1, histone deacetylases, the DNA helicase BLM (mutated in Bloom's Syndrome), and mismatch repair proteins [51, 81]. Consistent with these associations, BRCA1 affects homologous recombination, mismatch repair, and transcription-coupled repair [51]. Studies of the DNA damage responses in BRCA1-deficient cells are focusing increasing attention on the role of BRCA1 in promoting high fidelity DNA repair through homologous recombination between sister chromatids [51, 82]. BRCA1 also is involved in the regulation of centrosome duplication. In cell deficient in BRCA1, improper amplification of

functional centrosomes leads to the formation of multiple spindle poles within a single cell [83]. These abnormalities directly result in the unequal segregation of chromosomes, abnormal nuclear division and aneuploidy.

BRCA1 is the classic member of a family of checkpoint repair proteins that contain the conserved BRCT domains, which have recently been shown to be phosphospecific binding domains involved in the signaling process from the induction of the G2/M cell cycle checkpoint to the repair of damaged DNA [51, 84-86]. In addition to BRCA1, other members of this BRCT domain-containing family have recently been identified as substrates for ATM and are likely substrates of ATR as well. Both MDC1 and p53 binding protein 1 (53BP1) are large nuclear BRCT domain-containing proteins that rapidly localize to sites of DNA damage in cells treated with IR or other DNA-damaging agents [87, 88], although the functions of MDC1 and 53BP1 remain unclear. Within minutes following ionizing radiation, MDC1 associates with the MRN complex and with numerous other DNA damage response proteins including 53BP1 and BRCA1. Nbs1, BRCA1, 53BP1 and MDC1 all form nuclear foci that colocalize with H2AX foci induced by DNA damage. The exact role of how BRCA1 and its BRCT domains function to control the DNA damage response remains unclear.

Damage transducers: ATM, ATR, CHK1 and CHK2

The ATM/CHK1 and ATR/CHK2 pathways are responsible for regulating several points within cell cycle progression. Despite the importance of these pathways, there most likely remains unidentified substrates and phospho-binding

domains functioning downstream of these kinases. ATM and ATR are members of the phosphoinositide 3-kinase related kinases (PIKKs) and regulate several proteins within the same pathway, often by phosphorylation of proteins substrates on a common [Ser/Thr]-Gln motif, to control the cell cycle progression [2, 89]. CHK1 and CHK2 are serine-threonine kinases that are required for cell cycle arrest in response to DNA damage [90]. As downstream kinases, CHK1 and CHK2 are phosphorylated by ATM/ATR-dependent processes and potentiate phosphorylation of additional downstream targets [89, 91]. This pattern of dual regulation of substrate phosphorylation by ATM and ATR in cells exposed to different forms of genotoxic stress has become a recurrent theme in the checkpoint-signaling field. Of the PIKK family members, ATM represents the primary responder to IR or radiomimetic agent-induced DNA damage. In the absence of ATM, or in normal cells that incur a high level of IR-induced DNA damage, ATR serves mainly as a backup kinase for ATM [92, 93]. On the other hand, ATR takes on the front-line signaling responsibilities when cells are challenged with other forms of genotoxic stress, such as UV light exposure or treatment with agents that interfere with DNA replication (aphidicolin and hydroxyurea) [2]. ATR is essential for cell viability and ATR has been shown to form a heterodimer with the associated protein ATRIP, which is required for ATR stabilization and the checkpoint signaling pathway [2, 93, 94]. Though the mechanism of ATR-ATRIP activation remains elusive it is probable that, like the PIKK family member DNA-PK, kinase activity is activated upon association with additional protein partners at the sites of damaged DNA, such as single-stranded

DNA [2]. In fact, ATR and ATRIP colocalize to intranuclear foci after DNA damage or inhibition of replication [94]. Though ATR's essential function is not yet fully defined, it is likely to be critical for repairing the DNA damage sustained that occurs on a continuous basis. Furthermore, cells may require ATR for the constant monitoring to ensure viability [94]. Recent data clearly demonstrates that ATM, ATR and DNA-PK are required to associates with protein partners at the sites of DNA damage for efficient phosphorylation of their targets [42].

The ATM protein kinase has been studied more extensively than ATR for two reasons. First, ATM was identified as the gene defective in the syndrome ataxia-telangiectasia (AT), and little association between ATR deficiency and a disease yet exists (ATR has reciently been shown to be involved in Seckel syndrome [95]). Second, unlike ATR, ATM is not essential for cell viability [93, 96]. Cells lacking ATM display chromosomal instability, a RDS phenotype, and extreme sensitivity to IR and radiomimetic drugs. AT cells are defective for cell cycle checkpoints at G1/S, S, and G2/M phase transitions in response to radiation-induced damage [1]. For example, the topoisomerase inhibitor, camptothecin, induces double-strand breaks predominantly in replication forks, and ATM mutant cells are defective in repair of this particular subclass of double-strand breaks [46]. In response to DNA damage, the E2F1 protein is phosphorylated by ATM and ATR at a site in its amino terminus. This phosphorylation stabilizes E2F1, which transcriptionally activates the p73 promoter. Accumulation of p73 leads, in turn, to induction of apoptosis. ATM is also required for IR-induced apoptosis and is largely dependent on BAX, a

member of the Bcl-2 family of cell death regulators, which promotes apoptosis [97, 98]. At DSBs, ATM may associate with the MRN complex of proteins, which could then serve to recruit ATM substrates for phosphorylation much like the 9-1-1 and Rad17-RFC complexes do for ATR [1]. Again, the fact that ATM and MRN act together at DSBs is inferred from the fact that cells from patients with mutations in NBS1, presenting as Nijmegan breakage syndrome, also exhibit radiosensitivity and chromosomal fragility like AT cells, and patients with mutations in MRE11 present with clinical symptoms and cellular defects much like those seen in AT, thus giving rise to the name "AT-like disorder" [91, 99]. In one example of ATM mediated signaling, ATM activates CHK2 by phosphorylating an amino terminal Thr residue (Thr 68) [100, 101], and CHK2, in turn, phosphorylates yet another amino-terminal Ser residue (Ser 20) in p53 [102-105]. Unlike the Ser 15 modification, which increases p53 transcriptional activity, phosphorylation at Ser 20 interferes directly with the binding of p53 to MDM2, thereby favoring p53 accumulation in response to IR-induced DNA damage. In another example, ATM directly phosphorylates BRCA1 after activation by DSB caused by ionizing radiation, although the consequences of this phosphorylation are unknown [2]. Additionally, activated CHK2, downstream of ATM, also phosphorylates BRCA1 on another site that is required for the dissociation of BRCA1 and CHK2 [79]. This pattern of dual kinase phosphorylation mediated regulation of proteins is evident throughout the cell cycle and DNA damage response pathways making it difficult to unambiguously order specific kinases within these types of signaling networks. If fact, once a

kinase phosphorylation site is identified on a protein, it would be prudent to identify other kinases that are activated during the process of interest, as they will likely also phosphorylate this protein.

Damage transducers: p38 MAPK and MAPKAP Kinase-2

DNA damage, and other cellular stress, triggeres the activation of the mitogen-activated protein kinase signaling pathways (MAPKs) [91, 106]. Normally, MAPKs are involved in regulating several cellular processes such as development, growth, differentiation, proliferation, and programmed cell death [27, 107]. MAPK signaling is required for preventing UV-induced DNA damage and tumorigenesis by initiating cell cycle arrest and apoptosis [52, 91, 108]. The MAPK pathway is comprised of three levels of kinases that are sequentially activated by phosphorylation of specific amino acid residues within the activation loop [109-111]. Ras can also play an important role as upstream activators of the MAPK pathways, a role facilitated via several MAPK enzymes. For example, DNA damage may first trigger activation of the serine/threonine MAP kinase kinase kinases (MAPKKKs) such as MEKK1/2/3, MTK1 (MEKK4), MLK2, ASK1/2, TAK1, and Tlp2. Active MAPKKKs in turn will phosphorylate serines in the activation loop of MAPKKs (MEK1/2, MKK3/4/6/7) [106, 111-113]. Subsequently, active MAPKKs will phosphorylate [Thr-Xxx-Tyr] motifs within the activation loop of MAPKs (p38s, JNKs, ERKs), which ultimately phosphorylate proteins and effector MAPKAP kinases (MAPKAPKs) [91, 110, 114, 115].

Just like the ATM and ATR pathways, a great deal of cross talk exists between MAPK pathways, p38s, c-Jun N-terminal kinases (JNKs), and extracellular signal-regulated kinases (ERKs) constitute the three main arms of the MAPK signaling pathway [91, 116]. They also constitute evolutionarily conserved pathways and are comprised of multiple isoforms. p38 MAPK has four isoforms (α, β, γ and δ); JNK has three isoforms (1/2/3); and ERK has two isoforms (1/2) [106, 116]. For the most part, JNK and p38 MAPKs are activated in response to genotoxic stresses while ERKs are activated in response to mitogenic signals [27, 107, 116].

MAPKs regulate key oncogenes and tumor suppressors implicated in the pathogenesis of cancers, such as ras, p53, APC/β-catenin, and $p16^{INK4a}$ (p16) [27, She, 2002 #1040, 116]. JNK and p38 MAPKs can either block cell proliferation or promote cell death when activated by DNA damage through the regulation of p53 and Cdc25A/B/C [27, 91, 117, 118]. MAPKs are also known to phosphorylate p53 to increase its stability and activity [27, 91]. p38 will modulate p53 activity by directly targeting Ser33 and Ser37 for phosphorylation [108, 119]. Furthermore, the MAPK signaling pathways contribute to cell cycle regulation by controling p21 and Gadd45a [2, 46]. p21 can directly block Cdk4/6/cyclin D1 and Cdk2/cyclin E, while Gadd45a's effects contrubite to p53 activation [111, 120]. Parallel to p53, UV-induced activation of MAPK increases the expression of the Cdk inhibitor p16 [91, 111, 121]. Like p21, p16 blocks Cdk4/6/cyclin D activity and prevents cells from progressing into S-phase.

The p38 MAPK pathway was originally described as a mammalian homologue to a yeast osmolarity sensing pathway [106, 111]. It was soon discovered that many cellular stresses activated the p38 MAPK pathway [107]. There are several protein kinases downstream of p38 MAPK enzymes that are activated following phosphorylation by p38 including MAPKAP Kinase-2 (MK2) and MSK1/2 [111, 122, 123]. For example MK2 phosphorylates and activates heat-shock protein 27 (HSP27), while MSK1/2 can phosphorylate and activate transcription factors that regulate survival [106, 111, 116, 122].

MAPKs can also regulate proteins that are part of the WNT/β-catenin signaling pathway. The Wingless/INT-1 (WNT) signaling pathway regulates cytoplasmic β-catenin accumulation by blocking the activity of the adenomatous poliposis coli (APC) destruction complex, which phosphorylates β-catenin and targets it for degradation [111, 124, 125]. The APC complex is composed of several factors, including APC protein, protein phosphatase 2A (PP2A), glycogen synthase kinase 3β (GSK3β) and Axin [126-128]. WNT signaling can promote the accumulation β-catenin under certain conditions, however, UV-induced p38 MAPK signaling has been reported to suppress WNT signaling and allow the APC complex to remain active [2, 46, 52, 91, 124].

As stated above, activation of MAPK is achieved not only through activation of the MAPKKK/MAPKK/MAPK pathway, but also through the Ras family of G proteins [129-131]. Ras activation can elicit varying responses [129, 132]. Initially, activated Ras activates MEK1/2 that specifically targets ERK1/2. The MEK/ERK signaling cascade will promote cell growth [129]. However,

sustained Ras/MEK/ERK activation will eventually induce MKK3/6 MAPKK activation, leading to p38 activation and expression of p53 and p16 that most likely counteract ERK [128, 129, 131, 133]. In response to DNA damage, p38 activation is critical for Ras-induced senescence, and interestingly its activation may be blocked with the MEK inhibitor U0126, supporting the idea that MEK activation is necessary for eventual MKK3/6/p38 activation [128, 129, 131, 133]. Cytokine regulation also involves p38 MAPK signaling [130]. The p38/MK2 pathway plays an important role in regulating the expression of many genes by modulating events ranging from transcriptional and translational control to mRNA stability [106, 123]}. For example, IL-1 and TNFα, protein levels are regulated at the transcriptional level while IL-6 levels are dependent on mRNA stability induced in part by IL-1 [121, 130]. p38 inhibitors can suppress TNFα expression without altering mRNA levels, which is indicative of regulation at the translational level [106].

Complicating the issue it that fact that the exact role of p38 MAPK signaling is dependant on the cell type and stimulus. p38 MAPK signaling has been shown to both promote cell death as well as enhance cell growth and survival in different cells and under various conditions [27, 116, 118, 122]. For example, the ability of ionizing radiation to regulate p38 MAPK activity appears to be highly variable with different groups reporting either no activation, weak activation or strong activation [27, 116, 118, 122]. In the studies where p38 MAPK activation has been observed following exposure to ionizing radiation it has been required for causing the G2/M arrest [27, 46, 111]. Interestingly in

these studies, p38 signaling was dependent on expression of a functional ATM protein. In support of this finding, overexpression of constitutively active MKK6 also enhanced cell numbers in the G2/M phase [52, 91].

Recent finding have show that p38 also plays a role in the UV-induced G2/M arrest [107]. Specifically, this group claimed that p38 was the kinase directly responsible for the phosphorylation of the 14-3-3 binding site on CDC25B/C. The growing idea that p38 and ERK directly contribute to the function of p53 (by phosphorylation of Ser15) and CDC25A/B/C (by phosphorylation of multiple residues, including the 14-3-3 binding sites) is puzzling. Based on preliminary data from our lab, the sequence motifs phosphorylated by these kinases do match the phosphorylated residues on p53 and CDC25A/B/C [91, 106, 108, 111]. Furthermore, JNK1/2 has been reported to phosphorylate Ser20, despite the fact that the p53 site is not a match for the JNK1/2 phosphorylation motif [91, 106, 108, 111]. In addition to the identification of ATR/CHK1 and ATM/CHK2 dependent processes, it is necessary to identify how activation of these MAPK pathways with different stimuli or at different points within the cell cycle, can alter the downstream processes and determine cell fate. Part of my thesis project will involved the determination which kinases are responsible for some of the identified known phosphorylation events.

The cell cycle checkpoints

The exact roles of the proteins described above depend on the stage in the cell division cycle the cell is when DNA damage occurs.

The G1 checkpoint

Most eukaryotic cells that experience DNA damage in G1 exhibit a delay prior to entering S-phase. This arrest in G1 allows time for DNA repair, thus preventing replication of a damaged DNA template. The exact role of the G1 checkpoint is often the subject of debate because it is very different in higher and lower eukaryotes. In mammalian cells, the key process may well be the series of events that lead to the stabilization of the tumor suppressor p53. An intricate web of protein kinases and phosphatases, as well as histone acetylases and ubiquitin-conjugating enzymes, regulates the accumulation and transcriptional-activating functions of p53 [134, 135]. Although p53 exerts a pervasive influence on checkpoint functions during the mammalian cell cycle, the G1 checkpoint represents the only case in which loss of p53 leads to total checkpoint abrogation [134-136]. The G1 delay mechanism involves ATM/ATR and CHK2/CHK1 but can take up to several hours to initiate because regulation for this block to S-phase entry occurs at the transcriptional level. Here ATM/ATR and CHK2/CHK1 activate and stabilize p53, causing transcriptional induction of p21 which then inhibits the Cdk2/cyclin E complex [2, 46, 137, 138]. In addition to p21, the activated form of p53 stimulates the expression of a large panel of genes, which, depending on the cellular context and type of initiating insult, may modulate intracellular redox status or induce the host cell to undergo apoptosis [2, 46].

As we now know, one well defined role for ATM and ATR is the regulation of p53 where these kinases utilize several means to stabilize the p53 protein. However, determining the functional consequences of p53 phosphorylation after

DNA damage was far more challenging than discovering the phosphorylation site. The location of Ser 15 at the p53 amino terminus suggested that modification of this residue might trigger the dissociation of p53 from MDM2, a protein that targets p53 for ubiquitination, nuclear export, and proteosomal degradation [2, 46]. It turns out, however, that Ser 15 phosphorylation is not sufficient to disrupt the p53/MDM2 interaction and instead this modification stimulates the transactivating function of p53 by enhancing the binding of this protein to the transcriptional coactivator, p300 [139]. While this phosphorylation by ATM probably causes p53 transcriptional activation, it is the phosphorylation of p53 at Ser 20 by CHK2 acting downstream of ATM that appears to reduce the ability of ubiquitin ligase MDM2 to bind p53, thus promoting its stabilization [2, 46, 136]. The physiological relevance of CHK2 in the regulation of p53 is underscored by the finding that loss-of-function mutations in CHK2 can give rise to a variant form of Li-Fraumeni syndrome, a heritable, cancer-prone disorder typically associated with germ-line mutations in p53 [102, 140].

It is unclear how a parallel ATR/CHK1 or p38 pathway also drives p53 accumulation in cells that have incurred IR or UV light-induced DNA damage. It will be interesting to determine if these kinases further ensure p53 stabilization by phosphorylating MDM2 and preventing export of p53 to the cytoplasm where it is degraded. Also undetermined is whether these two checkpoint cascades can occur independently or whether cascades are always activated together, regardless of the extent of damage [2]? Whether G1 arrest or apoptosis is more important in mammalian cells in preventing cancer is as yet unresolved. If both

mechanisms function to remove damaged cells from cycling, then both may play prominent roles in cancer evasion.

The S-phase checkpoint

The traditional view for the S-phase checkpoint is predominantly based on studies in budding and fission yeast. S-phase cells activate one of two very similar checkpoint pathways (which may in fact be integrated into one pathway) to signal DNA damage through the intra-S checkpoint or aberrant replication forks through the replication checkpoint [141]. The first step in S-phase checkpoint activation is stalling of replication forks owing either to the depletion of dNTPs or to the presence of DNA damage on the template strand [2, 142].

Fortunately, DNA damage detected during S-phase is likely to be repaired precisely via homologous recombination mechanisms involving sister chromatids [143]. Nonhomologous repair mechanisms also play a very prominent role in DNA DSB repair during all phases of the cell cycle; however, these mechanisms are inherently less precise and therefore confer an increased risk that inaccurately repaired DNA will be carried forward into M phase. The canonical checkpoint defect displayed by A-T cells is radioresistant DNA synthesis [144]. In normal cells, exposure to IR provokes a rapid but reversible decrease in DNA synthesis, which reflects decreases in the rates of both replication origin firing and DNA strand elongation [144]. In the absence of ATM, the IR-induced decrease in DNA synthesis is dampened significantly, giving rise to the RDS phenotype.

Activation of ATM/CHK2 and ATR/CHK1 leads to phosphorylation of CDC25A, thereby priming it for ubiquitination and proteasome destruction [117, 145, 146]. Loss of CDC25A inhibits Cdk2 by maintaining its inhibitory phosphorylation on Tyr 15 and inhibiting its association with cyclin E, an association necessary for progression into S-phase and possibly progression [147]. CDC25A also regulates Cdk4 activity and, as indicated by a much earlier study performed with UV treatment, destruction of CDC25A results in maintenance of the Tyr 17 inhibitory phosphorylation on Cdk4 that also prevents S-phase entry or progression [148]. IR exposure during S-phase activates CHK2 which then phosphorylates Ser 123 in CDC25A; this modification targets CDC25A for ubiquitin-dependent degradation. Interestingly, mutant CHK2 alleles associated with a variant form of Li-Fraumeni syndrome [102] failed to bind and/or phosphorylate CDC25A [149], which implies that genetic lesions in the RDS pathway could promote genome instability and cancer development.

The G2/M checkpoint

The final gatekeeper that blocks the entry of DNA-damaged cells into mitosis is the G2/M checkpoint. Though well characterized in pombe systems, the details of G2/M arrest in higher eukaryotic cells are still being determined. The picture thus far supports that fission yeast and higher eukaryotes both target Cdc2 to maintain its inhibitory phosphorylations as a principal means to block the G2/M transition. Targeting of Cdc2 is achieved by various parallel pathways, including the phosphatases that promote mitosis, the kinases that block Cdc2

function, and other proteins that control these regulators, which all converge to regulate Cdc2 activity. DNA damage causes the activation of several different downstream kinases that independently block the activity of CDC25B/C, the phosphatase that promotes mitosis by removing phosphates at Cdc2 inhibitory sites. By one mechanism, activation of ATR by damage leads to CHK1 phosphorylation [150]. CHK1 then negatively regulates CDC25B/C by phosphorylating it at Ser 309 or Ser 216, respectively [4, 151]. This phosphorylation of CDC25B/C creates a binding site for 14-3-3 proteins, and the bound state renders CDC25B/C either catalytically less active, sequestered in the cytoplasm, or both [152, 153], as discussed previously. In additional to activation by ATR, CHK1 may need to be further activated by BRCA1 to induce a G2/M arrest, although this additional activation has yet to be confirmed [80]. By a second mechanism, ATM activation by DNA damage in G2 leads to Chk2 activation that also phosphorylates CDC25B/C at Ser 309 or Ser 216 to block its function [154-156].

Studies of the G2 checkpoint in A-T cells have led to conflicting results, at least until the emergence of ATR, and possibly now p38 as a parallel initiator of checkpoint signaling [107]. When A-T cells are exposed to IR during G1 or S-phase, any cells that reach G2 phase are effectively arrested before they initiate mitosis. In fact, these cells show a more protracted G2 arrest than do ATM-expressing cells. On the other hand, if A-T cells are irradiated while in G2 phase, then the cells fail to arrest, and proceed into mitosis [92, 157, 158]. These results indicate that ATM is dispensable for activation of checkpoint-mediated G2 arrest

unless the DNA damage occurs during G2 itself. The ATM-independent pathway that initiates G2 arrest in cells that have experienced a genotoxic insult before G2 phase has not been defined. However, it is still unclear what role ATR/CHK1 and p38 will play in this alternative pathway of G2 checkpoint activation [27, 117, 118].

The critical role of CHK1 in the implementation of the G2 checkpoint is supported by the finding that *Chk1*$^{-/-}$ embryonic stem cells display a substantial reduction in G2 arrest following IR exposure [96]. The current G2 checkpoint model positions ATR as the upstream activator of CHK1 in human cells. In light of the ATR/CHK1 pathway outlined earlier, how do we explain the fact the ATM-deficient cells fail to activate the G2 checkpoint when DNA damage occurs during G2 phase? One possibility is that ATM also contributes to the inhibition of CDC25B/C activity, particularly in IR-damaged cells, by activating CHK2, which is capable of phosphorylating Ser 216 of CDC25C, at least in vitro [159]. In cells that express both ATM and ATR, ATM may activate CHK2 to reinforce the block to cyclin B/CDC2 activation imposed by the ATR/CHK1 pathway. A defect in the maintenance of the checkpoint induced G2 arrest has been observed in *Chk2*$^{-/-}$ embryonic stem cells [103]. Hence the ATM/CHK2 pathway may play a secondary role in G2 checkpoint activation when cells incur DNA DSB during G1 or S-phase.

The exact role each of the aforementioned pathways play and the interplay between the pathways under various cellular stresses will most certainly be the focus of intense study in coming years. For my thesis project, I have

focued on the identifcation new kinases substrates in the DNA damage response pathway phosphorylated by the CHK1, CHK2 and p38 arms of DNA damage signaling, as well as identification of new phospho-binding domains the recognize proteins phosphorylated by ATM and ATR that may facilitate DNA damage signaling and repair.

Chapter 2

MAPKAP Kinase-2 is a Cell Cycle Checkpoint Kinase that Regulates the G2/M Transition and S-phase Progression in Response to UV Irradiation

Summary

The cellular response to DNA damage is mediated by evolutionarily conserved Ser/Thr kinases, phosphorylation of CDC25 protein phosphatases, binding to 14-3-3 proteins, and exit from the cell cycle. To investigate DNA damage responses mediated by the p38/stress-activated protein kinase (SAPK) axis of signaling, the optimal phosphorylation motifs of mammalian p38α SAPK and MAPKAP Kinase-2 were determined using oriented peptide library screening. The optimal substrate motif for MAPKAP Kinase-2, but not for p38 SAPK, closely matches the 14-3-3-binding site on CDC25B/C. We discovered that MAPKAP Kinase-2 is directly responsible for CDC25B/C phosphorylation and 14-3-3-binding *in vitro* and in response to UV-induced DNA damage within mammalian cells. Down-regulation of MAPKAP Kinase-2 eliminates DNA damage-induced G1, intra S-phase, and G2/M checkpoints. We propose that MAPKAP Kinase-2, more aptly named CHK3, is a new member of the DNA damage checkpoint kinase family that functions in parallel with CHK1 and CHK2 to integrate DNA damage signaling responses and cell cycle arrest in mammalian cells.

Contributions:

Andy Elia, Mike Yaffe, and Mary Stewart preformed the p38 kinase experiments shown in Figure 2.1 and discussed in the text. Dan Lim preformed the structural modeling experiment shown in Figure 2.6 and played a major role in the construction of Figure 2.7. Ancho Nguyen played a major role in the generation of the FACS data shown in Figures 2.4/2.5.

Introduction

The maintenance of genomic integrity is essential for the health of multi-cellular organisms. DNA damage checkpoints constitute a mechanism where cell division is delayed to allow repair of damaged DNA or if the extent of DNA damage is beyond repair, induce apoptosis. The three major DNA damage-responsive cell cycle checkpoints are the G1/S checkpoint, intra S-phase checkpoint, and the G2/M checkpoint [46].

Signal transduction events controlling the DNA damage response are mediated by evolutionarily conserved Ser/Thr kinases and phosphoserine/threonine-binding domains. Distinct types of genotoxic stress converge to trigger a limited repertoire of DNA damage checkpoint responses, presumably by funneling specific protein complexes that recognize different types of DNA damage into a few common pathways. For example, lesions commonly caused by IR and UV initiate the activation of the upstream kinases ATM and ATR [2]. These kinases transduce the signal that directly engages the DNA damage checkpoint.

ATM and ATR appear to have partially overlapping functions since some common Ser/Thr-Gln-containing substrates of both kinases have been identified. ATM responds primarily to double strand breaks whereas ATR responds to many types of DNA damage, including the bulky DNA lesions caused by UV. Once activated, ATM phosphorylates the downstream effector kinase CHK2 on Thr68, and ATR phosphorylates the downstream effector kinase CHK1 on Ser317 and Ser345 [2, 160]. In addition, studies in both *Xenopus* egg extracts and

mammalian cells have pointed to the existence of a checkpoint pathway that is independent of ATR/CHK1 and ATM/CHK2 [107, 120, 161-163].

A major mechanism by which CHK1 and CHK2 control the DNA damage response is through the phosphorylation-dependent inactivation of members of the CDC25 family of phosphatases, which are positive regulators of Cyclin/Cdk complexes [164]. The CDC25 family consists of three different isoforms: CDC25A, CDC25B (variants 1,2, and 3) and CDC25C. CDC25A and CDC25B are thought to be oncogenes since they are upregulated in many forms of human cancer [165, 166]. CDC25A controls both progression through S-phase and entry into, and maintenance of, mitosis [167, 168]. In response to DNA damage, CDC25A is phosphorylated on several sites including Ser78 and Ser123, targeting it for ubiquitin-mediated degradation [167]. CDC25B and CDC25C, on the other hand, are primarily involved in regulating mitotic entry through their activation of the cyclin-dependent kinase CDC2/CyclinB [164]. In response to DNA damage, CDC25B1/CDC25B2 and CDC25C become sequestered away from the nuclear pool of CDC2/CyclinB by phosphorylation on Ser-309/Ser-323 and Ser216, respectively, leading to 14-3-3 binding and cytosolic retention [169-172]. The exact roles of different CDC25 family members in establishing this G2/M checkpoint, however, remain a matter of active debate [173, 174].

In contrast to the IR-induced DNA damage checkpoint, the UV responsive checkpoint is less well understood. It was recently shown that, in addition to the ATR/CHK1 pathway, the p38 SAPK pathway is also required for full activation of the DNA damage response following UV irradiation [107]. We discovered that

MAPKAP Kinase-2, a direct downstream target of p38 SAPK is directly responsible for phosphorylating CDC25B and C and maintaining the G1, S, and G2/M checkpoints in response to UV-induced DNA damage. Thus, MAPKAP Kinase-2 constitutes a third checkpoint kinase, in addition to CHK1 and CHK2, involved in coordinating the DNA damage response of higher eukaryotic cells.

Results

Defining the optimal phosphorylation motif for p38 SAPK

To identify substrates and targets of the p38 SAPK signaling pathway involved in DNA damage responses, the optimal substrate phosphorylation motif for p38α SAPK was determined using oriented peptide library screening [11]. Efficient peptide phosphorylation by p38 SAPK required a fixed Pro residue in the Ser+1 position (data not shown), consistent with the known identification of p38 SAPK as a Pro-directed MAP kinase. Screening performed with a library containing the degenerate sequence X-X-X-X-Ser-Pro-X-X-X-X (X denotes all amino acids except Cys, Ser, Thr, and Tyr) displayed strongest selection for Pro in the Ser-2 position with weaker selection for other aliphatic residues (Figure 2.1A). Additional selection was also observed at the Ser-3, Ser-1 and Ser+2 positions.

To further refine the optimal phosphorylation motif, a secondary screen was performed based on results from the initial screen by using a library with Pro fixed in both the Ser-2 and Ser+1 positions, and Ser, Thr, and Tyr included in the X positions. This revealed selection for Gln, Met, and Gly in the Ser-1 position, along with slightly weaker selection for Pro, Ser and Thr (Figure 2.1A). Gly was the preferred residue in the Ser-3 position, along with Ile, Val, and Tyr. Hydrophobic residues, particularly aromatic and β-branched amino acids, were selected at the Ser+2 position. The resulting optimal motif for p38α SAPK determined by oriented peptide library screening closely matches the sequence

of mapped p38 MAPK phosphorylation sites on most, though not all, known substrates (Figure 2.1A) [112, 113, 175-179]

A peptide containing the optimal p38 SAPK consensus phosphorylation motif GPQSPI, "p38tide", was synthesized for kinetic analysis. This peptide was readily phosphorylated by p38 SAPK *in vitro*, however, it failed to display saturable Michaelis-Menton-type kinetics (Figure 2.1B). Instead, the initial velocity increased linearly with increasing p38tide concentration up to1400 μM. This finding suggests that additional interactions besides an optimal phosphorylation motif are likely to be involved in optimizing p38 SAPK-substrate binding, such as MAP kinase docking sites [180].

To search for potential p38 SAPK substrates, particularly those relevant to DNA damage signaling, the Swiss-Prot database was queried with the p38 SAPK consensus phosphorylation motif using Scansite [181]. Other than GADD153, a known p38 SAPK substrate, we were unable to identify any DNA damage response proteins in the top 250 hits. Database searching did, however, reveal two tandem near-optimal p38 SAPK phosphorylation sites (Ser-345 and Ser-348) in p47phox, a cytosolic component of the NADPH oxidase enzyme. A peptide containing this sequence, PGPQSPGSPL, "p47tide", was strongly phosphorylated by p38 SAPK, but like p38tide, the isolated peptide displayed linear non-saturable kinetics (Figure 2.1B).

Wild-type and mutant versions of GST-tagged full-length p47phox protein, rather than isolated peptides, were then used as substrates for *in vitro* phosphorylation reactions. The wild-type full-length p47phox protein was rapidly

phosphorylated by p38α SAPK (Figure 2.1C, D). Mutation of Ser-345→Ala had a more pronounced effect on p47phox phosphorylation than mutation of Ser-348→Ala, in excellent agreement with the observation that the Ser-345 site is a better match for the optimal p38 SAPK consensus motif than the Ser-348 site. Simultaneous mutation of both Ser-345 and Ser-348 to Ala eliminated phosphorylation of p47phox by p38 SAPK altogether. Kinetic analysis revealed classical Michaelis-Menton behavior for p38 SAPK phosphorylation of the wild-type p47phox with a K_m of 6.0 μM and a V_{max} of 36.6 nmol/min/μg. Mutation of Ser-345 to Ala both increased the K_m and reduced the V_{max}, while mutation of Ser-348 to Ala primarily increased the K_m (Figure 2.1E).

This data from isolated peptides and intact proteins argues that efficient substrate phosphorylation by p38 SAPK requires sequences with reasonable matches to the optimal substrate motif determined by oriented peptide library screening, and that additional interactions involving MAPK docking sites are likely to be critical for strong kinase-substrate interactions. Several docking motifs have been identified for p38 SAPK, particularly a short cluster of positively charged amino acid residues often flanked by hydrophobic amino acids [106, 111]. Two sequences corresponding to this type of docking motif are present near the p38SAPK phosphorylation sites in p47 phox, ^{311}IHQRSRKRLSQ^{321} and ^{329}VRFLQQRRRQA^{339}. Mutation of ^{335}RRR^{337} to LLL in the latter motif decreased the rate of p38α SAPK phosphorylation of p47phox by over 70%. The contribution of amino acids 311-321, or involvement of alternative p38 SAPK docking site(s) [112] is not yet known.

Bulavin et al. [107] implicated p38 SAPK in the DNA damage-response pathway and reported that p38 SAPK was directly responsible for generating a 14-3-3-binding site on CDC25B (Ser-323 in CDC25B2; Ser-309 in CDC25B1) in response to UV-C-induced DNA damage. Like p47phox, CDC25B contains a potential p38 SAPK docking motif, ^{345}PVQNKRRRSV^{354}, however the sequence flanking Ser-323, LXRSPSMP lacks a Pro in the Ser+1 position, and does not resemble the optimal p38 SAPK motif shown in Figure 2.1A. As shown in Figure 2.2A, recombinant p38 SAPK readily phosphorylated bacterially produced CDC25B *in vitro*. However, this phosphorylation did not induce 14-3-3-binding, and a Ser-323→Ala mutant form of CDC25B was phosphorylated by p38 SAPK equivalently to the wild-type CDC25B protein. This data argues that while CDC25B may be a p38 SAPK substrate, this phosphorylation event is not responsible for the 14-3-3-binding event that results in a G2/M checkpoint.

Defining the optimal phosphorylation motif for MAPKAP Kinase-2

A number of Ser/Thr kinases are activated downstream of p38 SAPK including MAPKAP kinases-2, and -3, MNK1 and MNK2, MSK1 and MSK2, and PRAK [116]. In response to UV-B-induced DNA damage, She et al (2002) reported that MAPKAP kinase-2 could phosphorylate p53 on Ser-20, the same site that is phosphorylated by two well-established checkpoint kinases, CHK1 and CHK2. Both CHK1 and CHK2 can also phosphorylate CDC25 family members to create 14-3-3 binding sites, suggesting that MAPKAP Kinase-2 might share a similar motif. The optimal substrate phosphorylation motif for

MAPKAP kinase-2 was therefore investigated using oriented peptide library screening.

Efficient peptide phosphorylation by MAPKAP Kinase-2 was only observed with a library containing a fixed Arg in the Ser-3 position (X-X-X-X-R-X-X-S-X-X-X-X, where X denotes all amino acids except Cys, Ser, Thr, or Tyr). A critical step in determining protein kinase phosphorylation motifs by peptide library screening involves purification of the phosphorylated peptides from the non-phosphorylated peptide background. In the case of MAPKAP Kinase-2, this was dramatically improved by conversion of all Glu and Asp residues to their methyl esters prior to metal-affinity chromatography and sequencing [12]. This resulting motif revealed clear amino acid selection at almost all degenerate positions (Figure 2.3A). MAPKAP Kinase-2 displayed strong selection for the hydrophobic residues Leu, Phe, Ile, and Val in the Ser-5 position, and the Ser+1 position. Strong selection was also observed for Gln in the Ser-2 position, and modest selection for Leu in the Ser-1 position. The motif determined for MAPKAP Kinase-2 using oriented peptide library screening is in remarkably good agreement with the sequence of mapped MAPKAP Kinase-2 phosphorylation sites on known substrates (Figure 2.3A, bottom) [110, 182-188], which primarily contain Leu, Ile or Phe in the Ser-5 position, Arg in the Ser-3 position, Gln, Ser, or Thr in the Ser-2 position, Leu, Val or Pro in the Ser-1 position, and hydrophobic residues along with Glu in the Ser+1 position. The preference for polar residues Ser and Thr in addition to Gln in the Ser-2 position in known

MAPKAP Kinase-2 substrates would not have been detected by oriented peptide library screening since Ser and Thr were not present in the library.

To verify the peptide library screening results, individual peptides (MK2tides) containing the optimal MAPKAP Kinase-2 consensus motif LQRQLSI, or mutant versions with Ala substituted at each position in the motif, were synthesized and used for kinetic analysis (Figure 2.3B, C). The optimal MK2tide displayed a K_m value two-fold lower than the best MAPKAP kinase-2 peptide substrate known to date, a sequence derived from HSP27 [188]. Substitution of Ala at each position in the motif affected K_m and V_{max} differently with some positions showing primarily a K_m effect (i.e. Arg in the Ser-3 position), while others revealed a primary effect on V_{max} (i.e. Leu in the Ser-5 position) (Figure 2.3C). The rank order of importance of key residues is Arg-3 > Leu-5 ≈ Ile+1 > Gln-3. The optimal MK2tide had neither the lowest K_m nor the highest V_{max}, but rather had the highest V_{max}/K_m ratio, consistent with the fact that the peptide library screening approach selects substrates on the basis of optimal V_{max}/K_m, rather than low K_m or high V_{max} alone [189]. Combining the data from oriented peptide library screening, known substrate sequences, and our kinetic studies, the optimal MAPKAP Kinase-2 phosphorylation motif is (Leu/Phe/Ile)-(Xxx)-(Arg)-(Gln/Ser/Thr)-(Leu)-(Ser/Thr)-(Hydrophobic).

The optimal MAPKAP Kinase-2 substrate motif is an excellent match for the known Ser-323 phosphorylation/14-3-3 binding motif in CDC25B, as well as the Ser-216 phosphorylation/14-3-3-binding site in CDC25C (Figure 2.3A). Initial experiments focused on CDC25B, since unlike CDC25C, CDC25B can be

produced in modest quantities in bacteria, and the Ser-323 site in CDC25B had been previously reported to be a direct p38 SAPK site. Incubation of recombinant CDC25B with purified MAPKAP Kinase-2 resulted in significant CDC25B phosphorylation and strong binding of the phosphorylated protein to 14-3-3 (Figure 2.2A). Mutation of Ser-323→Ala substantially reduced the ability of MAPKAP Kinase-2 to phosphorylate CDC25B, and completely eliminated the ability of CDC25B to bind to 14-3-3 (Figure 2.2A). These *in vitro* results strongly suggest that MAPKAP Kinase-2 is the critical CDC25/14-3-3 checkpoint kinase downstream of DNA damage signals relayed by the p38 SAPK pathway.

MAPKAP Kinase-2 is critical for the G2/M checkpoint following UV-induced DNA damage

The importance of MAPKAP Kinase-2 in DNA damage checkpoint function was investigated in U2OS cells. Activation of MAPKAP Kinase-2 in response to UV-C irradiation-induced DNA damage (Figure 2.4A) was monitored by its reduced mobility on SDS-PAGE gels, and by immunoblotting using a phospho-specific antibody against pThr-344, a site phosphorylated by p38 and required for MAPKAP Kinase-2 activation [177]. As shown in Figure 2.2B, MAPKAP kinase-2 was activated within 1 hr of irradiation, and remained activated for the 8 hr duration of the experiment. The kinetics of MAPKAP Kinase-2 activation paralleled the ability of CDC25B from these cells to bind to 14-3-3. Based on these data, a 2 hr time point was chosen for use in further studies.

RNA interference was used to confirm a direct role for endogenous MAPKAP Kinase-2 in the UV-induced DNA damage response. Treatment of U2OS cells with MAPKAP Kinase-2-specific siRNA oligonucleotides, but not with control GFP siRNA oligonucleotides, resulted in a substantial reduction of MAPKAP Kinase-2 to nearly undetectable levels by 48 hr after transfection (Figure 2.2C). No reduction in the levels or UV-C-induced activation of p38 SAPK, CHK1 or CHK2 was observed in these cells. Despite the presence of these other active kinases, siRNA-mediated knock-down of MAPKAP Kinase-2 caused a loss of both CDC25B- and CDC25C-binding to 14-3-3 after UV-C exposure (Figure 2.2C).

Cell cycle progression in the control GFP and MAPKAP Kinase-2 knock-down cells following UV-C-irradiation was studied using FACS (Figure 2.4). In these experiments, cells were irradiated with 20 J/m^2 of UV-C radiation, allowed to recover for 2 hr, then placed in nocodazole-containing media for an additional 16 hr to cause any cells progressing through the cell cycle to arrest in mitosis, where they can stained for the mitotic marker phosho-histone H3. Under these conditions, un-irradiated cultures of asynchronous GFP siRNA-transfected cells accumulated in a 4N-DNA-containing peak, with prominent levels of phospho-histone H3 staining (Figure 2.4B, C), consistent with a nocodazole-mediated M-phase arrest. In response to UV-irradiation, control cells displayed a prominent G1, S, and G2 distribution, with near-complete loss of phospho-histone H3 staining, indicating intact G1, S, and G2 checkpoints (Figure 2.4D, E).

The behavior of the MAPKAP Kinase-2 siRNA transfected cells was dramatically different. In the absence of UV irradiation, MAPKAP kinase-2 siRNA transfected cells, like control GFP siRNA-transfected cells, accumulate in a 4N DNA-containing peak with high levels of phospho-histone H3 staining (Figure 2.4F, G). Following UV-induced DNA damage, however, the MAPKAP Kinase-2 knock-down cells failed to arrest cell cycle progression. Instead, these cells proceeded to enter mitosis to the same extent as un-irradiated cells, as shown by a comparable 4N-DNA peak and similar levels of phosho-histone H3 staining as those observed in un-irradiated cells (Figure 2.4H, I). Together with the CDC25B/C:14-3-3 results in Figure 2.2C, this FACS data demonstrates that MAPKAP Kinase-2, is critical for the UV-induced G2/M checkpoint in response to UV-irradiation. In contrast to the UV response, summarized in Figure 2.4J, the G2/M checkpoint response to ionizing radiation in MAPKAP Kinase-2 knock-down cells is intact (Figure 2.4K).

MAPKAP Kinase-2 is critical for the S-phase checkpoint and G1 arrest following UV-induced DNA damage

The MAPKAP Kinase-2 knockdown cells in Figure 2.4 also showed a loss of the G1 and S-phase checkpoints following DNA damage, since UV-irradiation of asynchronous cultures resulted in accumulation of the cells in a 4N DNA-containing peak when the cells were transferred to nocodazole-containing medium. To investigate the direct role of MAPKAP Kinase-2 in S-phase checkpoint function, control or MAPKAP Kinase-2 knock-down U2OS cells were

UV-irradiated, allowed to recover for 30 min, and then labeled with BrdU for various times. In the absence of irradiation, 42% of the control siRNA-transfected cells showed substantial BrdU incorporation after 12 hr, compared with 53% of the MAPKAP Kinase-2-siRNA transfected cells (Figure 2.5A, B). When the cells were irradiated with 20 J/m^2 of UV light prior to BrdU labeling, only 3.5% of the control siRNA transfected cells showed BrdU incorporation at 12 hr. In marked contrast, 48% of the MAPKAP Kinase-2-knock-down cells continued to incorporate substantial amounts of BrdU. A similar difference in BrdU uptake between control siRNA-treated cells and MAPKAP Kinase-2-knock-down cells was also seen at shorter times after irradiation (Figure 2.5B).

Examination of the FACS profiles 12 hr following UV-irradiation revealed a dramatic decrease in the G1 population in the MAPKAP Kinase-2-knock-down cells compared with the control GFP siRNA-transduced cells (Figure 2.5A, right-most upper and lower FACS profiles). This loss of the G1 peak, together with the increased percentage of cells showing BrdU incorporation at 12 hr versus 2 hr of labeling, implies that endogenous MAPKAP Kinase-2 plays important roles in both the inhibition of DNA synthesis following damage (S-phase checkpoint function), and in the damage-induced arrest of cells in G1 prior to S-phase entry (G1/S checkpoint function). Loss of the G1/S and S-phase checkpoints in MAPKAP kinase-2 knock-down cells was associated with higher levels of CDC25A, decreased levels of p53, and reduced phosphorylation of p53 on Ser-20 following UV-irradiation compared with control siRNA-treated cells (Figure 2.2C).

The fate of S-phase control or MAPKAP Kinase-2 siRNA-treated cells in response to UV-C-induced DNA damage was examined by using FACS. In this experiment, asynchronous cells were mock-treated or irradiated with 20 J/m^2 of UV-C radiation and then pulse-labeled with BrdU. The ells showing BrdU uptake were subsequently analyzed 10 and 20 hr later (Figure 2.5C). In both non-irradiated control and MAPKAP Kinase-2 knock down cells, the BrdU pulse-labeled population showed a late S and G2/M distribution at 10 hr, and a re-appearance of a G1 peak at 20 hr, indicating full transit through the cell cycle. In response to UV-C irradiation, control siRNA-treated cells failed to show significant BrdU uptake upon which to gate for FACS analysis (Figure 2.5C, lower left panel). In contrast, the large population of MAPKAP Kinase-2 siRNA treated cells, which had lost the S-phase checkpoint and incorporated BrdU, went on to display a greatly reduced G1 peak at 20 hr with many cells showing DNA staining $\geq$ 4N (Figure 2.5C, bracket in lower right panel), consistent with mitotic death and exit from the cell cycle.

MAPKAP Kinase-2 Depleted Cells are More Sensitive to DNA Damage-Induced Cell Death

The experiments in Figures 2.4 and 2.5A-C indicate that MAPKAP Kinase-2 is involved in each of the cell cycle checkpoints triggered by UV-induced DNA damage. To determine the effect of MAPKAP Kinase-2 depletion on cell survival, cells were transfected with control siRNA or MAPKAP Kinase-2 siRNA for 48 hr, trypsinized, re-plated, and analyzed for colony formation in response to various

doses of UV-C irradiation 12 hr after re-plating. As shown in Figures 2.5D and E, MAPKAP Kinase-2 knock-down cells displayed a significant reduction in colony formation when compared to control-treated cells at all doses of UV-C irradiation examined. This difference in survival after UV-C exposure was most pronounced at low to moderate UV doses.

A structural model for MAPKAP Kinase-2 substrate selectivity

The optimal phosphorylation motif determined for MAPKAP Kinase-2 is strikingly similar to that determined for two other checkpoint kinases, CHK1 and CHK2 (Figure 2.6A; [90] and data not shown). All three of these CAMK superfamily members - MAPKAP Kinase-2, CHK1, and CHK2 - strongly select for aliphatic residues in the Ser–5 position, Arg in the Ser–3 position, and aromatic/aliphatic residues in the Ser+1 position, along with additional less stringent selection for particular amino acids in other positions (Figure 2.6A). In contrast, members of the AGC kinase superfamily such as Akt/PKB and conventional protein kinase C superfamily members preferentially phosphorylate sequences containing Arg residues in both the Ser–5 and Ser–3 positions, and play important roles in anti-apoptotic signaling and other signaling events unique to differentiated cell function, rather than critical roles in cell cycle control.

To investigate the structural basis for substrate motif selection, we performed molecular modeling studies of activated MAPKAP Kinase-2, using the published MAPKAP Kinase-2:ADP co-crystal structure [190] as a base model. The optimal substrate peptide Leu-Gln-Arg-Gln-Leu-Ser-Ile-Ala was modeled into

the kinase active site in an extended conformation (Figure 2.6D), and the kinase:substrate complex compared with the structures of Akt/PKB:AMP-PNP:GSK3-peptide ternary complex [191] (Figure 2.6C) and the CHK1 crystal structure containing a modeled CDC25C peptide [192] (Figure 2.6E). Strong selection for Arg in the Ser-3 position for MAPKAP Kinase-2, Akt/PKB and CHK1 is rationalized by the presence of a conserved glutamate residue at a similar location in all three kinases (Glu-145 in MAPKAP Kinase-2, Glu-236 in Akt/PKB and Glu-91 in CHK1), which in Akt/PKB forms a bidentate salt bridge with the Ser-3 arginine guanidino group on GSK3-peptide [191]. Similarly, selection for a hydrophobic residue at the Ser+1 position is explained by a hydrophobic pocket that is conserved at this position in all three kinases. The pocket is lined by Phe-310, Pro-314, Leu-317 and Phe-359 in Akt/PKB and by Met-167, Leu-171, Val-174, Leu-178 and Leu-179 in CHK1. The corresponding Ser+1 pocket in MAPKAP Kinase-2 is lined by Pro-223, Pro-227, Val-234 and Leu-235. Within this region, Gly-312 in Akt/PKB and Gly-169 in CHK1 are replaced by Tyr-225 in MAPKAP Kinase-2, which may reduce the depth of the MAPKAP Kinase-2 hydrophobic pocket and explain selection for branched chain aliphatic residues in this position compared with Phe selection by Akt/PKB and CHK1.

The marked contrast between Arg selection at the Ser-5 position in Akt/PKB with the corresponding selection for hydrophobic residues at this position by MAPKAP Kinase-2 and CHK1 is accounted for by the presence of Glu 342 in Akt/PKB at the base of the Ser-5 pocket. This residue is not conserved in MAPKAP Kinase-2 and CHK1, and is instead substituted by Ile-255

in MAPKAP Kinase-2 and by Ala-200 in CHK1. Additional residues, notably Phe-147, Pro-189, Pro-261 and Leu-342 in MAPKAP Kinase-2, and similarly Phe-93, Ile-96, Pro-98, Pro-133 and Leu-206 in CHK1, contribute a significant hydrophobic character to this region.

Discussion

In this study we have defined the optimal substrate motifs within the p38 SAPK/MAPKAP Kinase-2 axis of signaling using oriented peptide library screening. Our elucidation of the optimal phosphorylation motif for MAPKAP Kinase-2 expands considerably upon, and is in good agreement with, a more preliminary motif for this kinase determined previously [110]. Similarly, the optimal motif determined for p38 SAPK is in reasonable agreement with many mapped phosphorylation sites on p38 SAPK substrates. As with all consensus phosphorylation motifs, bona-fide substrates match the optimal motif at some, but not necessarily at all positions. Nearly all *in vivo* p38 MAPK substrates contain at least a minimum core SP motif, though Cohen and colleagues have recently identified TAB1 as a novel *in vivo* substrate of p38 SAPK in which one of the three mapped p38 SAPK phosphorylation sites lacks the Ser+1 Pro residue. This suggests that alternative phosphorylation and docking motifs may be present on some p38 SAPK substrates, and/or that local avidity effects may be important in some cases.

Our data suggests that a crucial role of p38 SAPK in response to UV-induced DNA damage is the phosphorylation and activation of MAPKAP Kinase-2, leading to MAPKAP Kinase-2-directed phosphorylation of CDC25 family members to induce 14-3-3-binding and subsequent cell cycle arrest. In this way, MAPKAP Kinase-2 performs similar functions after UV-C induced DNA damage as those performed by CHK1 and CHK2 after exposure of cells to ionizing radiation [193]. Recent data suggest that p38 SAPK (and therefore MAPKAP

Kinase-2) may play a similar role in certain types of chemotherapy-induced DNA damage [118, 120, 163].

Our finding that MAPKAP Kinase-2 is a central checkpoint kinase involved in DNA damage responses triggered by UV irradiation allows a different interpretation of the results of Bulavin et al [107], who demonstrated that inhibition of p38 SAPK by the chemical inhibitor SB202190, or reduction of p38 SAPK levels using anti-sense oligonucleotides blocked the G2/M checkpoint response in cells that received the same dose of UV-C radiation as the cells used in our study. The authors reported that p38 SAPK directly phosphorylated CDC25B and C to generate a 14-3-3 binding site. However, the experiments in that study were performed using Flag-tagged p38 SAPK that was immunoprecipitated from UV-irradiated cells. p38 SAPK and MAPKAP Kinase-2 form a tight complex within cells, and in response to cellular stress, p38 SAPK phosphorylation of MAPKAP Kinase-2 is required for the co-transport of the p38 SAPK:MAPKAP Kinase-2 complex from the nucleus to the cytoplasm [122, 123]. Thus, the p38 SAPK immunoprecipitates used in that study likely contained significant amounts of MAPKAP Kinase-2. Furthermore, the activity of MAPKAP Kinase-2 would have been strongly reduced by treatment with any p38 SAPK inhibitor.

MAPKAP Kinase-2 undergoes initial activation in the nucleus with subsequent export of the active kinase to the cytoplasm [122]. Thus, MAPKAP Kinase-2 is well positioned to function as both a nuclear initiator of CDC25B/C phosphorylation in response to DNA damage, and as a maintenance kinase that

keeps CDC25B/C inhibited in the cytoplasm. A unified model for kinase-dependent DNA damage checkpoints is presented in Figure 2.7. In response to ionizing radiation, ATM activation of CHK2 and ATR activation of CHK1 leads to phosphorylation of CDC25 family members on related sequences corresponding to the checkpoint kinase core "motif" LxRxx[S/T]ϕ. Similarly, in response to UV-induced DNA damage, ATR activates CHK1 and p38 SAPK activates MAPKAP Kinase-2, leading to phosphorylation of the same core motif on CDC25 family members. The exact role that different checkpoint kinases play in phosphorylating different CDC25 phosphatases remains incompletely understood. The major role of CHK1 appears to involve phosphorylation of CDC25A after IR ([167] and references therein), whereas CHK2 appears to phosphorylate all three CDC25 family members. In the absence of CHK2, CHK1 appears to be able to subsume at least part of this function [193]. Our data now suggests that MAPKAP Kinase-2 is the primary effector kinase that targets CDC25B/C after UV-C exposure. MAPKAP Kinase-2 may also be involved in CDC25A phosphorylation, since we observed that the G1 and S-phase checkpoints were eliminated in the MAPKAP Kinase-2 knock-down cells.

Given the convergence of optimal substrate motifs for MAPKAP Kinase-2, CHK1 and CHK2, the structural similarity between the substrate-binding cleft in CHK1 and MAPKAP Kinase-2, and the functional overlap between these 3 kinases in response to DNA damage, MAPKAP Kinase-2 could equivalently be referred to as "CHK3". Whether MAPKAP Kinase-2 plays a similar critical checkpoint role in the cellular response to altered chromatin topology and

chemically-induced DNA damage as that described here in response to UV-irradiation is not known. However, recent reports that p38 MAPK participates in checkpoint activation following Topoisomerase II inhibition, adriamycin-induced double-strand breaks [120], and temozolomide-induced DNA damage mismatch-repair [163], is consistent with such a model. Experiments to test this are currently in progress. In summary, our data implicate MAPKAP Kinase-2 as a third checkpoint kinase that functions in parallel with CHK1 and CHK2 to coordinately regulate the DNA damage response.

Experimental Procedures

Protein Production and Purification

Recombinant 14-3-3ε/ζ-MBP (maltose binding protein), 14-3-3β/ζ-GST (glutathione-S-transferase) and p47phox-GST proteins were produced as described previously [21]. A vector encoding CDC25B2-GST was a gift from B. Gabrielli (University of Queensland, Australia). Point mutations were generated using the Stratagene Quick Change Mutagenesis Kit and confirmed by sequencing the entire coding regions.

Kinase Motif Screening with Oriented Peptide Libraries and In Vitro Kinase Assays

Combinatorial peptide library screening was performed using recombinant purified p38α SAPK, MK2, CHK1 and CHK2 as previously described [11] with minor modifications. Kinase reactions were performed in 30 μl of kinase reaction buffer (20 mM HEPES, pH 7.5, 10 mM $MgCl_2$, 3 mM 2-mercaptoethanol, 100 μg/ml BSA, 50 μM ATP, 10 μCi ^{32}P-γ-ATP) containing 2.0 μg of recombinant p47 or CDC25B substrate protein or the specified amount of peptide and 0.10 μg of recombinant p38α SAPK or 0.03 μg of recombinant MAPKAP Kinase-2 at 30° C for the indicated time.

Tissue Culture and Transfections

U2OS cells were maintained and propagated in DMEM supplemented with 10% fetal bovine serum (FBS), L-glutamine and penicillin/streptomycin. siRNA oligonucleotides corresponding to MAPKAP Kinase-2 sense strand 5'-UGACCAUCACCGAGUUUAUdTdT-3' and anti-sense strand 5'-AUAAACUCGGUGAUGGUCAdTdT-3' and to GFP sense strand 5'-UCCCGGCUAUGUGCAGGAGdTdT-3' and anti-sense strand 5'-CUCCUGCACAUAGCCGGGAdTdT-3' were purchased from Dharmacon. siRNAs were used according to the manufacturer's suggested protocol and transfected into cells using Lipofectamine 2000 (Gibco Invitrogen).

14-3-3 pull-down assays, Immunoblotting, and Immunofluorescence

U2OS cells were lysed in lysis buffer: 50 mM Tris/HCl, pH7.8, 150 mM NaCl, 1.0% NP-40, 5 mM EDTA, 2 mM DTT, 8 µg/mL pepstatin, 8 µg/mL aprotinin, 8 µg/mL leupeptin, 2 mM Na_3VO_4, 10 mM NaF, 1 µM microcystin for 20 min at 4°C. Clarified lysates (0.5-2mg protein) were incubated with 20 µL glutathione beads or amylose beads containing 10-20 µg 14-3-3- GST or 14-3-3-MBP, respectively, for 120 min at 4°C. Following washing, lysates and bead-bound proteins were analysed by SDS-PAGE, followed by transfer to PVDF membranes and immunoblotted with the indicated antibodies. For immunofluorescence experiments, U2OS cells were seeded onto 18mm^2

coverslips, irradiated or mock-treated, fixed, extracted, and immunostained as described previously [86].

FACS Analysis

UV irradiation was performed at 254 nm (UV-C) using a Stratalinker 2400 (Stratagene). U2OS cells were fixed in 70% ethanol overnight at –20°C, permeabilized with PBS containing 0.2% Triton X-100 for 20 min at 4°C, blocked with 2% FBS in PBS and incubated with 1 μg of anti-phospho-histone H3 per 10^6 cells for 60 min on ice. Following washing, cells were incubated with FITC-conjugated goat anti-rabbit antibody (diluted 1:500) for 30 min on ice, washed, and resuspended in PBS containing 50 μg/ml PI for 20 minutes immediately prior to FACS analysis.

For BrdU incorporation experiments, cells were incubated with 30 μM BrdU for the indicated times, then fixed and permeabilized as above. Cells were denatured in 2N HCl for 20 min at room temperature, neutralized with 0.1M $Na_2B_4O_7$ (pH 8.5), blocked with 2% FBS in PBS and incubated with a murine anti-BrdU antibody for 60 min on ice. Following washing, cells were incubated with FITC-conjugated goat anti-mouse antibodies and PI as above. Analysis was performed using a Becton Dickinson FACS machine with CellQuest software.

Structural Modeling

Activated MAPKAP Kinase-2 (phosphorylated on Thr 222) was modeled using the crystal structure of the ADP complex [190] with the activation loop

(residues 213 to 241) deleted and rebuilt using the corresponding region (residues 299 to 328) from the structure of activated Akt/PKB in complex with AMP-PNP and GSK3-peptide [191] as a template. An optimal peptide (Leu-Gln-Arg-Gln-Leu-Ser-Ile-Ala) was modeled in the active site based on the GSK3-peptide. A substrate peptide (Leu-Tyr-Arg-Ser-Pro-Ser-Met-Pro-Leu, residues 211-219 of human CDC25C) in the CHK1 active site was similarly modeled using the GSK3-peptide as a template and manually adjusted to resemble the published model [192]. Structures were superimposed using ALIGN [194] and SUPERIMPOSE [195]. Manual adjustments of the models were made using XFIT from the XtalView suite [196].

Antibodies and Reagents

Anti-MAPKAP Kinase-2, anti-phospho-MAPKAP Kinase-2 (pT344), anti-p38, anti-phospho-p38 (pT180/pY182), anti-CHK1 and anti-phospho-CHK1 (pS345), anti-CHK2 and anti-phospho-CHK2 (pT68), anti-phospho(Ser/Thr) ATM/ATR substrate antibody, and anti-phospho-p53 (pS20) antibodies were purchased from Cell Signaling. Anti-CDC25B antibody was purchased from BD Transduction Labs. Anti-p53, anti-CDC25a, and anti-CDC25C antibody were purchased from Santa Cruz. Anti-phospho-histone H3 was purchased from Upstate Biotech, Inc. Anti-5-bromo-2-deoxyuridine (BrdU) was purchased from Sigma-Aldrich, Inc. Propidium Iodide (PI) was purchased from Calbiochem, amylose beads were purchased from New England Biolabs, Ni-NTA agarose

were purchased from QIAGEN, and glutathione beads and BrdU were purchased from Sigma-Aldrich.

Purification of Recombinant Proteins

Constructs encoding GST- and MBP-fusion proteins were transformed into DH5a or BL21(DE3) strains of E. coli and recombinant proteins obtained by inducing late log phase cells with 0.4 mM IPTG at 37oC for 3–5 hr. Cells were lysed by sonication in lysis buffer containing 50 mM Tris-HCl (pH 7.5), 250 mM NaCl, 1 mM DTT, 8 µg/mL pepstatin, 8 µg/mL aprotinin, and 8 µg/mL leupeptin. Fusion proteins were purified from cell lysates by using amylose or glutathione beads. After being extensively washed with PBS containing 0.5% NP-40 and a final wash with PBS, fusion proteins were eluted from the beads with HEPES (pH 7.2), containing 40 mM maltose or 20 mM glutathione, followed by exchange into PBS using duplicate Sephadex G-25 columns (NAP-10 columns, Pharmacia). Protein concentrations were determined using the bicinchoninic acid assay (Pierce) as recommended by the manufacturer, using BSA as the standard. Full-length CHK1-GST or full-length CHK2-His6 in pFASTBAC was expressed in Sf9 insect cells. CHK1-expressing cells were lysed in buffer containing 50 mM Tris-HCl (pH 7.5), 250 mM NaCl, 1 mM DTT, 1.0% NP-40, 8 µg/mL pepstatin, 8 µg/mL aprotinin, 8 µg/mL leupeptin, 2 mM Na3VO4, 10 mM NaF, and 1 µM microcystin, and CHK1 was purified using glutathione beads. CHK1 was eluted from the beads with 10 mM glutathione in 50 mM Tris-HCl (pH 8.0) and dialyzed into kinase buffer. CHK2-expressing cells were lysed in buffer containing 50 mM

Tris-HCl (pH 7.5), 250 mM NaCl, 1 mM DTT, 1.0% NP-40, 8 µg/mL pepstatin, 8 µg/mL aprotinin, 8 µg/mL leupeptin, 2 mM Na3VO4, 10 mM NaF, and 1 µM microcystin, and CHK2 was purified using Ni-NTA agrose beads. After being washed extensively with lysis buffer containing 40 mM imidazole, CHK2 was eluted from the beads with 100 mM imidazole in 50 mM Tris-HCl (pH 8.0) and dialyzed into kinase buffer.

Kinase Motif Screening with Oriented Peptide Libraries

Combinatorial peptide library screening was performed using recombinant purified p38a SAPK, MK2, CHK1, and CHK2. Briefly, 5.0 mg of recombinant p38a SAPK, 3.0 mg MK2, 2.0 mg CHK1, and 2.0 mg CHK2 were incubated with 1 mg of each peptide library in 300 ml reaction volumes containing 20 mM HEPES (pH 7.5), 10 mM MgCl2, 3 mM 2-mercaptoethanol, and 100 mM ATP containing 2.5 mCi of 32P-g-ATP for 120 min at 30oC. Under these conditions, approximately 1% of the peptide mixture was phosphorylated. The reaction mixture was diluted by addition of 300 ml of 30% acetic acid, and the phosphorylated peptides separated from unincorporated 32P-g-ATP by DEAE column chromatography (1 ml bed volume) by using isocratic elution with 30% acetic acid. The peptide mixture (both phosphorylated and unphosphorylated but free of ATP) eluted within the first 1 ml following the 600 ml void volume of the column. Samples were dried in a Speed-Vac apparatus.

For the p38a SAPK peptide library experiments, the sample was resuspended in 200 ml of 50 mM MES (pH 5.5) containing 1 M NaCl. Separation

of phosphorylated from nonphosphorylated peptides was achieved by IMAC using ferric-iminodiacetic acid beads. A 0.5 ml iminodiacetic acid column was charged with 2.5 ml of 20 mM FeCl3 and extensively washed with H2O and then with 3 ml of 500 mM NH4HCO3 (pH 8.0), 3 ml of H2O, and 3 ml of 50 mM MES (pH 5.5)/1 M NaCl. The peptide mixture was applied, and the column was developed with 3 ml 50 mM MES (pH 5.5) and 1 M NaCl followed by 4 ml of H2O to remove nonphosphorylated peptides. Phosphorylated peptides were then eluted with 2 ml of 500 mM NH4HCO3 (pH 8.0) and dried in a Speed-Vac apparatus and resuspended in 80 ml H2O.

Peptide library screens using basophilic kinase-directed libraries are complicated by a high background of nonphosphorylated Asp/Glu-rich peptides that copurified with the phosphorylated peptides during the immobilized metal affinity chromatography (IMAC) step prior to peptide sequencing, greatly complicating the analysis. To overcome this problem, we developed a new approach in which peptide libraries are first phosphorylated by the kinase of interest and then treated with methanolic HCl to convert Asp and Glu residues to their uncharged methyl esters. With this approach, the background of nonphosphorylated peptides that adhere to the IMAC column was reduced to insignificant levels. Furthermore, the Asp and Glu methyl esters were converted back to their free acids during the sequencing reaction, allowing selection for these residues, if present in the phosphorylation motif, to be accurately measured.

For the MAPKAP Kinase-2, CHK1, and CHK2 peptide library experiments, 40 ml of thionyl chloride was added drop wise in a hood to 1 ml of dry methanol. This solution was then used to dissolve each of the dried peptide libraries followed by stirring at room temperature for 1 hr. The peptide library was dried down overnight and resuspended in 100 ml of a 1:1:1 mixture of methanol/acetonitrile/water. A 0.5 ml iminodiacetic acid column was charged with 2.5 ml of 20 mM FeCl3 and extensively washed with H2O and then with 3 ml of 500 mM NH4HCO3 (pH 8.0), 3 ml H2O, and 3 ml of 50 mM MES (pH 5.5) and 1 M NaCl. The peptide mixture was applied, and the column was developed with 4 ml of H2O followed by 3 ml NH4HCO3 (pH 8.0) to remove nonphosphorylated peptides. Phosphorylated peptides were eluted with 2 ml of 500 mM NH4HCO3 (pH 11.0), dried in a Speed-Vac apparatus, and resuspended in 40–80 ml H2O.

After IMAC purification, libraries (0.5–1.5 nmol) were subjected to automated Edman sequencing using an Applied Biosystems model 477A peptide sequencer. Data analysis was performed by normalizing the abundance (mol%) of each amino acid in the phosphorylated peptide mixture to that present in the starting libraries. The sums of the final preference ratios were normalized to the total number of amino acids in the degenerate positions within the peptide libraries so that a particular amino acid would have a preference value of one in the absence of selectivity at a particular position. The degenerate peptide libraries used for in vitro kinase screening with p38 MAP kinase, MK2, CHK1, and CHK2 consisted of the sequences Gly-Ala-X-X-X-X-S-P-X-X-X-X-Ala-Lys-Lys-Lys [SP library] where X denotes all amino acids except Cys, Ser, Thr, and

Tyr; Gly-Ala-X-X-X-X-P-X-S-P-X-X-X-X-X-Ala-Lys-Lys-Lys [PxSP library] where X denotes all amino acids except Cys; or Gly-Ala-X-X-X-X-R-X-X-S-X-X-X-X-Ala-Lys-Lys-Lys [RxxS library] where X denotes all amino acids except Cys, Ser, Thr, and Tyr. In all libraries, S denotes Ser, P denotes Pro, and R denotes Arg.

Kinase reactions were performed in 30 ml of kinase reaction buffer (20 mM HEPES [pH 7.5], 10 mM MgCl2, 3 mM 2-mercaptoethanol, 100 mg/ml BSA, 50 mM ATP, and 10 mCi 32P-g-ATP) containing 2.0 μg of recombinant p47 or CDC25B substrate protein or the specified amount of peptide and 0.10 mg of recombinant p38a SAPK or 0.03 mg of recombinant MAPKAP Kinase-2 at 30oC for the indicated time. The sequences of the p38 optimal peptide and the p47phox peptide were KKAZGPQGPQSPIE and KKAZGPQSPGSPLE, respectively. For 14-3-3 pull-downs of CDC25B after in vitro phosphorylation by p38 or MAPKAP Kinase-2, 2.0 mg of CDC25B was incubated with 10-fold excess 14-3-3-MBP and analyzed by autoradiography. For kinetic measurements, the reactions were terminated by the addition of an equal volume of 0.5 percent phosphoric acid and 5 ml was spotted onto p81 paper. The p81 paper was washed 5′ in 0.5 percent phosphoric acid and added to scintillation fluid for scintillation counting. For in vitro phosphorylation reactions, the reactions were terminated by the addition of an equal volume of sample buffer followed by heating at 95oC for 3 min. Samples were analyzed by SDS-PAGE followed by transfer to nitrocellulose for autoradiography and immunoblotting. The rate of p38a phosphorylation of isolated peptides and full-length p47phox proteins was determined by scintillation counting with peptide concentrations of 100, 400, and

1400 μM and protein concentrations of 1, 5, 10, and 15 μM with time points taken at 5, 10, and 20 minutes. MAPKAP Kinase-2 phosphorylation of MK2tides was performed with peptide concentrations of 5, 10, 20, 40, 80, 160, 320, 500, and 1000 μM with time points taken at 3, 6, 9, and 12 min. From these enzymatic studies, Km, Vmax, and Vmax/Km values were then ascertained. All kinetic experiments were performed a minimum of three times. For each experimental condition in the determination of the Km and Vmax values, we verified that the reaction rates were linear with respect to time for all substrate concentrations and that less than 10% substrate was phosphorylated.

Figures

Figure 2.1. Substrate specificity and kinetic analysis of substrate phosphorylation by p38α SAPK.

(A) p38 substrate specificity determined using oriented peptide library screening.

Residues displaying the highest selectivity are shown; those with selection values > 1.7 in bold. MEF2A, Myocyte Enhancer Factor 2; ATF2, Activating Transcription Factor 2; 3PK1, MAP Kinase-activated Protein Kinase-3.

(B) Kinetics of *in vitro* phosphorylation of an optimal p38 peptide (p38tide) and a peptide from p47phox (p47tide) by p38α kinase.

(C) Kinetics of *in vitro* phosphorylation of wild-type GST-p47phox, the Ser-345→Ala mutant, and the Ser-348→Ala mutant. Typical data from n=3 experiments is shown.

(D) *In vitro* phosphorylation of full-length wild-type or mutant p47phox proteins. Samples were analyzed by SDS-PAGE/autoradiography.

(E) Table of kinetic parameters for the reactions in panel C.

Figure 2.1 Continued.

A

p38a MAP Kinase Phosphorylation Motif

	-3	-2	-1	S	P	+2
SP library	M (1.6) F (1.5) Q (1.5) N (1.4)	**P (2.1)** M (1.7) L (1.5) V (1.5) I (1.5)	**M (1.9)** L (1.6) Q (1.5)	↓	↓	P (1.7) V (1.4) I (1.3)

	-3	P	-1	S	P	+2
PxSP library	**G (2.1)** I (1.5) V (1.5) Y (1.4)	↓	**Q (1.9)** M (1.8) G (1.7) P (1.4) S (1.3) T (1.3)	↓	↓	**I (1.8)** W (1.7) Y (1.7) T (1.6) V (1.6)

Comparison of p38 MAP Kinase Substrates

Substrate	-3	-2	-1	S/T	P	+2
3PK1 (T313)	V	P	Q			L
3PK1 (T201)	A	L	Q			C
MAPKAP2 (T334)	V	P	Q			L
MAPKAP2 (S272)	L	A	I			G
MAPKAP2 (T222)	S	L	T			C
MAPKAP2 (T25)	Q	P	P			A
GADD153 (S78)	T	S	Q			R
GADD153 (S81)	S	P	R			D
MEF2A (T312)	P	L	A			V
MEF2A (T319)	S	V	T			S
ATF2 (T51)	A	D	Q			T
ATF2 (T53)	Q	T	P			T
p47*phox* (S345)	G	P	Q			G
p47*phox* (S348)	S	P	G			L

B

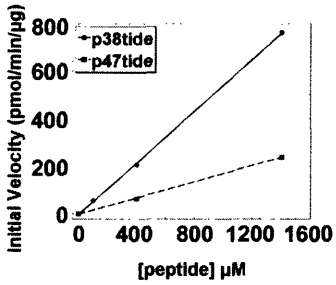

C

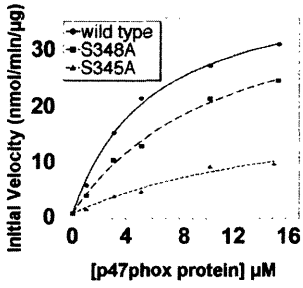

D

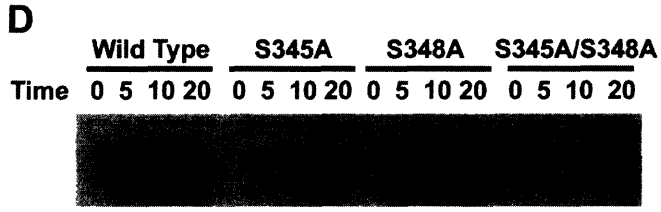

E

p47phox	K_m (µM)	V_{max}(nmol/min/µg)	V_{max}/K_m
Wild Type	6.0±1.8	36.6±2.5	6.1±2.2
S348A	8.3±2	36.8±0.3	4.4±1.1
S345A	10.7±0.7	17.3±4.4	1.6±0.5

Figure 2.2. Involvement of MAPKAP Kinase-2 in the phosphorylation of CDC25B and CDC25C after DNA damage.

(A) Phosphorylation of full-length wild type CDC25B or a Ser-323→Ala mutant by p38α SAPK or MAPKAP Kinase-2. After phosphorylation, generation of a 14-3-3 binding site on CDC25B was determined by a 14-3-3-MBP pulldown followed by SDS-PAGE/autoradiography.

(B) Kinetics of MAPKAP Kinase-2 phosphorylation and generation of a 14-3-3-binding site on CDC25B were measured in U2OS cells following 20 J/m^2 UV-irradiation.

(C) Signaling events in the G2/M, G1, and S-phase checkpoint response were analyzed in GFP siRNA- or MAPKAP Kinase-2 siRNA-treated U2OS cells before and 2 hrs after UV-induced DNA damage. Equal loading was determined by western blotting for β-actin.

Figure 2.2 Continued.

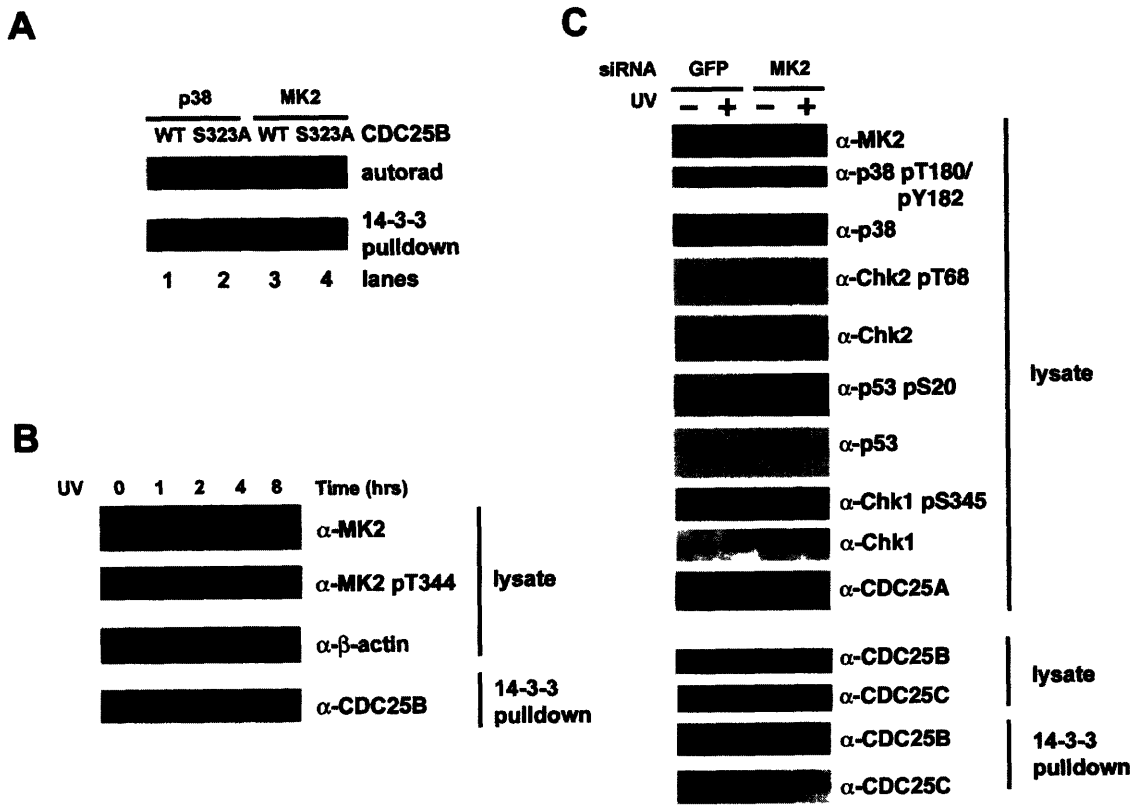

Figure 2.3. Substrate specificity and kinetic analysis of substrate phosphorylation by MAPKAP Kinase-2.

(A) MAPKAP Kinase-2 substrate specificity was determined by oriented peptide library screeing. HSP27, Heat Shock protein 27; 5-LO, 5-Lipoxygenase; LSP1, Lymphocyte-specific protein; SRF, Serum Response Factor; GS, Glycogen Synthase; TH, Tyrosine Hydroxylase.

(B) Kinetics of *in vitro* phosphorylation of the optimal MAPKAP Kinase-2 peptide (MK2tide) by MAPKAP Kinase-2.

(C) Table of kinetic parameters for MAPKAP Kinase-2 phosphorylation of wild-type and mutant MK2tides.

Figure 2.3 Continued.

A

MAPKAP Kinase-2 Phosphorylation Motif

	-5	-4	R	-2	-1	S	+1
RxxS library	L (2.5) F (1.9) I (1.6) V (1.3)	Q (1.3) A (1.2) M (1.2)	↓	Q (2.6) M (1.3)	L (1.6) N (1.3)	↓	I (1.8) V (1.7) F (1.4) L (1.3)

Comparisoh of MK2 Kinase Substrates

Substrate	-5	-4	R	-2	-1	S	+1
HSP-27 (82)	L	S		Q	L		S
5-LO (271)	L	E		Q	L		L
LSP1 (204)	I	D		T	E		L
LSP1 (252)	L	A		Q	A		I
SRF (103)	L	K		T	L		E
GS (7)	L	N		S	L		V
TH (19)	F	R		A	V		E
CDC25B (309)	L	F		S	P		M
CDC25C (216)	L	Y	↓	S	P	↓	M

B

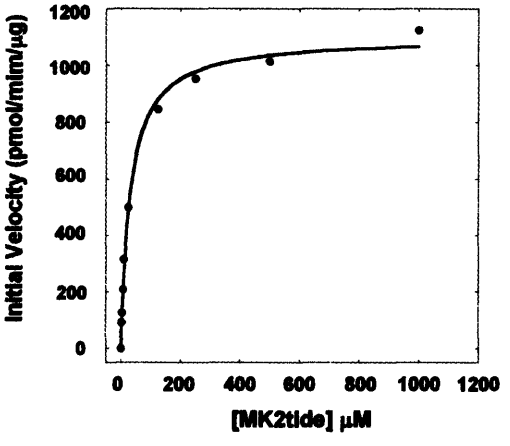

C

Optimal MK2tide

	-5	-4	-3	-2	-1	0	+1	Motif Position
1	2	3	4	5	6	7	8	9	10	11	12
Ala	His	Leu	Gln	Arg	Gln	Leu	Ser	Ile	Ala	His	His

Peptide	$Km_{\mu M}$	V_{max} (pmol/min/µg)	V_{max}/Km
MK2tide	31	1098	35
L3Atide	29	463	16
Q4Atide	41	1209	29
R5Atide	310	282	<1
Q6Atide	51	1058	21
L7Atide	35	955	27
I9Atide	43	627	15

Figure 2.4. MAPKAP Kinase-2 is required for G2/M arrest following DNA damage.

(A) UV-C irradiation induces DNA damage as revealed by nuclear foci formation. U2OS cells were mock irradiated or exposed to 20 J/m^2 of UV-C radiation and immunostained 2 hr later using an anti-phospho(Ser/Thr) ATM/ATR substrate antibody.

(B-I) GFP siRNA- or MAPKAP Kinase-2-siRNA-treated U2OS cells were irradiated as in panel A, then placed in 50ng/ml nocodazole-containing media for an additional 16 hours. Cells were analyzed by FACS for DNA content by PI staining (panels **B, D, F and H**) and for phospho-histone H3 staining as a marker of mitotic entry (panels **C, E, G, and I**).

(J-K) GFP siRNA- or MAPKAP Kinase-2-siRNA treated U2OS cells were either mock treated, exposed to 20 J/m^2 of UV-C irradiation **(J)**, or to 10 Gy of ionizing radiation **(K)** and analyzed as in panels **B-I**. Representative results of each experiment are shown.

Figure 2.4 Continued.

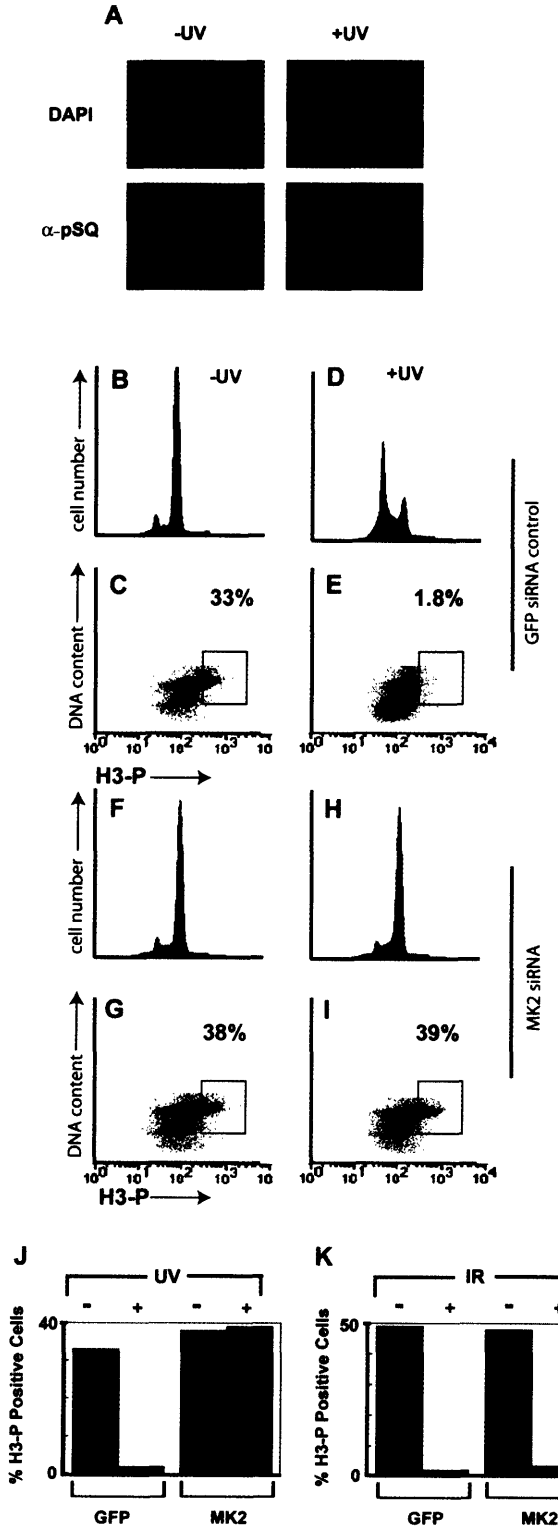

Figure 2.5. MAPKAP Kinase-2 is required for S-phase arrest and cell survival following DNA damage.

(A) GFP siRNA- or MAPKAP Kinase-2-siRNA treated U2OS cells were mock treated or UV-irradiated and allowed to recover for 30 min. BrdU was added and cells were fixed and analyzed by FACS for DNA content and BrdU-incorporation 12 hr later.

(B) Percentage of cells in panel **A** showing BrdU incorporation at 2 and 12 hr following BrdU addition were measured.

(C) GFP siRNA- or MAPKAP Kinase-2-siRNA treated U2OS cells were either mock treated or UV-irradiated, allowed to recover for 30 min, then pulse-labeled with BrdU for 30 minutes. At the indicated times after irradiation the distribution of DNA content analyzed in the BrdU-positive population.

(D) GFP siRNA- or MAPKAP Kinase-2-siRNA treated U2OS cells were either mock-treated or irradiated at the indicated UV-C dose. Cells were stained with Crystal Violet 48 hr later and visualized. Insets show a magnified view.

(E) Quantitative colony forming assays were performed by plating cells at a density of ~100 cells per 35 mm^2 dish. Cells were treated as in panel **D**, and assays performed in triplicate for each condition.

Figure 2.5 Continued.

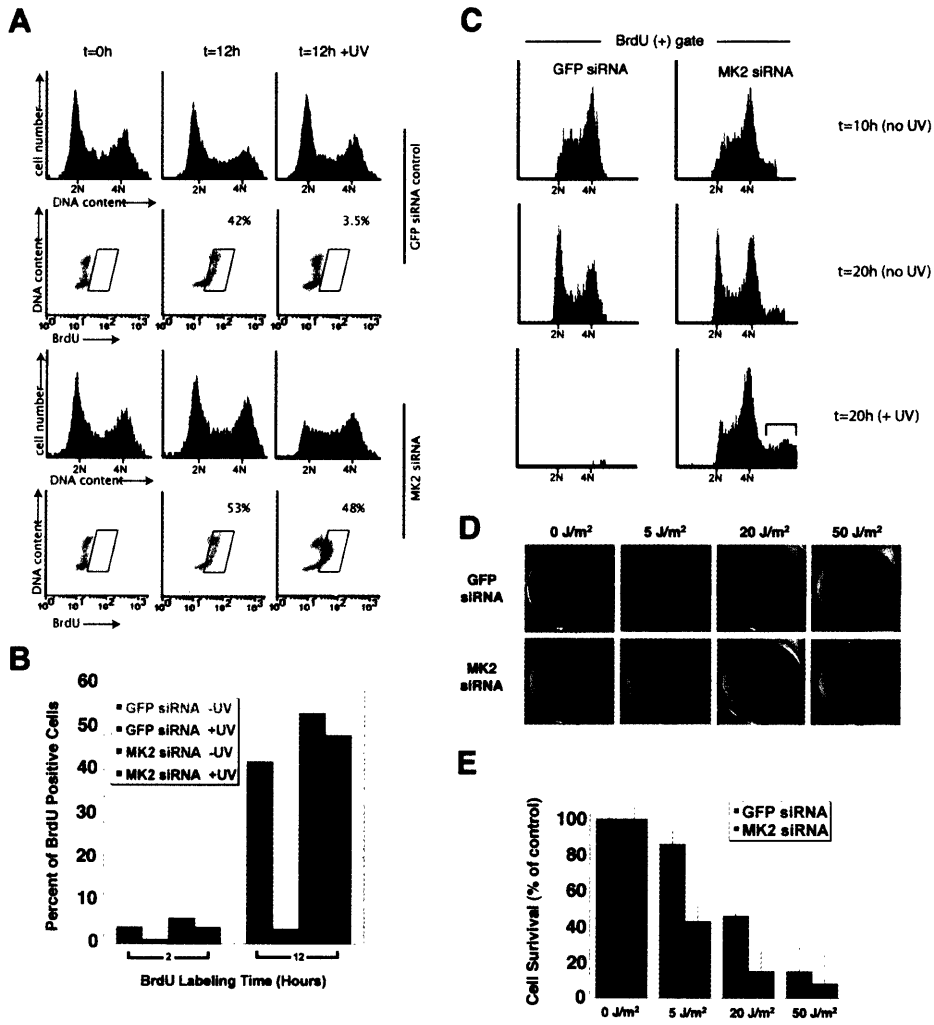

Figure 2.6. Comparison of active site electrostatic potentials and hydrophobicity for the substrate binding cleft of MAPKAP Kinase-2, Akt and CHK1.

(A) Optimal substrate phosphorylation motifs for Akt/PKB, CHK1, CHK2 and MAPKAP Kinase-2.

(B) Ribbons representation of the MAPKAP Kinase-2 kinase domain in a similar orientation as that shown in panels **C** through **E** (upper), and in an orthogonal orientation (lower) with stick representations of the substrate peptide in the active site cleft. Figure created using Molscript [197] and Raster3D [198].

(C) Molecular surface representations of the Akt/PKB active site (PDB code 1O6K) using GRASP [199]. Electrostatic potentials (left) are colored red (negative) and blue (positive). Hydrophobicity (right) is shaded grey, yellow and green for low, medium and high hydrophobic potentials, respectively. The GSK3 substrate peptide Gly-Arg-Pro-Arg-Thr-Thr-**Ser**-Phe-Ala-Glu, with the phospho-acceptor indicated in bold and underlined, is shown in stick representation.

(D) Molecular surface representations of the MAPKAP Kinase-2 active site (PDB code 1NY3). Electrostatic and hydrophobic potentials are colored as in **C**. The optimal substrate peptide Leu-Gln-Arg-Gln-Leu-**Ser**-Ile-Ala is shown in stick representation.

(E) Molecular surface representations of the CHK1 active site (PDB code 1IA8). Electrostatic and hydrophobic potentials are colored as in **C**. Stick representation of the modeled CDC25C substrate peptide (Leu-Tyr-Arg-Ser-Pro-**Ser**-Met-Pro-Leu) is shown. The region corresponding to the Ser-5, Ser-3 and

Ser+1 positions of the substrate peptides in panels **C**, **D** and **E** is indicated by dashed circles.

Figure 2.6 Continued.

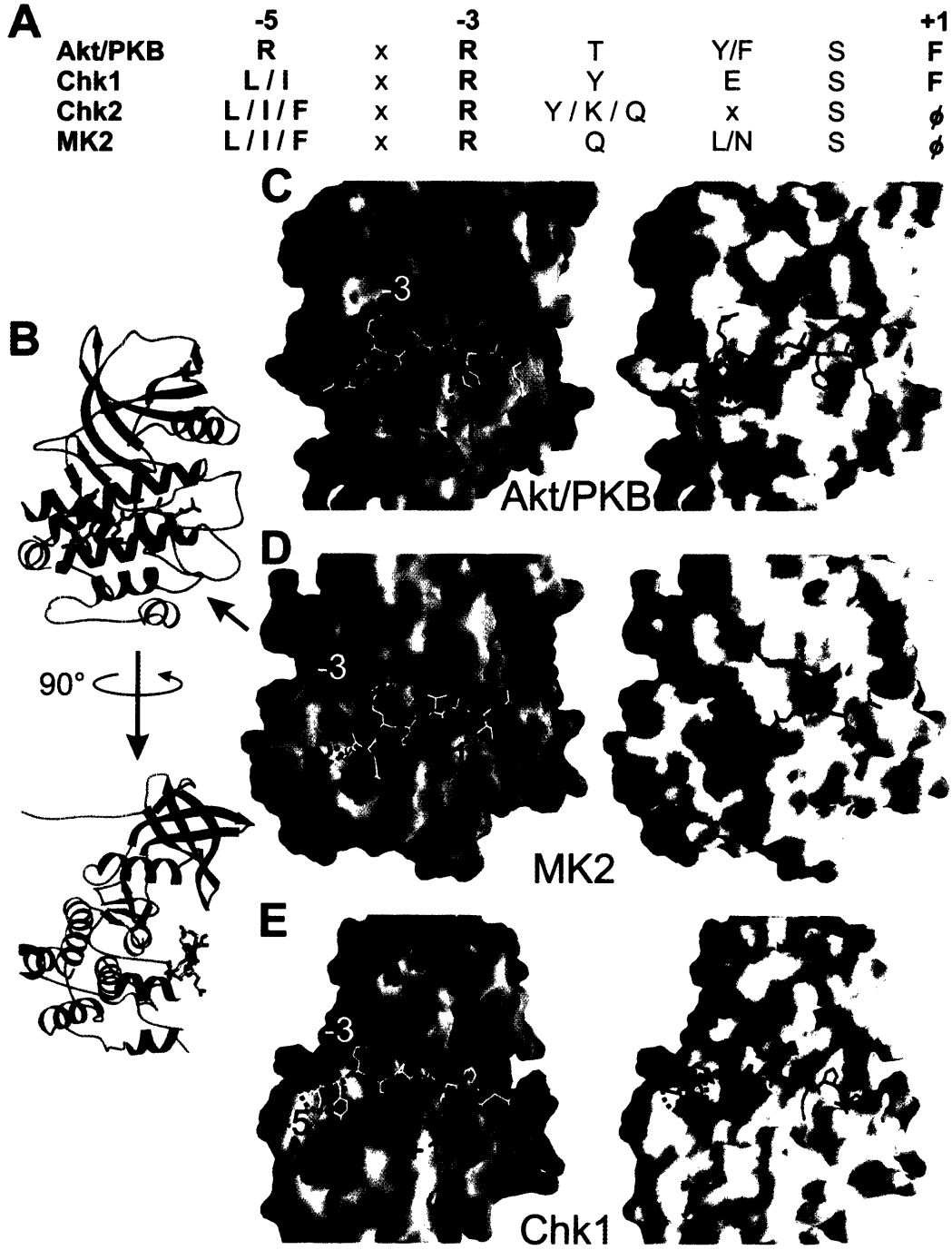

Figure 2.7. A unified model of the kinase-dependent DNA damage checkpoint.

Parallel pathways in the DNA damage checkpoint signal transduction network converge on common substrates by signaling to downstream kinases with similar phosphorylation motif specificities. ϕ indicates hydrophobic residues. The dashed line from CHK1 to CDC25B/C indicates that this phosphorylation event remains controversial in response to ionizing radiation.

Figure 2.7 Continued.

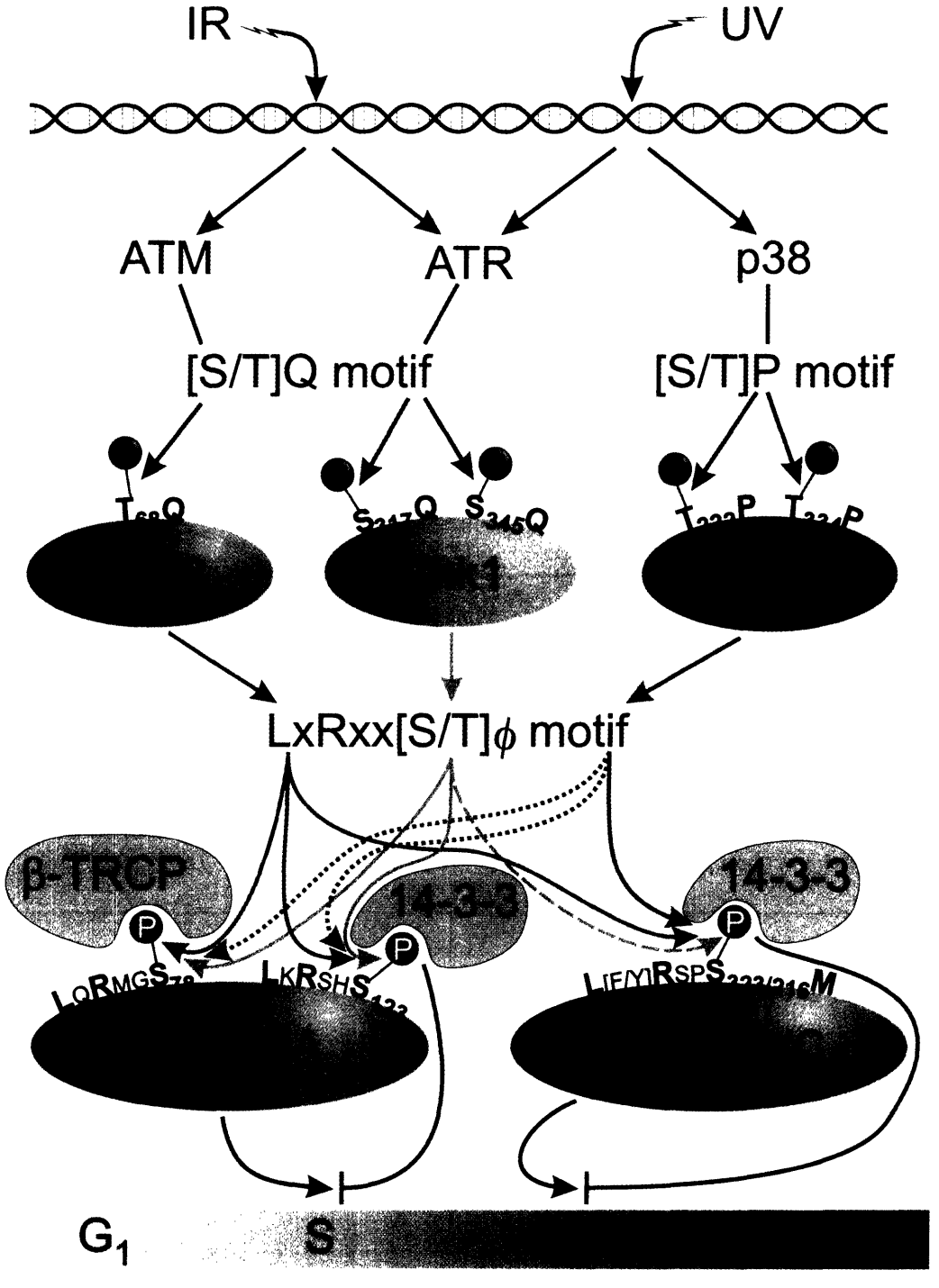

Chapter 3

BRCT Repeats as Phosphopeptide-Binding Modules Involved in Protein Targeting

Summary

We used a proteomic approach to identify phosphopeptide-binding modules mediating signal transduction events in the DNA damage response pathway. Using a library of partially degenerate phosphopeptides, we identified tandem BRCA1 carboxy-terminal (BRCT) domains in Pax transactivation domain-interacting protein (PTIP) and BRCA1 as phosphoserine (pSer)- or phosphothreonine (pThr)-specific binding modules that recognize a subset of substrates phosphorylated by the kinases ataxia-telangiectasia mutated (ATM) and ataxia-telangiectasia- and RAD3-related (ATR), in response to γ-irradiation. PTIP tandem BRCT domains are responsible for phosphorylation-dependent protein localization into 53BP1- and phospho-H2AX (γ-H2AX)-containing nuclear foci, a marker of DNA damage. These findings provide a molecular basis for BRCT domain function in the DNA damage response and may rationalize why the BRCA1 BRCT domain mutation M1775R, which fails to bind phosphopeptides, predisposes patients to breast and ovarian cancer.

Contributions:

Andy Elia initially adapted the small pool IVT screening process, developed in other labs, to identify phospho-binding domains. Katja Hoepker helped with the implementation and screening of the 96,000 clone library that led to the identification of PTIP in Figure 3.1. Bob Grant helped with BRCT domain protein purification for ITC analysis. Mike Yaffe assisted with the ITC analysis. Timmy Ho helped with BRCT domain protein production and figure 3.1/3.2/3.3 construction. Ancho Nguyen helped with the localization data shown in Figure 3.5/3.6. Drew Lowery cloned several of the constructs, helped with DNA purification and westernblot analysis.

Introduction

Signal transduction by protein kinases in eukaryotes results in the directed assembly of multi-protein complexes at specific locations within the cell [7]. This process is particularly evident following DNA damage, where activation of DNA damage response kinases results in the formation of protein-protein complexes at discrete foci within the nucleus [46]. In many cases, protein kinases directly control the formation of these multi-protein complexes by generating specific phosphorylated-motif sequences; modular binding domains then recognize these short phospho-motifs to mediate protein-protein interactions [15, 17].

Results

Identification of pSer- or pThr-binding domains

We used a proteomic screening approach [18] to identify novel modular pSer- or pThr-binding domains involved in the DNA damage response. In cells exposed to IR, the kinases ATM and ATR phosphorylate transcription factors, DNA repair proteins, protein kinases, and scaffolds on Ser-Gln and Thr-Gln motifs [2]. We therefore constructed an oriented phosphopeptide library biased to resemble the motif generated by ATM and ATR [89, 200] (Figure 3.1A). This library and its non-phosphorylated counterpart were immobilized and screened in a high-throughput multi-well format against ~96,000 in vitro translated (IVT) polypeptides (960 pools each containing ~100 transcripts) (Figure 3.1A).

Pool EE11 contained the strongest phosphopeptide-binding clone, EE11-9, encoding the C-terminal 70% of human PTIP (Figure 3.1B). PTIP, originally identified as a transcriptional regulatory protein, appears to also play a critical role in the DNA damage response pathway [201-203]. Human PTIP contains 4 BRCT domains, known protein-protein interaction modules present in many DNA damage response and cell cycle checkpoint proteins [204]. A construct containing only the tandem 3rd and 4th BRCT domains displayed strong and specific binding to the (pSer or pThr)-Gln library (Figure 3.1B). Constructs of PTIP lacking both of these domains either failed to bind or lacked phosphopeptide discrimination. Furthermore, neither the 3rd nor the 4th BRCT domain alone bound to phosphopeptides, suggesting that the tandem C-terminal

BRCT domains function as a single module that is necessary and sufficient for phospho-specific binding.

The optimal phosphopeptide binding motif of BRCT Domains

BRCT domains are often found in tandem pairs, $((BRCT)_2)$, or multiple copies of tandem pairs, and the tandem BRCA1 BRCT domains behave as a single stable fragment in limited proteolysis and X-ray crystallographic studies [84]. Like those of PTIP, the tandem BRCT domains of BRCA1, but not the individual BRCT domains alone, displayed phospho-specific binding (Figure 3.2A). However, little if any phospho-binding was seen for $(BRCT)_2$ modules from MDC1, 53BP1, *S. cerevisiae* Rad9p, or the PTIP N-terminal pair, suggesting that the phosphopeptide-binding function is present in only a subset of tandem BRCT domains.

We used oriented peptide library screening to determine the optimal phospho-binding motifs for the C-terminal $(BRCT)_2$ domains of PTIP and BRCA1 (Figure 3.2B and Table 3.1). PTIP- and BRCA1-$(BRCT)_2$ displayed strongest binding to similar, but not identical, motifs with extremely strong selection for either aromatic or aliphatic residues, and aromatic residues, respectively, in the (pSer or pThr)+3 position. More moderate selection was also observed at other positions, particularly (pSer or pThr)+2 and +5. We defined an optimal $(BRCT)_2$-binding peptide (BRCTide) as Y-D-I-(pSer or pThr)-Q-V-F-P-F and verified motif data using a solid-phase array of immobilized phosphopeptides (Figure 3.3). In the filter-array experiments (Figure 3.3), substitution of pSer for pThr enhanced

binding for both PTIP and BRCA1 BRCT domains, consistent with the ITC results. $(BRCT)_2$ domains are unusual in binding to pSer-containing peptides more strongly than to pThr-containing peptides since 14-3-3 proteins, WW domains, WD40 domains, FHA domains and Polobox domains either bind pThr-peptides better than pSer-peptides, or do not bind to pSer-peptides at all [4]. Substitution of pTyr for pThr eliminated binding altogether, verifying that tandem BRCT domains are pSer/pThr-specific binding modules. Replacement of pThr with Thr, Ser or Tyr abrogated tandem BRCT domain binding. The pTQ oriented blots on the left show strong selection at several positions for both PTIP and BRCA1 BRCT domains; especially for Phe in the +3 position in agreement with the oriented peptide library screening data. The pS oriented blots on the right show that the +3 position is the most important position for peptide selection.

Isothermal titration calorimetry showed that the optimal pSer-containing peptide bound to the C-terminal $(BRCT)_2$ of PTIP with a dissociation constant of 280 nM, and to the $(BRCT)_2$ of BRCA1 with a dissociation constant of 400 nM (Table 3.2). Replacement of pThr for pSer reduced the affinity of the peptide for the PTIP-$(BRCT)_2$ though binding was still observed. Interestingly, ATM and ATR prefer SQ to TQ motifs for phosphorylation suggesting a convergence of the kinase phosphorylation motif and tandem BRCT domain binding motif. Substitution of pTyr, Ser or Thr for pSer abrogated binding verifying that $(BRCT)_2$ modules are pSer- or pThr-specific (Figure 3.3).

BRCT Domains interact with phosphoproteins after DNA damage

After treatment of U2OS cells with 10 Gy of IR, both PTIP- and BRCA1-$(BRCT)_2$ bound distinct phospho-proteins, as detected by immunoblotting with a phospho-specific antibody against the (pSer or pThr)-Gln motif generated by ATM and ATR (Figure 3.3A, B, D). Binding to $(BRCT)_2$ was inhibited by incubation with specific phosphopeptides but not by non-phosphorylated peptides. Pretreatment of the cells with caffeine to inhibit the activity of ATM and ATR prior to irradiation also largely eliminated binding [205].

In response to IR, the DNA damage protein 53BP1 undergoes multi-site phosphorylation by ATM and forms nuclear foci [87, 88, 206]. 53BP1 bound to the C-terminal PTIP-$(BRCT)_2$ only after IR, in a phosphorylation-dependent manner (Figure 3.3C). In addition, in vivo association of full-length FLAG-PTIP with HA-53BP1 increased after IR treatment.

BRCT Domains are responsible for PITP localization after IR

The binding of tandem BRCT domains to ATM- or ATR-phosphorylated substrates could localize PTIP to sites of DNA damage in vivo. In the absence of DNA damage, GFP-PTIP was diffusely nuclear with a small amount of cytosolic staining (Figure 3.4). Two hours after IR, PTIP localized into discrete nuclear foci with (pSer or pThr)-Gln phosphoepitopes, 53BP1 and γ-H2AX (Figure 3.4A). PTIP lacking the C-terminal $(BRCT)_2$ did not form foci (Figure 3.4B). The isolated C-terminal $(BRCT)_2$, however, while diffusely nuclear in the absence of DNA damage, re-localized into these nuclear foci after IR (Figure

3.4C). Inhibition of ATM and ATR by caffeine prior to IR reduced the number and altered the appearance of full-length PTIP foci, and caused loss of co-localization with γ-H2AX (Figure 3.7).

Discussion

These findings strongly suggest that PTIP functions as a key component of the DNA damage response network and may provide a molecular rationale for the early embryonic lethality of PTIP knock-out mice with extensive unrepaired DNA ends [202]. $(BRCT)_2$ selection for aromatic and aliphatic residues in the (pSer or pThr)+3 positions exceeds their selection for Gln in the +1 position. Thus, only a subset of ATM and ATR phosphorylated substrates are likely to bind with high affinity, and other kinases might also generate $(BRCT)_2$-binding motifs. The important role for $(BRCT)_2$ domains as pSer- or pThr-binding modules is emphasized by the finding that ~80% of germline mutations in BRCA1 result in C-terminal truncations involving the BRCT region, predisposing patients to breast and ovarian cancer [204]. Interestingly, a BRCA1 cancer associated mutation in the $(BRCT)_2$ module that ablates critical BRCA1 protein interactions [51], M1775R, fails to bind phosphopeptides (Figure 3.2A), despite the fact the M1775R crystal structure is nearly identical to that of the wild-type $(BRCT)_2$ [85]. Since interference with DNA damage signaling results in both tumorigenesis, and presumably tumor cell death in the face of massive DNA damage by chemotherapeutic agents, the phosphopeptide-binding pocket of $(BRCT)_2$ modules may constitute a target for anti-cancer drug development.

Experimental Procedures

ATM/ATR Phospho-Motif Screen for Phosphoserine/threonine Binding Domains

An oriented (pSer/pThr) phosphopeptide library biased toward the phosphorylation motifs for ATM/ATR kinases, and its non-phosphorylated counterpart were constructed as follows: biotin-Z-Gly-Z-Gly-Gly-Ala-X-X-X-B-(pS/pT)-Gln-J-X-X-X-Ala-Lys-Lys-Lys and biotin-Z-Gly-Z-Gly-Gly-Ala-X-X-X-B-(Ser/Thr)-Gln-J-X-X-X-Ala-Lys-Lys-Lys where pS denotes phosphoserine, pT phosphothreonine, Z indicates aminohexanoic acid , B represents a biased mixture of the amino acids (Ala, Ile, Leu, Met, Asn, Pro, Ser, Thr, Val) and J represents a biased mixture of (25% Glu, 75% X), where X denotes all amino acids except (Cys, Arg, Lys, His). The amino acids Arg, Lys, and His were intentionally omitted from the degenerate positions in the peptide library to decrease the likelihood of identifying phosphopeptide-binding domains such as 14-3-3 which target basophilic motifs generated by kinases such as AKT, PKA, and PKCs. Streptavidin beads (Pierce, 75pmol/μL gel) were incubated with a ten-fold molar excess of each biotinylated library in 50 mM Tris/HCl (pH7.6), 150 mM NaCl, 0.5% NP-40, 1 mM EDTA, 2 mM DTT and washed five times with the same buffer to remove unbound peptide. The bead-immobilized libraries (10μL of gel) were added to 10 μL of an in vitro translated [^{35}S]-labeled protein pool in 150 μL binding buffer (50 mM Tris/HCl (pH7.6), 150 mM NaCl, 0.5% NP-40, 1 mM EDTA, 2 mM DTT, 8 μg/mL pepstatin, 8 μg/mL aprotinin, 8 μg/mL leupeptin, 800 μM Na_3VO_4, 25 mM NaF). Each pool consisted of ~100 radiolabeled proteins

produced by the ProteoLink in vitro expression cloning system (Promega). After incubation at 4°C for 3 hours, the beads were washed three times 200 µL with binding buffer prior to SDS-PAGE (12.5%) and autoradiography. Positively scoring hits were identified as protein bands that interacted more strongly with the phosphorylated immobilized library than with the unphosphorylated counterpart. Pools containing positively scoring clones were progressively subdivided and re-screened for phospho-binding until single clones were isolated and identified by DNA sequencing.

Cloning, Expression, and Purification of PTIP and BRCA1

For deletion mapping of the PTIP and BRCA1 BRCT phospho-binding region and for expression of MDC1, Rad9, and 53BP1 (Figure 3.1-2), fragments were generated by PCR, cloned into pcDNA3.1 (Invitrogen), and subjected to in vitro transcription and translation. The BRCA1 BRCT M1775R mutation was generated using the Stratagene Quick Change Mutagenesis Kit. For production of recombinant GST-PTIP BRCT domains and GST-BRCA1 BRCT domains, residues 550-757 of PTIP and residues 1634-1863 of BRCA1 were ligated into the EcoRI and Not1 sites of pGEX-4T1 (Pharmacia) and subsequently transformed into DH5α *E. Coli.* Protein induction occurred at 37°C for 4 hrs or at 25°C for 16 hrs in the presence of 0.2-0.4 mM IPTG. GST-PTIP BRCT domains and GST-BRCA1 BRCT domains were isolated from bacterial lysates using glutathione agarose, eluted with 40mM glutathione/50mM Tris/HCl (pH 8.1), and dialyzed into 50mM Tris/HCl (pH 8.1)/300mM NaCl. For ITC experiments,

purified GST-PTIP BRCT domains were dialyzed into cleavage buffer (25mM Tris-HCl, 100mM NaCl, 2mM $CaCl_2$), and cleaved in solution with thrombin (Sigma). Free GST was removed by incubation with glutathione agarose and the PTIP BRCT domains were further purified on a mono-Q column and eluted with a NaCl gradient. The appropriate fractions were dialyzed into 25mM Tris/HCl (pH 8.1), 100mM NaCl. The GFP-PTIP constructs FL (residues 1-757), ΔBRCT (residues 1-549), or $(BRCT)_2$ (residues 550-757) were cloned into the EcoRI and Sal1 sites of pEGFP-C2 (Clontech). All plasmid insert sequences were verified by sequencing.

Peptide Library Screening

Phosphoserine and phosphothreonine oriented degenerate peptide libraries consisting of the sequences Gly-Ala-X-X-X-B-(pS/pT)-Gln-J-X-X-X-Ala-Lys-Lys-Lys, Met-Ala-X-X-X-X-pThr-X-X-X-X-Ala-Lys-Lys-Lys, Met-Ala-X-X-X-X-pSer-X-X-X-X-X-Ala-Lys-Lys-Lys, and Gly-Ala-X-X-X-X-pSer-X-X-Phe-X-X-Ala-Tyr-Lys-Lys-Lys, where X denotes all amino acids except Cys. In the (pS/pT)-Gln library pS denotes phosphoserine, pT phosphothreonine, B represents a biased mixture of the amino acids (Ala, Ile, Leu, Met, Asn, Pro, Ser, Thr, Val) and J represents a biased mixture of (25% Glu, 75% X), where X denotes all amino acids except (Cys, Arg, Lys, His). Peptides were synthesized using N-α-FMOC-protected amino acids and standard BOP/HOBt coupling chemistry. Peptide library screening was performed using 125-250 μl of glutathione beads containing saturating amounts of GST-PTIP BRCT or GST-BRCA1 BRCT

domains (1-1.5 mg) (Figure 3.3). Beads were packed in a 1mL column and incubated with 0.45 mg of the peptide library mixture for 10 min at room temperature in PBS (150 mM NaCl, 3 mM KCl, 10 mM Na_2HPO_4, 2 mm KH_2PO_4, pH 7.6). Unbound peptides were removed from the column by three washes with PBS containing 1.0% NP-40 followed by three washes with PBS. Bound peptides were eluted with 30% acetic acid for 10 min at room temperature, lyophilized, resuspended in H_2O, and sequenced by automated Edman degradation on a Procise protein microsequencer. Selectivity values for each amino acid were determined by comparing the relative abundance (mole percentage) of each amino acid at a particular sequencing cycle in the recovered peptides to that of each amino acid in the original peptide library mixture at the same position.

Isothermal Titration Calorimetry

Peptides were synthesized by solid phase technique with three C-terminal lysines to enhance solubility. Peptides were then purified by reverse phase HPLC following deprotection and confirmed by MALDI-TOF mass spectrometry. Calorimetry measurements were performed using a VP-ITC microcalorimeter (MicroCal Inc.). Experiments involved serial 10μL injections of peptide solutions (20μM-150μM) into a sample cell containing 15μM PTIP BRCT domains (residues 550-757) or 15μM GST-BRCA1 BRCT domains (residues 1634-1863) in 25-50mM Tris/HCl (pH 8.1), 100-300mM NaCl. Twenty injections were performed with 240s intervals between injections and a reference power of 25

μCal/s. Binding isotherms were plotted and analyzed using Origin Software (MicroCal Inc.)

Peptide Filter Array

An ABIMED peptide arrayer with a computer controlled Gilson diluter and liquid handling robot was used to synthesize peptides onto an amino-PEG cellulose membrane using N-α-FMOC-protected amino acids and DIC/HOBT coupling chemistry. The membranes were blocked in 5% milk/TBS-T (0.1%) for 1hr at room temperature, incubated with 0.025-0.1 μM GST-PTIP BRCT domains (residues 550-757) or GST-BRCA1 BRCT domains (residues 1634-1863) in 5% milk, 50 mM Tris/HCl (pH 7.6), 150 mM NaCl, 2 mM EDTA, 2mM DTT for 1 hr at room temperature and washed four times with TBS-T (0.1%). The membranes were then incubated with anti-GST conjugated HRP (Amersham) in 5% milk/TBS-T (0.1%) for 1 hr at room temperature, washed five times with TBS-T (0.1%), and subjected to chemiluminescence.

PTIP BRCT Domains and BRCA1 BRCT Domains Binding to Cellular Substrates

U2OS cells were either treated with 10 Gy of ionizing radiation or mock irradiated and allowed to recover for 30-120 min. Cells were subsequently lysed in 50 mM Tris/HCl (pH7.6), 150 mM NaCl, 1.0% NP-40, 5 mM EDTA, 2 mM DTT, 8 μg/mL pepstatin, 8 μg/mL aprotinin, 8 μg/mL leupeptin, 2 mM Na_3VO_4, 10 mM NaF, 1 μM microcystin. The lysates (0.5-2mg) were incubated with 20 μL

glutathione beads containing 10-20 μg of GST-PTIP BRCT domains (residues 550-757), GST-BRCA1 BRCT domains (residues 1634-1863) or GST for 120 min at 4°C. Beads were washed three times with lysis buffer. Precipitated proteins were eluted in sample buffer and detected by blotting with anti-ATM/ATR substrate (pSer/pThr)Gln antibody (Cell Signaling), polyclonal anti-53BP1 (Oncogene), or monoclonal anti-HA (Covance). For peptide competition experiments, GST-PTIP BRCT domains or GST-BRCA1 BRCT domains were immobilized on glutathione beads and preincubated with 350 μM of BRCTtide-(7pSer, 7pThr, 7Thr, 7Ser), (pSer/pThr)Gln-library, (Ser/Thr)Gln-library, or pThrPro-library for 1 hr at 4°C and washed three times with lysis buffer. For the phosphatase experiment the lysate was treated for one hour with lambda protein phosphatase (Sigma) prior to incubation with glutathione beads containing GST-PTIP BRCT domains.

Immunofluorescence and Microscopy

U2OS cells were seeded onto 18mm^2 coverslips and transfected with GFP-PTIP constructs FL (residues 1-757), ΔBRCT (residues 1-549), or $(BRCT)_2$ (residues 550-757) using FuGene6 transfection reagent (Roche) according to manufacturer's protocol. Twenty to thirty hours following transfection, the cells were either treated with 10 Gy of ionizing radiation or mock irradiated and allowed to recover for 30-480 minutes. Cells were fixed in 3% paraformaldehyde/2% sucrose for 15 min at RT and permeabilized with a 0.5% Triton X-100 solution containing 20 mM Tris-HCl (pH 7.8), 75 mM NaCl, 300 mM

sucrose, and 3 mM $MgCl_2$ for 15 min at RT. When necessary, cytosolic proteins were extracted after IR treatment as described by O. K. Mirzoeva, J. H. Petrini, *Mol Cell Biol* **21**, 281 (2001). In brief: cells were incubated with cytoskeleton buffer (10mM PIPES pH6.8, 100mM NaCl, 300mM sucrose, 3mM $MgCl_2$, 1mM EGTA, 0.5% Triton X-100) for 5 minutes on ice followed by incubation with cytoskeleton stripping buffer (10mM Tris-Hcl pH 7.4, 10mM NaCl, 3mM $MgCl_2$, 1% Tween-40, 0.5% sodium deoxycholate) for 5 minutes on ice followed by successive washes in ice cold PBS. Slides were stained with primary antibodies at 4°C overnight, then stained with a Texas Red conjugated anti-mouse or anti-rabbit secondary antibody for 60 min (Molecular Probes) at RT. Primary antibodies used were rabbit polyclonal anti-53BP1 (Oncogene), mouse anti-γ-H2AX (Upstate), and rabbit anti-(pSer/pThr)Gln (Cell Signaling). Images were either collected on a Deltavision microscope (Carl Zeiss, Thornwood, NY) and digitally deconvolved using Softworx graphics processing software (SGI) or captured using a spinning disk confocal detector mounted on a Nikon TE2000 microscope using OpenLab software (Improvision).

Tables

Table 3.1. Phosphoserine and Phosphothreonine Peptide Motif Selection by PTIP and BRCA1 Tandem BRCT Domains

PTIP

-4	-3	-2	-1		+1	+2	+3	+4	+5
X	Y (1.5)	G (2.3) D (1.5) E (1.4)	L (2.6) I (2.5) M (2.5) V (1.9)	**pS/pT**		V (3.8) I (2.8)	F (7.0) L (4.3) I (4.1)	P (1.6)	I (2.9) F (2.7) L (2.4) V (2.0) Y (2.0)
X	X	E (1.3)	I (1.4) M (1.4) V (1.4) L (1.3)	**pS**	F (1.7) I (1.5) Q (1.5) Y (1.3)	V (1.8) T (1.5)		X	I (1.9) F (1.7) M (1.6) L (1.4)
G (1.6)	Y (1.1)	D (1.2) E (1.1)	L (1.2) I (1.2) M (1.2)	**pS**	Q (1.3) I (1.3) P (1.2)	V (2.1) I (1.7)	F (2.3) I (2.3) V (1.8) L (1.7) Y (1.5)	P (1.2)	Y (1.3)
X	X	X	I (2.1) L (1.8) W (1.3)	**pT**	Q (1.5) F (1.4) I (1.3)	Y (1.4)	I (1.4) L (1.3) V (1.2)	F (1.5) Y (1.4) P (1.3)	**A**

BRCA1

-4	-3	-2	-1		+1	+2	+3	+4	+5
X	F (1.7) Y (1.6)	D (1.2) E (1.1)	I (1.4) V (1.3) L (1.2) M (1.2)	**pS/pT**		V (3.1) T (2.6) I (2.2) S (1.7)	F (7.5) Y (5.2)	V (1.5) P (1.4)	F (4.5) G (1.8)
X	R (1.5) Y (1.4)	E (1.3) D (1.2)	V (1.4) I (1.3) M (1.3)	**pS**	F (2.1) Y (1.6) I (1.4) Q (1.4)	T (1.9) V (1.7)		X	F (1.6) M (1.4) Y (1.3)
X	X	Y (1.2)	X	**pS**	Q (1.4) F (1.3)	V (1.2) I (1.2)	F (2.4) Y (1.5)	I (1.2)	X
X	E (1.5)	D (1.9) E (1.5)	I (1.6) L (1.4)	**pT**	Q (1.5) E (1.4) F (1.3)	D (1.5) Y (1.3) I (1.2)	F (1.9) Y (1.2)	D (1.4) P (1.2)	

A GST fusion of the PTIP or BRCA1 tandem BRCT domains was screened for binding to four phosphopeptide libraries, which contained the sequences GAXXXB(pS/pT)QJXXXAKKK, GAXXXXpSXXFXXAYKKK, MAXXXXpTXXXXAKKK, and MAXXXXSpXXXXXAKKK, where X indicates all amino acids except Cys. In the library MAXXXB(pS/pT)QJXXXAKKK B indicates (A, I, L, M, N, P, S, T, V) and J represents a biased mixture of (25% E, 75% X), while X indicates all amino acids except (C, R, K, H) for all positions in this library. Residues showing strong enrichment are underlined [16].

Table 3.2. Peptide Binding Affinities for the Tandem BRCT Domains

Peptide	Sequence	$(BRCT)_2$ Domain	K_d
BRCTtide-7pS	GAAYDI-***p*S**-QVFPFAKKK	PTIP	280 nM
BRCTtide-7pT	GAAYDI-***p*T**-QVFPFAKKK	PTIP	14.3 μM
BRCTtide-7S	GAAYDI- **S**-QVFPFAKKK	PTIP	N.D.B.
BRCTtide-7T	GAAYDI- **T**-QVFPFAKKK	PTIP	N.D.B.
BRCTtide-7pS	GAAYDI-***p*S**-QVFPFAKKK	BRCA1	400 nm
BRCTtide-7S	GAAYDI- **S**-QVFPFAKKK	BRCA1	N.D.B.
BRCTtide-7T	GAAYDI- **T**-QVFPFAKKK	BRCA1	N.D.B.

Isothermal titration calorimetry (ITC) was used to determine binding constants (K_d). All observed binding stoichiometries were consistent with a 1:1 complex of protein and phosphopeptide. N.D.B indicates no detectable binding by ITC for a tandem BRCT domain with a concentration of at least 150μM. pS and pT denote phosphoserine and phosphothreoine, respectively.

Figures

Figure 3.1. Identification of pSer/pThr-binding domains using an ATM/ATR-motif library vs. expression library screen.

(A) An oriented (pSer/pThr) phosphopeptide library, biased toward the phosphorylation motifs of ATM and ATR, was immobilized on Streptavidin beads. The library [pSQ= biotin-ZGZGGAXXXB(pS/pT)QJXXXAKKK] and its non-phosphorylated counterpart (SQ) were screened against in vitro translated ^{35}S-Met labeled proteins. (pS/pT) denotes 50% phosphoserine and 50% phosphothreonine, Z indicates aminohexanoic acid, B represents a biased mixture of the amino acids (A, I, L, M, N, P, S, T, V) and J represents a biased mixture of (25% E, 75% X), where X denotes all amino acids except (C, H, K, R). In each panel, the first and second lanes show binding of proteins within the pool to the phosphorylated (pSQ) and non-phosphorylated (SQ) libraries, respectively. Identification of PTIP, denoted by arrow and asterisk, occurred through progressive subdivision of the EE11 pool to a single clone. The uppermost band is a fusion artifact of PTIP with vector sequences resulting in translation initiation at an upstream start codon in the vector.

(B) Deletion mapping of the phospho-binding domain of PTIP. Truncations of PTIP were assayed for selective binding to the pSQ library as in panel A. BRCT domain boundaries were determined from sequence alignments [207].

Figure 3.1 Continued.

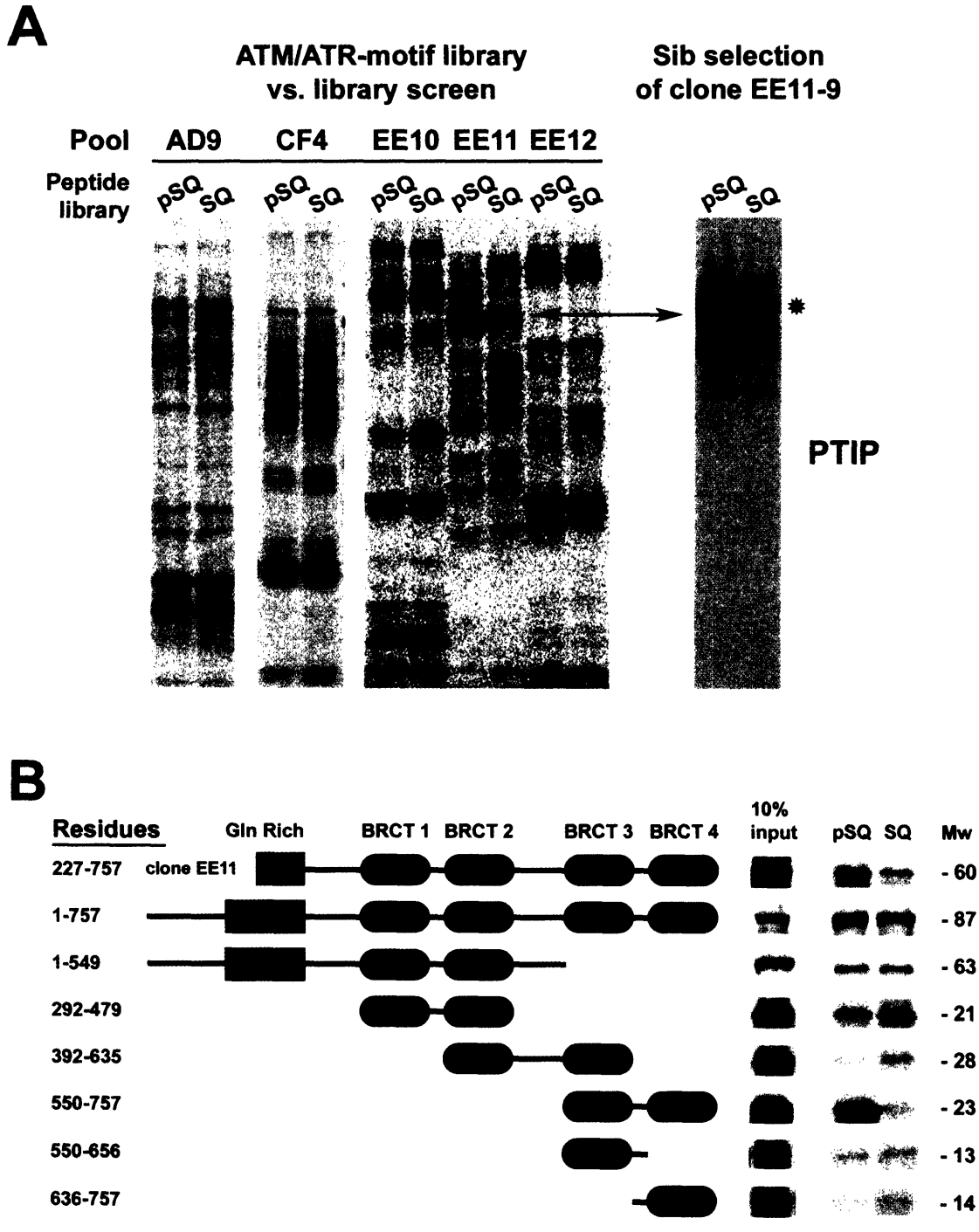

Figure 3.2. Comparison of the tandem BRCT domains and determination of the PTIP and BRCA1 BRCT optimal phosphopeptide-binding motifs.

(A) PTIP, BRCA1, BRCA1 M1775R, MDC1, 53BP1 and Rad9p $(BRCT)_2$ domains were assayed for binding as in Figure 3.1A. The peptide libraries used were pSQ (Figure 3.1A), pS= biotin-ZGZGGAXXXXpSXXXXXAKKK, pT=biotin-ZGZGGAXXXXpTXXXXXAKKK,pSXXF=biotin-ZGZGGAXXXXpSXXFXXAYKKK, where pS is phosphoserine, pT is phosphothreonine, Z indicates aminohexanoic acid, X denotes all amino acids except Cys. Domain boundaries: PTIP as indicated in Figure 3.1; BRCA1 BRCT1 and 2, aa 1633-1863; BRCT1 alone, aa 1633-1740; BRCT2 alone, 1741-1863; MDC1, aa 1874-2089; 53BP1, aa 1622-1972; Rad9p, 985-1309.

(B) Strong selection by the PTIP- and BRCA1-$(BRCT)_2$ domains for Phe at the (pSer/pThr)-Gln +3 position (7.0 or 7.5), respectively (Table 3.1). Bar graphs show the relative abundance of each amino acid at a given cycle of sequencing compared to its abundance in the starting peptide library mixture [16].

Figure 3.2 Continued.

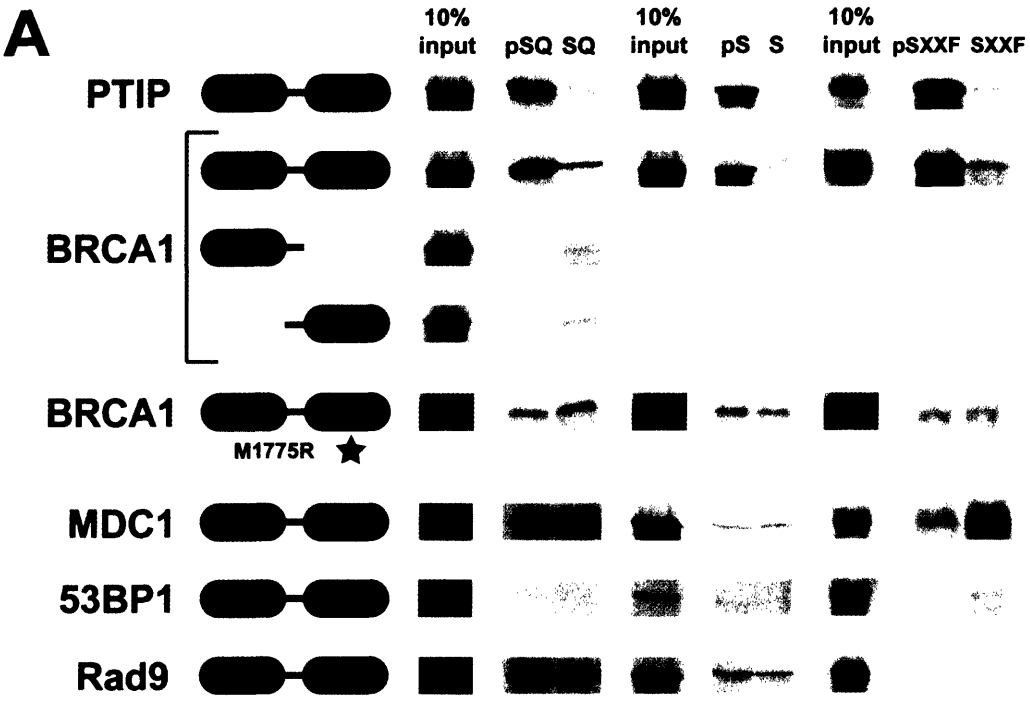

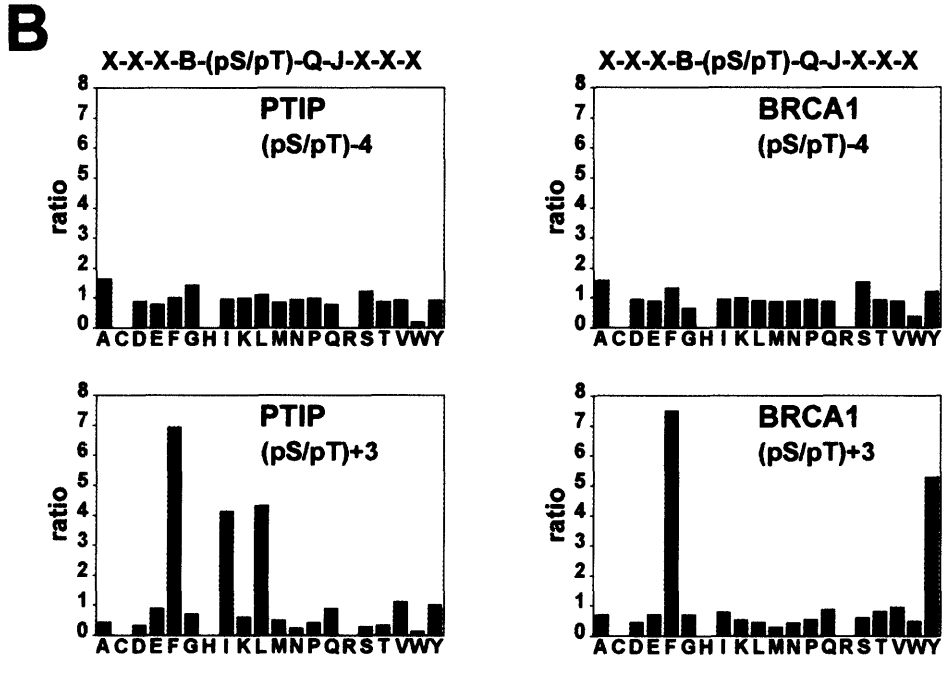

Figure 3.3. PTIP and BRCA1 BRCT domains binding to a filter array of phosphopeptides.

(A, B) Binding of GST-PTIP **(A)** and BRCA1 **(B)** tandem BRCT domains to a filter array of peptide spots, comprising single point mutants of the optimal BRCT domain phosphopeptide (left column). Bound GST-BRCT domains were detected by blotting with HRP-conjugated anti-GST antibody. The resulting consensus binding motif is indicated in the right column; X denotes no dominant selection, ϕ denotes residues with aliphatic or aromatic side chains, and letters enclosed in square brackets are specifically de-selected. The top row indicates the amino acid that was substituted for the optimal amino acid.

Figure 3.3 Continued.

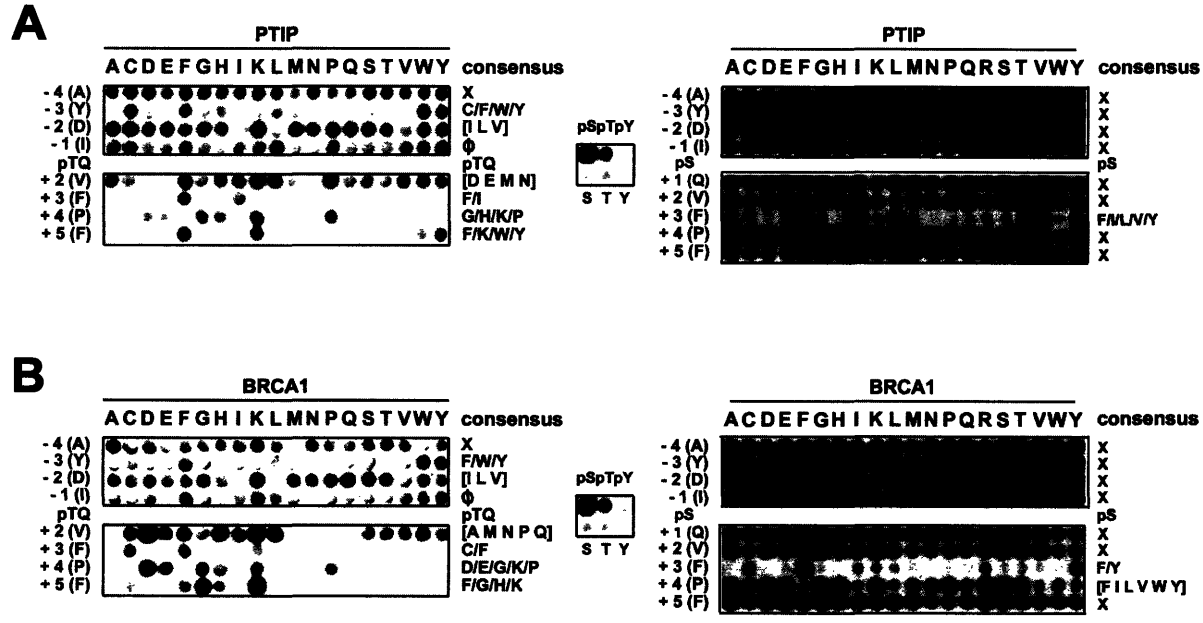

Figure 3.4. Association of tandem PTIP and BRCA1 BRCT domains with DNA damage-induced phosphoproteins through their phosphopeptide-binding pockets.

(A) Lysates from U2OS cells before or 2 hours after 10 Gy of IR were incubated with GST-PTIP-$(BRCT)_2$. Bound proteins were detected by immunoblotting with an antibody to the (pSer/pThr)-Gln motif generated by ATM and ATR. The interaction was disrupted by incubation with the pSQ peptide library, but not with the SQ peptide library or an unrelated pTP library [18].

(B) Interaction of the PTIP-$(BRCT)_2$ domain with phosphoproteins was disrupted by treatment of U2OS cells with caffeine (5 mM) before IR exposure or by incubating the beads with BRCTtide (7pT) but not by its non-phosphorylated counterpart (7T).

(C) Tandem BRCT domains of PTIP interact with 53BP1 following DNA damage. Endogenous 53BP1 from IR treated U2OS cells was precipitated with GST-PTIP-$(BRCT)_2$ and detected by immunoblotting with an antibody to 53BP1. U2OS cells were transfected with HA-tagged 53BP1 and the interaction with GST-PTIP-$(BRCT)_2$ was analyzed as in panels **A** and **B**. Treatment of the cell lysates with lambda phosphatase also abolished the interaction.

(D) Lysates from U2OS cells before or after IR were incubated with GST-BRCA1-$(BRCT)_2$ and analyzed as in panel **B**. In these experiments the pSer version of BRCTtide (7pS) and its non-phosphorylated counterpart (7S) were used.

Figure 3.4 Continued.

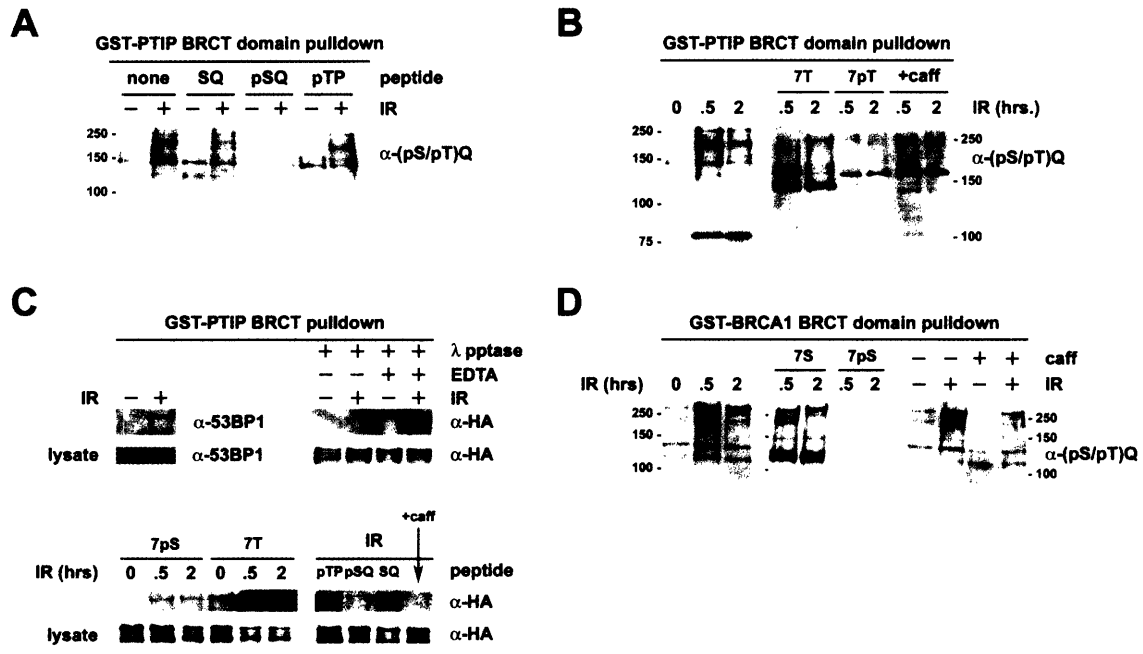

Figure 3.5. Full length PTIP forms DNA damage induced foci and co-localizes with (pSer/pThr)-Gln proteins, 53BP1, and γ-H2AX.

(A) U2OS cells were transfected with a full length GFP-PTIP construct (PTIP-FL residues 1-757).

(B) U2OS cells were transfected with a PTIP deletion construct in which the last two BRCT domains had been removed (PTIP-ΔBRCT, residues 1-550)

(C) U2OS cells were transfected with a PTIP construct containing only the last two BRCT domains ($(BRCT)_2$, residues 550-757). In **A-C**, 24 hrs following transfection cells were either treated with 10 Gy of ionizing radiation or mock irradiated, allowed to recover for 2 hrs, stained, and analyzed by immunofluorescence microscopy.

Figure 3.5 Continued.

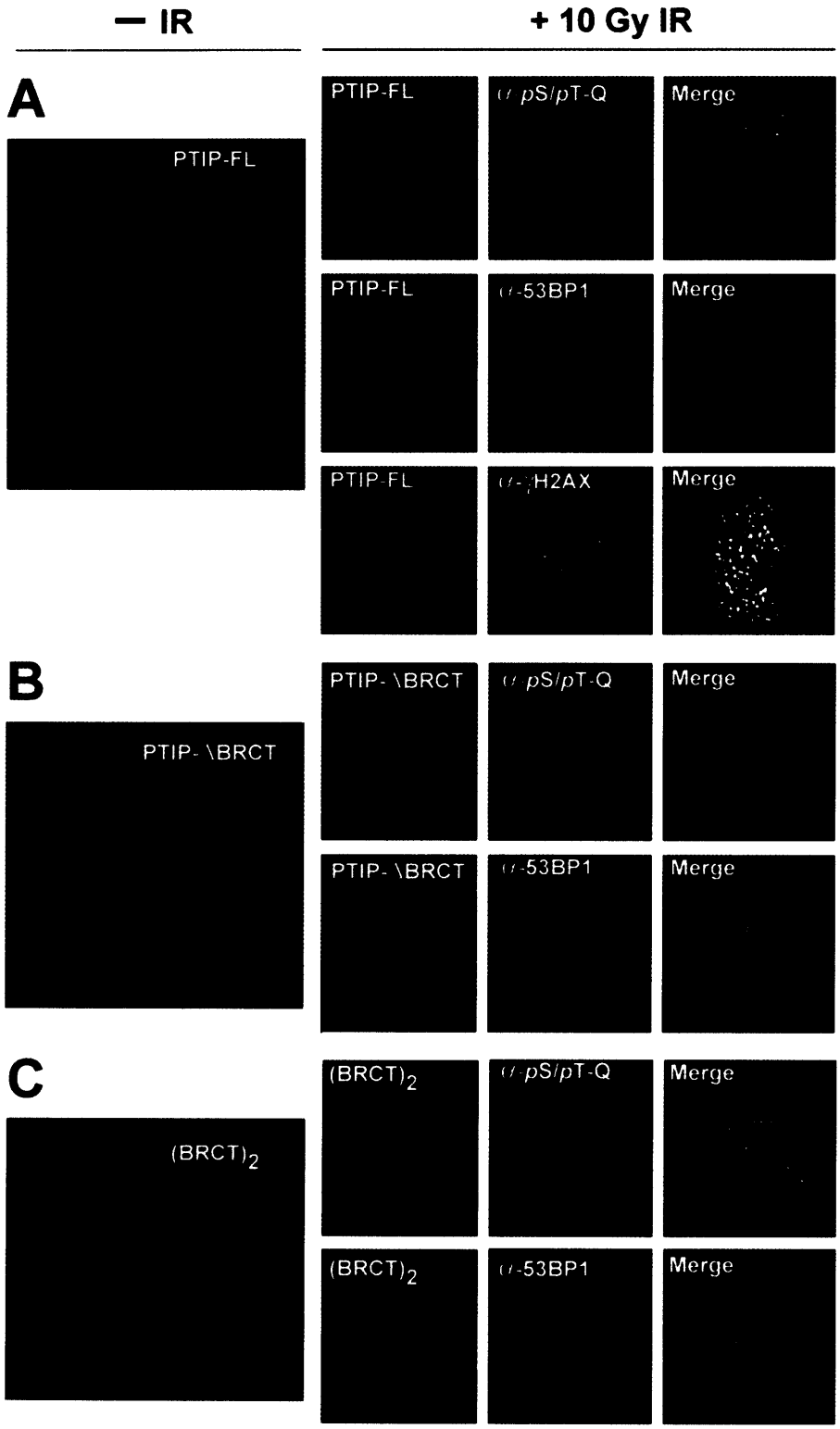

Figure 3.6. Caffeine attenuates recruitment of PTIP to DNA damage foci in response to ionizing radiation. U20S cells transfected with full-length GFP-PTIP cDNA were mock treated or treated with 10mM caffeine for 70 minutes before exposure to 10Gy ionizing radiation.

(A) In reponse to IR, mock-treated U20S cells formed nuclear foci containing PTIP (in green) and γ-H2AX (in red); these two proteins co-localize at sites of DNA damage (merge).

(B) In response to IR, caffeine treated U20S cells formed reduced numbers of nuclear foci; PTIP was mislocalized and did not form discrete nuclear foci and there were reduced numbers of γ-H2AX containing foci; pretreatment with caffeine effectively abolished co-localization of PTIP and γ -H2AX (merge).

Figure 3.6 Continued.

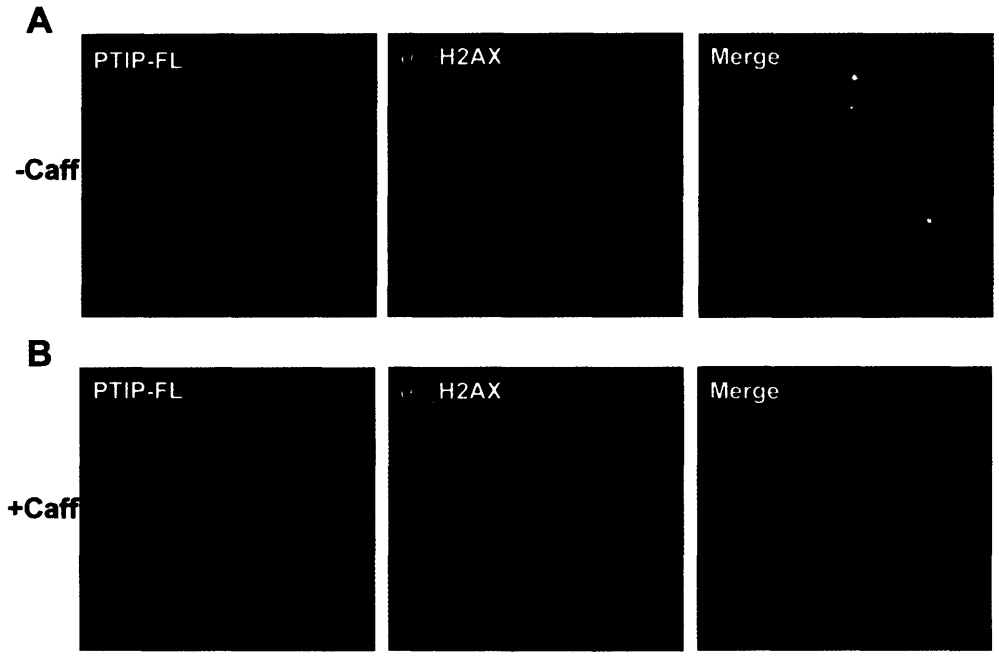

Chapter 4

Structure and Mechanism of BRCA1 BRCT Domain Recognition of Phosphorylated BACH1

Summary

Germline mutations in the BRCA1 tumor suppressor often result in a significant increase in susceptibility to breast and ovarian cancers. Although the molecular basis of their effects remains largely obscure, many are known to target the highly conserved C-terminal BRCT-repeats that function as a phosphoserine/phosphothreonine-binding module. We report the 1.85Å X-ray crystal structure of the BRCA1 tandem BRCT domains in complex with a phosphorylated peptide representing the minimal interacting region of the DEAH-box helicase BACH1. The structure reveals the determinants of this novel and important class of BRCA1 binding events. We show that a subset of disease-linked mutations appear to act through specific disruption of phospho-dependent BRCA1 interactions rather than through gross structural perturbation of the tandem BRCT domains.

Contributions:

Julie Clapperton and Steve Smerdon (with the assistance of Mike Yaffe) solved the X-tal structure and produced Figures 4.1, 4.2 and part of 4.4. Timmy Ho helped with the mutagenesis of BRCT domain constructs as well as DNA purification. Drew Lowery helped with the mutagenesis of several constructs, helped with DNA purification and westernblot analysis.

Introduction

The breast-cancer susceptibility gene product, BRCA1, plays important roles in cell cycle control, transcriptional regulation, chromatin remodelling, and the response to DNA-damage[51, 76, 83, 208]. BRCA1 is a large, modular protein of 1863 amino-acid residues containing an N-terminal RING domain, a central region rich in SQ/TQ dipeptide pairs, and tandem BRCT domains. BRCA1 interacts with a large number of protein partners at different stages of the cell cycle, or following genotoxic stress. For example, BRCA1 interacts with the DNA helicase BACH1 during S and G2 in normally cycling cells,[20, 209] whereas BRCA1 interacts with a subset of ATM/ATR substrates in response to DNA damage[19]. In both S-phase and irradiated/mutagen-treated cells, BRCA1 localizes to distinct nuclear foci thought to represent sites of DNA-damage[48, 78] where BRCA1 is thought to function, at least in part, as a scaffold for the assembly of DNA-repair complexes.

Mutations in BRCA1 occur in 50% of women with inherited breast cancer and up to 90% of women with combined breast and ovarian cancer[210-213]. Most frameshift and deletion mutants truncate all or part of the BRCT repeats, while more that 70 missense mutations lie within the BRCT domains themselves (http://research.nhgri.nih.gov/projects/bic/). BRCT domains are α/β structures that occur singly or as multiple repeats in a number of proteins in addition to BRCA1 that are involved in cell-cycle regulation and DNA-damage responses[204, 214]. Comprised of 80–100 amino acids, BRCT domains are generally thought to function as protein-protein recognition modules[204]. The

molecular basis underlying BRCA1 BRCT function, and how cancer-causing mutations in the BRCT domains act at the structural level, however, remains unresolved, despite significant structural, biochemical, and mutagenic analysis[84, 85, 204, 215, 216]. It has been suggested that mutational effects are manifested through structural destabilization, however a number of mutations are located on the protein surface, indicating that they may specifically affect BRCT interactions with other BRCA1-associated targets.

We recently discovered that a subset of tandem BRCT domains, including those of BRCA1, function as phosphoserine/phosphothreonine (pSer/pThr)-binding modules, suggesting that some BRCT-mediated interactions with proteins involved in DNA-damage and cell-cycle control are regulated by protein phosphorylation[19]. Oriented peptide library screening of tandem BRCT domains revealed phospho-dependent binding specificity extending from the pSer/pThr+1 to the pSer/pThr+5 position, with particularly strong selection for aromatic or aromatic/aliphatic residues in the pSer/pThr+3 position. High affinity phosphopeptides selected by *in vitro* oriented library screens were able to block the interaction of the tandem BRCT domains of BRCA1 and the transcriptional regulator PTIP with ATM/ATR-phosphorylated substrates[19]. Similar findings were reported by Chen and colleagues who were able to demonstrate that the BRCA1 BRCT domain repeat mediates interaction with the DEAH-box helicase BACH1 through a specific phosphoserine 990 located within a region (888–1063) previously shown to be sufficient for BRCA1-BACH1 binding[20, 209]. The tumor-suppressor function of BRCA1 may directly depend on this interaction since its

disruption is sufficient to abrogate the G2-M checkpoint following DNA damage[20, 217].

To determine the structural basis for phosphopeptide binding and phosphopeptide-motif selection, and investigate alternative structural mechanisms underlying BRCA1 BRCT mutations and cancer predisposition, we solved the high resolution X-ray crystal structure of the BRCA1 tandem BRCT repeats bound to a BACH1 phosphopeptide. We now provide a molecular rationale for phosphospecific binding, and show that a set of cancer-associated BRCA1 BRCT mutations eliminate phosphopeptide binding *in vitro* and BACH1 phosphoprotein binding *in vivo*, or alter the phosphopeptide recognition motif for the BRCA1 tandem BRCT domains, revealing a structural basis for mutation-associated loss of BRCA1 function.

Results

Structure of the BRCA1 BRCT:BACH1 Phosphopeptide Complex

The BRCA1 tandem BRCT domains bound to the interacting phosphopeptide from BACH1 (residues 986–995) was crystallized and its structure solved at 1.85Å resolution by X-ray diffraction (Figure 4.1A, B). Phases were determined by molecular replacement using the previously determined structure of the un-liganded BRCA1 tandem BRCT domains (PDB ID 1JNX) as a search model[84], (Table 1 and Methods). Difference Fourier maps revealed well-defined electron density for the phosphopeptide allowing modelling of eight residues corresponding to BACH1 Ser988 – Lys995. Each BRCT repeat forms a compact domain (Figure 4.1) in which a central, four-stranded beta-sheet is packed against two helices, α1 and α3, on one side and a single helix, α2 on the other. The two domains pack together through interaction between α2 of BRCT1 and the α1'/α3' pair of BRCT2. A linker region connecting the two BRCT domains contains a β-hairpin-like structure βL and a short helical region, αL, that forms part of the interface through interactions with α2 of BRCT1 and the N-terminal end of α3' from BRCT2. Overall, the structure of the tandem BRCT domain:phosphopeptide complex is similar to that of the un-liganded domains (rmsd ~ 0.4Å for all Cα atoms). However, superposition of the individual BRCT repeats reveals that phosphopeptide-binding is associated with a slight relative rotation of each BRCT domain and a translation of BRCT1 helix α1 towards the cleft between the domains.

The BACH1 phosphopeptide binds in an extended conformation to a groove

located at the highly conserved interface between the N- and C-terminal BRCT domains (Figures 4.1A, 4.2A), consistent with the requirement of both domains for efficient phosphopeptide binding[19, 217]. This mode of binding is distinct from that observed in the phospho-independent interaction between p53 and the tandem BRCT domains of 53BP-1, which occurs primarily through the linker region[218, 219]. Our structure clearly shows that the phospho-dependent interactions that are necessary and sufficient for formation of the BACH1/BRCA1 complex occur on the opposite side of the BRCT-BRCT interface from those involved in the p53:53BP-1 interaction.

BRCA1 BRCT:Phosphopeptide Specificity

BRCA1 tandem BRCT domain binding to library-selected peptides *in vitro*[19, 217], and to phosphorylated BACH1 *in vivo*[20] is dominated by the presence of a phosphoserine/threonine and a phenylalanine three residues C-terminal to it (Phe +3). This is now confirmed by our structure which shows that the BACH1 pSer 990 phosphate moiety binds to a basic pocket through three direct hydrogen-bonding interactions involving the side chains of Ser1655 and Lys1702, and the main-chain NH of Gly1656 (Figure 4.3A). All three of these residues are located in BRCT1 and all are absolutely conserved in BRCA1 homologues. Ser1655 and Gly1656 are situated within the loop preceding α1 and are brought into proximity with the phosphate moiety as a result of the conformational change that occurs upon phosphopeptide binding. Intriguingly, a S1655F mutation has been identified in a single breast cancer patient, although

its link to disease has not been confirmed. In addition to these direct interactions, the phosphate, and some peptide main-chain atoms are also tethered through networks of water molecules, many of which are tetrahedrally hydrogen bonded (Figure 4.3A). Indirect protein-solvent-phosphate contacts are unusual in phospho-dependent protein-protein interactions but have been observed previously in structures of phosphopeptide complexes of the human Plk1 Polo-box domain[220, 221].

The Phe +3 peptide side-chain fits into a hydrophobic pocket at the BRCT interface consisting of the side chains of Phe1704, Met1775 and Leu1839 contributed from both BRCT domains (Figures 4.3A, 4.4A). This finding rationalizes the strong selection for aromatic amino acids in the +3 position of the binding motif seen in peptide library experiments[19, 217], as well as the observation of Yu et al that mutation of Phe993 to Ala eliminates BRCA1:BACH1 binding[20]. Additional hydrogen-bonds with the main-chain N and C=O atoms of Phe +3 are supplied by main- and side-chain atoms from Arg1699, a site of mutation also associated with cancer predisposition. The phosphorylated Ser990 of BACH1 is preceded by an Arg residue in the –3 position and followed by a proline residue in the +1 position, suggesting potential Ser990 phosphorylation by either basophilic and/or proline-directed kinases. The BRCA1 tandem BRCT domains are also known to interact with pSQ-containing motifs characteristic of PI 3-kinase-like kinases such as ATM and ATR[19]. In the tandem BRCT:BACH1 phosphopeptide co-crystal structure, there are no direct interactions between the +1 Pro side chain and the BRCT domains. Instead, this residue participates in

only a single water-mediated hydrogen bond involving its carbonyl oxygen (Figure 4.3A), consistent with the idea that various types of protein kinases can generate tandem BRCT phospho-binding motifs. The Lys +5 side chain makes two salt-bridging interactions with residues in BRCT2 (Figure 4.3A), consistent with the Lys selection observed in this position by spot blot and peptide library experiments[19, 217].

Cancer-Associated BRCA1 BRCT Mutations

Residues that form or stabilize the phosphopeptide binding surface, and the domain-domain interface, are among the most highly conserved portions of the molecule in BRCA1 orthologues from humans, primates, rats and mice (Figure 4.2B). Interestingly, these regions correlate strongly with the location of cancer-associated mutations (Figure 4.2A). Some cancer-associated mutations may disrupt the global BRCT fold while others are more likely to specifically interfere with ligand binding[85, 204, 215, 216, 218]. Approximately 80 tumor-derived mutations have been identified within the BRCA1 tandem BRCT domains, though only a few of these have been subsequently confirmed to result in cancer predisposition including D1692Y, C1697R, R1699W, A1708E, S1715R, G1738E, P1749R, M1775R, 5382InsC (a frameshift mutation that results in a stop codon at position 1829), and Y1853X (which truncates the last 11 residues). Most of these cluster at or near the phosphopeptide-interacting surface (Figure 4.2A). Two of these mutated residues, Arg1699 and Met1775, directly interact with residues in the phosphopeptide (Figure 4.3A). Two others, Pro1749 and

Gly1738, are located at the BRCT1/BRCT2 interface beneath the molecular surface and their effects are likely to be mediated through alterations in the relative orientation of the tandem BRCT motifs that our structure suggests is necessary for phospho-dependent interactions with partner proteins.

To verify the phosphoserine phosphate interactions observed in the X-ray structure and to investigate the effects of the most common tumor-derived point mutations, we investigated the binding of a panel of site-directed mutant BRCA1 tandem BRCT domains to the interacting region of BACH1. Binding was determined by measuring the ability of *in vitro* transcribed and translated proteins to bind to either phosphorylated and non-phosphorylated biotinylated peptides (Figure 4.3B). Wild-type BRCA1 tandem BRCT domains clearly bind to phosphorylated but not non-phosphorylated peptides, while mutation of the conserved Ser1655 and Lys1702, alone or in combination, completely abolished the interaction. Five *bona fide* cancer-linked mutations, P1749R, G1738E, M1775R, Y1853X and 5382InsC all result in complete loss of phosphopeptide binding. A mutation R1699W is cancer-linked and a second, R1699Q, has been detected in breast cancer patients but has not yet been directly related to disease-predisposition. We surmised that the glutamine side-chain might still participate in main-chain hydrogen bonding to the peptide and this is, indeed, the only BRCA1 tandem BRCT domain mutant that retained a small degree of binding in our assays. Somewhat surprisingly, however, the R1699Q mutant largely loses phospho-specificity, and instead bound to both phosphorylated and non-phosphorylated peptides.

To investigate the *in vivo* binding of cancer-predisposing mutant BRCA1 tandem BRCT domains to endogenous BACH1, we transfected U2OS cells with a vector encoding the C-terminal 550 amino acids of BRCA1 containing a myc tag and an SV40 nuclear localization sequence as described by Chen et al[222]. As shown in Figure 4.3C, interaction between the wild type BRCA1 tandem BRCT domains with full-length BACH1 was easily detected. In contrast, no *in vivo* interaction was observed between BACH1 and mutant BRCA1 tandem BRCT domains that disrupt phosphate-binding or predispose to breast and ovarian cancer. All of these cancer-associated mutant proteins were expressed at comparable levels when transfected into mammalian cells[81] (Figure 4.3C), suggesting that gross structural destabilization is unlikely to account for their cancer proclivity.

Interpretation of the structural effects of the M1775R mutation is simplified since the X-ray crystal structure of the M1775R tandem BRCT domain mutant has been determined (PDB ID 1N5O)[85], revealing a nearly identical structure as the wild-type protein with an average rmsd of 0.35 Å for all Cα atoms. Superposition of the mutant structure with that of our BACH1 complex shows that the guanidine portion of the substituent arginine side-chain extrudes into the tandem BRCT cleft, where it occupies the binding site for the essential Phe +3 of the phosphopeptide (Figure 4.4A, B). In this case, loss of phosphopeptide-binding *in vitro* and BACH1 binding *in vivo* appear to be attributable to the severe steric clash of the Arg1775 side-chain with an important determinant of phospholigand specificity and affinity. The M1775R mutant protein does,

however, bind weakly to a BACH1 phosphopeptide in which the +3 Phe is mutated to Asp or Glu (Figure 4.4C). This is consistent with the introduction of a basic residue at the pSer +3 binding site and with the observation that this mutation creates new anion binding sites in the M1775R crystal structure[85]. Thus, in addition to disrupting the native BRCA1:BACH1 interaction, this mutation may also result in the formation of inappropriate BRCA1 BRCT interactions.

Phosphopeptide-Binding and Nuclear Foci Formation

Subcellular localization and nuclear foci formation by the wild type, S1655A/K1702M phosphopeptide-binding mutant and the M1775R cancer-associated mutant BRCA1 BRCT domains were studied before and after DNA damage in unsynchronized U2OS cells (Figure 4.5). To maximize visualization of nuclear foci, the cells were permeabilized with buffers containing 0.5% Triton X-100 prior to fixation and immunostaining[69]. In un-extracted cells the wild-type BRCT domains and both of the mutant BRCT proteins showed equivalent diffuse nuclear localization. Extraction of the un-irradiated cells prior to fixation resulted in near complete loss of BRCT domain staining in all cases (Figure 4.5A). Under these conditions, less than 5% of the wild-type and M1775R tandem BRCT-containing cells displayed 5 or more nuclear foci, and no foci were observed with the S1655A/K1702M double mutant. When the cells were irradiated with 10 Gy of γ-irradiation, and 2 hrs later permeabilized, fixed, and stained, nearly all of the cells containing the wild-type BRCA1 tandem BRCT

domains demonstrated sharp punctate nuclear foci that largely co-localized with the staining pattern of an anti-pSer/pThr-Gln epitope antibody that recognizes ATM- and ATR-phosphorylated substrates (Figure 4.5B). In contrast, the S1655A/K1702M mutant protein displayed only faint staining with a very fine granular pattern that completely failed to co-localize with pSer/pThr-Gln staining. This failure of foci formation and pSer/pThr-Gln co-localization is strong evidence that the phospho-binding function of the BRCA1 tandem BRCT domains is critical for normal subcellular localization following DNA damage. The M1775R mutant protein that binds weakly to phosphopeptides with a different specificity than the wild-type BRCA1 BRCT domains also formed punctate nuclear foci, although these were slightly reduced in number and showed less co-localization with pSer/pThr-Gln staining foci than the wild-type protein. This localization might result from synergistic weak binding to alternative non-optimal phosphorylated ligands present in high abundance in nuclear foci following DNA damage, as has been observed for other phosphopeptide-binding domain interactions[223].

Discussion

The 1.85Å BRCA1 tandem BRCT domain:phosphopeptide structure described here is the highest resolution X-ray structure of any BRCT domain structure solved to date, and provides an enhanced structural framework within which the molecular basis of breast and ovarian cancer can be further investigated. The structure reveals why tandem BRCT repeats, rather than single BRCT domains, are required for binding to pSer- or pThr-containing phosphopeptides with high affinity and specificity, since motif recognition is mediated by residues contributed from both domains across the domain-domain interface. In addition, the structure rationalizes the observation that the BRCA1 BRCT domains do not bind to pTyr-containing sequences[7], since the phosphate recognition pocket appears too shallow to accept a bulky phenyl ring. Despite the fact that not all tandem BRCT domains appear to bind phosphopeptides, several residues involved in the binding are relatively conserved. Structures of additional BRCT:phosphopeptide complexes will be necessary to better understand negative determinants of binding.

The BRCA1 tandem BRCT:phosphopeptide structure, in combination with biochemical and cell biological analysis, shows that some pro-oncogenic mutations in the BRCA1 C-terminal domains directly disrupt phosphopeptide binding or perturb the BRCT interface that forms the phospho-dependent binding surface. Similar conclusions were reached by Williams et al [36] who report the structure of the BRCA1 tandem BRCT domains bound to an alternative phosphopeptide determined from oriented peptide library screening[7], and the un-

liganded structures of the M1775R and V1809F mutants in an accompanying paper in this issue.

Like the BRCT domains in PTIP, the BRCT domains in BRCA1 are sufficient for nuclear foci formation in response to DNA damage, and the phospho-binding function appears to be involved in this phenomenon. Four *bona fide* cancer-linked mutations, P1749R, G1738E, 5382InsC, and Y1853X all result in loss of phosphopeptide binding. A fifth mutation, M1775R, binds weakly to phosphopeptides with altered motif specificity, and can still form nuclear foci after DNA damage, however it completely loses the ability to interact with wild-type BACH1. These effects of the Pro1749 and Met1775 lesions confirm the previous observations that these mutations are sufficient to abrogate BRCA1-BACH1 interactions *in vivo*[209]. Since BACH1 mutations have also been shown to be associated with the development of cancer[224], these findings suggest that the loss of this critical BRCA1 M1775R:BACH1 interaction may be the critical event responsible for cancer predisposition[20, 224].

Despite the fact that mutations in BRCA1 ultimately predispose women to cancer, wild-type BRCA1 paradoxically constitutes a target for anti-cancer therapy. Given the importance of BRCA1 in homologous recombination and DNA repair[82, 208, 225, 226], disruption of the pSer-binding function would be expected to result in enhanced sensitivity to chemotherapy and radiation[26], as has been observed in BRCA1 null murine embryonic stem cells[82]. The structural delineation of the pSer binding surface provides a new target for rational drug design.

Experimental Procedures

Protein Cloning, Expression, and Purification

For crystallization experiments, human BRCA1 BRCTs (residues 1646–1859) were expressed as glutathione *S*-transferase (GST) fusions in pGEX-4T1 (Amersham Pharmacia Biotech) in *Escherichia coli* BL21 at 18°C. The GST was removed by 48-hour treatment with thrombin before gel filtration. Synthetic peptides were prepared by W. Mawby, University of Bristol, U.K. A BRCA1 BRCT clone (residues 1313–1863) in pcDNA3 containing a N-terminal Myc-tag and a SV40 nuclear localization sequence was a gift from R. Scully and D. Livingston[222], and was used for the co-immunoprecipitation and immunofluorescence assays. Mutations were generated using the Stratagene Quick Change Mutagenesis Kit, and verified by sequencing. The pGEX-BRCA1 BRCT clone (residues 1633–1863) was described previously [19] and was used for the peptide filter array. Induction of recombinant GST-BRCA1 BRCT domain protein was performed at 37°C for 3 hrs in the presence of 0.4 mM IPTG. The GST-BRCA1 BRCT domains were isolated from bacterial lysates using glutathione agarose, followed by elution with 40mM glutathione, 50mM Tris/HCl (pH 8.1), and dialysis into 50mM Tris/HCl (pH 8.1), 300mM NaCl.

Crystallization and Structure Determination

Crystals were grown at 18°C by microbatch methods. The BACH1 phosphopeptide (SRSTpS^{990}PTFNK) was mixed with the BRCA1 BRCTs in a

1.5:1 stoichiometric excess and concentrated to 0.35mM in a buffer containing 50mM Tris-HCl (pH 7.5), 0.4M NaCl, and 3mM DTT. Crystals grew from 50 mM MES (pH 6.5), 0.1 M $(NH_4)_2SO_4$, and 13% PEG 8K (w/v). Crystals belonged to the trigonal space group $P3_221$ (a = b = 65.8 Å, c = 93.1 Å, $\alpha = \beta = 90.0°$, $\gamma = 120.0°$) with one complex in the asymmetric unit. Data were collected from flash-cooled crystals at 100K on a Raxis-II detector mounted on a Rigaku RU200 generator. Diffraction data were integrated and scaled using DENZO and SCALEPACK [227]. The structure was solved by molecular replacement using the coordinates 1JNX.brk[84] as a model with AMORE[228]. Subsequent refinement was carried out using REFMAC5[228] and manual model building in O[229]. Figures were constructed using Pymol.

Peptide Binding

An optimal phosphopeptide for binding the BRCA1 BRCTs was determined by oriented peptide library screening as described previously[19]. This peptide was synthesized in both its phosphorylated and non-phosphorylated form with a biotin group at the N-terminus using N-α-FMOC-protected amino acids and standard BOP/HOBt coupling chemistry. These peptides were conjugated to streptavidin coated beads (Sigma-Aldrich). The wild-type and mutant BRCA1 BRCT domain-containing constructs (residues 1313–1863) were transcribed and translated *in vitro* in the presence of [^{35}S]-methionine using the TNT kit (Promega). The bead-immobilized peptides (10μL of beads) were added to 10 μL of the in vitro translated [^{35}S]-labeled protein pool in 150 μL binding

buffer (50 mM Tris-HCl (pH7.6), 150 mM NaCl, 0.5% NP-40, 1 mM EDTA, 2 mM DTT, 8 µg/mL pepstatin, 8 µg mL^{-1} aprotinin, 8 µg mL^{-1} leupeptin, 800 µM Na3VO4, 25 mM NaF). After incubation at 4°C for 3 hours, the beads were washed three times with 200 µL of binding buffer prior to analysis by SDS-PAGE (12.5% (w/v)) and autoradiography.

Peptide Filter Array

An ABIMED peptide arrayer with a computer controlled Gilson diluter and liquid handling robot was used to synthesize peptides onto an amino-PEG cellulose membrane using N-α-FMOC-protected amino acids and DIC/HOBT coupling chemistry. The membranes were blocked in 5% (w/v) milk in Tris-buffered saline containing 0.1% (v/v) Tween-20 (TBS-T) for 1hr at room temperature, incubated with 0.025µM GST-BRCA1 BRCTs or 0.25 µM GST-BRCA1 BRCTs M1775R (residues 1633–1863) in 5% (w/v) milk, 50 mM Tris-HCl (pH 7.6), 150 mM NaCl, 2 mM EDTA, 2mM DTT for 1 hr at room temperature and washed four times with TBS-T. The membranes were then incubated with anti-GST conjugated HRP (Amersham) in 5% (w/v) milk/TBS-T for 1 hr at room temperature, washed five times with TBS-T, and binding analysed by ECL (Perkin-Elmer).

Co-immunoprecipitation of BRCA1 BRCTs and BACH1

U2OS cells were grown to 50% confluency in 100cm^2 dishes and transfected with the myc-tagged wild-type or mutant BRCA1 BRCT constructs

(residues 1313–1863) using FuGene6 transfection reagent (Roche) according to manufacturer's protocol. Cells were collected 30 hrs following transfection, lysed in lysis buffer (50 mM Tris-HCl (pH7.6), 150 mM NaCl, 1.0% NP-40, 5 mM EDTA, 2 mM DTT, 8 μg/mL AEBSF, 8 μg mL^{-1} aprotinin, 8 μg mL^{-1} leupeptin, 2 mM Na_3VO_4, 10 mM NaF and the phosphatase inhibitors microcystin and okadaic acid). Lysates containing equal amounts of protein (3 mg) was incubated with 3 μL of a mouse anti-myc antibody (Cell Signaling) for 2 hr at 4°C and then 10 μL of protein G-sepharose beads (Sigma-Aldrich) were added and samples incubated for an additional 2 hr at 4°C. Beads were washed four times with lysis buffer, bound proteins eluted in SDS-PAGE sample buffer, analysed on 6% polyacrylamide gels, transferred to PVDF membrane, and detected by blotting with rabbit anti-BACH1 antibody (a gift from D. Livingston). A portion of the lysates were also run and blotted with the anti-BACH1 antibody and the anti-myc antibody to further ensure equal protein loading.

Immunofluorescence and Microscopy

U2OS cells were seeded onto 18mm^2 coverslips and transfected with the BRCA1 BRCT construct (residues 1313–1863) and various mutants using FuGene6 transfection reagent (Roche) according to manufacturer's protocol. Thirty hours following transfection, the cells were either treated with 10 Gy of ionizing radiation or mock irradiated and allowed to recover for 120 minutes. Cells were fixed in 3% (v/v) paraformaldehyde/2% (w/v) sucrose for 15 min at RT and permeabilized with a 0.5% (v/v) Triton X-100 solution containing 20 mM Tris-

HCl (pH 7.8), 75 mM NaCl, 300 mM sucrose, and 3 mM $MgCl_2$ for 15 min at RT. When necessary, proteins were extracted after IR treatment as described previously [69]. In brief, cells were incubated with extraction buffer (10mM PIPES pH6.8, 100mM NaCl, 300mM sucrose, 3mM $MgCl_2$, 1mM EGTA, 0.5% (v/v) Triton X-100) for 5 minutes on ice followed by incubation with extraction stripping buffer (10mM Tris-HCl pH 7.4, 10mM NaCl, 3mM $MgCl_2$, 0.5% (v/v) Triton X-100) for 5 minutes on ice followed by successive washes in ice cold PBS. Slides were fixed as above, stained with primary antibodies at 37°C for 20 min, then stained with a anti-mouse or anti-rabbit secondary antibody for 20 min (Molecular Probes) at 37°C. Primary antibodies used were mouse anti-myc (Cell Signaling) and rabbit anti-(pSer/pThr)Gln (Cell Signaling). Images were collected on a Axioplan2 microscope (Carl Zeiss) and processed using OpenLab software (Improvision).

Coordinates

The atomic coordinates and structure factors have been deposited in the Protein Data Bank (Accession code 1T15).

Table 4.1. Summary of crystallographic analysis. Details of the crystallization and structure determination are provided in the supplementary information. $^{*}R_{sym} = \Sigma_j | \langle I \rangle - I_j | / \Sigma \langle I \rangle$ where I_j is the intensity of the j^{th} reflection and $\langle I \rangle$ is the average intensity. $^{\S}R_{work} = \Sigma_{hkl} | F_{obs} - F_{calc} | / \Sigma_{hkl} F_{obs}$, where R_{free} is equivalent to R_{work} but is calculated for a randomly chosen 5% of reflections omitted from the refinement process.

Data Collection:	
Space group	$P3_221$
Unit cell dimensions	$a = b = 65.8$ Å, $c = 93.1$ Å,
	$\alpha = \beta = 90°$, $\gamma = 120°$
Resolution range (Å)	15.0-1.85
Completeness (%)	93.9
Total observations	165,151
Unique reflections	19,219
Average $I/\sigma(I)$	35.6
R_{sym} * (%)	5.4
Model refinement:	
Resolution (Å)	15.0-1.85
No. of reflections (free)	18,225 (911)
R_{work}/R_{free} § (%)	20.6/22.2
No. of protein atoms	1,750
No. of water atoms	157
rms deviations	
bonds (Å)	0.01
angles (°)	1.35

Figures

Figure 4.1. Structure of the BRCA1 tandem BRCT domains:BACH1 phosphopeptide complex.

(A) Ribbons representation of the BRCA1 tandem BRCT domains in complex with the pSer-containing BACH1 peptide shown as stick representation in yellow. The BACH1 phosphopeptide binds at the interface between the two BRCT repeats. The secondary-structure elements in BRCT2 are labelled 'prime' to differentiate them from the secondary-structure elements in BRCT1. The BRCT inter-domain liker is shown in green. Areas of 3_{10}-helix are not labelled.

(B) Electron density map ($2F_o$-F_c) covering the BACH1 phosphopeptide.

Figure 4.1 Continued.

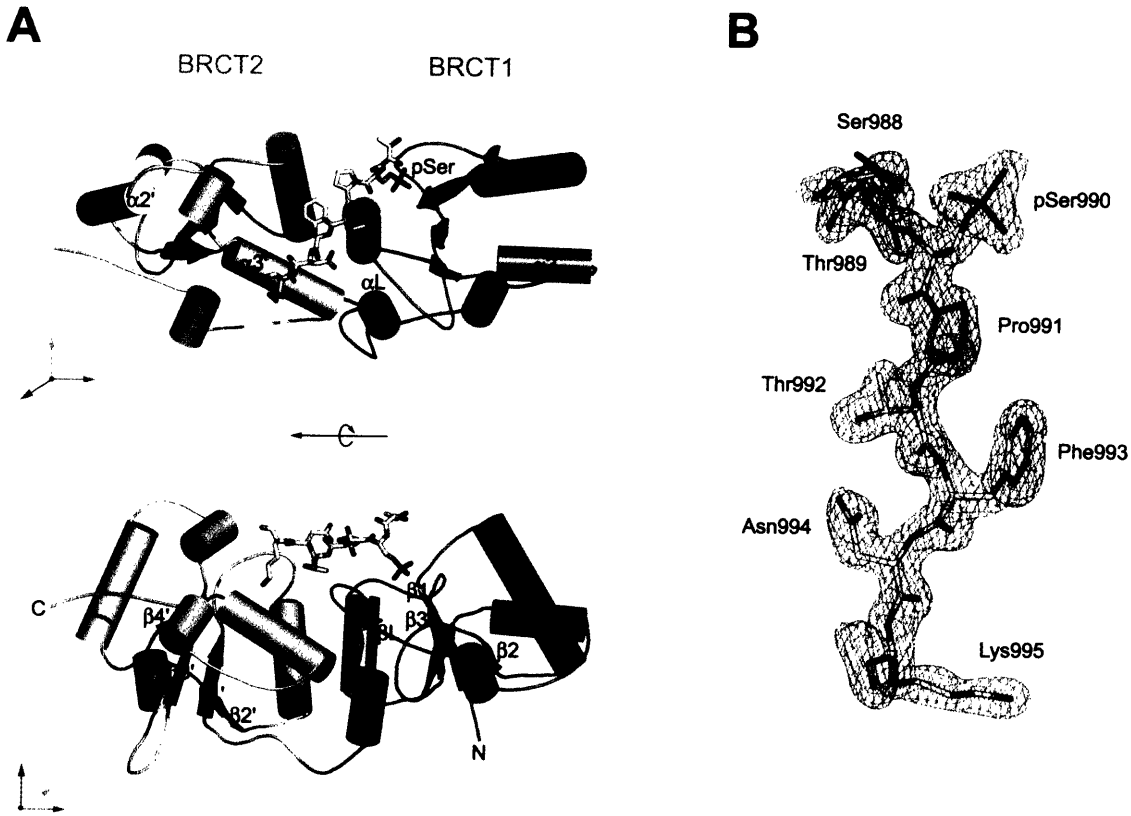

Figure 4.2. BRCA1 BRCT cancer-linked mutations and sequence conservation in relation to the BACH1 phosphopeptide binding-site.

(A) A molecular surface representation of BRCA1 tandem BRCT domains showing how the cancer-associated mutations S1655F, D1692Y, C1697R, R1699Q, S1715R, M1775R and Y1853X cluster with respect to the phosphopeptide binding-site. BRCT1 is colored blue, BRCT2 is colored grey, and the mutations are colored red, except for S1655 which is colored green as its cancer predisposition has not been confirmed by pedigree analysis.

(B) Comparison of the front and back views of the molecular surface showing the clustering of residues (magenta) conserved in human, chimp, mouse, rat, chicken and Xenopus BRCA1 tandem BRCT domains. The BACH1 peptide binds in a conserved phosphopeptide binding-groove.

Figure 4.2 Continued.

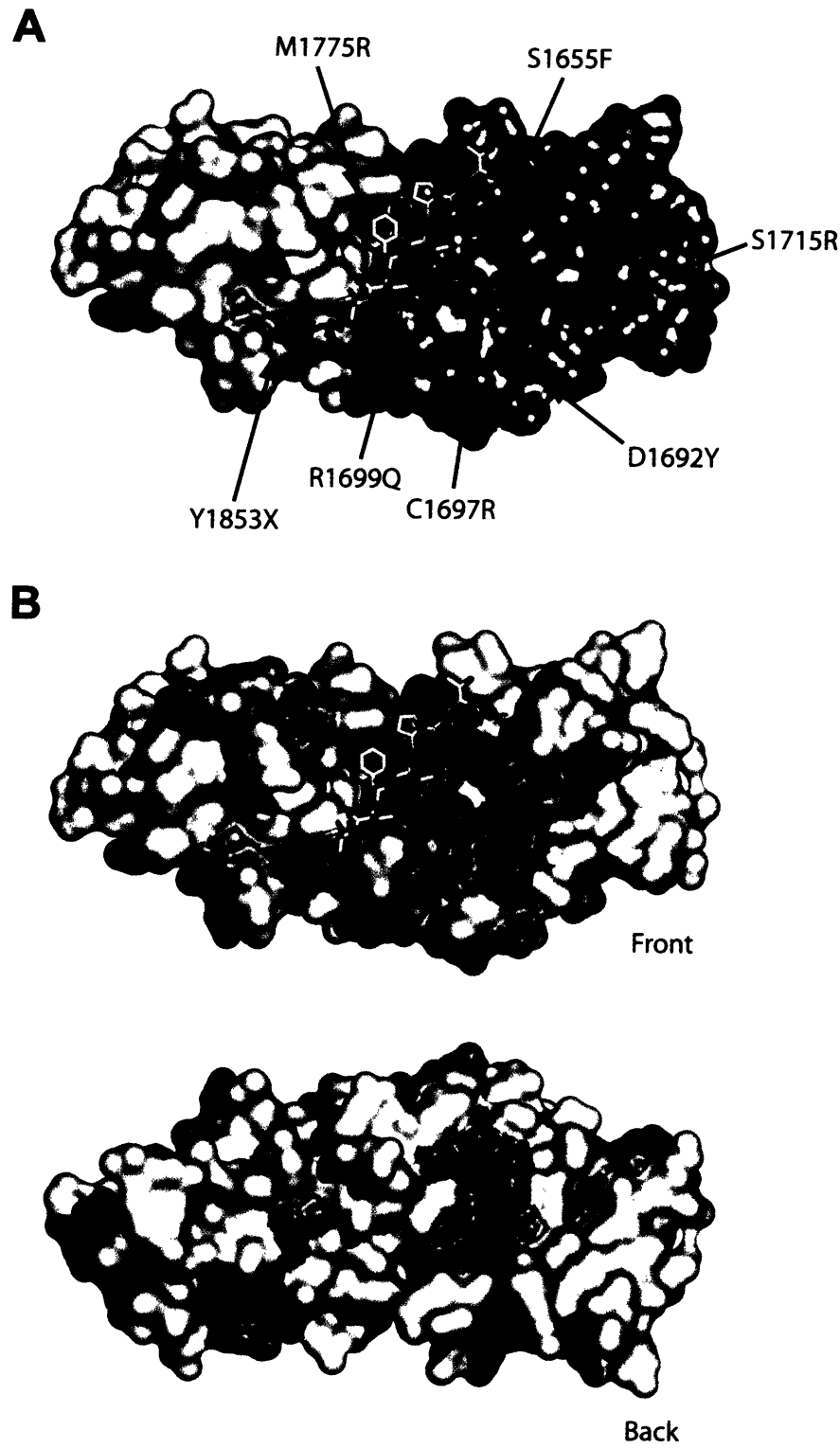

Figure 4.3. Functional effects of tandem BRCT domain mutations.

(A) Schematic representation of protein-peptide contacts between BRCA1 tandem BRCT domains and the BACH1 phosphopeptide. Hydrogen bonds, Van der Waals interactions and water molecules are denoted by dashed lines, pink crescents, and green circles respectively.

(B) The wild-type and mutant myc-tagged BRCA1 tandem BRCT domain constructs containing the indicated mutations were analysed for binding to a bead-immobilized optimal tandem BRCT domain-interacting phosphopeptide, YDIpSQVFPF, or its non-phosphorylated counterpart. The weak phospho-independent binding of the R1699Q mutant was observed using 10-fold more sample input than used in the other lanes.

(C) U2OS cells transfected with wild-type and mutant myc-tagged BRCA1 tandem BRCT domain constructs were analysed for association with endogenous BACH1.

Figure 4.3 Continued.

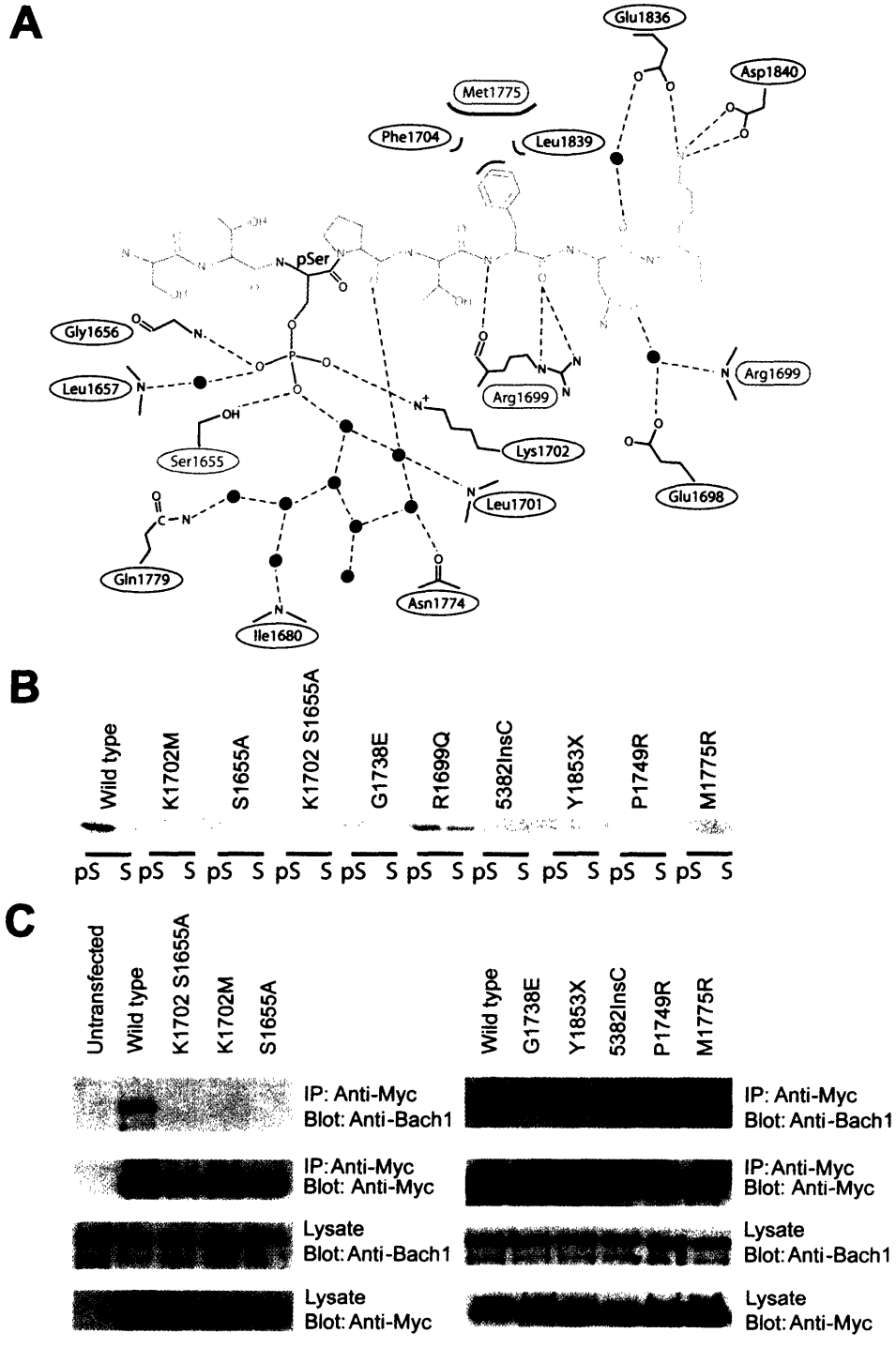

Figure 4.4. The Phe +3 position of the BACH1 phosphopeptide is essential for BRCA1 tandem BRCT domain binding-specificity.

(A) Residues Phe 1704, Met 1775, and Leu 1704 from BRCA1 tandem BRCT domains form a hydrophobic pocket to accommodate the Phe +3 position of the BACH1 phosphopeptide.

(B) Superposition of the crystal structure of BRCA1 M1775R tandem BRCT domain mutant [85] with the wild-type:BACH1 phosphopeptide complex reveals that this mutation occludes the BACH1 Phe +3 position.

(C) BRCA1 wild type tandem BRCT domains and the M1775R mutant binding to a BACH1 phosphopeptide spot array. The M1775R mutant spot blot was performed using 10 times the amount of protein and was exposed to film for a significantly longer amount of time than the wild-type protein.

Figure 4.4 Continued.

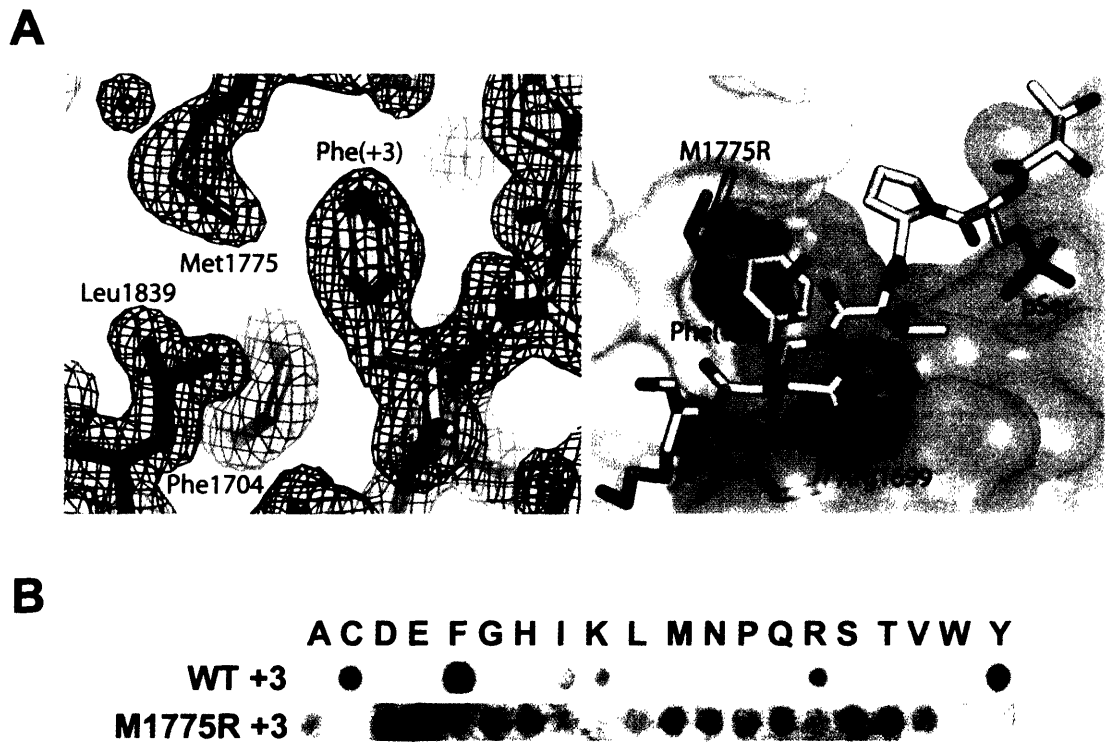

Figure 4.5. Localization of the BRCA1-BRCT domains to nuclear phosphoproteins.

(A) Localization of wild-type, M1775R, or K1702M/S1655A versions of myc-tagged BRCA1 tandem BRCT domains in un-irradiated U2OS cells prior to (left panels) or following (right panels) extraction using Triton X-100-containing buffers. Bars indicate 25 μm.

(B) Localization following Triton X-100 extraction as in (a) two hours following exposure of cells to 10 Gy of γ-radiation. Extracted cells were also stained using an anti-pSer/pThr-Gln epitope antibody that recognizes the phosphorylation motif generated by the DNA damage-response kinases ATM and ATR. Bars indicate 10 μm.

Figure 4.5 Continued.

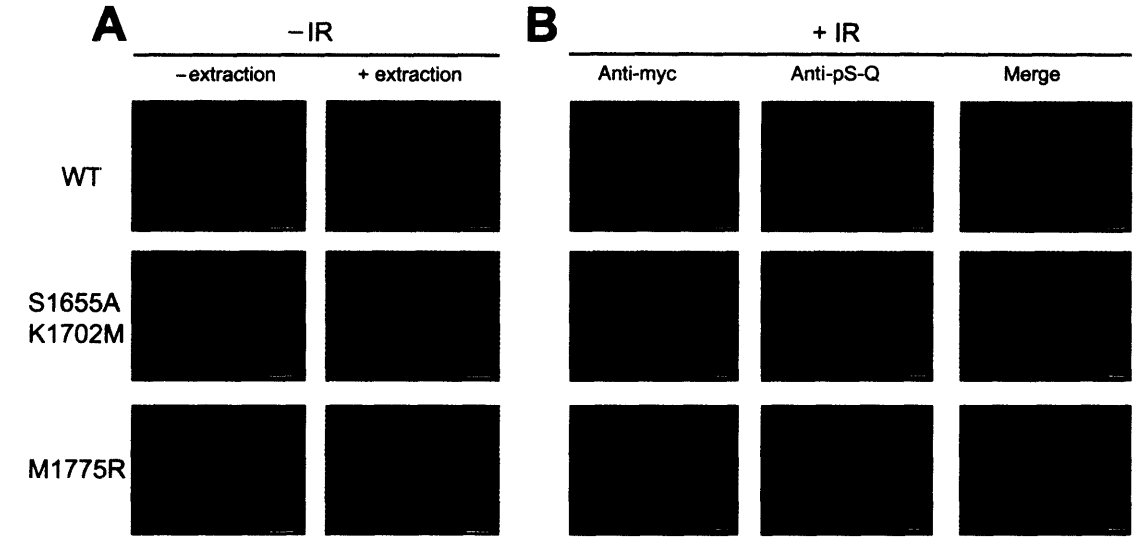

Chapter 5

Future Directions

Multiple pathways in cellular responses to DNA damage

The results presented here have detailed independent discoveries of the requirement of MK2 in the DNA damage signaling pathway and have identified the PTIP and BRCA1 BRCT domains as a new class of phospho-binding domains that interact with proteins phosphorylated by ATM and ATR in response to DNA damage. In addition, the screening techniques developed will help facilitate further advances in the kinase signaling field. The determination of the optimal phosphorylation motif of kinases will continue to provide important data on kinases of interest and help identify their potential downstream targets. The kinase motif data will prove even more valuable as an increasing amount of computational biology research is performed. The identification of posttranslational modification specific binding domains will continue to be an important and exciting area of research. The screen discussed here is one of the only proven approaches to directly identify specific phosphorlyation dependent interactions. Work is already in progress to modify our screen to isolate domains that recognize additional posttranslational modifications, such as methyl arginine.

The relationship of the p38/MK2 pathway to the ATR/CHK1 and ATM/CHK2 pathways

It is not clear why cells have evolved three seeminly parallel pathways that respond to DNA damage. If there are multiple parallel pathways functioning, as the current data suggests, these pathways may not be active at similar locations, times or intensities within the cell. Recent data have emerged that suggest both

the p38/MK2 and the ATR/CHK1 pathways are required for the cellular response to DNA lesions caused by UV light or chemotherapeutic agents [67, 107]. It will be necessary to determine both the temporal and spatial kinetics for each of these pathways. Do cells require activation of multiple pathways for the full checkpoint response, or is the p38/MK2 pathway somehow inseparably integrated with these other pathways where inhibition of one component could affect the activation of other members? It appears more likely that the activation of redundant pathways is required because the inhibition of p38 or MK2 does not appear to affect CHK1 activation [107, 117, 118]. It remains unclear how CHK1 is unable to regulate CDC25A levels and generate the 14-3-3 binding sites on CDC25B/C without active MK2. It is also unclear how MK2 is unable to regulate CDC25A and generate the 14-3-3 binding sites on CDC25B/C without active CHK1 [27, 117]. Based on the current motif data, the regulation of CDC25B/C appears to be one convergent point for MK2 and CHK1 in the DNA damage checkpoint signaling pathway. Before the discovery that MK2 plays a critical role in DNA damage signaling, a significant amount of the CHK1 data was generated by using UCN-01 to inhibit CHK1. In fact, UCN-01 inhibits MK2 in vitro at similar concentrations to those used to inhibit CHK1, and it is likely that UCN-01 inhibits MK2 in vivo (C. Reinhardt, unpublished data). Therefore, results obtained with the use of UCN-O1 may have been misinterpreted [167]. Recently, however, a few labs have used CHK1 RNAi experiments to reproduce some of the UCN-01 data, which supports the requirement of CHK1, as the UCN-01 data implied [91, 118].

However it is possible that CHK1 and MK2 are in the same pathway, and that CHK1 is responsible for the activation of MK2. The best approach to resolve this issue will require examining the activation and/or phosphorylation status of the classic members involved in these pathways (as in Figure 2.2). By using siRNA approaches that deplete MK2, CHK1, or both MK2 and CHK1 in an epistasis study it might be possible to order these signaling events and place them into discrete pathways. For example, if depletion of MK2 does not affect CHK1 activation, but depletion of CHK1 alters MK2 activation, CHK1 would be placed upstream of MK2. This result would explain some conflicting previous work. However, one problem that arises in epistasis studies involving the RNAi depletion of an enzyme, experimental results from a 90% reduction in protein levels may not be sufficient to create the null phenotype required. In spite of this potential problem, loss of the checkpoint when MK2 or CHK1 is RNAi depleted indicates that the kinase activities are impaired and supports the idea that an RNAi epistasis study could generate meaningful results. Additionally, overexpression of MK2 or CHK1 in CHK1 or MK2 RNAi depleted backgrounds, respectively, may reveal compensation that takes place and explain why the activity of one kinase is not sufficient to trigger the checkpoint.

Other types of DNA damage may activate MK2

How does the p38/MK2 pathway respond to different types of DNA damage? The p38/MK2 pathway is activated by cellular stress, but our data suggest that this pathway may also be activated directly by DNA damage or

sensor proteins that localize with damaged DNA. It is unclear how the p38/MK2 pathway is activated by DNA damage. However, in response to alkylating agents, the MMR proteins are required for the activation of p38, and most likely MK2 [163]. p38 and MK2 exist in a heterotrimeric complex located within the nucleus so these kinases are perfectly positioned to be proximal respondes to DNA damage. The p38/MK2 pathway may sense and transmit signals in a similar fashion to ATM/CHK2 and ATR/CHK1, or there may be different undiscovered upstream activators. BRCA1 plays an important, but yet undefined, role in the DNA damage induced activation of CHK1. BRCA1 also plays a role in the taxol mediated activation of p38 [230]. Is BRCA1 also required for the DNA damage dependent activation of p38/MK2? Are the MRN or 911 complexes involved in the activation of p38/MK2? And if so, are ATM/ATR also involved in the p38 mediated activation of MK2? It would also be interesting to determine if there are differences in MK2 activation or target phosphorylation based on the type of DNA lesion encountered. Specific pathway activation data, after DNA damage, may provide insight into what types of cancers depend more heavily on different repair pathways or kinases for proliferation. Inhibiting critical nodes in these networks may prove more tractable than the current approaches which may not sufficiently account for redundant signaling mechanisms, thus making certain pathways more sensitive to inhibition. In the future, answers to these questions may more efficiently direct cancer treatment choices and improve patient survival rates.

Additional MK2 functions and targets

What are the other targets of MK2 in the DNA damage response pathway? MK2 appears to phosphorylate the same targets as CHK1 and CHK2 following DNA damage. However MK2 regulates multiple pathways at the transcriptional level and there are only a few identified roles for CHK1 and CHK2 regulating gene expression after DNA damage. Recently, Ueda et al. [231] used comparative mass spectrometry analysis of protein samples to identify substrates of MK2. It would be interesting to use similar genomic and proteomic approaches to identify additional transcriptional and protein targets of MK2, including those that are p53 dependent and independent.

BRCA1 and the requirement of its BRCT domains

The understanding of the multiple roles BRCA1 plays in the cellular response to DNA damage remains incomplete. BRCA1 appears to function both upstream and downstream of ATM/CHK2 and ATR/CHK1. How is this possible? One explanation is an autocatalytic activation loop, where a kinase reaches a low level of activity due to DNA damage, which in turn activates BRCA1 and facilitates further activation of the kinase. It is unknown how the phosphorylation of BRCA1 is involved in its activation of the checkpoint pathways. A few non-mutually exclusive ideas are that phosphorylation could alter the structure of BRCA1 exposing important domains, increase the activity of the RING finger domain or the BRCT domains of BRCA1, or improve the ability of BRCA1 to act as a protein scaffold localizing substrates in proximity to the relevant kinases.

Is the role of BRCA1 in checkpoint signaling dependent on the phospho-binding function of its BRCT domains, as recent data suggests [19, 20, 217]? It is unclear how BRCA1 uses its BRCT domains to propagate signals in the DNA damage response. How do the cancer-associated mutations found in BRCA1 disrupt this as yet undefined role? While BRCA1 BRCT domain destabilization is one way function is lost, clearly not all BRCA1 BRCT domain mutations destabilize the protein [85, 86, 232]. What is the function of the BRCA1-BACH1 interaction that is lost in BRCA1 cancer-associated mutations? Highlighting the importance of this BRCA1-BACH1 interaction, there are also cancer-associated mutations detected in BACH1 [224]. It is not known how the cancer-associated mutations that do not disrupt phospho-binding prevent BRCA1 BRCT domain function. Is there another surface on the BRCT domains that is required for certain protein-protein interactions? It is likely that the phospho-binding pocket of the BRCT domains only provides some of the necessary requirements of ligand specificity and binding. One BRCA1 BRCT domain mutation, M1775R, appears to alter phospho-binding specificity. It is not clear what interactions are lost and what new ligands result from this mutation [86]. In addition to ATM and ATR that generate the phospho-motif recognized by the BRCT domains, the PTIP and BRCA1 BRCT domains show phospho-binding selectivity towards a Pro in the +1 position. It is possible that p38 also phosphorylates BRCT binding partners, such as BACH1, in the DNA damage response pathway.

Multiple functions of BRCT domain-containing proteins

The identification and crystallization of the BRCA1 BRCT domains provides another example of the growing family of pSer/pThr binding domains. Interestingly these domains are all structurally distinct supporting the idea that phospho-binding developed as a type of convergent evolution [9, 22]. Though BRCT domains are known protein-protein interaction modules present in many DNA damage response and cell cycle checkpoint proteins, based on experimental data and crystal structure based sequence alignments, it appears that only a subset of BRCT domain posses a phospho-binding capability [86, 233]. It is not known how the phospho-binding motifs differ between BRCT domains and if the short phospho-motif is the only means by which BRCT domains interact with proteins. As predicted from the sequence alignments, little if any phospho-binding was detected for 53BP1 or the PTIP N-terminal pair, further suggesting that the phosphopeptide-binding function is present in only a subset of tandem BRCT domains. The functions of the nonphospho-binding and phospho-binding BRCT domain proteins remain to be determined. For example human PTIP contains 5 BRCT domains, only two of which posses a phospho-binding function; the function of the other three is yet undefined. The BRCT domains probably mediate nonphospho-dependent protein interactions as well, just like the FHA domains [234]. Though BRCT domains often exist in tandem pairs, there are multiple examples of proteins that contain only one BRCT domain or several BRCT domains. Based on crystal structure data BRCT domains can dimerize [86, 233]. As BRCT domains are commonly found in

proteins that function in the cell cycle, one possibility is that the proteins use the BRCT domains as a common adaptor to facilitate necessary interactions, whether phospho-dependent or phospho-independent.

The role of PTIP in the DNA damage response pathway

PITP shares many similarities to other proteins in the DNA damage response pathway; PTIP contains BRCT domains, PTIP interacts with other DNA damage response proteins, PTIP forms nuclear foci following IR, and (like ATR, CHK1 and BRCA1) the PTIP knockout mouse is not viable [202]. What is the exact role for PTIP in the DNA damage response pathway? PTIP may be involved with S-phase progression and the recovery of stalled replication forks, like ATR and CHK1. Based on the data available, PTIP does appear to play an essential role for progression into mitosis, but it is unclear if that role is in S-phase or G2, as cells lacking PITP do not display an S-phase entry defect [202]. Recent data also suggest that PTIP may have multiple splice forms [165]. While PITP interacts with 53BP1 to form nuclear foci following DNA damage, the functions of this interaction in unknown [19]. In addition, in vivo association of full-length FLAG-PTIP with HA-53BP1 increases after IR treatment. If PTIP is involved in the S-phase response, what then is the role of 53BP1?

Multiple pathways in cellular responses to DNA damage

While much has been learned during my time at MIT, several intriguing opportunities exist to improve our understanding of how protein-protein interactions function in the DNA damage signaling response network. Determining the exact role of MK2 in the DNA damage response pathway and understanding how the BRCT domain-containing proteins function in signal transduction pathways will be crucial. Recently, much research has been focused on the development of drugs that inhibit DNA repair as chemosensitizing compounds [67]. Because our discoveries expand the molecular understanding as to how kinases signal to phospho-binding domains in the DNA damage response signaling network they also provide novel validated targets for the development of chemosensitizing therapeutic agents.

References

1. Zhou, B.B. and S.J. Elledge, *The DNA damage response: putting checkpoints in perspective.* Nature, 2000. **408**(6811): p. 433-9.
2. Abraham, R.T., *Cell cycle checkpoint signaling through the ATM and ATR kinases.* Genes Dev, 2001. **15**(17): p. 2177-96.
3. Bulavin, D.V., et al., *Dual phosphorylation controls Cdc25 phosphatases and mitotic entry.* Nat Cell Biol, 2003. **5**(6): p. 545-51.
4. Walworth, N.C., *DNA damage: Chk1 and Cdc25, more than meets the eye.* Curr Opin Genet Dev, 2001. **11**(1): p. 78-82.
5. Yaffe, M.B., *How do 14-3-3 proteins work?-- Gatekeeper phosphorylation and the molecular anvil hypothesis.* FEBS Lett, 2002. **513**(1): p. 53-7.
6. Venter, J.C., et al., *The sequence of the human genome.* Science, 2001. **291**.
7. Pawson, T. and P. Nash, *Assembly of cell regulatory systems through protein interaction domains.* Science, 2003. **300**(5618): p. 445-52.
8. Manning, B.D. and L.C. Cantley, *Hitting the target: emerging technologies in the search for kinase substrates.* Sci STKE, 2002. **2002**(162): p. PE49.
9. McLachlin, D.T. and B.T. Chait, *Analysis of phosphorylated proteins and peptides by mass spectrometry.* Curr Opin Chem Biol, 2001. **5**(5): p. 591-602.
10. Yaffe, M.B., et al., *A motif-based profile scanning approach for genome-wide prediction of signaling pathways.* Nat Biotechnol, 2001. **19**(4): p. 348-53.
11. Songyang, Z. and L.C. Cantley, *The use of peptide library for the determination of kinase peptide substrates.* Methods Mol Biol, 1998. **87**: p. 87-98.
12. Ficarro, S.B., et al., *Phosphoproteome analysis by mass spectrometry and its application to Saccharomyces cerevisiae.* Nat Biotechnol, 2002. **20**(3): p. 301-5.
13. Pawson, T. and J.D. Scott, *Signaling through scaffold, anchoring, and adaptor proteins.* Science, 1997. **278**(5346): p. 2075-80.
14. Kuriyan, J. and D. Cowburn, *Modular peptide recognition domains in eukaryotic signaling.* Annu Rev Biophys Biomol Struct, 1997. **26**: p. 259-88.
15. Yaffe, M.B., *Phosphotyrosine-binding domains in signal transduction.* Nat Rev Mol Cell Biol, 2002. **3**(3): p. 177-86.
16. Yaffe, M.B. and L.C. Cantley, *Mapping specificity determinants for protein-protein association using protein fusions and random peptide libraries.* Methods Enzymol, 2000. **328**: p. 157-70.
17. Yaffe, M.B. and A.E. Elia, *Phosphoserine/threonine-binding domains.* Curr Opin Cell Biol, 2001. **13**(2): p. 131-8.
18. Elia, A.E., L.C. Cantley, and M.B. Yaffe, *Proteomic screen finds pSer/pThr-binding domain localizing Plk1 to mitotic substrates.* Science, 2003. **299**(5610): p. 1228-31.

19. Manke, I.A., et al., *BRCT repeats as phosphopeptide-binding modules involved in protein targeting.* Science, 2003. **302**(5645): p. 636-9.
20. Yu, X., et al., *The BRCT domain is a phospho-protein binding domain.* Science, 2003. **302**(5645): p. 639-42.
21. Yaffe, M.B., et al., *The structural basis for 14-3-3:phosphopeptide binding specificity.* Cell, 1997. **91**(7): p. 961-71.
22. Fantl, W.J., et al., *Activation of Raf-1 by 14-3-3 proteins.* Nature, 1994. **371**(6498): p. 612-4.
23. Pallas, D.C., et al., *Association of polyomavirus middle tumor antigen with 14-3-3 proteins.* Science, 1994. **265**(5171): p. 535-7.
24. Freed, E., et al., *Binding of 14-3-3 proteins to the protein kinase Raf and effects on its activation.* Science, 1994. **265**(5179): p. 1713-6.
25. Yaffe, M.B. and S.J. Smerdon, *PhosphoSerine/threonine binding domains: you can't pSERious?* Structure, 2001. **9**(3): p. R33-8.
26. Conklin, D.S., K. Galaktionov, and D. Beach, *14-3-3 proteins associate with cdc25 phosphatases.* Proc Natl Acad Sci U S A, 1995. **92**(17): p. 7892-6.
27. Bulavin, D.V., S.A. Amundson, and A.J. Fornace, *p38 and Chk1 kinases: different conductors for the G(2)/M checkpoint symphony.* Curr Opin Genet Dev, 2002. **12**(1): p. 92-7.
28. Kumagai, A., P.S. Yakowec, and W.G. Dunphy, *14-3-3 proteins act as negative regulators of the mitotic inducer Cdc25 in Xenopus egg extracts.* Mol Biol Cell, 1998. **9**(2): p. 345-54.
29. Lopez-Girona, A., et al., *Nuclear localization of Cdc25 is regulated by DNA damage and a 14-3-3 protein.* Nature, 1999. **397**(6715): p. 172-5.
30. Hofmann, K. and P. Bucher, *The FHA domain: a putative nuclear signalling domain found in protein kinases and transcription factors [letter].* Trends Biochem Sci, 1995. **20**(9): p. 347-9.
31. Stone, J.M., et al., *Interaction of a protein phosphatase with an Arabidopsis serine-threonine receptor kinase.* Science, 1994. **266**(5186): p. 793-5.
32. Durocher, D., et al., *The molecular basis of FHA Domain:phosphopeptide binding specificity and implications for phosphodependent signaling mechanisms.* Mol Cell, 2000.
33. Ahn, J. and C. Prives, *Checkpoint kinase 2 (Chk2) monomers or dimers phosphorylate Cdc25C after DNA damage regardless of threonine 68 phosphorylation.* J Biol Chem, 2002. **277**(50): p. 48418-26.
34. McGowan, C.H., *Checking in on Cds1 (Chk2): A checkpoint kinase and tumor suppressor.* Bioessays, 2002. **24**(6): p. 502-11.
35. Ahn, J.Y., et al., *Phosphorylation of threonine 68 promotes oligomerization and autophosphorylation of the Chk2 protein kinase via the forkhead-associated domain.* J Biol Chem, 2002. **277**(22): p. 19389-95.
36. Xu, X., L.M. Tsvetkov, and D.F. Stern, *Chk2 activation and phosphorylation-dependent oligomerization.* Mol Cell Biol, 2002. **22**(12): p. 4419-32.

37. Li, J., et al., *Structural and functional versatility of the FHA domain in DNA-damage signaling by the tumor suppressor kinase Chk2.* Mol Cell, 2002. **9**(5): p. 1045-54.
38. Obenauer, J.C., L.C. Cantley, and M.B. Yaffe, *Scansite 2.0: Proteome-wide prediction of cell signaling interactions using short sequence motifs.* Nucleic Acids Res, 2003. **31**(13): p. 3635-41.
39. Wood, R.D., *DNA repair in eukaryotes.* Annu Rev Biochem, 1996. **65**: p. 135-67.
40. Sinha, R.P. and D.P. Hader, *UV-induced DNA damage and repair: a review.* Photochem Photobiol Sci, 2002. **1**(4): p. 225-36.
41. Meira, L.B., et al., *Cancer predisposition in mutant mice defective in multiple genetic pathways: uncovering important genetic interactions.* Mutat Res, 2001. **477**(1-2): p. 51-8.
42. Falck, J., J. Coates, and S.P. Jackson, *Conserved modes of recruitment of ATM, ATR and DNA-PKcs to sites of DNA damage.* Nature, 2005. **434**(7033): p. 605-11.
43. van den Bosch, M., P.H. Lohman, and A. Pastink, *DNA double-strand break repair by homologous recombination.* Biol Chem, 2002. **383**(6): p. 873-92.
44. Pfeiffer, P., et al., *Pathways of DNA double-strand break repair and their impact on the prevention and formation of chromosomal aberrations.* Cytogenet Genome Res, 2004. **104**(1-4): p. 7-13.
45. Abraham, R.T., *Checkpoint signalling: focusing on 53BP1.* Nat Cell Biol, 2002. **4**(12): p. E277-9.
46. Zhou, B.B. and S.J. Elledge, *The DNA damage response: putting checkpoints in perspective.* Nature, 2000. **408**(6811): p. 433-9.
47. Zhang, J., et al., *Chk2 phosphorylation of BRCA1 regulates DNA double-strand break repair.* Mol Cell Biol, 2004. **24**(2): p. 708-18.
48. Wang, Y., et al., *BASC, a super complex of BRCA1-associated proteins involved in the recognition and repair of aberrant DNA structures.* Genes Dev, 2000. **14**(8): p. 927-39.
49. Iliakis, G., et al., *Mechanisms of DNA double strand break repair and chromosome aberration formation.* Cytogenet Genome Res, 2004. **104**(1-4): p. 14-20.
50. Daboussi, F., et al., *DNA double-strand break repair signalling: the case of RAD51 post-translational regulation.* Cell Signal, 2002. **14**(12): p. 969-75.
51. Scully, R. and D.M. Livingston, *In search of the tumour-suppressor functions of BRCA1 and BRCA2.* Nature, 2000. **408**(6811): p. 429-32.
52. Stojic, L., R. Brun, and J. Jiricny, *Mismatch repair and DNA damage signalling.* DNA Repair (Amst), 2004. **3**(8-9): p. 1091-101.
53. Pastwa, E. and J. Blasiak, *Non-homologous DNA end joining.* Acta Biochim Pol, 2003. **50**(4): p. 891-908.
54. Collis, S.J., et al., *The life and death of DNA-PK.* Oncogene, 2005. **24**(6): p. 949-61.
55. Lage, C., et al., *New insights on how nucleotide excision repair could remove DNA adducts induced by chemotherapeutic agents and psoralens*

plus UV-A (PUVA) in Escherichia coli cells. Mutat Res, 2003. **544**(2-3): p. 143-57.
56. Costa, R.M., et al., *The eukaryotic nucleotide excision repair pathway.* Biochimie, 2003. **85**(11): p. 1083-99.
57. Cleaver, J.E., R.R. Laposa, and C.L. Limoli, *DNA replication in the face of (In)surmountable odds.* Cell Cycle, 2003. **2**(4): p. 310-5.
58. Ura, K. and J.J. Hayes, *Nucleotide excision repair and chromatin remodeling.* Eur J Biochem, 2002. **269**(9): p. 2288-93.
59. Hanawalt, P.C., J.M. Ford, and D.R. Lloyd, *Functional characterization of global genomic DNA repair and its implications for cancer.* Mutat Res, 2003. **544**(2-3): p. 107-14.
60. Sarasin, A., *The molecular pathways of ultraviolet-induced carcinogenesis.* Mutat Res, 1999. **428**(1-2): p. 5-10.
61. Bartek, J., C. Lukas, and J. Lukas, *Checking on DNA damage in S phase.* Nat Rev Mol Cell Biol, 2004. **5**(10): p. 792-804.
62. Melo, J. and D. Toczyski, *A unified view of the DNA-damage checkpoint.* Curr Opin Cell Biol, 2002. **14**(2): p. 237-45.
63. Zabkiewicz, J. and A.R. Clarke, *DNA damage-induced apoptosis: insights from the mouse.* Biochim Biophys Acta, 2004. **1705**(1): p. 17-25.
64. Parrilla-Castellar, E.R., S.J. Arlander, and L. Karnitz, *Dial 9-1-1 for DNA damage: the Rad9-Hus1-Rad1 (9-1-1) clamp complex.* DNA Repair (Amst), 2004. **3**(8-9): p. 1009-14.
65. Bartek, J. and J. Lukas, *DNA repair: Damage alert.* Nature, 2003. **421**(6922): p. 486-8.
66. Sorensen, C.S., et al., *ATR, Claspin and the Rad9-Rad1-Hus1 complex regulate Chk1 and Cdc25A in the absence of DNA damage.* Cell Cycle, 2004. **3**(7): p. 941-5.
67. Ljungman, M., *Dial 9-1-1 for p53: mechanisms of p53 activation by cellular stress.* Neoplasia, 2000. **2**(3): p. 208-25.
68. Karanjawala, Z.E. and M.R. Lieber, *DNA damage and aging.* Mech Ageing Dev, 2004. **125**(6): p. 405-16.
69. Mirzoeva, O.K. and J.H. Petrini, *DNA damage-dependent nuclear dynamics of the Mre11 complex.* Mol Cell Biol, 2001. **21**(1): p. 281-8.
70. Shiloh, Y., *ATM and related protein kinases: safeguarding genome integrity.* Nat Rev Cancer, 2003. **3**(3): p. 155-68.
71. Carney, J.P., et al., *The hMre11/hRad50 protein complex and Nijmegen breakage syndrome: linkage of double-strand break repair to the cellular DNA damage response.* Cell, 1998. **93**(3): p. 477-86.
72. Petrini, J.H., *The Mre11 complex and ATM: collaborating to navigate S phase.* Curr Opin Cell Biol, 2000. **12**(3): p. 293-6.
73. Kobayashi, J., et al., *NBS1 localizes to gamma-H2AX foci through interaction with the FHA/BRCT domain.* Curr Biol, 2002. **12**(21): p. 1846-51.
74. Tauchi, H., et al., *The forkhead-associated domain of NBS1 is essential for nuclear foci formation after irradiation but not essential for*

hRAD50[middle dot]hMRE11[middle dot]NBS1 complex DNA repair activity. J Biol Chem, 2001. **276**(1): p. 12-5.
75. Petrini, J.H., *S-phase functions of the Mre11 complex.* Cold Spring Harb Symp Quant Biol, 2000. **65**: p. 405-11.
76. Venkitaraman, A.R., *Cancer susceptibility and the functions of BRCA1 and BRCA2.* Cell, 2002. **108**(2): p. 171-82.
77. Thomas, J.E., et al., *Induction of phosphorylation on BRCA1 during the cell cycle and after DNA damage.* Cell Growth Differ, 1997. **8**(7): p. 801-9.
78. Scully, R., et al., *Dynamic changes of BRCA1 subnuclear location and phosphorylation state are initiated by DNA damage.* Cell, 1997. **90**(3): p. 425-35.
79. Foray, N., et al., *A subset of ATM- and ATR-dependent phosphorylation events requires the BRCA1 protein.* Embo J, 2003. **22**(11): p. 2860-71.
80. Yarden, R.I., et al., *BRCA1 regulates the G2/M checkpoint by activating Chk1 kinase upon DNA damage.* Nat Genet, 2002. **30**(3): p. 285-9.
81. Scully, R., et al., *Genetic analysis of BRCA1 function in a defined tumor cell line.* Mol Cell, 1999. **4**(6): p. 1093-9.
82. Moynahan, M.E., et al., *Brca1 controls homology-directed DNA repair.* Mol Cell, 1999. **4**(4): p. 511-8.
83. Starita, L.M. and J.D. Parvin, *The multiple nuclear functions of BRCA1: transcription, ubiquitination and DNA repair.* Curr Opin Cell Biol, 2003. **15**(3): p. 345-50.
84. Williams, R.S., R. Green, and J.N. Glover, *Crystal structure of the BRCT repeat region from the breast cancer-associated protein BRCA1.* Nat Struct Biol, 2001. **8**(10): p. 838-42.
85. Williams, R.S. and J.N. Glover, *Structural consequences of a cancer-causing BRCA1-BRCT missense mutation.* J Biol Chem, 2003. **278**(4): p. 2630-5.
86. Clapperton, J.A., et al., *Structure and mechanism of BRCA1 BRCT domain recognition of phosphorylated BACH1 with implications for cancer.* Nat Struct Mol Biol, 2004. **11**(6): p. 512-8.
87. Schultz, L.B., et al., *p53 binding protein 1 (53BP1) is an early participant in the cellular response to DNA double-strand breaks.* J Cell Biol, 2000. **151**(7): p. 1381-90.
88. Rappold, I., et al., *Tumor suppressor p53 binding protein 1 (53BP1) is involved in DNA damage-signaling pathways.* J Cell Biol, 2001. **153**(3): p. 613-20.
89. O'Neill, T., et al., *Utilization of oriented peptide libraries to identify substrate motifs selected by ATM.* J Biol Chem, 2000. **275**(30): p. 22719-27.
90. O'Neill, T., et al., *Determination of substrate motifs for human Chk1 and hCds1/Chk2 by the oriented peptide library approach.* J Biol Chem, 2002. **277**(18): p. 16102-15.
91. Kawabe, T., *G2 checkpoint abrogators as anticancer drugs.* Mol Cancer Ther, 2004. **3**(4): p. 513-9.

92. Xu, B., et al., *Two molecularly distinct G(2)/M checkpoints are induced by ionizing irradiation.* Mol Cell Biol, 2002. **22**(4): p. 1049-59.
93. Zhao, H. and H. Piwnica-Worms, *ATR-mediated checkpoint pathways regulate phosphorylation and activation of human Chk1.* Mol Cell Biol, 2001. **21**(13): p. 4129-39.
94. Cortez, D., et al., *ATR and ATRIP: partners in checkpoint signaling.* Science, 2001. **294**(5547): p. 1713-6.
95. O'Driscoll, M., et al., *A splicing mutation affecting expression of ataxia-telangiectasia and Rad3-related protein (ATR) results in Seckel syndrome.* Nat Genet, 2003. **33**(4): p. 497-501.
96. Liu, Q., et al., *Chk1 is an essential kinase that is regulated by Atr and required for the G(2)/M DNA damage checkpoint.* Genes Dev, 2000. **14**(12): p. 1448-59.
97. Wang, J.Y., *Regulation of cell death by the Abl tyrosine kinase.* Oncogene, 2000. **19**(49): p. 5643-50.
98. Wang, B., et al., *A role for 14-3-3 tau in E2F1 stabilization and DNA damage-induced apoptosis.* J Biol Chem, 2004. **279**(52): p. 54140-52.
99. Varon, R., et al., *Nibrin, a novel DNA double-strand break repair protein, is mutated in Nijmegen breakage syndrome.* Cell, 1998. **93**(3): p. 467-76.
100. Ahn, J.Y., et al., *Threonine 68 phosphorylation by ataxia telangiectasia mutated is required for efficient activation of Chk2 in response to ionizing radiation.* Cancer Res, 2000. **60**(21): p. 5934-6.
101. Melchionna, R., et al., *Threonine 68 is required for radiation-induced phosphorylation and activation of Cds1.* Nat Cell Biol, 2000. **2**(10): p. 762-5.
102. Bell, D.W., et al., *Heterozygous germ line hCHK2 mutations in Li-Fraumeni syndrome.* Science, 1999. **286**(5449): p. 2528-31.
103. Hirao, A., et al., *DNA damage-induced activation of p53 by the checkpoint kinase Chk2.* Science, 2000. **287**(5459): p. 1824-7.
104. Chehab, N.H., et al., *Chk2/hCds1 functions as a DNA damage checkpoint in G(1) by stabilizing p53.* Genes Dev, 2000. **14**(3): p. 278-88.
105. Shieh, S.Y., et al., *The human homologs of checkpoint kinases Chk1 and Cds1 (Chk2) phosphorylate p53 at multiple DNA damage-inducible sites.* Genes Dev, 2000. **14**(3): p. 289-300.
106. Roux, P.P. and J. Blenis, *ERK and p38 MAPK-activated protein kinases: a family of protein kinases with diverse biological functions.* Microbiol Mol Biol Rev, 2004. **68**(2): p. 320-44.
107. Bulavin, D.V., et al., *Initiation of a G2/M checkpoint after ultraviolet radiation requires p38 kinase.* Nature, 2001. **411**(6833): p. 102-7.
108. She, Q.B., W.Y. Ma, and Z. Dong, *Role of MAP kinases in UVB-induced phosphorylation of p53 at serine 20.* Oncogene, 2002. **21**(10): p. 1580-9.
109. Pearce, A.K. and T.C. Humphrey, *Integrating stress-response and cell-cycle checkpoint pathways.* Trends Cell Biol, 2001. **11**(10): p. 426-33.
110. Stokoe, D., et al., *The substrate specificity and structure of mitogen-activated protein (MAP) kinase-activated protein kinase-2.* Biochem J, 1993. **296 (Pt 3)**: p. 843-9.

111. Tanoue, T. and E. Nishida, *Molecular recognitions in the MAP kinase cascades.* Cell Signal, 2003. **15**(5): p. 455-62.
112. Cheung, P.C., et al., *Feedback control of the protein kinase TAK1 by SAPK2a/p38alpha.* Embo J, 2003. **22**(21): p. 5793-805.
113. Yang, S.H., A. Galanis, and A.D. Sharrocks, *Targeting of p38 mitogen-activated protein kinases to MEF2 transcription factors.* Mol Cell Biol, 1999. **19**(6): p. 4028-38.
114. Tanoue, T., et al., *Identification of a docking groove on ERK and p38 MAP kinases that regulates the specificity of docking interactions.* Embo J, 2001. **20**(3): p. 466-79.
115. Lehner, M.D., et al., *Mitogen-activated protein kinase-activated protein kinase 2-deficient mice show increased susceptibility to Listeria monocytogenes infection.* J Immunol, 2002. **168**(9): p. 4667-73.
116. Obata, T., G.E. Brown, and M.B. Yaffe, *MAP kinase pathways activated by stress: the p38 MAPK pathway.* Crit Care Med, 2000. **28**(4 Suppl): p. N67-77.
117. Manke, I.A., et al., *MAPKAP kinase-2 is a cell cycle checkpoint kinase that regulates the G2/M transition and S phase progression in response to UV irradiation.* Mol Cell, 2005. **17**(1): p. 37-48.
118. Hirose, Y., et al., *Cooperative function of Chk1 and p38 pathways in activating G2 arrest following exposure to temozolomide.* J Neurosurg, 2004. **100**(6): p. 1060-5.
119. Kishi, H., et al., *Osmotic shock induces G1 arrest through p53 phosphorylation at Ser33 by activated p38MAPK without phosphorylation at Ser15 and Ser20.* J Biol Chem, 2001. **276**(42): p. 39115-22.
120. Mikhailov, A., M. Shinohara, and C.L. Rieder, *Topoisomerase II and histone deacetylase inhibitors delay the G2/M transition by triggering the p38 MAPK checkpoint pathway.* J Cell Biol, 2004. **166**(4): p. 517-26.
121. Kotlyarov, A. and M. Gaestel, *Is MK2 (mitogen-activated protein kinase-activated protein kinase 2) the key for understanding post-transcriptional regulation of gene expression?* Biochem Soc Trans, 2002. **30**(Pt 6): p. 959-63.
122. Ben-Levy, R., et al., *Nuclear export of the stress-activated protein kinase p38 mediated by its substrate MAPKAP kinase-2.* Curr Biol, 1998. **8**(19): p. 1049-57.
123. Kotlyarov, A., et al., *Distinct cellular functions of MK2.* Mol Cell Biol, 2002. **22**(13): p. 4827-35.
124. Korswagen, H.C., *Canonical and non-canonical Wnt signaling pathways in Caenorhabditis elegans: variations on a common signaling theme.* Bioessays, 2002. **24**(9): p. 801-10.
125. McEwen, D.G. and M. Peifer, *Wnt signaling: Moving in a new direction.* Curr Biol, 2000. **10**(15): p. R562-4.
126. Luo, W. and S.C. Lin, *Axin: a master scaffold for multiple signaling pathways.* Neurosignals, 2004. **13**(3): p. 99-113.
127. Salahshor, S. and J.R. Woodgett, *The links between axin and carcinogenesis.* J Clin Pathol, 2005. **58**(3): p. 225-36.

128. Harris, S.L. and A.J. Levine, *The p53 pathway: positive and negative feedback loops.* Oncogene, 2005. **24**(17): p. 2899-908.
129. Martin-Blanco, E., *p38 MAPK signalling cascades: ancient roles and new functions.* Bioessays, 2000. **22**(7): p. 637-45.
130. Kyriakis, J.M. and J. Avruch, *Protein kinase cascades activated by stress and inflammatory cytokines.* Bioessays, 1996. **18**(7): p. 567-77.
131. Rennefahrt, U., et al., *Stress kinase signaling in cancer: fact or fiction?* Cancer Lett, 2005. **217**(1): p. 1-9.
132. Lowes, V.L., N.Y. Ip, and Y.H. Wong, *Integration of signals from receptor tyrosine kinases and g protein-coupled receptors.* Neurosignals, 2002. **11**(1): p. 5-19.
133. Yee, A.S., et al., *The HBP1 transcriptional repressor and the p38 MAP kinase: unlikely partners in G1 regulation and tumor suppression.* Gene, 2004. **336**(1): p. 1-13.
134. Giaccia, A.J. and M.B. Kastan, *The complexity of p53 modulation: emerging patterns from divergent signals.* Genes Dev, 1998. **12**(19): p. 2973-83.
135. Ko, L.J. and C. Prives, *p53: puzzle and paradigm.* Genes Dev, 1996. **10**(9): p. 1054-72.
136. North, S. and P. Hainaut, *p53 and cell-cycle control: a finger in every pie.* Pathol Biol (Paris), 2000. **48**(3): p. 255-70.
137. Zhu, J., et al., *The potential tumor suppressor p73 differentially regulates cellular p53 target genes.* Cancer Res, 1998. **58**(22): p. 5061-5.
138. Chiarle, R., et al., *Increased proteasome degradation of cyclin-dependent kinase inhibitor p27 is associated with a decreased overall survival in mantle cell lymphoma.* Blood, 2000. **95**(2): p. 619-26.
139. Dumaz, N. and D.W. Meek, *Serine15 phosphorylation stimulates p53 transactivation but does not directly influence interaction with HDM2.* Embo J, 1999. **18**(24): p. 7002-10.
140. IVahteristo, P., et al., *p53, CHK2, and CHK1 genes in Finnish families with Li-Fraumeni syndrome: further evidence of CHK2 in inherited cancer predisposition.* Cancer Res, 2001. **61**(15): p. 5718-22.
141. Bartek, J. and J. Lukas, *Mammalian G1- and S-phase checkpoints in response to DNA damage.* Curr Opin Cell Biol, 2001. **13**(6): p. 738-47.
142. Nilsson, I. and I. Hoffmann, *Cell cycle regulation by the Cdc25 phosphatase family.* Prog Cell Cycle Res, 2000. **4**: p. 107-14.
143. Johnson, R.D. and M. Jasin, *Sister chromatid gene conversion is a prominent double-strand break repair pathway in mammalian cells.* Embo J, 2000. **19**(13): p. 3398-407.
144. Painter, R.B. and B.R. Young, *Radiosensitivity in ataxia-telangiectasia: a new explanation.* Proc Natl Acad Sci U S A, 1980. **77**(12): p. 7315-7.
145. Shimuta, K., et al., *Chk1 is activated transiently and targets Cdc25A for degradation at the Xenopus midblastula transition.* Embo J, 2002. **21**(14): p. 3694-703.

146. Sorensen, C.S., et al., *Chk1 regulates the S phase checkpoint by coupling the physiological turnover and ionizing radiation-induced accelerated proteolysis of Cdc25A.* Cancer Cell, 2003. **3**(3): p. 247-58.
147. Mailand, N., et al., *Regulation of G(2)/M events by Cdc25A through phosphorylation-dependent modulation of its stability.* Embo J, 2002. **21**(21): p. 5911-20.
148. Xiao, Z., et al., *Chk1 mediates S and G2 arrests through Cdc25A degradation in response to DNA-damaging agents.* J Biol Chem, 2003. **278**(24): p. 21767-73.
149. Falck, J., et al., *The ATM-Chk2-Cdc25A checkpoint pathway guards against radioresistant DNA synthesis.* Nature, 2001. **410**(6830): p. 842-7.
150. Sanchez, Y., et al., *Conservation of the Chk1 checkpoint pathway in mammals: linkage of DNA damage to Cdk regulation through Cdc25.* Science, 1997. **277**(5331): p. 1497-501.
151. Chen, L., T.H. Liu, and N.C. Walworth, *Association of Chk1 with 14-3-3 proteins is stimulated by DNA damage.* Genes Dev, 1999. **13**(6): p. 675-85.
152. Muslin, A.J. and H. Xing, *14-3-3 proteins: regulation of subcellular localization by molecular interference.* Cell Signal, 2000. **12**(11-12): p. 703-9.
153. Forrest, A. and B. Gabrielli, *Cdc25B activity is regulated by 14-3-3.* Oncogene, 2001. **20**(32): p. 4393-401.
154. Ouyang, B., et al., *The physical association and phosphorylation of Cdc25C protein phosphatase by Prk.* Oncogene, 1999. **18**(44): p. 6029-36.
155. Fu, H., R.R. Subramanian, and S.C. Masters, *14-3-3 proteins: structure, function, and regulation.* Ann. Rev Pharmacol Toxicol, 2000. **40**: p. 617-47.
156. Raleigh, J.M. and M.J. O'Connell, *The G(2) DNA damage checkpoint targets both Wee1 and Cdc25.* J Cell Sci, 2000. **113 (Pt 10)**: p. 1727-36.
157. Beamish, H. and M.F. Lavin, *Radiosensitivity in ataxia-telangiectasia: anomalies in radiation-induced cell cycle delay.* Int J Radiat Biol, 1994. **65**(2): p. 175-84.
158. Scott, D., A.R. Spreadborough, and S.A. Roberts, *Radiation-induced G2 delay and spontaneous chromosome aberrations in ataxia-telangiectasia homozygotes and heterozygotes.* Int J Radiat Biol, 1994. **66**(6 Suppl): p. S157-63.
159. Brown, A.L., et al., *A human Cds1-related kinase that functions downstream of ATM protein in the cellular response to DNA damage.* Proc Natl Acad Sci U S A, 1999. **96**(7): p. 3745-50.
160. Guo, Z., et al., *Requirement for Atr in phosphorylation of Chk1 and cell cycle regulation in response to DNA replication blocks and UV-damaged DNA in Xenopus egg extracts.* Genes Dev, 2000. **14**(21): p. 2745-56.
161. Stokes, M.P. and W.M. Michael, *DNA damage-induced replication arrest in Xenopus egg extracts.* J Cell Biol, 2003. **163**(2): p. 245-55.

162. Goldstone, S., et al., *Cdc25-dependent activation of cyclin A/cdk2 is blocked in G2 phase arrested cells independently of ATM/ATR.* Oncogene, 2001. **20**(8): p. 921-32.
163. Hirose, Y., et al., *The p38 mitogen-activated protein kinase pathway links the DNA mismatch repair system to the G2 checkpoint and to resistance to chemotherapeutic DNA-methylating agents.* Mol Cell Biol, 2003. **23**(22): p. 8306-15.
164. Donzelli, M. and G.F. Draetta, *Regulating mammalian checkpoints through Cdc25 inactivation.* EMBO Rep, 2003. **4**(7): p. 671-7.
165. Galaktionov, K., et al., *CDC25 phosphatases as potential human oncogenes.* Science, 1995. **269**(5230): p. 1575-7.
166. Gasparotto, D., et al., *Overexpression of CDC25A and CDC25B in head and neck cancers.* Cancer Res, 1997. **57**(12): p. 2366-8.
167. Busino, L., et al., *Cdc25A phosphatase: combinatorial phosphorylation, ubiquitylation and proteolysis.* Oncogene, 2004. **23**(11): p. 2050-6.
168. Zhao, H., J.L. Watkins, and H. Piwnica-Worms, *Disruption of the checkpoint kinase 1/cell division cycle 25A pathway abrogates ionizing radiation-induced S and G2 checkpoints.* Proc Natl Acad Sci U S A, 2002. **99**(23): p. 14795-800.
169. Peng, C.Y., et al., *Mitotic and G2 checkpoint control: regulation of 14-3-3 protein binding by phosphorylation of Cdc25C on serine-216.* Science, 1997. **277**(5331): p. 1501-5.
170. Furnari, B., N. Rhind, and P. Russell, *Cdc25 mitotic inducer targeted by chk1 DNA damage checkpoint kinase.* Science, 1997. **277**(5331): p. 1495-7.
171. Kumagai, A. and W.G. Dunphy, *Binding of 14-3-3 proteins and nuclear export control the intracellular localization of the mitotic inducer Cdc25.* Genes Dev, 1999. **13**(9): p. 1067-72.
172. Giles, N., A. Forrest, and B. Gabrielli, *14-3-3 acts as an intramolecular bridge to regulate cdc25B localization and activity.* J Biol Chem, 2003. **278**(31): p. 28580-7.
173. Chen, M.S., et al., *Absence of apparent phenotype in mice lacking Cdc25C protein phosphatase.* Mol Cell Biol, 2001. **21**(12): p. 3853-61.
174. Mailand, N., et al., *Regulation of G(2)/M events by Cdc25A through phosphorylation-dependent modulation of its stability.* Embo J, 2002. **21**(21): p. 5911-20.
175. Raingeaud, J., et al., *Pro-inflammatory cytokines and environmental stress cause p38 mitogen-activated protein kinase activation by dual phosphorylation on tyrosine and threonine.* J Biol Chem, 1995. **270**(13): p. 7420-6.
176. McLaughlin, M.M., et al., *Identification of mitogen-activated protein (MAP) kinase-activated protein kinase-3, a novel substrate of CSBP p38 MAP kinase.* J Biol Chem, 1996. **271**(14): p. 8488-92.
177. Ben-Levy, R., et al., *Identification of novel phosphorylation sites required for activation of MAPKAP kinase-2.* Embo J, 1995. **14**(23): p. 5920-30.

178. El Benna, J., et al., *Phosphorylation of the respiratory burst oxidase subunit p47phox as determined by two-dimensional phosphopeptide mapping. Phosphorylation by protein kinase C, protein kinase A, and a mitogen-activated protein kinase.* J Biol Chem, 1996. **271**(11): p. 6374-8.
179. Wang, X.Z. and D. Ron, *Stress-induced phosphorylation and activation of the transcription factor CHOP (GADD153) by p38 MAP Kinase.* Science, 1996. **272**(5266): p. 1347-9.
180. Tanoue, T., et al., *A conserved docking motif in MAP kinases common to substrates, activators and regulators.* Nat Cell Biol, 2000. **2**(2): p. 110-6.
181. Yaffe, M.B., et al., *A motif-based profile scanning approach for genome-wide prediction of signaling pathways.* Nat Biotechnol, 2001. **19**(4): p. 348-53.
182. Stokoe, D., et al., *MAPKAP kinase-2; a novel protein kinase activated by mitogen-activated protein kinase.* Embo J, 1992. **11**(11): p. 3985-94.
183. Rouse, J., et al., *A novel kinase cascade triggered by stress and heat shock that stimulates MAPKAP kinase-2 and phosphorylation of the small heat shock proteins.* Cell, 1994. **78**(6): p. 1027-37.
184. Huang, C.K., et al., *LSP1 is the major substrate for mitogen-activated protein kinase-activated protein kinase 2 in human neutrophils.* J Biol Chem, 1997. **272**(1): p. 17-9.
185. Heidenreich, O., et al., *MAPKAP kinase 2 phosphorylates serum response factor in vitro and in vivo.* J Biol Chem, 1999. **274**(20): p. 14434-43.
186. Cheng, T.J. and Y.K. Lai, *Identification of mitogen-activated protein kinase-activated protein kinase-2 as a vimentin kinase activated by okadaic acid in 9L rat brain tumor cells.* J Cell Biochem, 1998. **71**(2): p. 169-81.
187. Werz, O., et al., *Arachidonic acid promotes phosphorylation of 5-lipoxygenase at Ser-271 by MAPK-activated protein kinase 2 (MK2).* J Biol Chem, 2002. **277**(17): p. 14793-800.
188. Landry, J., et al., *Human HSP27 is phosphorylated at serines 78 and 82 by heat shock and mitogen-activated kinases that recognize the same amino acid motif as S6 kinase II.* J Biol Chem, 1992. **267**(2): p. 794-803.
189. Nishikawa, K., et al., *Determination of the specific substrate sequence motifs of protein kinase C isozymes.* J Biol Chem, 1997. **272**(2): p. 952-60.
190. Underwood, K.W., et al., *Catalytically active MAP KAP kinase 2 structures in complex with staurosporine and ADP reveal differences with the autoinhibited enzyme.* Structure (Camb), 2003. **11**(6): p. 627-36.
191. Yang, J., et al., *Crystal structure of an activated Akt/protein kinase B ternary complex with GSK3-peptide and AMP-PNP.* Nat Struct Biol, 2002. **9**(12): p. 940-4.
192. Chen, P., et al., *The 1.7 A crystal structure of human cell cycle checkpoint kinase Chk1: implications for Chk1 regulation.* Cell, 2000. **100**(6): p. 681-92.
193. Bartek, J. and J. Lukas, *Chk1 and Chk2 kinases in checkpoint control and cancer.* Cancer Cell, 2003. **3**(5): p. 421-9.

194. Cohen, G.E., *ALIGN: a program to superimpose protein coordinates, accounting for insertions and deletions.* J Appl Crystallogr, 1997. **30**: p. 1160–1161.
195. Diederichs, K., *Structural Superposition of Proteins with Unknown Alignment and Detection of Topological Similarity using a Six-dimensional Search Algorithm.* Proteins, 1995. **23**: p. 187-195.
196. McRee, D.E., *XtalView/Xfit--A versatile program for manipulating atomic coordinates and electron density.* J Struct Biol, 1999. **125**(2-3): p. 156-65.
197. Kraulis, P.J., *MOLSCRIPT: a program to produce both detailed and schematic plots of protein structures.* J Appl Crystallogr, 1991. **24**: p. 946–950.
198. Merritt, E.A. and M.E.P. Murphy, *Raster3D version 2.0. A program for photorealistic molecular graphics.* Acta Crystallogr D, 1994. **50**: p. 869–873.
199. Nicholls, A., R. Bharadwaj, and B. Honig, *GRASP: graphical representation and analysis of surface properties.* Biophys J, 1993. **64**: p. A166–A166.
200. Kim, S.T., et al., *Substrate specificities and identification of putative substrates of ATM kinase family members.* J Biol Chem, 1999. **274**(53): p. 37538-43.
201. Lechner, M.S., I. Levitan, and G.R. Dressler, *PTIP, a novel BRCT domain-containing protein interacts with Pax2 and is associated with active chromatin.* Nucleic Acids Res, 2000. **28**(14): p. 2741-51.
202. Cho, E.A., M.J. Prindle, and G.R. Dressler, *BRCT domain-containing protein PTIP is essential for progression through mitosis.* Mol Cell Biol, 2003. **23**(5): p. 1666-73.
203. Shimizu, K., et al., *Swift is a novel BRCT domain coactivator of Smad2 in transforming growth factor beta signaling.* Mol Cell Biol, 2001. **21**(12): p. 3901-12.
204. Huyton, T., et al., *The BRCA1 C-terminal domain: structure and function.* Mutat Res, 2000. **460**(3-4): p. 319-32.
205. Sarkaria, J.N., et al., *Inhibition of ATM and ATR kinase activities by the radiosensitizing agent, caffeine.* Cancer Res, 1999. **59**(17): p. 4375-82.
206. Wang, B., et al., *53BP1, a mediator of the DNA damage checkpoint.* Science, 2002. **298**(5597): p. 1435-8.
207. Bateman, A., et al., *Pfam 3.1: 1313 multiple alignments and profile HMMs match the majority of proteins.* Nucleic Acids Res, 1999. **27**(1): p. 260-2.
208. Powell, S.N. and L.A. Kachnic, *Roles of BRCA1 and BRCA2 in homologous recombination, DNA replication fidelity and the cellular response to ionizing radiation.* Oncogene, 2003. **22**(37): p. 5784-91.
209. Cantor, S.B., et al., *BACH1, a novel helicase-like protein, interacts directly with BRCA1 and contributes to its DNA repair function.* Cell, 2001. **105**(1): p. 149-60.
210. Miki, Y., et al., *A strong candidate for the breast and ovarian cancer susceptibility gene BRCA1.* Science, 1994. **266**(5182): p. 66-71.

211. Couch, F.J. and B.L. Weber, *Mutations and polymorphisms in the familial early-onset breast cancer (BRCA1) gene. Breast Cancer Information Core.* Hum Mutat, 1996. **8**(1): p. 8-18.
212. Nathanson, K.L., et al., *Breast cancer genetics: what we know and what we need.* Nat Med, 2001. **7**(5): p. 552-6.
213. Ford, D., et al., *Genetic heterogeneity and penetrance analysis of the BRCA1 and BRCA2 genes in breast cancer families. The Breast Cancer Linkage Consortium.* Am J Hum Genet, 1998. **62**(3): p. 676-89.
214. Callebaut, I. and J.P. Mornon, *From BRCA1 to RAP1: a widespread BRCT module closely associated with DNA repair.* FEBS Lett, 1997. **400**(1): p. 25-30.
215. Ekblad, C.M., et al., *Characterisation of the BRCT domains of the breast cancer susceptibility gene product BRCA1.* J Mol Biol, 2002. **320**(3): p. 431-42.
216. Vallon-Christersson, J., et al., *Functional analysis of BRCA1 C-terminal missense mutations identified in breast and ovarian cancer families.* Hum Mol Genet, 2001. **10**(4): p. 353-60.
217. Rodriguez, M., et al., *Phosphopeptide binding specificities of BRCA1 COOH-terminal (BRCT) domains.* J Biol Chem, 2003. **278**(52): p. 52914-8.
218. Joo, W.S., et al., *Structure of the 53BP1 BRCT region bound to p53 and its comparison to the Brca1 BRCT structure.* Genes Dev, 2002. **16**(5): p. 583-93.
219. Derbyshire, D.J., et al., *Crystal structure of human 53BP1 BRCT domains bound to p53 tumour suppressor.* Embo J, 2002. **21**(14): p. 3863-72.
220. Elia, E.A.H., et al., *The Molecular Basis for Phosphodependent Substrate Targeting and Regulation of Plks by the Polo-box Domain.* Cell, 2003.
221. Cheng, K.Y., et al., *The crystal structure of the human polo-like kinase-1 polo box domain and its phospho-peptide complex.* Embo J, 2003. **22**(21): p. 5757-68.
222. Chen, J., et al., *Stable interaction between the products of the BRCA1 and BRCA2 tumor suppressor genes in mitotic and meiotic cells.* Mol Cell, 1998. **2**(3): p. 317-28.
223. Nash, P., et al., *Multisite phosphorylation of a CDK inhibitor sets a threshold for the onset of DNA replication.* Nature, 2001. **414**(6863): p. 514-21.
224. Cantor, S., et al., *The BRCA1-associated protein BACH1 is a DNA helicase targeted by clinically relevant inactivating mutations.* Proc Natl Acad Sci U S A, 2004. **101**(8): p. 2357-62.
225. Snouwaert, J.N., et al., *BRCA1 deficient embryonic stem cells display a decreased homologous recombination frequency and an increased frequency of non-homologous recombination that is corrected by expression of a brca1 transgene.* Oncogene, 1999. **18**(55): p. 7900-7.
226. Westermark, U.K., et al., *BARD1 participates with BRCA1 in homology-directed repair of chromosome breaks.* Mol Cell Biol, 2003. **23**(21): p. 7926-36.

227. Otwinowski, Z., *Oscillation data reduction program*, in *Data Collection and Processing*, L. Sawyers, N. Isaacs, and S. Bailey, Editors. 1993, SERC Daresbury Laboratory: Warrington, UK. p. 56-62.
228. CCP4, *The CCP4 suite: programs for protein crystallography.* Acta Crystallogr., 1994. **D50**: p. 760-763.
229. Jones, T.A., et al., *Improved methods for binding protein models in electron density maps and the location of errors in these models.* Acta Crystallogr A, 1991. **47**(Pt 2): p. 110-9.
230. Gilmore, P.M., et al., *BRCA1 interacts with and is required for paclitaxel-induced activation of mitogen-activated protein kinase kinase kinase 3.* Cancer Res, 2004. **64**(12): p. 4148-54.
231. Ueda, K., et al., *Proteomic identification of Bcl2-associated athanogene 2 as a novel MAPK-activated protein kinase 2 substrate.* J Biol Chem, 2004. **279**(40): p. 41815-21.
232. Williams, R.S., et al., *Detection of protein folding defects caused by BRCA1-BRCT truncation and missense mutations.* J Biol Chem, 2003. **278**(52): p. 53007-16.
233. Williams, R.S., et al., *Structural basis of phosphopeptide recognition by the BRCT domain of BRCA1.* Nat Struct Mol Biol, 2004. **11**(6): p. 519-25.
234. Li, J., et al., *The FHA domain mediates phosphoprotein interactions.* J Cell Sci, 2000. **113 Pt 23**: p. 4143-9.

Appendices

Molecular Cell, Vol. 17, 37–48, January 7, 2005, Copyright ©2005 by Elsevier Inc. DOI 10.1016/j.molcel.2004.11.021

MAPKAP Kinase-2 Is a Cell Cycle Checkpoint Kinase that Regulates the G_2/M Transition and S Phase Progression in Response to UV Irradiation

Isaac A. Manke,[1,2] Anhco Nguyen,[1,2] Daniel Lim,[1,2] Mary Q. Stewart,[1,2] Andrew E.H. Elia,[1,2] and Michael B. Yaffe[1,2,3,*]
[1]Center for Cancer Research
[2]Department of Biology
[3]Division of Biological Engineering
Massachusetts Institute of Technology
77 Massachusetts Avenue
Cambridge, Massachusetts 02139

Summary

The cellular response to DNA damage is mediated by evolutionarily conserved Ser/Thr kinases, phosphorylation of Cdc25 protein phosphatases, binding to 14-3-3 proteins, and exit from the cell cycle. To investigate DNA damage responses mediated by the p38/stress-activated protein kinase (SAPK) axis of signaling, the optimal phosphorylation motifs of mammalian p38α SAPK and MAPKAP kinase-2 were determined. The optimal substrate motif for MAPKAP kinase-2, but not for p38 SAPK, closely matches the 14-3-3 binding site on Cdc25B/C. We show that MAPKAP kinase-2 is directly responsible for Cdc25B/C phosphorylation and 14-3-3 binding in vitro and in response to UV-induced DNA damage within mammalian cells. Downregulation of MAPKAP kinase-2 eliminates DNA damage-induced G_2/M, G_1, and intra S phase checkpoints. We propose that MAPKAP kinase-2 is a new member of the DNA damage checkpoint kinase family that functions in parallel with Chk1 and Chk2 to integrate DNA damage signaling responses and cell cycle arrest in mammalian cells.

Introduction

The maintenance of genomic integrity is essential for the health of multicellular organisms. DNA damage checkpoints constitute a mechanism where cell division is delayed to allow repair of damaged DNA or, if the extent of DNA damage is beyond repair, induce apoptosis. The three major DNA damage-responsive cell cycle checkpoints are the G_1/S checkpoint, intra S phase checkpoint, and the G_2/M checkpoint (Zhou and Elledge, 2000).

Signal transduction events controlling the DNA damage response are mediated by evolutionarily conserved Ser/Thr kinases and phosphoserine/threonine binding domains. Distinct types of genotoxic stress converge to trigger a limited repertoire of DNA damage checkpoint responses, presumably by funneling specific protein complexes that recognize different types of DNA damage into a few common pathways. For example, lesions commonly caused by ionizing radiation (IR) and ultraviolet light (UV) initiate the activation of the upstream kinases ataxia-telangiectasia mutated (ATM) and ataxia-telangiectasia- and RAD3-related (ATR) (Abraham, 2001). These kinases transduce the signal that directly engages the DNA damage checkpoint.

ATM and ATR appear to have partially overlapping functions since some common Ser/Thr-Gln-containing substrates of both kinases have been identified. ATM responds primarily to double-strand breaks, whereas ATR responds to many types of DNA damage, including the bulky DNA lesions caused by UV. Once activated, ATM phosphorylates the downstream effector kinase Chk2 on Thr68, and ATR phosphorylates the downstream effector kinase Chk1 on Ser317 and Ser345 (Abraham, 2001; Guo et al., 2000). In addition, studies in both *Xenopus* egg extracts and mammalian cells have pointed to the existence of a checkpoint pathway that is independent of ATR/Chk1 and ATM/Chk2 (Bulavin et al., 2001; Goldstone et al., 2001; Hirose et al., 2003; Mikhailov et al., 2004; Stokes and Michael, 2003).

A major mechanism by which Chk1 and Chk2 control the DNA damage response is through the phosphorylation-dependent inactivation of members of the Cdc25 family of phosphatases, which are positive regulators of Cyclin/Cdk complexes (Donzelli and Draetta, 2003 and references therein). The Cdc25 family consists of three different isoforms: Cdc25A, Cdc25B (variants 1, 2, and 3), and Cdc25C. Cdc25A and Cdc25B are thought to be oncogenes since they are upregulated in many forms of human cancer (Galaktionov et al., 1995; Gasparotto et al., 1997). Cdc25A controls both progression through S phase and entry into, and maintenance of, mitosis (Busino et al., 2004; Zhao et al., 2002). In response to DNA damage, Cdc25A is phosphorylated on several sites, including Ser78 and Ser123, targeting it for ubiquitin-mediated degradation (Busino et al., 2004 and references therein). Cdc25B and Cdc25C, on the other hand, are primarily involved in regulating mitotic entry through their activation of the cyclin-dependent kinase Cdc2/CyclinB (Donzelli and Draetta, 2003). In response to DNA damage, Cdc25B1/Cdc25B2 and Cdc25C become sequestered away from the nuclear pool of Cdc2/CyclinB by phosphorylation on Ser309/Ser323 and Ser216, respectively, leading to 14-3-3 binding and cytosolic retention (Furnari et al., 1997; Giles et al., 2003; Kumagai and Dunphy, 1999; Peng et al., 1997). The exact roles of different Cdc25 family members in establishing this G_2/M checkpoint, however, remain a matter of active debate (Chen et al., 2001; Mailand et al., 2002).

In contrast to the IR-induced DNA damage checkpoint, the UV-responsive checkpoint is less well understood. It was recently shown that, in addition to the ATR-Chk1 pathway, the p38 SAPK pathway is also required for full activation of the DNA damage response following UV irradiation (Bulavin et al., 2001). We now demonstrate that MAPKAP kinase-2, a direct downstream target of p38 SAPK, is directly responsible for phosphorylating Cdc25B and C and maintaining the G_1, S, and G_2/M checkpoints in response to UV-induced DNA damage. Thus, MAPKAP kinase-2 constitutes a third checkpoint kinase, in addition to Chk1 and Chk2,

*Correspondence: myaffe@mit.edu

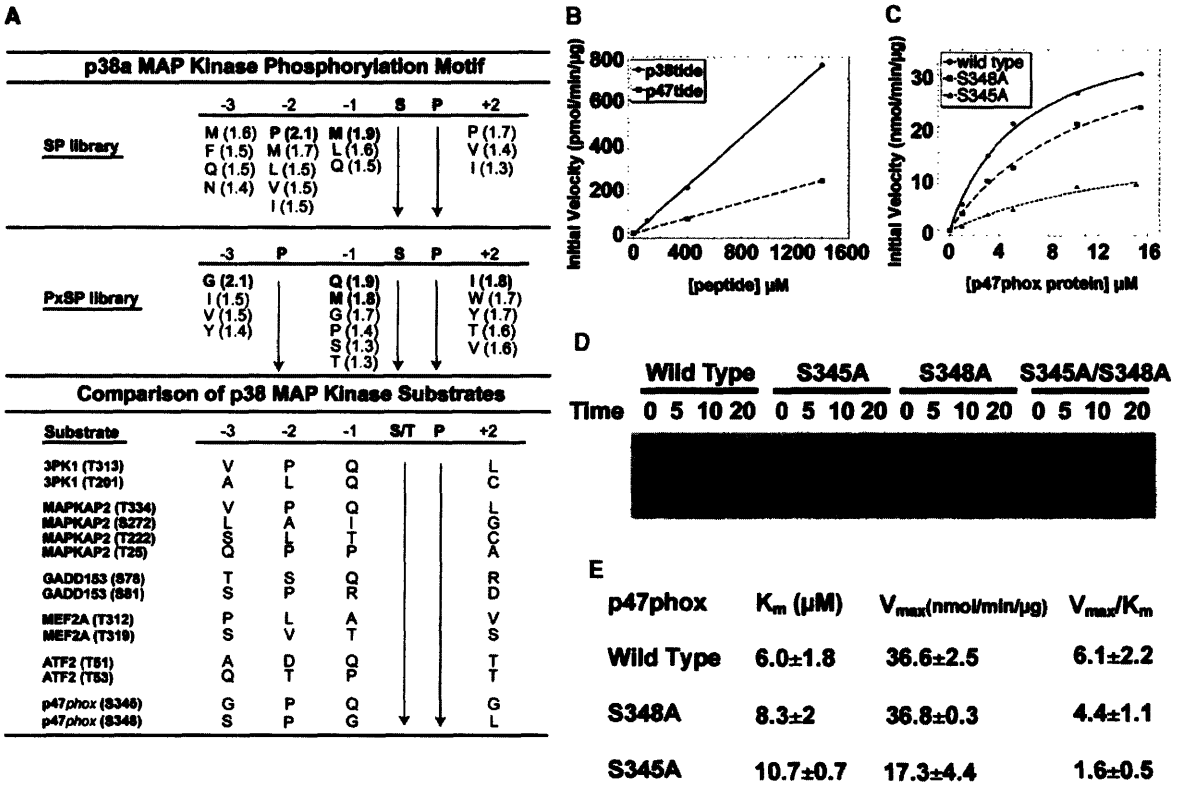

Figure 1. Substrate Specificity and Kinetic Analysis of Substrate Phosphorylation by p38α SAPK

(A) p38 substrate specificity determined using oriented peptide library screening. Residues displaying the highest selectivity are shown; those with selection values >1.7 are in bold. MEF2A, myocyte enhancer factor 2; ATF2, activating transcription factor 2; 3PK1, MAP kinase-activated protein kinase-3.

(B) Kinetics of in vitro phosphorylation of an optimal p38 peptide (p38tide) and a peptide from p47phox (p47tide) by p38α kinase.

(C) Kinetics of in vitro phosphorylation of wild-type GST-p47phox, the Ser345→Ala mutant, and the Ser348→Ala mutant. Typical data from n = 3 experiments is shown.

(D) In vitro phosphorylation of full-length wild-type or mutant p47phox proteins. Samples were analyzed by SDS-PAGE/autoradiography.

(E) Table of kinetic parameters for the reactions in (C).

involved in coordinating the DNA damage response of higher eukaryotic cells.

Results

Defining the Optimal Phosphorylation Motif for p38 SAPK

To identify substrates and targets of the p38 SAPK signaling pathway involved in DNA damage responses, the optimal substrate phosphorylation motif for p38α SAPK was determined using oriented peptide library screening (Songyang and Cantley, 1998). Efficient peptide phosphorylation by p38 SAPK required a fixed Pro residue in the Ser+1 position (data not shown), consistent with the known identification of p38 SAPK as a Pro-directed MAP kinase. Screening performed with a library containing the degenerate sequence X-X-X-X-Ser-Pro-X-X-X-X (X denotes all amino acids except Cys, Ser, Thr, and Tyr) displayed strongest selection for Pro in the Ser−2 position with weaker selection for other aliphatic residues (Figure 1A). Additional selection was also observed at the Ser−3, Ser−1, and Ser+2 positions.

To further refine the optimal phosphorylation motif, a secondary screen was performed based on results from the initial screen by using a library with Pro fixed in both the Ser−2 and Ser+1 positions, and Ser, Thr, and Tyr included in the X positions. This revealed selection for Gln, Met, and Gly in the Ser−1 position, along with slightly weaker selection for Pro, Ser, and Thr (Figure 1A). Gly was the preferred residue in the Ser−3 position, along with Ile, Val, and Tyr. Hydrophobic residues, particularly aromatic and β-branched amino acids, were selected at the Ser+2 position. The resulting optimal motif for p38α SAPK determined by oriented peptide library screening closely matches the sequence of mapped p38 MAPK phosphorylation sites on most, though not all, known substrates (Figure 1A) (Ben-Levy et al., 1995; Cheung et al., 2003; El Benna et al., 1996; McLaughlin et al., 1996; Raingeaud et al., 1995; Wang and Ron, 1996; Yang et al., 1999)

A peptide containing the optimal p38 SAPK consensus phosphorylation motif GPQSPI, "p38tide," was synthesized for kinetic analysis. This peptide was readily phosphorylated by p38 SAPK in vitro; however, it failed to display saturable Michaelis-Menton-type kinetics (Figure 1B). Instead, the initial velocity increased linearly

with increasing p38tide concentration up to1400 μM. This finding suggests that additional interactions besides an optimal phosphorylation motif are likely to be involved in optimizing p38 SAPK-substrate binding, such as MAP kinase docking sites (Tanoue et al., 2000).

To search for potential p38 SAPK substrates, particularly those relevant to DNA damage signaling, the Swiss-Prot database was queried with the p38 SAPK consensus phosphorylation motif using Scansite (Yaffe et al., 2001) (Supplemental Table S1). Other than GADD153, a known p38 SAPK substrate, we were unable to identify any DNA damage response proteins in the top 250 hits. Database searching did, however, reveal two tandem near-optimal p38 SAPK phosphorylation sites (Ser345 and Ser348) in p47phox, a cytosolic component of the NADPH oxidase enzyme. A peptide containing this sequence, PGPQSPGSPL, "p47tide," was strongly phosphorylated by p38 SAPK, but like p38tide, the isolated peptide displayed linear nonsaturable kinetics (Figure 1B).

Wild-type and mutant versions of GST-tagged full-length p47phox protein, rather than isolated peptides, were then used as substrates for in vitro phosphorylation reactions. The wild-type full-length p47phox protein was rapidly phosphorylated by p38α SAPK (Figures 1C and 1D). Mutation of Ser345→Ala had a more pronounced effect on p47phox phosphorylation than mutation of Ser348→Ala, in excellent agreement with the observation that the Ser345 site is a better match for the optimal p38 SAPK consensus motif than the Ser348 site. Simultaneous mutation of both Ser345 and Ser348 to Ala eliminated phosphorylation of p47phox by p38 SAPK altogether. Kinetic analysis revealed classical Michaelis-Menton behavior for p38 SAPK phosphorylation of the wild-type p47phox with a K_m of 6.0 μM and a V_{max} of 36.6 nmol/min/μg. Mutation of Ser345 to Ala both increased the K_m and reduced the V_{max}, while mutation of Ser348 to Ala primarily increased the K_m (Figure 1E).

This data from isolated peptides and intact proteins argues that efficient substrate phosphorylation by p38 SAPK requires sequences with reasonable matches to the optimal substrate motif determined by oriented peptide library screening, and that additional interactions involving MAPK docking sites are likely to be critical for strong kinase-substrate interactions. Several docking motifs have been identified for p38 SAPK, particularly a short cluster of positively charged amino acid residues often flanked by hydrophobic amino acids (Roux and Blenis, 2004; Tanoue and Nishida, 2003). Two sequences corresponding to this type of docking motif are present near the p38SAPK phosphorylation sites in p47 phox, ^{311}IHQRSRKRLSQ^{321} and ^{329}VRFLQQRRRQA^{339}. Mutation of ^{335}RRR^{337} to LLL in the latter motif decreased the rate of p38α SAPK phosphorylation of p47phox by over 70% (data not shown). The contribution of amino acids 311–321, or involvement of alternative p38 SAPK docking site(s) (cf. Cheung et al., 2003), is not yet known.

Bulavin et al. (2001) implicated p38 SAPK in the DNA damage-response pathway and reported that p38 SAPK was directly responsible for generating a 14-3-3 binding site on Cdc25B (Ser323 in Cdc25B2; Ser309 in Cdc25B1) in response to UV-C-induced DNA damage. Like p47phox, Cdc25B contains a potential p38 SAPK docking motif, ^{345}PVQNKRRRSV^{354}; however, the sequence flanking Ser323, LXRSPSMP, lacks a Pro in the Ser+1 position and does not resemble the optimal p38 SAPK motif shown in Figure 1A. As shown in Figure 2A, recombinant p38 SAPK readily phosphorylated bacterially produced Cdc25B in vitro. However, this phosphorylation did not induce 14-3-3 binding, and a Ser323→Ala mutant form of Cdc25B was phosphorylated by p38 SAPK equivalently to the wild-type Cdc25B protein. This data argues that while Cdc25B may be a p38 SAPK substrate, this phosphorylation event is not responsible for the 14-3-3 binding event that results in a G_2/M checkpoint.

Defining the Optimal Phosphorylation Motif for MAPKAP Kinase-2

A number of Ser/Thr kinases are activated downstream of p38 SAPK, including MAPKAP kinases-2, and -3, MNK1 and MNK2, MSK1 and MSK2, and PRAK (Obata et al., 2000). In response to UV-B-induced DNA damage, She et al. (2002) reported that MAPKAP kinase-2 could phosphorylate p53 on Ser20, the same site that is phosphorylated by two well-established checkpoint kinases, Chk1 and Chk2. Both Chk1 and Chk2 can also phosphorylate Cdc25 family members to create 14-3-3 binding sites, suggesting that MAPKAP kinase-2 might share a similar motif. The optimal substrate phosphorylation motif for MAPKAP kinase-2 was therefore investigated using oriented peptide library screening.

Efficient peptide phosphorylation by MAPKAP kinase-2 was only observed with a library containing a fixed Arg in the Ser−3 position (X-X-X-X-R-X-X-S-X-X-X-X, where X denotes all amino acids except Cys, Ser, Thr, or Tyr). A critical step in determining protein kinase phosphorylation motifs by peptide library screening involves purification of the phosphorylated peptides from the nonphosphorylated peptide background. In the case of MAPKAP kinase-2, this was dramatically improved by conversion of all Glu and Asp residues to their methyl esters prior to metal-affinity chromatography and sequencing (Ficarro et al., 2002). This resulting motif revealed clear amino acid selection at almost all degenerate positions (Figure 3A). MAPKAP kinase-2 displayed strong selection for the hydrophobic residues Leu, Phe, Ile, and Val in the Ser−5 position, and the Ser+1 position. Strong selection was also observed for Gln in the Ser−2 position, and modest selection for Leu in the Ser−1 position. The motif determined for MAPKAP kinase-2 using oriented peptide library screening is in remarkably good agreement with the sequence of mapped MAPKAP kinase-2 phosphorylation sites on known substrates (Figure 3A, bottom) (Cheng and Lai, 1998; Heidenreich et al., 1999; Huang et al., 1997; Landry et al., 1992; Rouse et al., 1994; Stokoe et al., 1992, 1993; Werz et al., 2002), which primarily contain Leu, Ile, or Phe in the Ser−5 position; Arg in the Ser−3 position; Gln, Ser, or Thr in the Ser−2 position; Leu, Val, or Pro in the Ser−1 position; and hydrophobic residues along with Glu in the Ser+1 position. The preference for polar residues Ser and Thr in addition to Gln in the Ser−2 position in known MAPKAP kinase-2 substrates would not have been detected by oriented peptide library screening since Ser and Thr were not present in the library.

To verify the peptide library screening results, individ-

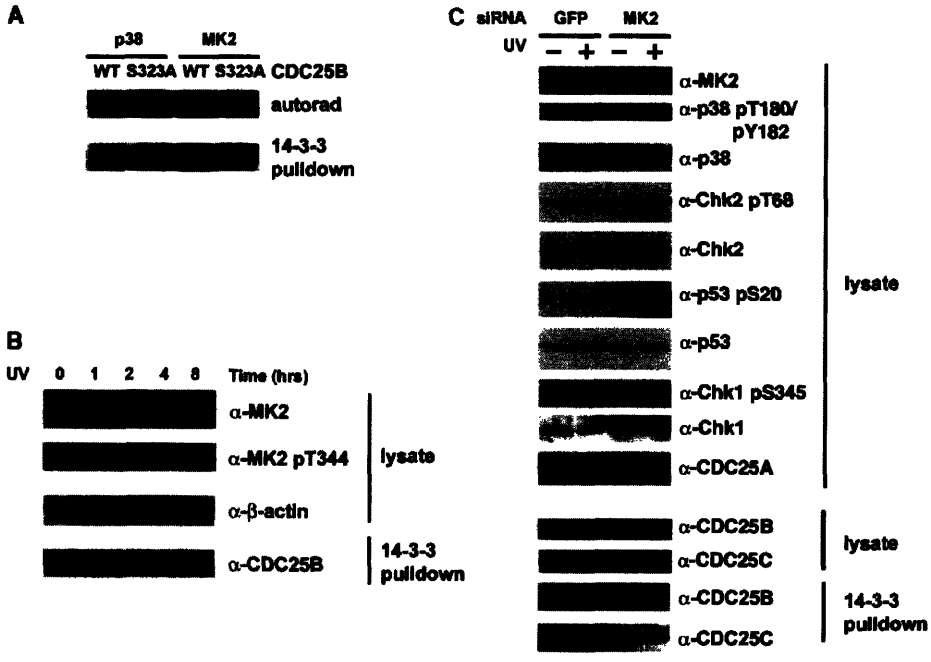

Figure 2. Involvement of MAPKAP Kinase-2 in the Phosphorylation of Cdc25B and Cdc25C after DNA Damage

(A) Phosphorylation of full-length wild-type Cdc25B or a Ser323→Ala mutant by p38α SAPK or MAPKAP kinase-2. After phosphorylation, generation of a 14-3-3 binding site on Cdc25B was determined by a 14-3-3-MBP pull-down followed by SDS-PAGE/autoradiography.

(B) Kinetics of MAPKAP kinase-2 phosphorylation and generation of a 14-3-3 binding site on Cdc25B were measured in U2OS cells following 20 J/m^2 UV irradiation.

(C) Signaling events in the G_2/M, G_1, and S phase checkpoint response were analyzed in GFP siRNA- or MAPKAP kinase-2 siRNA-treated U2OS cells before and 2 hr after UV-induced DNA damage. Equal loading was determined by Western blotting for β-actin.

ual peptides (MK2tides) containing the optimal MAPKAP kinase-2 consensus motif LQRQLSI, or mutant versions with Ala substituted at each position in the motif, were synthesized and used for kinetic analysis (Figures 3B and 3C). The optimal MK2tide displayed a K_m value 2-fold lower than the best MAPKAP kinase-2 peptide substrate known to date, a sequence derived from HSP27 (Landry et al., 1992). Substitution of Ala at each position in the motif affected K_m and V_{max} differently, with some positions showing primarily a K_m effect (i.e., Arg in the Ser−3 position), while others revealed a primary effect on V_{max} (i.e., Leu in the Ser−5 position) (Figure 3C). The rank order of importance of key residues is Arg−3 > Leu−5 ≈ Ile+1 > Gln−3. The optimal MK2tide had neither the lowest K_m nor the highest V_{max}, but rather had the highest V_{max}/K_m ratio, consistent with the fact that the peptide library screening approach selects substrates on the basis of optimal V_{max}/K_m, rather than low K_m or high V_{max} alone (Nishikawa et al., 1997). Combining the data from oriented peptide library screening, known substrate sequences, and our kinetic studies, the optimal MAPKAP kinase-2 phosphorylation motif is (Leu/Phe/Ile)-(Xxx)-(Arg)-(Gln/Ser/Thr)-(Leu)-(Ser/Thr)-(Hydrophobic).

The optimal MAPKAP kinase-2 substrate motif is an excellent match for the known Ser323 phosphorylation/14-3-3 binding motif in Cdc25B, as well as the Ser216 phosphorylation/14-3-3 binding site in Cdc25C (Figure 3A, Supplemental Table S2). Initial experiments focused on Cdc25B, since unlike Cdc25C, Cdc25B can be produced in modest quantities in bacteria, and the Ser323 site in Cdc25B had been previously reported to be a direct p38 SAPK site. Incubation of recombinant Cdc25B with purified MAPKAP kinase-2 resulted in significant Cdc25B phosphorylation and strong binding of the phosphorylated protein to 14-3-3 (Figure 2A). Mutation of Ser323→Ala substantially reduced the ability of MAPKAP kinase-2 to phosphorylate Cdc25B, and completely eliminated the ability of Cdc25B to bind to 14-3-3 (Figure 2A). These in vitro results strongly suggest that MAPKAP kinase-2 is the critical Cdc25/14-3-3 checkpoint kinase downstream of DNA damage signals relayed by the p38 SAPK pathway.

MAPKAP Kinase-2 Is Critical for the G_2/M Checkpoint following UV-Induced DNA Damage

The importance of MAPKAP kinase-2 in DNA damage checkpoint function was investigated in U2OS cells. Activation of MAPKAP kinase-2 in response to UV-C irradiation-induced DNA damage (Figure 4A) was monitored by its reduced mobility on SDS-PAGE gels, and by immunoblotting using a phospho-specific antibody against pThr344, a site phosphorylated by p38 and required for MAPKAP kinase-2 activation (Ben-Levy et al., 1995). As shown in Figure 2B, MAPKAP kinase-2 was activated within 1 hr of irradiation and remained activated for the 8 hr duration of the experiment. The kinetics of MAPKAP kinase-2 activation paralleled the ability of Cdc25B from these cells to bind to 14-3-3. Based on these data, a 2 hr time point was chosen for use in further studies.

RNA interference was used to confirm a direct role for endogenous MAPKAP kinase-2 in the UV-induced

A

MAPKAP Kinase-2 Phosphorylation Motif

	-5	-4	R	-2	-1	S	+1
RxxS library	L (2.5) Q (1.3) F (1.9) A (1.2) I (1.6) M (1.2) V (1.3)		↓	Q (2.6) M (1.3)	L (1.6) N (1.3)	↓	I (1.8) V (1.7) F (1.4) L (1.3)

Comparison of MK2 Kinase Substrates

Substrate	-5	-4	R	-2	-1	S	+1
HSP-27 (82)	L	S		Q	L		S
5-LO (271)	L	E		Q	L		L
LSP1 (204)	I	D		T	E		L
LSP1 (252)	L	A		Q	A		I
SRF (103)	L	K		T	L		E
GS (7)	L	N		S	L		V
TH (19)	F	R		A	V		E
CDC25B (309)	L	F		S	P		M
CDC25C (216)	L	Y	↓	S	P	↓	M

B

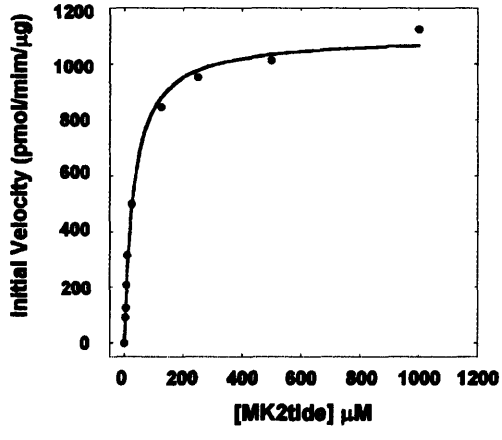

C

Optimal MK2tide

	-5	-4	-3	-2	-1	0	+1	Motif Position
1 2	3	4	5	6	7	8	9	10 11 12
Ala His	Leu	Gln	Arg	Gln	Leu	Ser	Ile	Ala His His

Peptide	$Km_{\mu M}$	V_{max} (pmol/min/µg)	V_{max}/Km
MK2tide	31	1098	35
L3Atide	29	463	16
Q4Atide	41	1209	29
R5Atide	310	282	<1
Q6Atide	51	1058	21
L7Atide	35	955	27
I9Atide	43	627	15

Figure 3. Substrate Specificity and Kinetic Analysis of Substrate Phosphorylation by MAPKAP Kinase-2

(A) MAPKAP kinase-2 substrate specificity was determined by oriented peptide library screeing. HSP27, heat shock protein 27; 5-LO, 5-lipoxygenase; LSP1, lymphocyte-specific protein; SRF, serum response factor; GS, glycogen synthase; TH, tyrosine hydroxylase.

(B) Kinetics of in vitro phosphorylation of the optimal MAPKAP kinase-2 peptide (MK2tide) by MAPKAP kinase-2.

(C) Table of kinetic parameters for MAPKAP kinase-2 phosphorylation of wild-type and mutant MK2tides.

DNA damage response. Treatment of U2OS cells with MAPKAP kinase-2-specific siRNA oligonucleotides, but not with control GFP siRNA oligonucleotides, resulted in a substantial reduction of MAPKAP kinase-2 to nearly undetectable levels by 48 hr after transfection (Figure 2C). No reduction in the levels or UV-C-induced activation of p38 SAPK, Chk1, or Chk2 was observed in these cells. Despite the presence of these other active kinases, siRNA-mediated knockdown of MAPKAP kinase-2 caused a loss of both Cdc25B- and Cdc25C binding to 14-3-3 after UV-C exposure (Figure 2C).

Cell cycle progression in the control GFP and MAPKAP kinase-2 knockdown cells following UV-C-irradiation was studied using FACS (Figure 4). In these experiments, cells were irradiated with 20 J/m^2 of UV-C radiation, allowed to recover for 2 hr, and then placed in nocodazole-containing media for an additional 16 hr to cause any cells progressing through the cell cycle to arrest in mitosis, where they can be stained for the mitotic marker phosho-histone H3. Under these conditions, unirradiated cultures of asynchronous GFP siRNA-transfected cells accumulated in a 4N-DNA-containing peak, with prominent levels of phospho-histone H3 staining (Figures 4B and 4C), consistent with a nocodazole-mediated M phase arrest. In response to UV irradiation, control cells displayed a prominent G_1, S, and G_2 distribution, with near-complete loss of phospho-histone H3 staining, indicating intact G_1, S, and G_2 checkpoints (Figures 4D and 4E).

The behavior of the MAPKAP kinase-2 siRNA-transfected cells was dramatically different. In the absence of UV irradiation, MAPKAP kinase-2 siRNA-transfected cells, like control GFP siRNA-transfected cells, accumulate in a 4N DNA-containing peak with high levels of phospho-histone H3 staining (Figures 4F and 4G). Following UV-induced DNA damage, however, the MAPKAP kinase-2 knockdown cells failed to arrest cell cycle progression. Instead, these cells proceeded to enter mitosis to the same extent as unirradiated cells, as shown by a comparable 4N-DNA peak and similar levels of phospho-histone H3 staining as those observed in unirradiated cells (Figures 4H and 4I). Together with the Cdc25B/C:14-3-3 results in Figure 2C, this FACS data demonstrates that MAPKAP kinase-2 is critical for the UV-induced G_2/M checkpoint in response to UV irradiation. In contrast to the UV response, summarized in Figure 4J, the G_2/M checkpoint response to ionizing radiation in MAPKAP kinase-2 knockdown cells is intact (Figure 4K).

MAPKAP Kinase-2 Is Critical for the S Phase Checkpoint and G_1 Arrest following UV-Induced DNA Damage

The MAPKAP kinase-2 knockdown cells in Figure 4 also showed a loss of the G_1 and S phase checkpoints following DNA damage, since UV irradiation of asynchronous cultures resulted in accumulation of the cells in a 4N DNA-containing peak when the cells were transferred to nocodazole-containing medium. To investigate the direct role of MAPKAP kinase-2 in S phase checkpoint function, control or MAPKAP kinase-2 knockdown U2OS cells were UV irradiated, allowed to recover for 30 min, and then labeled with BrdU for various times. In the

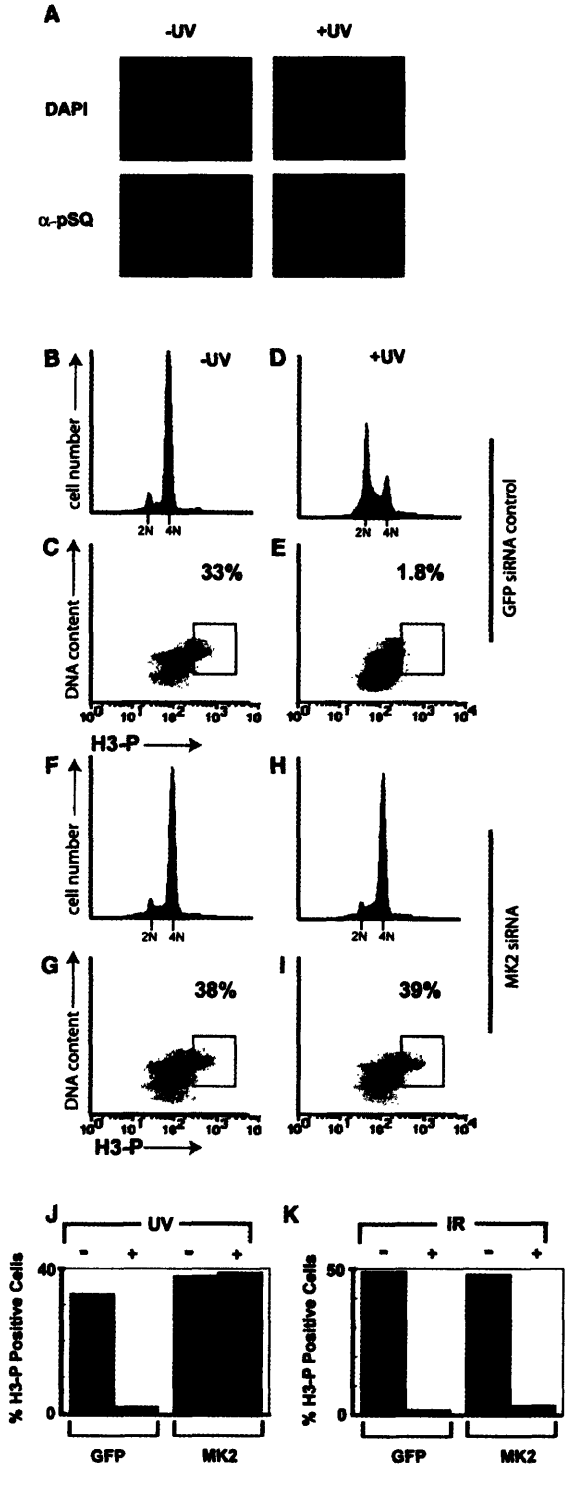

Figure 4. MAPKAP Kinase-2 Is Required for G_2/M Arrest following DNA Damage

(A) UV-C irradiation induces DNA damage as revealed by nuclear foci formation. U2OS cells were mock irradiated or exposed to 20 J/m² of UV-C radiation and immunostained 2 hr later using an anti-phospho(Ser/Thr) ATM/ATR substrate antibody.

(B–I) GFP siRNA- or MAPKAP kinase-2 siRNA-treated U2OS cells were irradiated as in (A), then placed in 50 ng/ml nocodazole-containing media for an additional 16 hr. Cells were analyzed by FACS for DNA content by PI staining (B, D, F, and H) and for phosphohistone H3 staining as a marker of mitotic entry (C, E, G, and I).

(J–K) GFP siRNA- or MAPKAP kinase-2 siRNA-treated U2OS cells were either mock treated, exposed to 20 J/m² of UV-C irradiation (J), or to 10 Gy of ionizing radiation (K) and analyzed as in (B)–(i). Representative results of each experiment are shown.

absence of irradiation, 42% of the control siRNA-transfected cells showed substantial BrdU incorporation after 12 hr, compared with 53% of the MAPKAP kinase-2 siRNA-transfected cells (Figures 5A and 5B). When the cells were irradiated with 20 J/m² of UV light prior to BrdU labeling, only 3.5% of the control siRNA-transfected cells showed BrdU incorporation at 12 hr. In marked contrast, 48% of the MAPKAP kinase-2 knockdown cells continued to incorporate substantial amounts of BrdU. A similar difference in BrdU uptake between control siRNA-treated cells and MAPKAP kinase-2 knockdown cells was also seen at shorter times after irradiation (Figure 5B).

Examination of the FACS profiles 12 hr following UV irradiation revealed a dramatic decrease in the G_1 population in the MAPKAP kinase-2 knockdown cells compared with the control GFP siRNA-transduced cells (Figure 5A, right-most upper and lower FACS profiles). This loss of the G_1 peak, together with the increased percentage of cells showing BrdU incorporation at 12 hr versus 2 hr of labeling, implies that endogenous MAPKAP kinase-2 plays important roles in both the inhibition of DNA synthesis following damage (S phase checkpoint function), and in the damage-induced arrest of cells in G_1 prior to S phase entry (G_1/S checkpoint function). Loss of the G_1/S and S phase checkpoints in MAPKAP kinase-2 knockdown cells was associated with higher levels of Cdc25A, decreased levels of p53, and reduced phosphorylation of p53 on Ser20 following UV irradiation compared with control siRNA-treated cells (Figure 2C).

The fate of S phase control or MAPKAP kinase-2 siRNA-treated cells in response to UV-C-induced DNA damage was examined by using FACS. In this experiment, asynchronous cells were mock treated or irradiated with 20 J/m² of UV-C radiation and then pulse labeled with BrdU. The cells showing BrdU uptake were subsequently analyzed 10 and 20 hr later (Figure 5C). In both nonirradiated control and MAPKAP kinase-2 knockdown cells, the BrdU pulse-labeled population showed a late S and G_2/M distribution at 10 hr, and a reappearance of a G_1 peak at 20 hr, indicating full transit through the cell cycle. In response to UV-C irradiation, control siRNA-treated cells failed to show significant BrdU uptake upon which to gate for FACS analysis (Figure 5C, lower left panel). In contrast, the large population of MAPKAP kinase-2 siRNA-treated cells, which had lost the S phase checkpoint and incorporated BrdU, went on to display a greatly reduced G_1 peak at 20 hr, with many cells showing DNA staining ≥4N (Figure 5C, bracket in lower right panel), consistent with mitotic death and exit from the cell cycle.

MAPKAP Kinase-2 Depleted Cells Are More Sensitive to DNA Damage-Induced Cell Death

The experiments in Figures 4 and 5A–5C indicate that MAPKAP kinase-2 is involved in each of the cell cycle

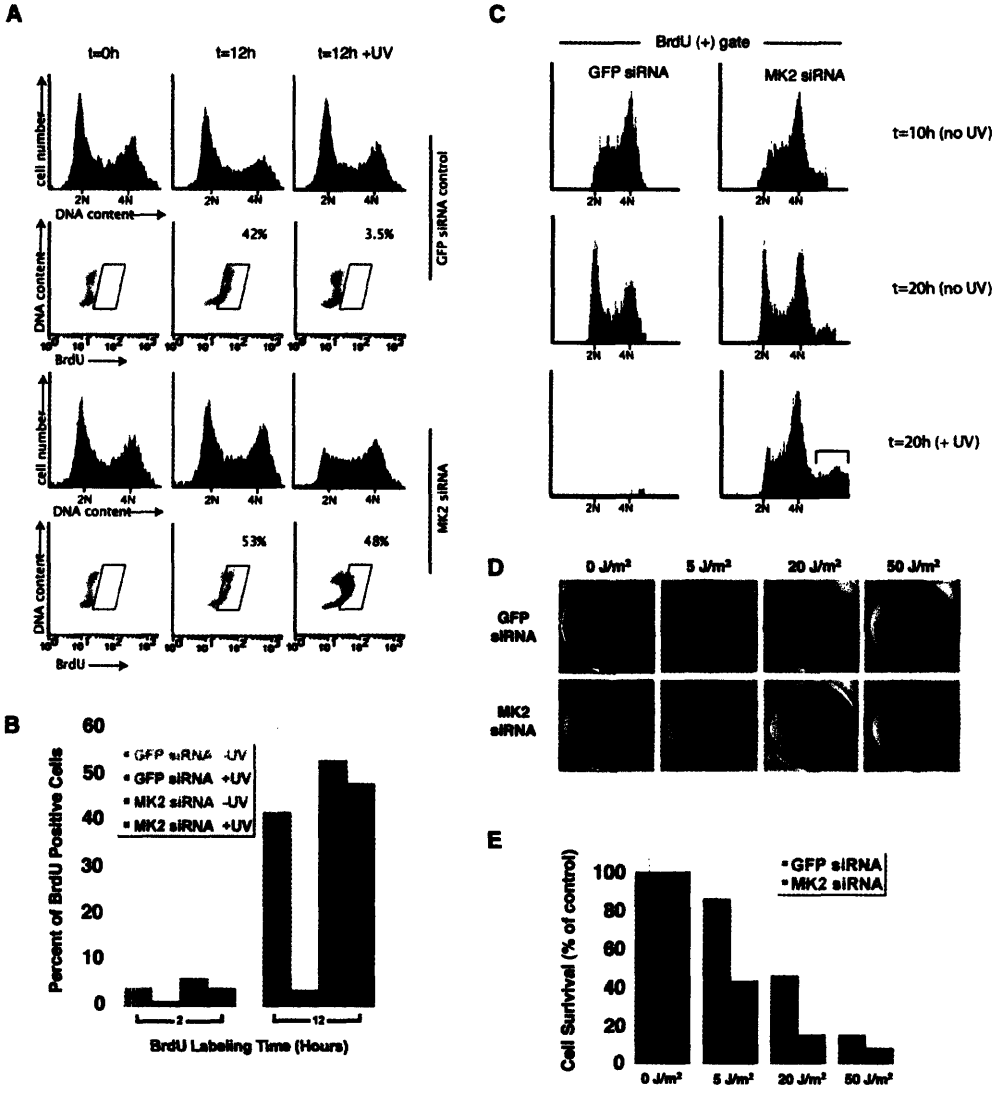

Figure 5. MAPKAP Kinase-2 Is Required for S Phase Arrest and Cell Survival following DNA Damage

(A) GFP siRNA- or MAPKAP kinase-2 siRNA-treated U2OS cells were mock treated or UV irradiated and allowed to recover for 30 min. BrdU was added and cells were fixed and analyzed by FACS for DNA content and BrdU incorporation 12 hr later.

(B) Percentage of cells in (A) showing BrdU incorporation at 2 and 12 hr following BrdU addition were measured.

(C) GFP siRNA- or MAPKAP kinase-2 siRNA-treated U2OS cells were either mock treated or UV irradiated, allowed to recover for 30 min, then pulse labeled with BrdU for 30 min. At the indicated times after irradiation the distribution of DNA content was analyzed in the BrdU-positive population.

(D) GFP siRNA- or MAPKAP kinase-2 siRNA-treated U2OS cells were either mock treated or irradiated at the indicated UV-C dose. Cells were stained with Crystal Violet 48 hr later and visualized. Insets show a magnified view.

(E) Quantitative colony forming assays were performed by plating cells at a density of ~100 cells per 35 mm² dish. Cells were treated as in (D), and assays were performed in triplicate for each condition.

checkpoints triggered by UV-induced DNA damage. To determine the effect of MAPKAP kinase-2 depletion on cell survival, cells were transfected with control siRNA or MAPKAP kinase-2 siRNA for 48 hr, trypsinized, replated, and analyzed for colony formation in response to various doses of UV-C irradiation 12 hr after replating. As shown in Figures 5D and 5E, MAPKAP kinase-2 knockdown cells displayed a significant reduction in colony formation when compared to control-treated cells at all doses of UV-C irradiation examined. This difference in survival after UV-C exposure was most pronounced at low to moderate UV doses.

A Structural Model for MAPKAP Kinase-2 Substrate Selectivity

The optimal phosphorylation motif determined for MAPKAP kinase-2 is strikingly similar to that determined for two other checkpoint kinases, Chk1 and Chk2 (Figure 6A; O'Neill et al. [2002]) and data not shown). All three of these CAMK superfamily members—MAPKAP kinase-2,

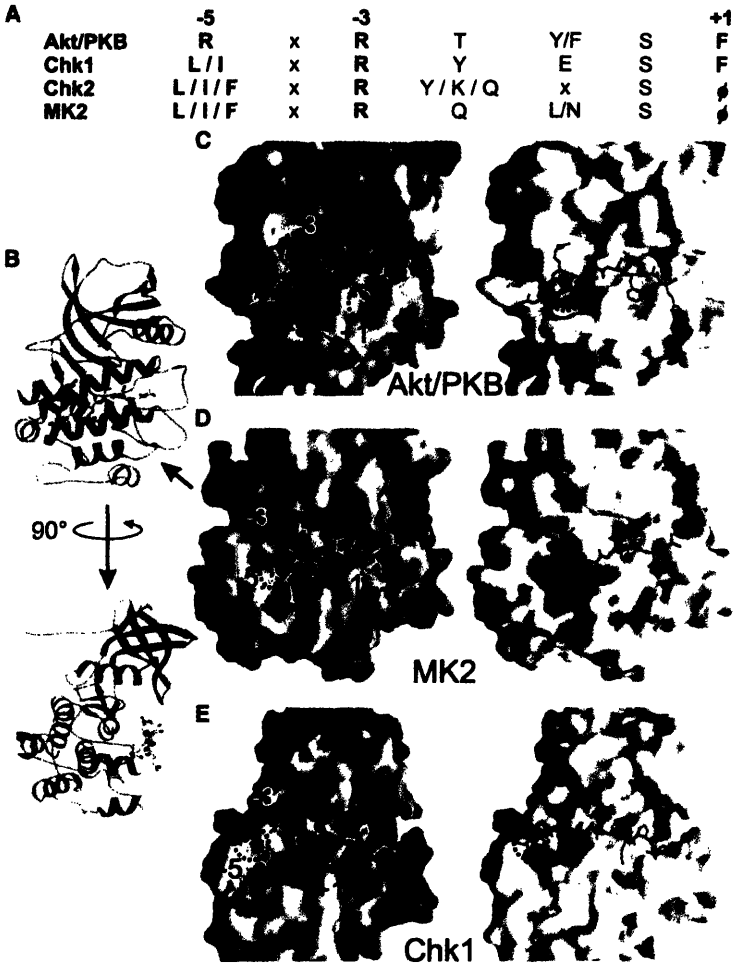

Figure 6. Comparison of Active Site Electrostatic Potentials and Hydrophobicity for the Substrate Binding Cleft of MAPKAP Kinase-2, Akt, and Chk1

(A) Optimal substrate phosphorylation motifs for Akt/PKB, Chk1, Chk2, and MAPKAP kinase-2.

(B) Ribbons representation of the MAPKAP kinase-2 kinase domain in a similar orientation as that shown in (C)–(E) (upper), and in an orthogonal orientation (lower) with stick representations of the substrate peptide in the active site cleft. Figure created using Molscript (Kraulis, 1991) and Raster3D (Merritt and Murphy, 1994).

(C) Molecular surface representations of the Akt/PKB active site (PDB code 1O6K) using GRASP (Nicholls et al., 1993). Electrostatic potentials (left) are colored red (negative) and blue (positive). Hydrophobicity (right) is shaded gray, yellow, and green for low, medium, and high hydrophobic potentials, respectively. The GSK3 substrate peptide Gly-Arg-Pro-Arg-Thr-Thr-Ser-Phe-Ala-Glu, with the phospho-acceptor indicated in bold and underlined, is shown in stick representation.

(D) Molecular surface representations of the MAPKAP kinase-2 active site (PDB code 1NY3). Electrostatic and hydrophobic potentials are colored as in (C). The optimal substrate peptide Leu-Gln-Arg-Gln-Leu-Ser-Ile-Ala is shown in stick representation.

(E) Molecular surface representations of the Chk1 active site (PDB code 1IA8). Electrostatic and hydrophobic potentials are colored as in (C). Stick representation of the modeled Cdc25C substrate peptide (Leu-Tyr-Arg-Ser-Pro-Ser-Met-Pro-Leu) is shown.

The region corresponding to the Ser−5, Ser−3, and Ser+1 positions of the substrate peptides in (C), (D), and (E) is indicated by dashed circles.

Chk1, and Chk2—strongly select for aliphatic residues in the Ser−5 position, Arg in the Ser−3 position, and aromatic/aliphatic residues in the Ser+1 position, along with additional less stringent selection for particular amino acids in other positions (Figure 6A). In contrast, members of the AGC kinase superfamily such as Akt/PKB and conventional protein kinase C superfamily members preferentially phosphorylate sequences containing Arg residues in both the Ser−5 and Ser−3 positions, and play important roles in antiapoptotic signaling and other signaling events unique to differentiated cell function, rather than critical roles in cell cycle control.

To investigate the structural basis for substrate motif selection, we performed molecular modeling studies of activated MAPKAP kinase-2, using the published MAPKAP kinase-2:ADP cocrystal structure (Underwood et al., 2003) as a base model. The optimal substrate peptide Leu-Gln-Arg-Gln-Leu-Ser-Ile-Ala was modeled into the kinase active site in an extended conformation (Figure 6D), and the kinase:substrate complex compared with the structures of Akt/PKB:AMP-PNP:GSK3-peptide ternary complex (Yang et al., 2002) (Figure 6C) and the Chk1 crystal structure containing a modeled Cdc25C peptide (Chen et al., 2000) (Figure 6E). Strong selection for Arg in the Ser−3 position for MAPKAP kinase-2, Akt/PKB, and Chk1 is rationalized by the presence of a conserved glutamate residue at a similar location in all three kinases (Glu145 in MAPKAP kinase-2, Glu236 in Akt/PKB, and Glu91 in Chk1), which in Akt/PKB forms a bidentate salt bridge with the Ser−3 arginine guanidino group on GSK3 peptide (Yang et al., 2002). Similarly, selection for a hydrophobic residue at the Ser+1 position is explained by a hydrophobic pocket that is conserved at this position in all three kinases. The pocket is lined by Phe310, Pro314, Leu317, and Phe359 in Akt/PKB and by Met167, Leu171, Val174, Leu178, and Leu179 in Chk1. The corresponding Ser+1 pocket in MAPKAP kinase-2 is lined by Pro223, Pro227, Val234, and Leu235. Within this region, Gly312 in Akt/PKB and Gly169 in Chk1 are replaced by Tyr225 in MAPKAP kinase-2, which may reduce the depth of the MAPKAP kinase-2 hydrophobic pocket and explain selection for branched chain aliphatic residues in this position compared with Phe selection by Akt/PKB and Chk1.

The marked contrast between Arg selection at the Ser−5 position in Akt/PKB with the corresponding selection for hydrophobic residues at this position by MAPKAP kinase-2 and Chk1 is accounted for by the presence of Glu342 in Akt/PKB at the base of the Ser−5 pocket. This residue is not conserved in MAPKAP ki-

nase-2 and Chk1 and is instead substituted by Ile255 in MAPKAP kinase-2 and by Ala200 in Chk1. Additional residues, notably Phe147, Pro189, Pro261, and Leu342 in MAPKAP kinase-2 and, similarly, Phe93, Ile96, Pro98, Pro133, and Leu206 in Chk1, contribute a significant hydrophobic character to this region.

Discussion

In this study we have defined the optimal substrate motifs within the p38 SAPK/MAPKAP kinase-2 axis of signaling using oriented peptide library screening. Our elucidation of the optimal phosphorylation motif for MAPKAP kinase-2 expands considerably upon, and is in good agreement with, a more preliminary motif for this kinase determined previously (Stokoe et al., 1993). Similarly, the optimal motif determined for p38 SAPK is in reasonable agreement with many mapped phosphorylation sites on p38 SAPK substrates. As with all consensus phosphorylation motifs, bona fide substrates match the optimal motif at some, but not necessarily at all, positions. Nearly all in vivo p38 MAPK substrates contain at least a minimum core SP motif, though Cohen and colleagues have recently identified TAB1 as a novel in vivo substrate of p38 SAPK in which one of the three mapped p38 SAPK phosphorylation sites lacks the Ser+1 Pro residue. This suggests that alternative phosphorylation and docking motifs may be present on some p38 SAPK substrates, and/or that local avidity effects may be important in some cases.

Our data suggests that a crucial role of p38 SAPK in response to UV-induced DNA damage is the phosphorylation and activation of MAPKAP kinase-2, leading to MAPKAP kinase-2-directed phosphorylation of Cdc25 family members to induce 14-3-3 binding and subsequent cell cycle arrest. In this way, MAPKAP kinase-2 performs similar functions after UV-C induced DNA damage as those performed by Chk1 and Chk2 after exposure of cells to ionizing radiation (Bartek and Lukas, 2003). Recent data suggest that p38 SAPK (and therefore MAPKAP kinase-2) may play a similar role in certain types of chemotherapy-induced DNA damage (Hirose et al., 2003, 2004; Mikhailov et al., 2004).

Our finding that MAPKAP kinase-2 is a central checkpoint kinase involved in DNA damage responses triggered by UV irradiation allows a different interpretation of the results of Bulavin et al. (2001), who demonstrated that inhibition of p38 SAPK by the chemical inhibitor SB202190, or reduction of p38 SAPK levels using antisense oligonucleotides, blocked the G_2/M checkpoint response in cells that received the same dose of UV-C radiation as the cells used in our study. The authors reported that p38 SAPK directly phosphorylated Cdc25B and C to generate a 14-3-3 binding site. However, the experiments in that study were performed using Flag-tagged p38 SAPK that was immunoprecipitated from UV-irradiated cells. p38 SAPK and MAPKAP kinase-2 form a tight complex within cells, and in response to cellular stress, p38 SAPK phosphorylation of MAPKAP kinase-2 is required for the cotransport of the p38 SAPK:MAPKAP kinase-2 complex from the nucleus to the cytoplasm (Ben-Levy et al., 1998; Kotlyarov et al., 2002). Thus, the p38 SAPK immunoprecipitates used in that study likely contained significant amounts of MAPKAP kinase-2. Furthermore, the activity of MAPKAP kinase-2 would have been strongly reduced by treatment with any p38 SAPK inhibitor.

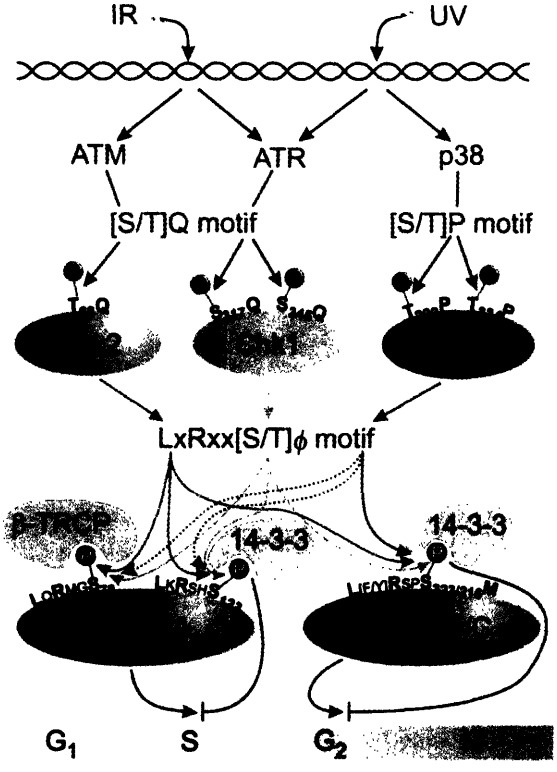

Figure 7. A Unified Model of the Kinase-Dependent DNA Damage Checkpoint

Parallel pathways in the DNA damage checkpoint signal transduction network converge on common substrates by signaling to downstream kinases with similar phosphorylation motif specificities. ϕ indicates hydrophobic residues. The dashed line from Chk1 to Cdc25B/C indicates that this phosphorylation event remains controversial in response to ionizing radiation.

MAPKAP kinase-2 undergoes initial activation in the nucleus with subsequent export of the active kinase to the cytoplasm (Ben-Levy et al., 1998). Thus, MAPKAP kinase-2 is well positioned to function as both a nuclear initiator of Cdc25B/C phosphorylation in response to DNA damage and as a maintenance kinase that keeps Cdc25B/C inhibited in the cytoplasm. A unified model for kinase-dependent DNA damage checkpoints is presented in Figure 7. In response to ionizing radiation, ATM activation of Chk2 and ATR activation of Chk1 leads to phosphorylation of Cdc25 family members on related sequences corresponding to the checkpoint kinase core "motif" LxRxx[S/T]ϕ. Similarly, in response to UV-induced DNA damage, ATR activates Chk1 and p38 SAPK activates MAPKAP kinase-2, leading to phosphorylation of the same core motif on Cdc25 family members. The exact role that different checkpoint kinases play in phosphorylating different Cdc25 phosphatases remains incompletely understood. The major role of Chk1 appears to involve phosphorylation of Cdc25A after IR (Busino et al., 2004 and references therein),

whereas Chk2 appears to phosphorylate all three Cdc25 family members. In the absence of Chk2, Chk1 appears to be able to subsume at least part of this function (Bartek and Lukas, 2003). Our data now suggests that MAPKAP kinase-2 is the primary effector kinase that targets Cdc25B/C after UV-C exposure. MAPKAP kinase-2 may also be involved in Cdc25A phosphorylation, since we observed that the G_1 and S phase checkpoints were eliminated in the MAPKAP kinase-2 knockdown cells.

Given the convergence of optimal substrate motifs for MAPKAP kinase-2, Chk1, and Chk2, the structural similarity between the substrate binding cleft in Chk1 and MAPKAP kinase-2, and the functional overlap between these three kinases in response to DNA damage, MAPKAP kinase-2 could equivalently be referred to as "Chk3." Whether MAPKAP kinase-2 plays a similar critical checkpoint role in the cellular response to altered chromatin topology and chemically induced DNA damage as that described here in response to UV irradiation is not known. However, recent reports that p38 MAPK participates in checkpoint activation following Topoisomerase II inhibition, adriamycin-induced double-strand breaks (Mikhailov et al., 2004), and temozolomide-induced DNA damage mismatch repair (Hirose et al., 2003) is consistent with such a model. Experiments to test this are currently in progress. In summary, our data implicate MAPKAP kinase-2 as a third checkpoint kinase that functions in parallel with Chk1 and Chk2 to coordinately regulate the DNA damage response.

Experimental Procedures

Protein Production and Purification

Recombinant 14-3-3ε/ζ-MBP (maltose binding protein), 14-3-3β/ζ-GST (glutathione S-transferase), and p47phox-GST proteins were produced as described previously (Yaffe et al., 1997). A vector encoding Cdc25B2-GST was a gift from B. Gabrielli (University of Queensland, Australia). Point mutations were generated using the Stratagene QuickChange Mutagenesis Kit and confirmed by sequencing the entire coding regions.

Kinase Motif Screening with Oriented Peptide Libraries and In Vitro Kinase Assays

Combinatorial peptide library screening was performed using recombinant purified p38α SAPK, MK2, Chk1, and Chk2 as previously described (Songyang and Cantley, 1998), with minor modifications. Kinase reactions were performed in 30 μl of kinase reaction buffer (20 mM HEPES, pH 7.5, 10 mM $MgCl_2$, 3 mM 2-mercaptoethanol, 100 μg/ml BSA, 50 μM ATP, 10 μCi ^{32}P-γ-ATP) containing 2.0 μg of recombinant p47 or Cdc25B substrate protein or the specified amount of peptide and 0.10 μg of recombinant p38α SAPK or 0.03 μg of recombinant MAPKAP kinase-2 at 30°C for the indicated time. Additional details are provided in the Supplemental Data, which can be found at http://www.molecule.org/cgi/content/full/17/1/37/DC1/.

Tissue Culture and Transfections

U2OS cells were maintained and propagated in DMEM supplemented with 10% fetal bovine serum (FBS), L-glutamine, and penicillin/streptomycin. siRNA oligonucleotides corresponding to MAPKAP kinase-2 sense strand 5′-UGACCAUCACCGAGUUUAUdTdT-3′ and antisense strand 5′-AUAAACUCGGUGAUGGUCAdTdT-3′ and to GFP sense strand 5′-UCCCGGCUAUGUGCAGGAGdTdT-3′ and antisense strand 5′-CUCCUGCACAUAGCCGGGAdTdT-3′ were purchased from Dharmacon. siRNAs were used according to the manufacturer's suggested protocol and transfected into cells using Lipofectamine 2000 (GIBCO Invitrogen).

14-3-3 Pull-Down Assays, Immunoblotting, and Immunofluorescence

U2OS cells were lysed in lysis buffer: 50 mM Tris/HCl, pH 7.8, 150 mM NaCl, 1.0% NP-40, 5 mM EDTA, 2 mM DTT, 8 μg/ml pepstatin, 8 μg/ml aprotinin, 8 μg/ml leupeptin, 2 mM Na_3VO_4, 10 mM NaF, and 1 μM microcystin for 20 min at 4°C. Clarified lysates (0.5–2 mg protein) were incubated with 20 μl glutathione beads or amylose beads containing 10–20 μg 14-3-3-GST or 14-3-3-MBP, respectively, for 120 min at 4°C. Following washing, lysates and bead bound proteins were analyzed by SDS-PAGE, followed by transfer to PVDF membranes, and immunoblotted with the indicated antibodies. For immunofluorescence experiments, U2OS cells were seeded onto 18 mm^2 coverslips, irradiated or mock treated, fixed, extracted, and immunostained as described previously (Clapperton et al., 2004).

FACS Analysis

UV irradiation was performed at 254 nm (UV-C) using a Stratalinker 2400 (Stratagene). U2OS cells were fixed in 70% ethanol overnight at −20°C, permeabilized with PBS containing 0.2% Triton X-100 for 20 min at 4°C, blocked with 2% FBS in PBS, and incubated with 1 μg of anti-phospho-histone H3 per 10^6 cells for 60 min on ice. Following washing, cells were incubated with FITC-conjugated goat anti-rabbit antibody (diluted 1:500) for 30 min on ice, washed, and resuspended in PBS containing 50 μg/ml PI for 20 min immediately prior to FACS analysis.

For BrdU incorporation experiments, cells were incubated with 30 μM BrdU for the indicated times, then fixed and permeabilized as above. Cells were denatured in 2 N HCl for 20 min at room temperature, neutralized with 0.1 M $Na_2B_4O_7$ (pH 8.5), blocked with 2% FBS in PBS, and incubated with a murine anti-BrdU antibody for 60 min on ice. Following washing, cells were incubated with FITC-conjugated goat anti-mouse antibodies and PI as above. Analysis was performed using a Becton Dickinson FACS machine with CellQuest software.

Structural Modeling

Activated MAPKAP kinase-2 (phosphorylated on Thr222) was modeled using the crystal structure of the ADP complex (Underwood et al., 2003) with the activation loop (residues 213–241) deleted and rebuilt using the corresponding region (residues 299–328) from the structure of activated Akt/PKB in complex with AMP-PNP and GSK3-peptide (Yang et al., 2002) as a template. An optimal peptide (Leu-Gln-Arg-Gln-Leu-Ser-Ile-Ala) was modeled in the active site based on the GSK3-peptide. A substrate peptide (Leu-Tyr-Arg-Ser-Pro-Ser-Met-Pro-Leu, residues 211–219 of human Cdc25C) in the Chk1 active site was similarly modeled using the GSK3-peptide as a template and manually adjusted to resemble the published model (Chen et al., 2000). Structures were superimposed using ALIGN (Cohen, 1997) and SUPERIMPOSE (Diederichs, 1995). Manual adjustments of the models were made using XFIT from the XtalView suite (McRee, 1999).

Supplemental data including additional data and detailed Experimental Procedures used in this work are available online at http://www.molecule.org/cgi/content/full/17/1/37/DC1/.

Acknowledgments

We thank Joe Budmann, Irma Alarcon-Rangel, Timmy Ho, Drew Lowery, and Duaa Mohammad for technical and editorial assistance, and Steve Smerdon for helpful discussions. We apologize to authors whose work we were unable to site due to space limitations. This work was funded by a David Koch Graduate Student Fellowship to I.A.M., a Jane Coffin Childs Memorial Fund postdoctoral fellowship to D.L., and NIH grant GM60594 and a Burroughs-Wellcome Career Development Award to M.B.Y.

Received: July 21, 2004
Revised: October 5, 2004
Accepted: October 27, 2004
Published: January 6, 2005

References

Abraham, R.T. (2001). Cell cycle checkpoint signaling through the ATM and ATR kinases. Genes Dev. *15*, 2177–2196.

Bartek, J., and Lukas, J. (2003). Chk1 and Chk2 kinases in checkpoint control and cancer. Cancer Cell *3*, 421–429.

Ben-Levy, R., Leighton, I.A., Doza, Y.N., Attwood, P., Morrice, N., Marshall, C.J., and Cohen, P. (1995). Identification of novel phosphorylation sites required for activation of MAPKAP kinase-2. EMBO J. *14*, 5920–5930.

Ben-Levy, R., Hooper, S., Wilson, R., Paterson, H.F., and Marshall, C.J. (1998). Nuclear export of the stress-activated protein kinase p38 mediated by its substrate MAPKAP kinase-2. Curr. Biol. *8*, 1049–1057.

Bulavin, D.V., Higashimoto, Y., Popoff, I.J., Gaarde, W.A., Basrur, V., Potapova, O., Appella, E., and Fornace, A.J., Jr. (2001). Initiation of a G2/M checkpoint after ultraviolet radiation requires p38 kinase. Nature *411*, 102–107.

Busino, L., Chiesa, M., Draetta, G.F., and Donzelli, M. (2004). Cdc25A phosphatase: combinatorial phosphorylation, ubiquitylation and proteolysis. Oncogene *23*, 2050–2056.

Chen, P., Luo, C., Deng, Y., Ryan, K., Register, J., Margosiak, S., Tempczyk-Russell, A., Nguyen, B., Myers, P., Lundgren, K., et al. (2000). The 1.7 Å crystal structure of human cell cycle checkpoint kinase Chk1: implications for Chk1 regulation. Cell *100*, 681–692.

Chen, M.S., Hurov, J., White, L.S., Woodford-Thomas, T., and Piwnica-Worms, H. (2001). Absence of apparent phenotype in mice lacking Cdc25C protein phosphatase. Mol. Cell. Biol. *21*, 3853–3861.

Cheng, T.J., and Lai, Y.K. (1998). Identification of mitogen-activated protein kinase-activated protein kinase-2 as a vimentin kinase activated by okadaic acid in 9L rat brain tumor cells. J. Cell. Biochem. *71*, 169–181.

Cheung, P.C., Campbell, D.G., Nebreda, A.R., and Cohen, P. (2003). Feedback control of the protein kinase TAK1 by SAPK2a/p38alpha. EMBO J. *22*, 5793–5805.

Clapperton, J.A., Manke, I.A., Lowery, D.M., Ho, T., Haire, L.F., Yaffe, M.B., and Smerdon, S.J. (2004). Structure and mechanism of BRCA1 BRCT domain recognition of phosphorylated BACH1 with implications for cancer. Nat. Struct. Mol. Biol. *11*, 512–518.

Cohen, G.E. (1997). ALIGN: a program to superimpose protein coordinates, accounting for insertions and deletions. J. Appl. Crystallogr. *30*, 1160–1161.

Diederichs, K. (1995). Structural superposition of proteins with unknown alignment and detection of topological similarity using a six-dimensional search algorithm. Proteins *23*, 187–195.

Donzelli, M., and Draetta, G.F. (2003). Regulating mammalian checkpoints through Cdc25 inactivation. EMBO Rep. *4*, 671–677.

El Benna, J., Faust, R.P., Johnson, J.L., and Babior, B.M. (1996). Phosphorylation of the respiratory burst oxidase subunit p47phox as determined by two-dimensional phosphopeptide mapping. Phosphorylation by protein kinase C, protein kinase A, and a mitogen-activated protein kinase. J. Biol. Chem. *271*, 6374–6378.

Ficarro, S.B., McCleland, M.L., Stukenberg, P.T., Burke, D.J., Ross, M.M., Shabanowitz, J., Hunt, D.F., and White, F.M. (2002). Phosphoproteome analysis by mass spectrometry and its application to Saccharomyces cerevisiae. Nat. Biotechnol. *20*, 301–305.

Furnari, B., Rhind, N., and Russell, P. (1997). Cdc25 mitotic inducer targeted by chk1 DNA damage checkpoint kinase. Science *277*, 1495–1497.

Galaktionov, K., Lee, A.K., Eckstein, J., Draetta, G., Meckler, J., Loda, M., and Beach, D. (1995). CDC25 phosphatases as potential human oncogenes. Science *269*, 1575–1577.

Gasparotto, D., Maestro, R., Piccinin, S., Vukosavljevic, T., Barzan, L., Sulfaro, S., and Boiocchi, M. (1997). Overexpression of CDC25A and CDC25B in head and neck cancers. Cancer Res. *57*, 2366–2368.

Giles, N., Forrest, A., and Gabrielli, B. (2003). 14-3-3 acts as an intramolecular bridge to regulate cdc25B localization and activity. J. Biol. Chem. *278*, 28580–28587.

Goldstone, S., Pavey, S., Forrest, A., Sinnamon, J., and Gabrielli, B. (2001). Cdc25-dependent activation of cyclin A/cdk2 is blocked in G2 phase arrested cells independently of ATM/ATR. Oncogene *20*, 921–932.

Guo, Z., Kumagai, A., Wang, S.X., and Dunphy, W.G. (2000). Requirement for Atr in phosphorylation of Chk1 and cell cycle regulation in response to DNA replication blocks and UV-damaged DNA in Xenopus egg extracts. Genes Dev. *14*, 2745–2756.

Heidenreich, O., Neininger, A., Schratt, G., Zinck, R., Cahill, M.A., Engel, K., Kotlyarov, A., Kraft, R., Kostka, S., Gaestel, M., et al. (1999). MAPKAP kinase 2 phosphorylates serum response factor in vitro and in vivo. J. Biol. Chem. *274*, 14434–14443.

Hirose, Y., Katayama, M., Stokoe, D., Haas-Kogan, D.A., Berger, M.S., and Pieper, R.O. (2003). The p38 mitogen-activated protein kinase pathway links the DNA mismatch repair system to the G2 checkpoint and to resistance to chemotherapeutic DNA-methylating agents. Mol. Cell. Biol. *23*, 8306–8315.

Hirose, Y., Katayama, M., Berger, M.S., and Pieper, R.O. (2004). Cooperative function of Chk1 and p38 pathways in activating G2 arrest following exposure to temozolomide. J. Neurosurg. *100*, 1060–1065.

Huang, C.K., Zhan, L., Ai, Y., and Jongstra, J. (1997). LSP1 is the major substrate for mitogen-activated protein kinase-activated protein kinase 2 in human neutrophils. J. Biol. Chem. *272*, 17–19.

Kotlyarov, A., Yannoni, Y., Fritz, S., Laass, K., Telliez, J.B., Pitman, D., Lin, L.L., and Gaestel, M. (2002). Distinct cellular functions of MK2. Mol. Cell. Biol. *22*, 4827–4835.

Kraulis, P.J. (1991). MOLSCRIPT: a program to produce both detailed and schematic plots of protein structures. J. Appl. Crystallogr. *24*, 946–950.

Kumagai, A., and Dunphy, W.G. (1999). Binding of 14-3-3 proteins and nuclear export control the intracellular localization of the mitotic inducer Cdc25. Genes Dev. *13*, 1067–1072.

Landry, J., Lambert, H., Zhou, M., Lavole, J.N., Hickey, E., Weber, L.A., and Anderson, C.W. (1992). Human HSP27 is phosphorylated at serines 78 and 82 by heat shock and mitogen-activated kinases that recognize the same amino acid motif as S6 kinase II. J. Biol. Chem. *267*, 794–803.

Mailand, N., Podtelejnikov, A.V., Groth, A., Mann, M., Bartek, J., and Lukas, J. (2002). Regulation of G(2)/M events by Cdc25A through phosphorylation-dependent modulation of its stability. EMBO J. *21*, 5911–5920.

McLaughlin, M.M., Kumar, S., McDonnell, P.C., Van Horn, S., Lee, J.C., Livi, G.P., and Young, P.R. (1996). Identification of mitogen-activated protein (MAP) kinase-activated protein kinase-3, a novel substrate of CSBP p38 MAP kinase. J. Biol. Chem. *271*, 8488–8492.

McRee, D.E. (1999). XtalView/Xfit: a versatile program for manipulating atomic coordinates and electron density. J. Struct. Biol. *125*, 156–165.

Merritt, E.A., and Murphy, M.E.P. (1994). Raster3D version 2.0. A program for photorealistic molecular graphics. Acta Crystallogr. D Biol. Crystallogr. *50*, 869–873.

Mikhailov, A., Shinohara, M., and Rieder, C.L. (2004). Topoisomerase II and histone deacetylase inhibitors delay the G2/M transition by triggering the p38 MAPK checkpoint pathway. J. Cell Biol. *166*, 517–526.

Nicholls, A., Bharadwaj, R., and Honig, B. (1993). GRASP: graphical representation and analysis of surface properties. Biophys. J. *64*, A166.

Nishikawa, K., Toker, A., Johannes, F.J., Songyang, Z., and Cantley, L.C. (1997). Determination of the specific substrate sequence motifs of protein kinase C isozymes. J. Biol. Chem. *272*, 952–960.

Obata, T., Brown, G.E., and Yaffe, M.B. (2000). MAP kinase pathways activated by stress: the p38 MAPK pathway. Crit. Care Med. *28*, N67–N77.

O'Neill, T., Giarratani, L., Chen, P., Iyer, L., Lee, C.H., Bobiak, M., Kanai, F., Zhou, B.B., Chung, J.H., and Rathbun, G.A. (2002). Determination of substrate motifs for human Chk1 and hCds1/Chk2 by the oriented peptide library approach. J. Biol. Chem. *277*, 16102–16115.

Peng, C.Y., Graves, P.R., Thoma, R.S., Wu, Z., Shaw, A.S., and

Piwnica-Worms, H. (1997). Mitotic and G2 checkpoint control: regulation of 14-3-3 protein binding by phosphorylation of Cdc25C on serine-216. Science *277*, 1501–1505.

Raingeaud, J., Gupta, S., Rogers, J.S., Dickens, M., Han, J., Ulevitch, R.J., and Davis, R.J. (1995). Pro-inflammatory cytokines and environmental stress cause p38 mitogen-activated protein kinase activation by dual phosphorylation on tyrosine and threonine. J. Biol. Chem. *270*, 7420–7426.

Rouse, J., Cohen, P., Trigon, S., Morange, M., Alonso-Llamazares, A., Zamanillo, D., Hunt, T., and Nebreda, A.R. (1994). A novel kinase cascade triggered by stress and heat shock that stimulates MAPKAP kinase-2 and phosphorylation of the small heat shock proteins. Cell *78*, 1027–1037.

Roux, P.P., and Blenis, J. (2004). ERK and p38 MAPK-activated protein kinases: a family of protein kinases with diverse biological functions. Microbiol. Mol. Biol. Rev. *68*, 320–344.

She, Q.B., Ma, W.Y., and Dong, Z. (2002). Role of MAP kinases in UVB-induced phosphorylation of p53 at serine 20. Oncogene *21*, 1580–1589.

Songyang, Z., and Cantley, L.C. (1998). The use of peptide library for the determination of kinase peptide substrates. Methods Mol. Biol. *87*, 87–98.

Stokes, M.P., and Michael, W.M. (2003). DNA damage-induced replication arrest in Xenopus egg extracts. J. Cell Biol. *163*, 245–255.

Stokoe, D., Campbell, D.G., Nakielny, S., Hidaka, H., Leevers, S.J., Marshall, C., and Cohen, P. (1992). MAPKAP kinase-2; a novel protein kinase activated by mitogen-activated protein kinase. EMBO J. *11*, 3985–3994.

Stokoe, D., Caudwell, B., Cohen, P.T., and Cohen, P. (1993). The substrate specificity and structure of mitogen-activated protein (MAP) kinase-activated protein kinase-2. Biochem. J. *296*, 843–849.

Tanoue, T., and Nishida, E. (2003). Molecular recognitions in the MAP kinase cascades. Cell. Signal. *15*, 455–462.

Tanoue, T., Adachi, M., Moriguchi, T., and Nishida, E. (2000). A conserved docking motif in MAP kinases common to substrates, activators and regulators. Nat. Cell Biol. *2*, 110–116.

Underwood, K.W., Parris, K.D., Federico, E., Mosyak, L., Czerwinski, R.M., Shane, T., Taylor, M., Svenson, K., Liu, Y., Hsiao, C.L., *et al.* (2003). Catalytically active MAP KAP kinase 2 structures in complex with staurosporine and ADP reveal differences with the autoinhibited enzyme. Structure (Camb) *11*, 627–636.

Wang, X.Z., and Ron, D. (1996). Stress-induced phosphorylation and activation of the transcription factor CHOP (GADD153) by p38 MAP Kinase. Science *272*, 1347–1349.

Werz, O., Szellas, D., Steinhilber, D., and Radmark, O. (2002). Arachidonic acid promotes phosphorylation of 5-lipoxygenase at Ser-271 by MAPK-activated protein kinase 2 (MK2). J. Biol. Chem. *277*, 14793–14800.

Yaffe, M.B., Rittinger, K., Volinia, S., Caron, P.R., Aitken, A., Leffers, H., Gamblin, S.J., Smerdon, S.J., and Cantley, L.C. (1997). The structural basis for 14-3-3:phosphopeptide binding specificity. Cell *91*, 961–971.

Yaffe, M.B., Leparc, G.G., Lai, J., Obata, T., Volinia, S., and Cantley, L.C. (2001). A motif-based profile scanning approach for genome-wide prediction of signaling pathways. Nat. Biotechnol. *19*, 348–353.

Yang, S.H., Galanis, A., and Sharrocks, A.D. (1999). Targeting of p38 mitogen-activated protein kinases to MEF2 transcription factors. Mol. Cell. Biol. *19*, 4028–4038.

Yang, J., Cron, P., Good, V.M., Thompson, V., Hemmings, B.A., and Barford, D. (2002). Crystal structure of an activated Akt/protein kinase B ternary complex with GSK3-peptide and AMP-PNP. Nat. Struct. Biol. *9*, 940–944.

Zhao, H., Watkins, J.L., and Piwnica-Worms, H. (2002). Disruption of the checkpoint kinase 1/cell division cycle 25A pathway abrogates ionizing radiation-induced S and G2 checkpoints. Proc. Natl. Acad. Sci. USA *99*, 14795–14800.

Zhou, B.B., and Elledge, S.J. (2000). The DNA damage response: putting checkpoints in perspective. Nature *408*, 433–439.

nature
structural &
molecular biology

Structure and mechanism of BRCA1 BRCT domain recognition of phosphorylated BACH1 with implications for cancer

Julie A Clapperton[1,3], Isaac A Manke[2,3], Drew M Lowery[2], Timmy Ho[2], Lesley F Haire[1], Michael B Yaffe[2] & Stephen J Smerdon[1]

Germline mutations in the *BRCA1* tumor suppressor gene often result in a significant increase in susceptibility to breast and ovarian cancers. Although the molecular basis of their effects remains largely obscure, many mutations are known to target the highly conserved C-terminal BRCT repeats that function as a phosphoserine/phosphothreonine-binding module. We report the X-ray crystal structure at a resolution of 1.85 Å of the BRCA1 tandem BRCT domains in complex with a phosphorylated peptide representing the minimal interacting region of the DEAH-box helicase BACH1. The structure reveals the determinants of this novel class of BRCA1 binding events. We show that a subset of disease-linked mutations act through specific disruption of phospho-dependent BRCA1 interactions rather than through gross structural perturbation of the tandem BRCT domains.

The breast cancer susceptibility gene product, BRCA1, has important roles in cell cycle control, transcriptional regulation, chromatin remodeling and the response to DNA damage[1–4]. BRCA1 is a large, modular protein of 1,863 residues containing an N-terminal RING domain, a central region rich in SQ and TQ dipeptide pairs and tandem BRCT (BRCA1 C-terminal) domains. BRCA1 interacts with many protein partners at different stages of the cell cycle, or after genotoxic stress. For example, BRCA1 interacts with the DNA helicase BACH1 during S and G2 phases in normally cycling cells[5,6], whereas BRCA1 interacts with a subset of ATM and ATR substrates in response to DNA damage[7]. In both S phase and irradiated or mutagen-treated cells, BRCA1 localizes to distinct nuclear foci thought to represent sites of DNA damage[8,9] where BRCA1 is thought to function, at least in part, as a scaffold for the assembly of DNA repair complexes.

Mutations in BRCA1 occur in 50% of women with inherited breast cancer and up to 90% of women with combined breast and ovarian cancer[10–13]. Most frameshift and deletion mutants truncate all or part of the BRCT repeats, whereas >70 missense mutations lie within the BRCT domains themselves (http://research.nhgri.nih.gov/projects/bic/). BRCT domains are α/β structures that occur singly or as multiple repeats in several proteins in addition to BRCA1 that are involved in cell cycle regulation and DNA damage responses[14,15]. Composed of 80–100 amino acids, BRCT domains are generally thought to function as protein-protein recognition modules[15]. The molecular basis of BRCT function, and how cancer-causing mutations in the BRCA1 BRCT domains act at the structural level, however, remain unresolved, despite considerable structural, biochemical and mutagenic analysis[15,17–20]. It has been suggested that mutational effects are manifested through structural destabilization; however, several mutations are located on the protein surface, indicating that they may specifically affect BRCT interactions with other BRCA1-associated targets.

We recently discovered that a subset of tandem BRCT domains, including those of BRCA1, function as phosphoserine/phosphothreonine (pSer/pThr)-binding modules, suggesting that some BRCT-mediated interactions with proteins involved in DNA damage and cell cycle control are regulated by protein phosphorylation[7]. Oriented peptide library screening of tandem BRCT domains revealed phospho-dependent binding specificity extending from the pSer/pThr(+1) to the pSer/pThr(+5) position, with particularly strong selection for aromatic or aromatic/aliphatic residues in the pSer/pThr(+3) position[7,16]. High-affinity phosphopeptides selected by *in vitro*–oriented library screens blocked the interaction of the tandem BRCT domains of BRCA1 and the transcriptional regulator PTIP with ATM- and ATR-phosphorylated substrates[7]. Similar findings were reported in a study[6] demonstrating that the BRCT domain repeat mediates interaction with the DEAH-box helicase BACH1 through a specific phosphoserine (pSer990) located in a region (residues 888–1063) previously shown to be sufficient for BRCA1-BACH1 binding[5,6]. The tumor suppressor function of BRCA1 may directly depend on this interaction as its disruption is sufficient to abrogate the G2-M checkpoint after DNA damage[6,16].

To determine the structural basis for phosphopeptide binding and phosphopeptide-motif selection, and to investigate alternative structural mechanisms underlying BRCT mutations and cancer predisposi-

[1]National Institute for Medical Research, Division of Protein Structure, The Ridgeway, Mill Hill, London NW7 1AA, UK. [2]Center for Cancer Research, E18-580, Massachusetts Institute of Technology, 77 Massachusetts Avenue, Cambridge, Massachusetts 02139, USA. [3]These authors contributed equally to this work. Correspondence should be addressed to M.B.Y. (myaffe@mit.edu) or S.J.S. (stephen.smerdon@nimr.mrc.ac.uk)

Published online 9 May 2004; doi:10.1038/nsmb775

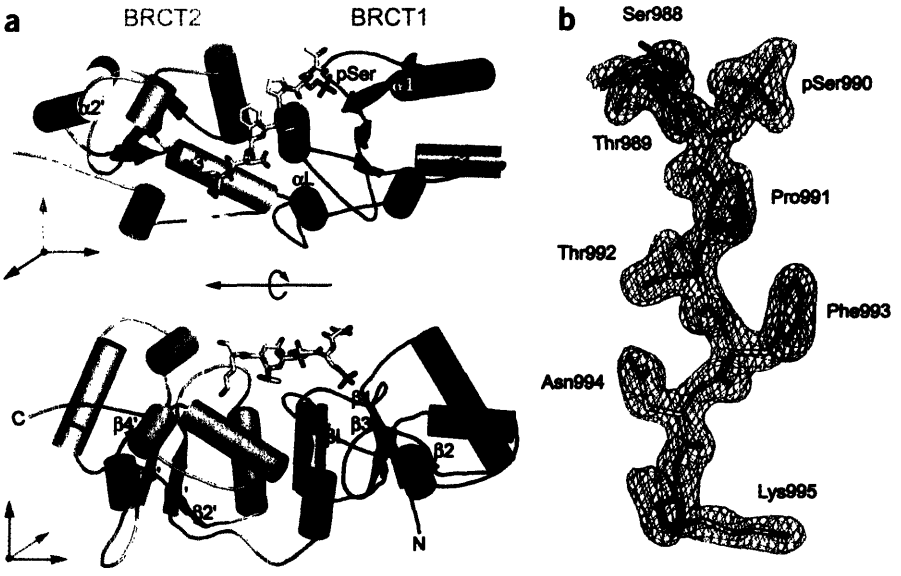

Figure 1 Structure of the tandem BRCT domain–BACH1 phosphopeptide complex. (**a**) Ribbons representation of the tandem BRCT domains in complex with the pSer-containing BACH1 peptide (yellow stick representation). The BACH1 phosphopeptide binds at the interface between the two BRCT repeats. The secondary-structure elements in BRCT2 are labeled with primes to differentiate them from the secondary-structure elements in BRCT1. The BRCT interdomain linker is green. Areas of the 3_{10}-helix are not labeled. (**b**) Electron density map ($2F_o - F_c$) covering the BACH1 phosphopeptide.

tion, we solved the high-resolution X-ray crystal structure of the tandem BRCT repeats bound to a BACH1 phosphopeptide. We provide here a molecular rationale for phosphospecific binding, and show that a set of cancer-associated BRCT mutations eliminate phosphopeptide binding *in vitro* and BACH1 phosphoprotein binding *in vivo*, or alter the phosphopeptide recognition motif for the tandem BRCT domains, revealing a structural basis for mutation-associated loss of BRCA1 function.

RESULTS

Structure of the BRCA1 BRCT–BACH1 complex

The tandem BRCT domains bound to the interacting phosphopeptide from BACH1 (residues 986–995) was crystallized and its structure solved at a resolution of 1.85 Å by X-ray diffraction (**Fig. 1**). Phases were determined by molecular replacement using the previously determined structure of the unliganded tandem BRCT domains (PDB entry 1JNX) as a search model[17] (see **Table 1** and Methods). Difference Fourier maps revealed well-defined electron density for the phosphopeptide, allowing modeling of eight residues corresponding to BACH1 Ser988–Lys995. Each BRCT repeat forms a compact domain (**Fig. 1a**) in which a central, four-stranded β-sheet is packed against two α-helices, α1 and α3, on one side and a single α-helix, α2, on the other. The two domains pack together through interaction between α2 of BRCT1 and the α1′-α3′ pair of BRCT2. A linker region connecting the two BRCT domains contains a β-hairpin-like structure, βL, and a short helical region, αL, which forms part of the interface through interactions with α2 of BRCT1 and the N-terminal end of α3′ from BRCT2. Overall, the structure of the tandem BRCT domain–phosphopeptide complex is similar to that of the unliganded domains (r.m.s. deviation ~0.4 Å for all Cα atoms). However, superposition of the individual BRCT repeats reveals that phosphopeptide binding is associated with a slight relative rotation of each BRCT domain and a translation of BRCT1 helix α1 toward the cleft between the domains.

The BACH1 phosphopeptide binds in an extended conformation to a groove located at the highly conserved interface between the N- and C-terminal BRCT domains (**Figs. 1a** and **2a**), consistent with the requirement of both domains for efficient phosphopeptide binding[7,16]. This mode of binding is distinct from that observed in the phospho-independent interaction between p53 and the tandem BRCT domains of 53BP-1, which occurs primarily through the linker region[21,22]. Our structure clearly shows that the phospho-dependent interactions that are necessary and sufficient for formation of the BACH1–BRCA1 complex occur on the opposite side of the BRCT-BRCT interface from those involved in the interaction between p53 and 53BP-1.

BRCT-phosphopeptide specificity

The binding of tandem BRCT domains to library-selected peptides *in vitro*[7,16] and to phosphorylated BACH1 *in vivo*[6] is dominated by the presence of a pSer/pThr and a phenylalanine three residues C-terminal to it (Phe(+3)). This is confirmed by our structure, which shows that the BACH1 pSer990 phosphate moiety binds to a basic pocket through three direct hydrogen-bonding interactions involving the side chains of Ser1655 and Lys1702, and the main chain NH of Gly1656 (**Fig. 3a**). All three of these residues are located in BRCT1 and all are absolutely conserved in BRCA1 homologs. Ser1655 and Gly1656 are situated within the loop preceding α1 and are brought near to the phosphate moiety as a result of the conformational change that occurs upon phosphopeptide binding. Notably, a S1655F mutation has been identified in a single breast cancer patient, although its link to disease has not been confirmed. In addition to these direct interactions, the phosphate and some peptide main chain atoms are also tethered through networks of water molecules, many of which are tetrahedrally hydrogen-bonded (**Fig. 3a**). Indirect protein-solvent-phosphate contacts are unusual in phospho-dependent protein-protein interactions but have been observed previously in structures of phosphopeptide complexes of the human Plk1 Polo-box domain[23,24].

The Phe(+3) peptide side chain fits into a hydrophobic pocket at the BRCT interface consisting of the side chains of Phe1704, Met1775 and Leu1839 from both BRCT domains (**Figs. 3a** and **4a**). This finding rationalizes the strong selection for aromatic amino acids in the +3 position of the binding motif seen in peptide library experiments[7,16], as well as the observation that a BACH1 F993A mutation eliminates BRCA1-BACH1 binding[6]. Additional hydrogen bonds with the main chain N and O atoms of Phe(+3) are supplied by main and side chain atoms from Arg1699, a site of mutation also associated with cancer predisposition. The phosphorylated Ser990 of BACH1 is preceded by an arginine in the –3 position and followed by a proline in the +1 position, suggesting potential Ser990 phosphorylation by either basophilic and/or proline-directed kinases. The tandem BRCT domains are also known to interact with pSQ-containing motifs characteristic of PI 3–kinase-like kinases such as ATM and ATR[7]. In the tandem BRCT–BACH1 phosphopeptide cocrystal structure, there are no direct interactions between the Pro(+1) side chain and the BRCT domains. Instead, this residue participates in only a single

water-mediated hydrogen bond involving its carbonyl oxygen (Fig. 3a), consistent with the idea that various types of protein kinases can generate tandem BRCT phospho-binding motifs. The Lys(+5) side chain makes two salt-bridging interactions with residues in BRCT2 (Fig. 3a), consistent with the lysine selection observed in this position by spot blot and peptide library experiments[7,16].

Cancer-associated BRCT mutations

Residues that form or stabilize the phosphopeptide-binding surface and the domain-domain interface are among the most highly conserved portions of the molecule in BRCA1 orthologs from humans, primates, rats and mice (Fig. 2b). Notably, these regions correlate strongly with the location of cancer-associated mutations (Fig. 2a). Some cancer-associated mutations may disrupt the global BRCT fold whereas others are more likely to specifically interfere with ligand binding[15,18–21]. About 80 tumor-derived mutations have been identified in the tandem BRCT domains, though only a few of these have been subsequently confirmed to result in cancer predisposition, including D1692Y, C1697R, R1699W, A1708E, S1715R, G1738E, P1749R, M1775R, 5382InsC (a frameshift mutation that results in a stop codon at position 1829) and Y1853X (which truncates the C-terminal 11 residues). Most of these cluster at or near the phosphopeptide-interacting surface (Fig. 2a). Two of these mutated residues, Arg1699 and Met1775, directly interact with residues in the phosphopeptide (Fig. 3a). Two others, Pro1749 and Gly1738, are located at the BRCT1-BRCT2 interface beneath the molecular surface and their effects are probably mediated through alterations in the relative orientation of the tandem BRCT motifs that our structure suggests are necessary for phospho-dependent interactions with partner proteins.

To verify the phosphoserine phosphate interactions observed in the X-ray structure and to investigate the effects of the most common tumor-derived point mutations, we investigated the binding of a panel of site-directed mutant tandem BRCT domains to the interacting region of BACH1. We determined binding by measuring the ability of *in vitro*–transcribed and translated proteins to bind to either phosphorylated or nonphosphorylated biotinylated peptides (Fig. 3b). Wild-type tandem BRCT domains clearly bound to phosphorylated but not nonphosphorylated peptides, whereas mutation of the conserved Ser1655 and Lys1702, alone or in combination, completely abolished the interaction. Five genuine cancer-linked mutations, P1749R, G1738E, M1775R, Y1853X and 5382InsC, all resulted in complete loss of phosphopeptide binding. The R1699W mutation is cancer-linked and a second mutation, R1699Q, has been detected in breast cancer patients but has not yet been directly correlated to disease predisposition. We surmised that the glutamine side chain might still participate in main chain hydrogen bonding to the peptide; this was, indeed, the only tandem BRCT domain mutant that retained a small degree of binding in our assays. Notably, the R1699Q mutant largely lost phospho-specificity, and instead bound to both phosphorylated and nonphosphorylated peptides.

To investigate the *in vivo* binding to endogenous BACH1 of tandem BRCT domains with cancer-predisposing mutations, we transfected U2OS cells with a vector encoding the C-terminal 550 amino acids of BRCA1 containing a myc tag and an SV40 nuclear localization sequence as described[25]. Interaction between the wild-type tandem BRCT domains and full-length BACH1 was easily detected (Fig. 3c). In contrast, no *in vivo* interaction was observed between BACH1 and mutant tandem BRCT domains that disrupt phosphate binding or cause predisposition to breast and ovarian cancer. All of these cancer-associated mutant proteins were expressed at comparable levels when transfected into mammalian cells[26] (Fig. 3c),

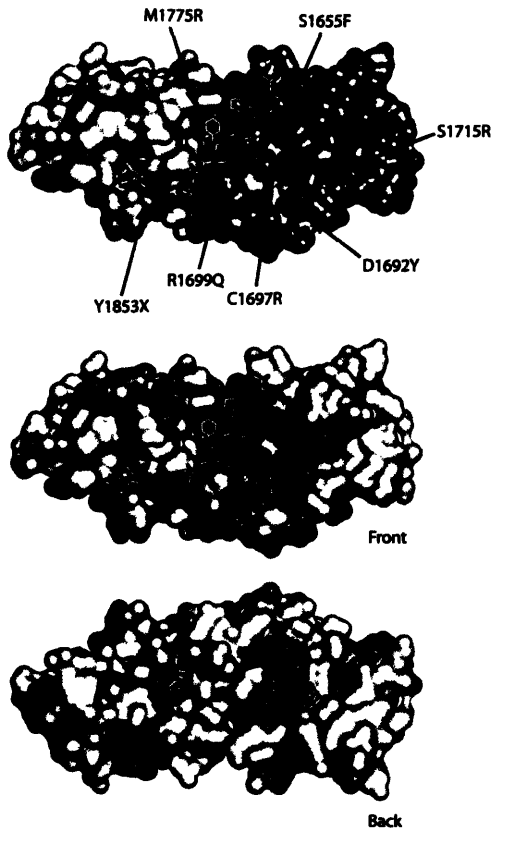

Figure 2 BRCT cancer-linked mutations and sequence conservation in relation to the BACH1 phosphopeptide-binding site. (**a**) Molecular surface representation of tandem BRCT domains. Cancer-associated mutations S1655F, D1692Y, C1697R, R1699Q, S1715R, M1775R and Y1853X cluster near the phosphopeptide-binding site. BRCT1 is blue, BRCT2 is gray, and the mutations are red, except for S1655F, which is green, as its cancer predisposition has not been confirmed by pedigree analysis. (**b**) Comparison of the front and back views of the molecular surface showing the clustering of residues (pink) conserved in human, chimp, mouse, rat, chicken and *Xenopus laevis* BRCA1 tandem BRCT domains. The BACH1 peptide binds in a conserved phosphopeptide-binding groove.

suggesting that gross structural destabilization is unlikely to account for their cancer proclivity.

Interpretation of the structural effects of the M1775R mutation is simplified because the X-ray crystal structure of the M1775R tandem BRCT domain mutant has been determined (PDB entry 1N5O)[18], revealing a nearly identical structure to that of the wild-type protein with an average r.m.s. deviation of 0.35 Å for all Cα atoms. Superposition of the mutant structure with that of our BACH1 complex shows that the guanidine portion of the substituent arginine side chain extrudes into the tandem BRCT cleft, where it occupies the binding site for the essential Phe(+3) of the phosphopeptide (Fig. 4a,b). In this case, loss of phosphopeptide binding *in vitro* and BACH1 binding *in vivo* seem to be attributable to the severe steric clash of the Arg1775 side chain with an important determinant of phospholigand specificity and affinity. The M1775R mutant protein does, however, bind weakly to a BACH1 phosphopeptide in which Phe(+3) is mutated to aspartate or glutamate (Fig. 4c). This is consistent with the introduction of a basic residue at the pSer(+3)-binding site and with the observation that this mutation creates new anion-binding sites in the M1775R crystal structure[18]. Thus, in addition to

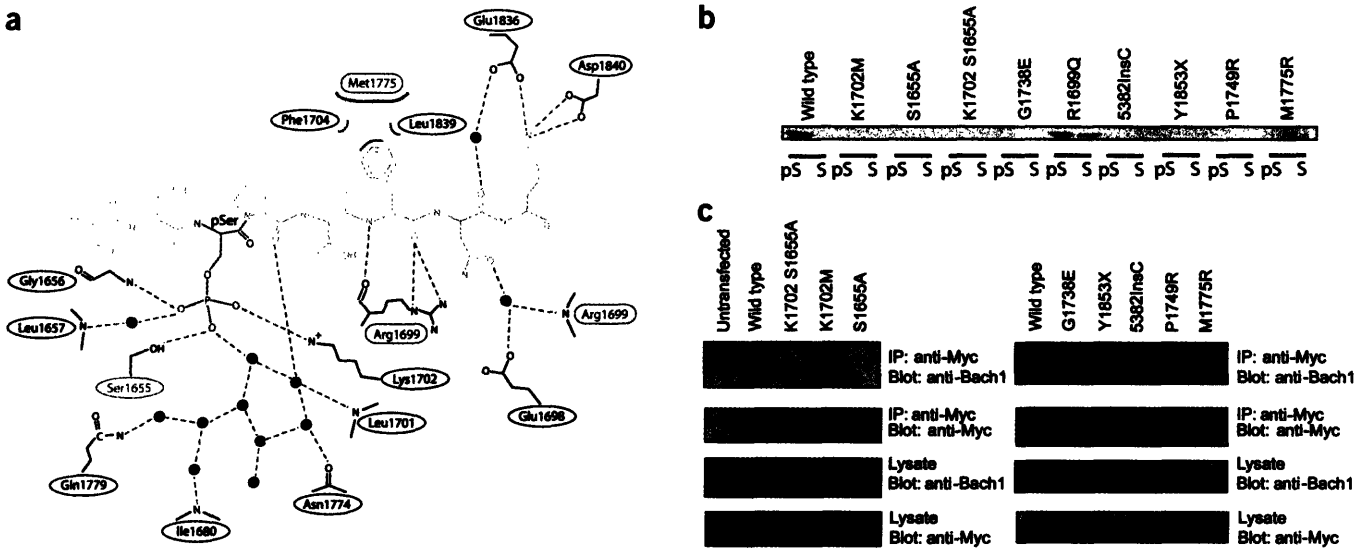

Figure 3 Functional effects of tandem BRCT domain mutations. (**a**) Schematic representation of protein-peptide contacts between tandem BRCT domains and the BACH1 phosphopeptide. Dashed lines, hydrogen bonds; pink crescents, van der Waals interactions; green circles, water molecules. (**b**) The wild-type and mutant myc-tagged tandem BRCT domain constructs containing the indicated mutations were analyzed for binding to a bead-immobilized optimal tandem BRCT domain-interacting phosphopeptide, YDIpSQVFPF, or its nonphosphorylated counterpart. The weak phospho-independent binding of the R1699Q mutant was observed using ten-fold more sample input than was used in the other lanes. (**c**) U2OS cells transfected with wild-type and mutant myc-tagged tandem BRCT domain constructs were analyzed for association with endogenous BACH1.

disrupting the native BRCA1-BACH1 interaction, this mutation may also result in the formation of inappropriate BRCT interactions.

Phosphopeptide binding and nuclear foci formation

Subcellular localization and nuclear foci formation by wild-type, phosphopeptide-binding mutant S1655A K1702M, and cancer-associated mutant M1775R BRCT domains were studied before and after DNA damage in unsynchronized U2OS cells (Fig. 5). To maximize visualization of nuclear foci, the cells were permeabilized with buffers containing 0.5% (v/v) Triton X-100 before fixation and immunostaining[27]. In unextracted cells, the wild-type BRCT domains and both of the mutant BRCT proteins showed equivalent diffuse nuclear localization. Extraction of the unirradiated cells before fixation caused almost complete loss of BRCT domain staining in all cases (Fig. 5a). Under these conditions, <5% of the wild-type and M1775R tandem BRCT–containing cells exhibited five or more nuclear foci, and no foci were observed with the S1655A K1702M double mutant. When the cells were irradiated with 10 Gy of γ-irradiation, and permeabilized, fixed and stained 2 h later, nearly all of the cells containing the wild-type tandem BRCT domains demonstrated sharp punctate nuclear foci that largely colocalized with the staining pattern of an antibody against the pSer/pThr-Gln epitope that recognizes ATM- and ATR-phosphorylated substrates (Fig. 5b). In contrast, the S1655A K1702M mutant showed only faint staining with a very fine granular pattern that completely failed to colocalize with pSer/pThr-Gln staining. This failure of foci formation and pSer/pThr-Gln colocalization is strong evidence that the phospho-binding function of the tandem BRCT domains is critical for normal subcellular localization after DNA damage. The M1775R mutant protein that binds weakly to phosphopeptides with a different specificity than the wild-type BRCT domains also formed punctate nuclear foci, although these were slightly reduced in number and showed less colocalization with pSer/pThr-Gln staining foci than the

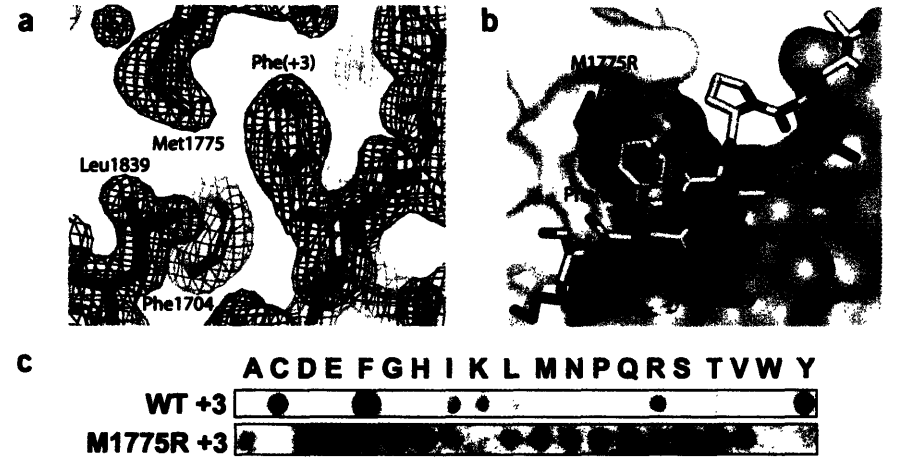

Figure 4 The Phe(+3) position of the BACH1 phosphopeptide is essential for tandem BRCT domain binding specificity. (**a**) Phe1704, Met1775 and Leu1704 from tandem BRCT domains form a hydrophobic pocket to accommodate the Phe(+3) position of the BACH1 phosphopeptide. (**b**) Superposition of the crystal structure of the M1775R tandem BRCT domain mutant[18] with the wild-type BACH1–phosphopeptide complex reveals that this mutation occludes the BACH1 Phe(+3) position. (**c**) Wild-type (WT) tandem BRCT domains and the M1775R mutant binding to a BACH1 phosphopeptide spot array. The M1775R mutant spot blot was carried out using ten times the amount of protein and was exposed to film for a substantially longer amount of time than the wild-type protein.

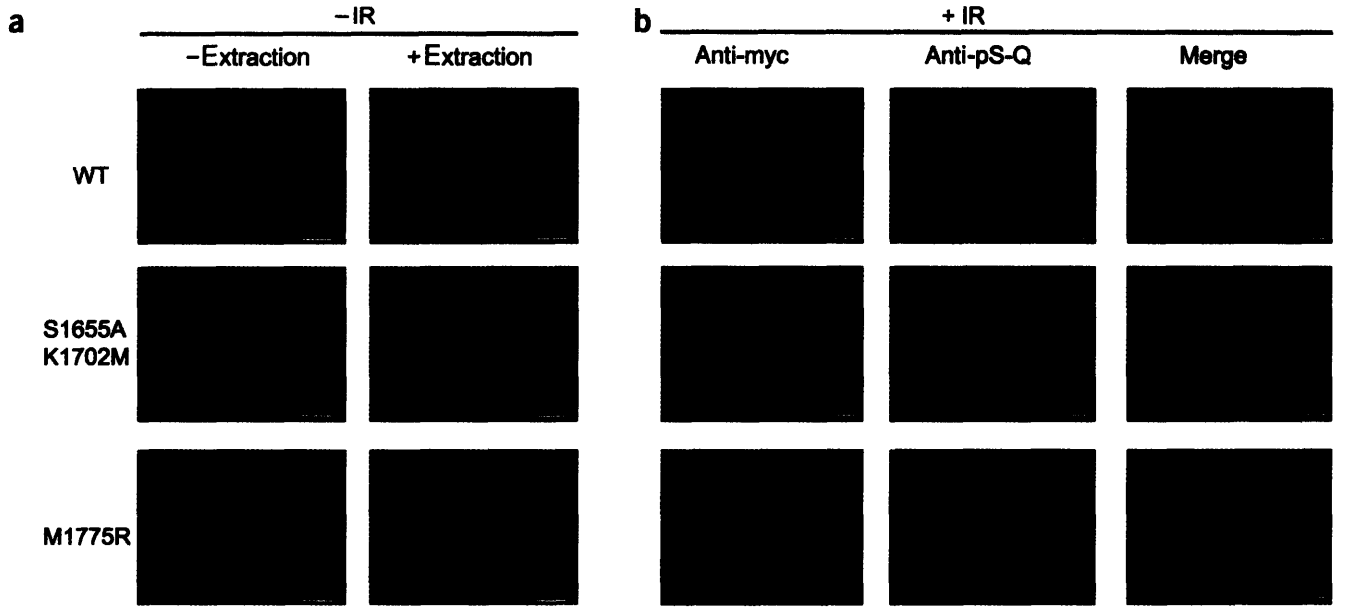

Figure 5 Localization of the BRCT domains to nuclear phosphoproteins. (**a**) Localization of wild-type, M1775R or K1702M S1655A mutants of myc-tagged tandem BRCT domains in unirradiated U2OS cells before (left panels) or after (right panels) extraction using Triton X-100-containing buffers. Bars, 25 μm. (**b**) Localization after Triton X-100 extraction as in **a** at 2 h after exposure of cells to 10 Gy of γ-radiation. Extracted cells were also stained using an anti-pSer/pThr-Gln epitope that recognizes the phosphorylation motif generated by the DNA damage-response kinases ATM and ATR. Bars, 10 μm.

wild-type protein. This localization might result from synergistic weak binding to alternative nonoptimal phosphorylated ligands present in high abundance in nuclear foci after DNA damage, as has been observed for other phosphopeptide-binding domain interactions[28].

DISCUSSION

The structure of the tandem BRCA1 BRCT domain–phosphopeptide complex described here is the highest-resolution X-ray structure of any BRCT domain structure solved to date, and provides an enhanced structural framework for investigating the molecular basis of breast and ovarian cancer. The structure reveals why tandem BRCT repeats, rather than single BRCT domains, are required for binding to pSer/pThr-containing phosphopeptides with high affinity and specificity; motif recognition is mediated by residues contributed by both domains across the domain-domain interface. In addition, the structure rationalizes the observation that the BRCT domains do not bind to phosphotyrosine-containing sequences[7], as the phosphate recognition pocket seems too shallow to accept a bulky phenyl ring. Despite the fact that not all tandem BRCT domains seem to bind phosphopeptides, several residues involved in the binding are relatively conserved. Structures of additional BRCT–phosphopeptide complexes will be necessary to better understand negative determinants of binding.

The tandem BRCT–phosphopeptide structure, in combination with biochemical and cell biological analysis, shows that some pro-oncogenic mutations in the BRCA1 C-terminal domains directly disrupt phosphopeptide binding or perturb the BRCT interface that forms the phospho-dependent binding surface. Similar conclusions have been reached in a study[36] reporting the structure of the tandem BRCT domains bound to an alternative phosphopeptide determined from oriented peptide library screening[7], and the unliganded structures of the M1775R and V1809F mutants in an accompanying paper in this issue[36].

Like the BRCT domains in PTIP, the BRCT domains in BRCA1 are sufficient for nuclear foci formation in response to DNA damage, and the phospho-binding function seems to be involved in this phenomenon. Four genuine cancer-linked mutations, P1749R, G1738E, 5382InsC and Y1853X, all result in loss of phosphopeptide binding. A fifth mutation, M1775R, binds weakly to phosphopeptides with altered motif specificity, and can still form nuclear foci after DNA damage; however, it completely loses the ability to interact with wild-type BACH1. These effects of the Pro1749 and Met1775 lesions confirm previous observations that these mutations are sufficient to abrogate BRCA1-BACH1 interactions *in vivo*[5]. Because BACH1 mutations are also associated with the development of cancer[29], these findings suggest that loss of this BRCA1-BACH1 interaction may be the critical event responsible for cancer predisposition[6,29].

Despite the fact that mutations in BRCA1 ultimately predispose women to cancer, wild-type BRCA1 paradoxically constitutes a target for anticancer therapy. Given the importance of BRCA1 in homologous recombination and DNA repair[4,30–32], disruption of the phosphoserine-binding function would be expected to cause enhanced sensitivity to chemotherapy and radiation[26], as has been observed in BRCA1-null murine embryonic stem cells[31]. The structural delineation of the phosphoserine-binding surface provides a new target for rational drug design.

METHODS

Protein cloning, expression and purification. For crystallization experiments, human BRCTs (residues 1646–1859) were expressed as glutathione *S*-transferase (GST) fusions in pGEX-4T1 (Amersham Pharmacia Biotech) in *Escherichia coli* BL21 at 18 °C. The GST was removed by 48-h treatment with thrombin before gel filtration. Synthetic peptides were prepared by W. Mawby (University of Bristol). A BRCT clone (residues 1313–1863) in pcDNA3 containing a N-terminal myc tag and a SV40 nuclear localization sequence was a gift from R. Scully (Beth Israel Deaconess Medical Center) and D. Livingston (Dana-Farber Cancer Institute)[25], and was used for the coimmunoprecipitation and immunofluorescence assays. Mutations were generated using the Stratagene QuikChange mutagenesis kit, and verified by sequencing. The pGEX-BRCT clone (residues 1633–1863) has been described[7] and was used for the peptide filter array. Induction of recombinant GST-BRCT domain protein

Table 1 Data collection and refinement statistics

Data collection	
Resolution range (Å)	15.0–1.85
Completeness (%)	93.9
Total observations	165,151
Unique reflections	19,219
Average $I / \sigma(I)$	35.6
R_{sym} (%)[a]	5.4
Refinement	
Resolution (Å)	15.0–1.85
No. of reflections (free)	18,225 (911)
R_{work} (%)[b]	20.6
R_{free} (%)[b]	22.2
No. of protein atoms	1,750
No. of water atoms	157
R.m.s. deviations	
Bonds (Å)	0.01
Angles (°)	1.35

[a] $R_{sym} = \Sigma_j |<I> - I_j| / \Sigma <I>$ where I_j is the intensity of the j^{th} reflection and $<I>$ is the average intensity. [b] $R_{work} = \Sigma_{hkl} | F_o - F_c | / \Sigma_{hkl} F_o$, where R_{free} is equivalent to R_{work} but is calculated for a randomly chosen 5% of reflections omitted from the refinement process.

was done at 37 °C for 3 h in the presence of 0.4 mM IPTG. The GST-BRCT domains were isolated from bacterial lysates using glutathione agarose, followed by elution with 40 mM glutathione, 50 mM Tris-HCl, pH 8.1, and dialysis into 50 mM Tris-HCl, pH 8.1, 300 mM NaCl.

Crystallization and structure determination. Crystals were grown at 18 °C by microbatch methods. The BACH1 phosphopeptide (SRST-pS990-PTFNK) was mixed with the BRCTs in a 1.5:1 stoichiometric excess and concentrated to 0.35 mM in a buffer containing 50 mM Tris-HCl, pH 7.5, 0.4 M NaCl and 3 mM DTT. Crystals grew from 50 mM MES, pH 6.5, 0.1 M $(NH_4)_2SO_4$ and 13% (w/v) PEG 8K. Crystals belonged to the trigonal space group $P3_221$ ($a = b = 65.8$ Å, $c = 93.1$ Å, $\alpha = \beta = 90.0°$, $\gamma = 120.0°$) with one complex in the asymmetric unit. Data were collected from flash-cooled crystals at 100 K on a Raxis-II detector mounted on a Rigaku RU200 generator. Diffraction data were integrated and scaled using DENZO and SCALEPACK[33]. The structure was solved by molecular replacement using the coordinates of PDB entry 1JNX[17] as a model with AmoRe[34]. Subsequent refinement was carried out using REFMAC5 (ref. 34) and manual model building in O[35]. Figures were constructed using PyMOL (http://www.pymol.org).

Peptide binding. An optimal phosphopeptide for binding the BRCTs was determined by oriented peptide library screening as described[7]. This peptide was synthesized in both its phosphorylated and nonphosphorylated forms with a biotin group at the N terminus using N-α-FMOC-protected amino acids and standard BOP-HOBt coupling chemistry. These peptides were conjugated to streptavidin-coated beads (Sigma-Aldrich). The wild-type and mutant BRCT domain-containing constructs (residues 1313–1863) were transcribed and translated *in vitro* in the presence of [^{35}S]methionine using the TNT kit (Promega). The bead-immobilized peptides (10 μl beads) were added to 10 μl of the *in vitro*–translated ^{35}S-labeled protein pool in 150 μl binding buffer (50 mM Tris-HCl, pH 7.6, 150 mM NaCl, 0.5% (v/v) NP-40, 1 mM EDTA, 2 mM DTT, 8 μg ml^{-1} pepstatin, 8 μg ml^{-1} aprotinin, 8 μg ml^{-1} leupeptin, 800 μM Na3VO4, 25 mM NaF). After incubation at 4 °C for 3 h, the beads were washed three times with 200 μl binding buffer before analysis by SDS-PAGE (12.5% (w/v)) and autoradiography.

Peptide filter array. An ABIMED peptide arrayer with a computer-controlled Gilson diluter and liquid handling robot was used to synthesize peptides onto an amino-PEG cellulose membrane using N-α-FMOC-protected amino acids and DIC-HOBT coupling chemistry. The membranes were blocked in 5% (w/v) milk in Tris-buffered saline containing 0.1% (v/v) Tween-20 (TBS-T) for 1h at room temperature, incubated with 0.025 μM GST-BRCTs or 0.25 μM M1775R GST-BRCTs (residues 1633–1863) in 5% (w/v) milk, 50 mM Tris-HCl, pH 7.6, 150 mM NaCl, 2 mM EDTA, 2 mM DTT for 1 h at room temperature and washed four times with TBS-T. The membranes were then incubated with anti-GST-conjugated HRP (Amersham) in 5% (w/v) milk and TBS-T for 1 h at room temperature, washed five times with TBS-T, and binding analyzed by ECL (Perkin-Elmer).

Coimmunoprecipitation of BRCTs and BACH1. U2OS cells were grown to 50% confluence in 100-cm^2 dishes and transfected with the myc-tagged wild-type or mutant BRCT constructs (residues 1313–1863) using FuGene6 transfection reagent (Roche) according to manufacturer's protocol. Cells were collected 30 h after transfection, lysed in lysis buffer (50 mM Tris-HCl, pH 7.6, 150 mM NaCl, 1.0% (v/v) NP-40, 5 mM EDTA, 2 mM DTT, 8 μg ml^{-1} AEBSF, 8 μg ml^{-1} aprotinin, 8 μg ml^{-1} leupeptin, 2 mM Na_3VO_4, 10 mM NaF and the phosphatase inhibitors microcystin and okadaic acid). Lysates containing equal amounts of protein (3 mg) were incubated with 3 μl of a mouse anti-myc (Cell Signaling) for 2 h at 4 °C, and then 10 μl of protein G–Sepharose beads (Sigma-Aldrich) were added and samples incubated for an additional 2 h at 4 °C. Beads were washed four times with lysis buffer, and bound proteins were eluted in SDS-PAGE sample buffer, analyzed on 6% (w/v) PAGE, transferred to PVDF membrane, and detected by blotting with rabbit anti-BACH1 (a gift from D. Livingston). A portion of the lysates were also run and blotted with anti-BACH1 and anti-myc to further ensure equal protein loading.

Immunofluorescence and microscopy. U2OS cells were seeded onto 18-mm^2 coverslips and transfected with the BRCT construct (residues 1313–1863) and various mutants using FuGene6 transfection reagent (Roche) according to the manufacturer's protocol. At 30 h after transfection, the cells were either treated with 10 Gy ionizing radiation or mock-irradiated and allowed to recover for 120 min. Cells were fixed in 3% (v/v) paraformaldehyde and 2% (w/v) sucrose for 15 min at room temperature and permeabilized with a 0.5% (v/v) Triton X-100 solution containing 20 mM Tris-HCl, pH 7.8, 75 mM NaCl, 300 mM sucrose, and 3 mM $MgCl_2$ for 15 min at room temperature. When necessary, proteins were extracted after IR treatment as described[27]. In brief, cells were incubated with extraction buffer (10 mM PIPES, pH 6.8, 100 mM NaCl, 300 mM sucrose, 3 mM $MgCl_2$, 1 mM EGTA, 0.5% (v/v) Triton X-100) for 5 min on ice followed by incubation with extraction stripping buffer (10 mM Tris-HCl, pH 7.4, 10 mM NaCl, 3 mM $MgCl_2$, 0.5% (v/v) Triton X-100) for 5 min on ice followed by successive washes in ice-cold PBS. Slides were fixed as above, stained with primary antibodies at 37 °C for 20 min, then stained with a anti-mouse or anti-rabbit secondary antibody for 20 min (Molecular Probes) at 37 °C. Primary antibodies used were mouse anti-myc (Cell Signaling) and rabbit anti-(pSer/pThr)Gln (Cell Signaling). Images were collected on a Axioplan2 microscope (Carl Zeiss) and processed using OpenLab (Improvision).

Coordinates. The atomic coordinates and structure factors have been deposited in the Protein Data Bank (accession code 1T15).

ACKNOWLEDGMENTS

We thank R. Scully and D. Livingston for vectors and helpful discussions, D. Livingston and R. Drapkin for the anti-BACH1 antibody, M. Glover for sharing unpublished information, members of the Yaffe and Smerdon laboratories for assistance and helpful comments, and S. Gamblin for assistance with crystal handling. This work was supported by US National Institutes of Health grant GM 60594 and a Burroughs-Wellcome Career Development Award to M.B.Y. D.L. was supported by a Howard Hughes Medical Institute predoctoral fellowship.

COMPETING INTERESTS STATEMENT

The authors declare that they have no competing financial interests.

Received 5 April; accepted 22 April 2004
Published online at http://www.nature.com/nsmb/

1. Scully, R. & Livingston, D.M. In search of the tumour-suppressor functions of BRCA1 and BRCA2. *Nature* **408**, 429–432 (2000).
2. Venkitaraman, A.R. Cancer susceptibility and the functions of BRCA1 and BRCA2. *Cell* **108**, 171–182 (2002).
3. Starita, L.M. & Parvin, J.D. The multiple nuclear functions of BRCA1: transcription, ubiquitination and DNA repair. *Curr. Opin. Cell Biol.* **15**, 345–350 (2003).

4. Powell, S.N. & Kachnic, L.A. Roles of BRCA1 and BRCA2 in homologous recombination, DNA replication fidelity and the cellular response to ionizing radiation. *Oncogene* **22**, 5784–5791 (2003).
5. Cantor, S.B. *et al.* BACH1, a novel helicase-like protein, interacts directly with BRCA1 and contributes to its DNA repair function. *Cell* **105**, 149–160 (2001).
6. Yu, X., Chini, C.C., He, M., Mer, G. & Chen, J. The BRCT domain is a phospho-protein binding domain. *Science* **302**, 639–642 (2003).
7. Manke, I.A., Lowery, D.M., Nguyen, A. & Yaffe, M.B. BRCT repeats as phosphopeptide-binding modules involved in protein targeting. *Science* **302**, 636–639 (2003).
8. Scully, R. *et al.* Dynamic changes of BRCA1 subnuclear location and phosphorylation state are initiated by DNA damage. *Cell* **90**, 425–435 (1997).
9. Wang, Y. *et al.* BASC, a super complex of BRCA1-associated proteins involved in the recognition and repair of aberrant DNA structures. *Genes Dev.* **14**, 927–939 (2000).
10. Miki, Y. *et al.* A strong candidate for the breast and ovarian cancer susceptibility gene BRCA1. *Science* **266**, 66–71 (1994).
11. Couch, F.J. & Weber, B.L. Mutations and polymorphisms in the familial early-onset breast cancer (BRCA1) gene. Breast Cancer Information Core. *Hum. Mutat.* **8**, 8–18 (1996).
12. Nathanson, K.L., Wooster, R., Weber, B.L. & Nathanson, K.N. Breast cancer genetics: what we know and what we need. *Nat. Med.* 7, 552–556 (2001).
13. Ford, D. *et al.* Genetic heterogeneity and penetrance analysis of the BRCA1 and BRCA2 genes in breast cancer families. The Breast Cancer Linkage Consortium. *Am. J. Hum. Genet.* **62**, 676–689 (1998).
14. Callebaut, I. & Mornon, J.P. From BRCA1 to RAP1: a widespread BRCT module closely associated with DNA repair. *FEBS Lett.* **400**, 25–30 (1997).
15. Huyton, T., Bates, P.A., Zhang, X., Sternberg, M.J. & Freemont, P.S. The BRCA1 C-terminal domain: structure and function. *Mutat. Res.* **460**, 319–332 (2000).
16. Rodriguez, M., Yu, X., Chen, J. & Songyang, Z. Phosphopeptide binding specificities of BRCA1 COOH-terminal (BRCT) domains. *J. Biol. Chem.* **278**, 52914–52918 (2003).
17. Williams, R.S., Green, R. & Glover, J.N. Crystal structure of the BRCT repeat region from the breast cancer-associated protein BRCA1. *Nat. Struct. Biol.* **8**, 838–842 (2001).
18. Williams, R.S. & Glover, J.N. Structural consequences of a cancer-causing BRCA1-BRCT missense mutation. *J. Biol. Chem.* **278**, 2630–2635 (2003).
19. Ekblad, C.M. *et al.* Characterisation of the BRCT domains of the breast cancer susceptibility gene product BRCA1. *J. Mol. Biol.* **320**, 431–442 (2002).
20. Vallon-Christersson, J. *et al.* Functional analysis of BRCA1 C-terminal missense mutations identified in breast and ovarian cancer families. *Hum. Mol. Genet.* **10**, 353–360 (2001).
21. Joo, W.S. *et al.* Structure of the 53BP1 BRCT region bound to p53 and its comparison to the BRCA1 BRCT structure. *Genes Dev.* **16**, 583–593 (2002).
22. Derbyshire, D.J. *et al.* Crystal structure of human 53BP1 BRCT domains bound to p53 tumour suppressor. *EMBO J.* **21**, 3863–3872 (2002).
23. Elia, E.A.H. *et al.* The molecular basis for phosphodependent substrate targeting and regulation of Plks by the polo-box domain. *Cell* **115**, 83–95 (2003).
24. Cheng, K.Y., Lowe, E.D., Sinclair, J., Nigg, E.A. & Johnson, L.N. The crystal structure of the human polo-like kinase-1 polo box domain and its phospho-peptide complex. *EMBO J.* **22**, 5757–5768 (2003).
25. Chen, J. *et al.* Stable interaction between the products of the BRCA1 and BRCA2 tumor suppressor genes in mitotic and meiotic cells. *Mol. Cell* **2**, 317–328 (1998).
26. Scully, R. *et al.* Genetic analysis of BRCA1 function in a defined tumor cell line. *Mol. Cell* **4**, 1093–1099 (1999).
27. Mirzoeva, O.K. & Petrini, J.H. DNA damage-dependent nuclear dynamics of the Mre11 complex. *Mol. Cell. Biol.* **21**, 281–288 (2001).
28. Nash, P. *et al.* Multisite phosphorylation of a CDK inhibitor sets a threshold for the onset of DNA replication. *Nature* **414**, 514–521 (2001).
29. Cantor, S. *et al.* The BRCA1-associated protein BACH1 is a DNA helicase targeted by clinically relevant inactivating mutations. *Proc. Natl. Acad. Sci. USA* **101**, 2357–2362 (2004).
30. Snouwaert, J.N. *et al.* BRCA1 deficient embryonic stem cells display a decreased homologous recombination frequency and an increased frequency of non-homologous recombination that is corrected by expression of a *brca1* transgene. *Oncogene* **18**, 7900–7907 (1999).
31. Moynahan, M.E., Chiu, J.W., Koller, B.H. & Jasin, M. BRCA1 controls homology-directed DNA repair. *Mol. Cell* **4**, 511–518 (1999).
32. Westermark, U.K. *et al.* BARD1 participates with BRCA1 in homology-directed repair of chromosome breaks. *Mol. Cell. Biol.* **23**, 7926–7936 (2003).
33. Otwinowski, Z. & Minor, W. Processing of X-ray diffraction data collected in oscillation mode. *Methods Enzymol.* **276**, 307–326 (1997).
34. Collaborative Computational Project, Number 4. The CCP4 suite: programs for protein crystallography. *Acta Crystallogr. D* **50**, 760–763 (1994).
35. Jones, T.A., Zou, J.Y., Cowan, S.W. & Kjeldgaard. Improved methods for binding protein models in electron density maps and the location of errors in these models. *Acta Crystallogr. A* **47**, 110–119 (1991).
36. Williams, R.S., Lee, M.S., Hau, D. & Glover, J.N.M. Structural basis of phosphopeptide recognition by the BRCT domain of BRCA1. *Nat. Struct. Mol. Biol.* advance online publication, 9 May 2004 (doi:10.1038/nsmb776).

Our results provide support for a role of kin selection in favoring helping behavior within cooperative vertebrates. Moreover, we show that the importance of kin selection varies across species, consistent with the predictions of Hamilton's rule (*6*). Specifically, preferential helping of relatives is more common in species where helping provides a greater benefit. It should be noted that our results do not imply that the direct fitness benefits of helping are unimportant or show anything about the relative importance of direct and indirect fitness benefits. Ideally, the next step would be an equivalent study on the effect size of direct fitness benefits.

References and Notes

1. T. H. Clutton-Brock, *Science* **296**, 69 (2002).
2. A. Cockburn, *Annu. Rev. Ecol. Syst.* **29**, 141 (1998).
3. P. B. Stacey, W. D. Koenig, *Cooperative Breeding in Birds: Longterm Studies in Ecology and Behaviour* (Cambridge Univ. Press, Cambridge, 1990).
4. S. T. Emlen, in *Behavioral Ecology*, J. R. Krebs, N. B. Davies, Eds. (Blackwell, Oxford, 1997), pp. 228–253.
5. L. A. Dugatkin, *Cooperation Among Animals*, R. M. May, P. H. Harvey, Eds. (Oxford Series in Ethology and Evolution, Oxford Univ. Press, New York, 1997).
6. W. D. Hamilton, *Am. Nat.* **97**, 354 (1963).
7. W. D. Hamilton, *J. Theor. Biol.* **7**, 1 (1964).
8. A. Bourke, N. Franks, *Social Evolution in Ants* (Princeton Univ. Press, Princeton, NJ, 1995).
9. L. Keller, H. K. Reeve, *Kin Selection*, M. Pagel, Ed. (Encyclopedia of Evolution, Oxford Univ. Press, Oxford, 2002).
10. A. S. Griffin, S. A. West, *Trends Ecol. Evol.* **17**, 15 (2002).
11. S. T. Emlen, *Proc. Natl. Acad. Sci. U.S.A.* **92**, 8092 (1995).
12. A. J. Gaston, *Am. Nat.* **112**, 1091 (1978).
13. H. Kokko, R. A. Johnstone, T. H. Clutton-Brock, *Proc. R. Soc. London Ser. B* **268**, 187 (2001).
14. H. Kokko, R. A. Johnstone, J. Wright, *Behav. Ecol.* **13**, 291 (2002).
15. J. Komdeur, B. J. Hatchwell, *Trends Ecol. Evol.* **14**, 237 (1999).
16. A. Grafen, *Anim. Behav.* **39**, 42 (1990).
17. A. F. Russell, B. J. Hatchwell, *Proc. R. Soc. London Ser. B* **268**, 2169 (2001).
18. J. Komdeur, *Proc. R. Soc. London Ser. B* **256**, 47 (1994).
19. S. T. Emlen, P. Wrege, *Behav. Ecol. Sociobiol.* **23**, 305 (1988).
20. T. H. Clutton-Brock *et al.*, *Science* **284**, 1577 (1999).
21. T. H. Clutton-Brock *et al.*, *Proc. R. Soc. London Ser. B* **267**, 301 (2000).
22. P. O. Dunn, A. Cockburn, R. A. Mulder, *Proc. R. Soc. London Ser. B* **259**, 339 (1995).
23. M. A. Du Plessis, *Behaviour* **127**, 49 (1993).
24. G. Arnqvist, D. Wooster, *Trends Ecol. Evol.* **10**, 236 (1995).
25. R. Rosenthal, *Meta-Analytic Procedures for Social Research* (Sage Foundation, Thousand Oaks, CA, 1991).
26. Materials and methods are available as supporting material on *Science* Online.
27. We used standard meta-analytic methods, described in detail elsewhere (*25*), implemented with the package MetaWin 2.0 (*31*). Effect sizes from each test statistic were averaged to obtain a single value per species. Effect sizes were *Z*-transformed before analysis to correct for the asymptotic behavior of *r*, and in all analyses individual effect sizes were weighted by the inverse of the variance associated with the effect size estimate. We used random effect models, because these are more appropriate for ecological data, and our underlying hypothesis is that effect sizes may differ between species.
28. A. Moller, M. Jennions, *Oecologia* **132**, 492 (2002).
29. Several lines of evidence suggest that the pattern observed was not greatly affected by publication bias: the tendency to publish only significant results (*24*, *25*, *31*, *32*). First, the subject area is one in which there can be as much incentive to publish nonsignificant results as significant results. Second, a scatter plot of effect size versus sample size did not show a pattern suggesting missing data for cases with nonsignificant effect sizes and small sample sizes (Fig. 1). Third, the rank correlation coefficient between effect size and sample size was not significantly negative ($R_s = -0.14$, $P = 0.58$). Fourth, we calculated the "fail-safe number," which is the number of unpublished studies with an effect size of zero that would have to exist in order for the overall mean effect size to be not significantly different from zero. The fail-safe number was 71, which suggests that our result is extremely robust, because there are unlikely to be unpublished studies with $r_{kin} = 0$ on this many species. Fifth, we used the trim and fill method of Duvall and Tweedie (*33*) to estimate the number of missing studies and their effect sizes (*32*). This method estimated that there were no missing studies ($L_0 = 0$). Sixth, a common problem in studies on cooperative breeding vertebrates is pseudoreplication. In many cases where the appropriate independent data point is a group, data has been analyzed using individuals or multiple observations from individuals. However, even when we analyzed the data weighting studies by the number of groups rather then the given sample sizes, the mean effect size was still significantly greater than zero (Table 1). Seventh, we found no significant difference in the effect size between studies based on pedigree or genetic data ($P_{rand} = 0.28$), suggesting that how relatedness was measured was not biasing the results.
30. K. N. Rabenold, *Behav. Ecol. Sociobiol.* **17**, 1 (1985).
31. M. S. Rosenberg, D. C. Adams, J. Gurevitch, *MetaWin: Statistical Software for Meta-Analysis, version 2.0* (Sinauer, Sunderland, MA, 2000).
32. M. D. Jennions, A. P. Moller, *Biol. Rev.* **77**, 211 (2002).
33. S. Duvall, R. Tweedie, *Biometrics* **56**, 455 (2000).

34. We thank A. Russell, B. Sheldon, D. Shuker, and three anonymous referees for comments; L. Bennun, P. Finn, and A. Russell for supplying and clarifying data; M. Jennions for supplying a spreadsheet for trim and fill analyses; and the Natural Environment Research Council, Biotechnology and Biological Sciences Research Council, and Royal Society for funding.

Supporting Online Material

www.sciencemag.org/cgi/content/full/302/5645/634/DC1
Materials and Methods
Tables S1 and S2
References

21 July 2003; accepted 8 September 2003

BRCT Repeats As Phosphopeptide-Binding Modules Involved in Protein Targeting

Isaac A. Manke, Drew M. Lowery,* Anhco Nguyen,* Michael B. Yaffe†

We used a proteomic approach to identify phosphopeptide-binding modules mediating signal transduction events in the DNA damage response pathway. Using a library of partially degenerate phosphopeptides, we identified tandem BRCT (BRCA1 carboxyl-terminal) domains in PTIP (Pax transactivation domain-interacting protein) and in BRCA1 as phosphoserine- or phosphothreonine-specific binding modules that recognize substrates phosphorylated by the kinases ATM (ataxia telangiectasia–mutated) and ATR (ataxia telangiectasia– and RAD3-related) in response to γ-irradiation. PTIP tandem BRCT domains are responsible for phosphorylation-dependent protein localization into 53BP1- and phospho-H2AX (γ-H2AX)–containing nuclear foci, a marker of DNA damage. These findings provide a molecular basis for BRCT domain function in the DNA damage response and may help to explain why the BRCA1 BRCT domain mutation Met^{1775} → Arg, which fails to bind phosphopeptides, predisposes women to breast and ovarian cancer.

Signal transduction by protein kinases in eukaryotes results in the directed assembly of multiprotein complexes at specific locations within the cell (*1*). This process is particularly evident after DNA damage, where activation of DNA damage response kinases results in the formation of protein-protein complexes at discrete foci within the nucleus (*2*). In many cases, protein kinases directly control the formation of these multiprotein complexes by generating specific phosphorylated-motif sequences; modular binding domains then recognize these short phospho-motifs to mediate protein-protein interactions (*3*, *4*).

We used a proteomic screening approach (*5*) to identify novel modular pSer- or pThr-binding domains involved in the DNA damage response. In cells exposed to γ-irradiation, the kinases ATM and ATR phosphorylate transcription factors, DNA repair proteins, protein kinases, and scaffolds on Ser-Gln and Thr-Gln motifs (*6*). We therefore constructed an oriented phosphopeptide library biased to resemble the motif generated by ATM and ATR (*7*, *8*) (Fig. 1A). This library and its nonphosphorylated counterpart were immobilized and screened against ~96,000 in vitro translated polypeptides (960 pools each containing ~100 transcripts) (Fig. 1A).

Center for Cancer Research, Department of Biology, Massachusetts Institute of Technology, Cambridge, MA 02139, USA.

*These authors contributed equally to this work.
†To whom correspondence should be addressed. E-mail: myaffe@mit.edu

Pool EE11 contained the strongest phosphopeptide-binding clone, EE11-9, encoding the C-terminal 70% of human PTIP (Fig. 1B). PTIP, originally identified as a transcriptional regulatory protein, appears to also play a critical role in the DNA damage response pathway (*9*–*11*). Human PTIP contains four BRCT domains, known protein-protein interaction modules that are present in many DNA damage response and cell cycle checkpoint proteins (*12*). A construct containing only the tandem third and fourth BRCT domains displayed strong and specific binding to the (pSer/pThr)-Gln library (Fig. 1B). Constructs of PTIP lacking both of these domains either failed to bind or lacked phosphopeptide discrimination. Moreover, neither the third nor the fourth BRCT domain alone bound to phosphopeptides, which suggests that the tandem C-terminal BRCT domains function as a single module that is necessary and sufficient for phospho-specific binding.

BRCT domains are often found in tandem pairs [$(BRCT)_2$] or multiple copies of tandem pairs, and the BRCA1 $(BRCT)_2$ domains behave as a single stable fragment in limited proteolysis and x-ray crystallographic studies (*13*). Like those of PTIP, the $(BRCT)_2$ domains of BRCA1, but not the individual BRCT domains alone, displayed phospho-specific binding (Fig. 2A). However, little if any phospho-binding was seen for $(BRCT)_2$ modules from the human DNA damage-response proteins 53BP1 and MDC1, *Saccharomyces cerevisiae* Rad9p, or the PTIP N-terminal pair, which suggests that the phosphopeptide-binding function is present in only a subset of $(BRCT)_2$ domains.

We used oriented peptide library screening to determine the optimal phospho-binding motifs

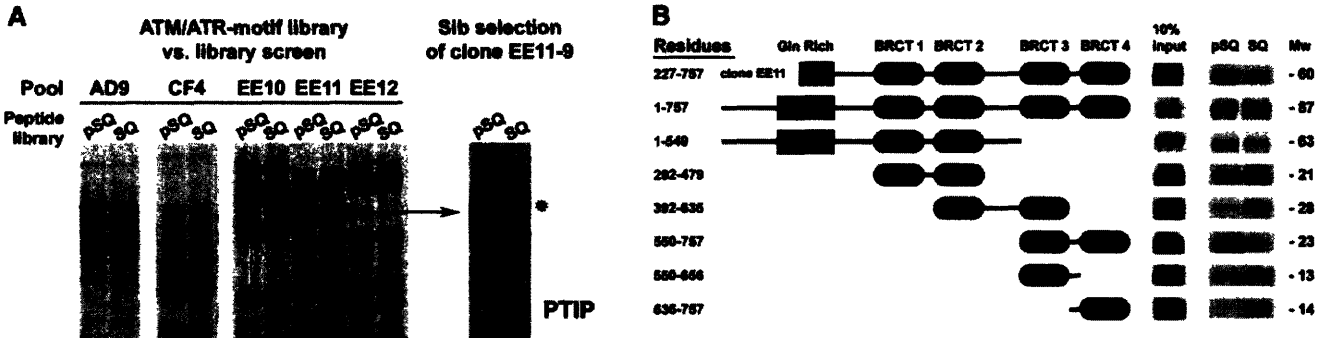

Fig. 1. Identification of pSer- or pThr-binding domains with an ATM/ATR-motif library versus an expression library screen. (**A**) An oriented (pSer/pThr) phosphopeptide library, biased toward the phosphorylation motifs of ATM and ATR, was immobilized on Streptavidin beads. The library [pSQ = biotin-ZGZGGAXXXB(pS/pT)QJXXXAKKK] and its nonphosphorylated counterpart (SQ) were screened against in vitro translated, [^{35}S]Met-labeled proteins. Notation code: (pS/pT), 50% pSer and 50% pThr; Z, aminohexanoic acid; B, a biased mixture of the amino acids Ala (A), Ile, Lys (K), Met, Asn, Pro, Ser, Thr, and Val; J, a biased mixture of 25% Glu and 75% X, where X denotes all amino acids except Cys, His, Lys, and Arg (*21*); G, Gly; Q, Gln. In each panel, the first and second lanes show binding of proteins within the pool to the phosphorylated (pSQ) and nonphosphorylated (SQ) libraries, respectively. Identification of PTIP, denoted by arrow and asterisk, occurred through progressive subdivision of the EE11 pool to a single clone. The uppermost band is a fusion artifact of PTIP with vector sequences resulting in translation initiation at an upstream start codon in the vector. (**B**) Deletion mapping of the phospho-binding domain of PTIP. Truncations of PTIP were assayed for selective binding to the pSQ library as in (A). BRCT domain boundaries were determined from sequence alignments (*22*).

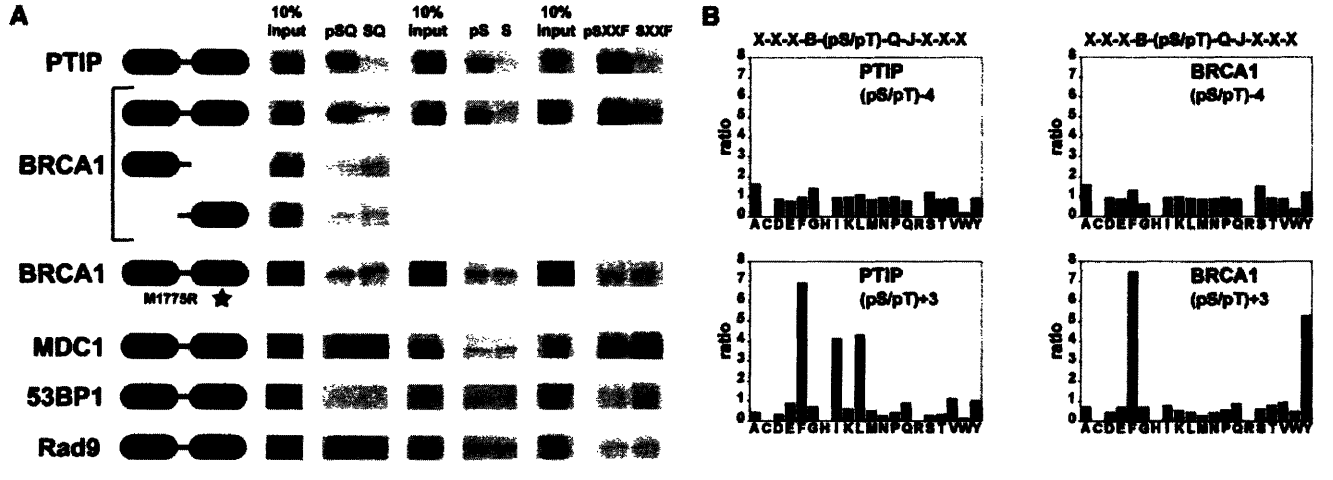

Fig. 2. Comparison of the $(BRCT)_2$ domains and determination of the optimal phosphopeptide-binding motifs. (**A**) PTIP, BRCA1, BRCA1 M1775R, MDC1, 53BP1, and Rad9p $(BRCT)_2$ domains were assayed for binding as in Fig. 1A. The peptide libraries used were pSQ (Fig. 1A), pS = biotin-ZGZGGAXXXXpSXXXX-XAKKK; pSXXF = biotinZGZGGAXXXXpSXXFX-XAYKKK (pS, pSer; pT, pThr; Z, aminohexanoic acid; X, all amino acids except Cys). Domain boundaries: PTIP, as indicated in Fig. 1; BRCA1 BRCT1 and BRCT2, amino acids 1633 to 1863; BRCT1 alone, amino acids 1633 to 1740; BRCT2 alone, amino acids 1741 to 1863; MDC1, amino acids 1874 to 2089; 53BP1, amino acids 1622 to 1972; Rad9p, amino acids 985 to 1309. (**B**) Strong selection by the PTIP-$(BRCT)_2$ and BRCA1-$(BRCT)_2$ domains for Phe (F) at the (pSer/pThr)-Gln +3 position (7.0 or 7.5), respectively (table S1) (*21*). Bar graphs show the relative abundance of each amino acid at a given cycle of sequencing versus its abundance in the starting peptide library mixture (*23*).

for the C-terminal $(BRCT)_2$ domains of PTIP and BRCA1 (Fig. 2B) (table S1). PTIP-$(BRCT)_2$ and BRCA-$(BRCT)_2$ displayed strongest binding to similar but not identical motifs, with extremely strong selection in the (pSer/pThr) +3 position for aromatic and aliphatic residues, or aromatic residues, respectively. More moderate selection was also observed at other positions, particularly (pSer/pThr) +2 and +5. We defined an optimal $(BRCT)_2$-binding peptide (BRCTide) as Tyr-Asp-Ile-(pSer/pThr)-Gln-Val-Phe-Pro-Phe and verified motif data with

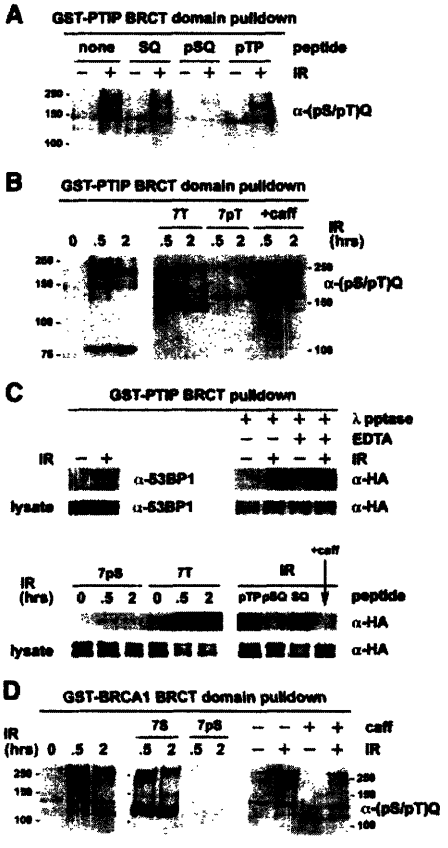

Fig. 3. Association of PTIP and BRCA1 $(BRCT)_2$ domains with DNA damage–induced phosphoproteins through their phosphopeptide-binding pockets. (**A**) Lysates from U2OS cells before or 2 hours after 10 Gy of γ-irradiation were incubated with GST-PTIP-$(BRCT)_2$. Bound proteins were detected by immunoblotting with an antibody to the (pSer/pThr)-Gln motif generated by ATM and ATR. The interaction was disrupted by incubation with the pSQ peptide library, but not with the SQ peptide library or an unrelated pTP library (*5*). (**B**) Interaction of the PTIP-$(BRCT)_2$ domain with phosphoproteins was disrupted by treatment of U2OS cells with caffeine (5 mM) before irradiation or by incubating the beads with BRCTtide (7pT), but not by its nonphosphorylated counterpart (*7T*). (**C**) $(BRCT)_2$ domains of PTIP interact with 53BP1 after DNA damage. Endogenous 53BP1 from irradiated U2OS cells was precipitated with GST-PTIP-$(BRCT)_2$ and detected by immunoblotting with an antibody to 53BP1. U2OS cells were transfected with HA-tagged 53BP1, and the interaction with GST-PTIP-$(BRCT)_2$ was analyzed as in (A) and (B). Treatment of the cell lysates with lambda phosphatase also abolished the interaction. (**D**) Lysates from U2OS cells before or after irradiation were incubated with GST-BRCA1-$(BRCT)_2$ and analyzed as in (B). In these experiments, the pSer version of BRCTtide (7pS) and its nonphosphorylated counterpart (7S) were used.

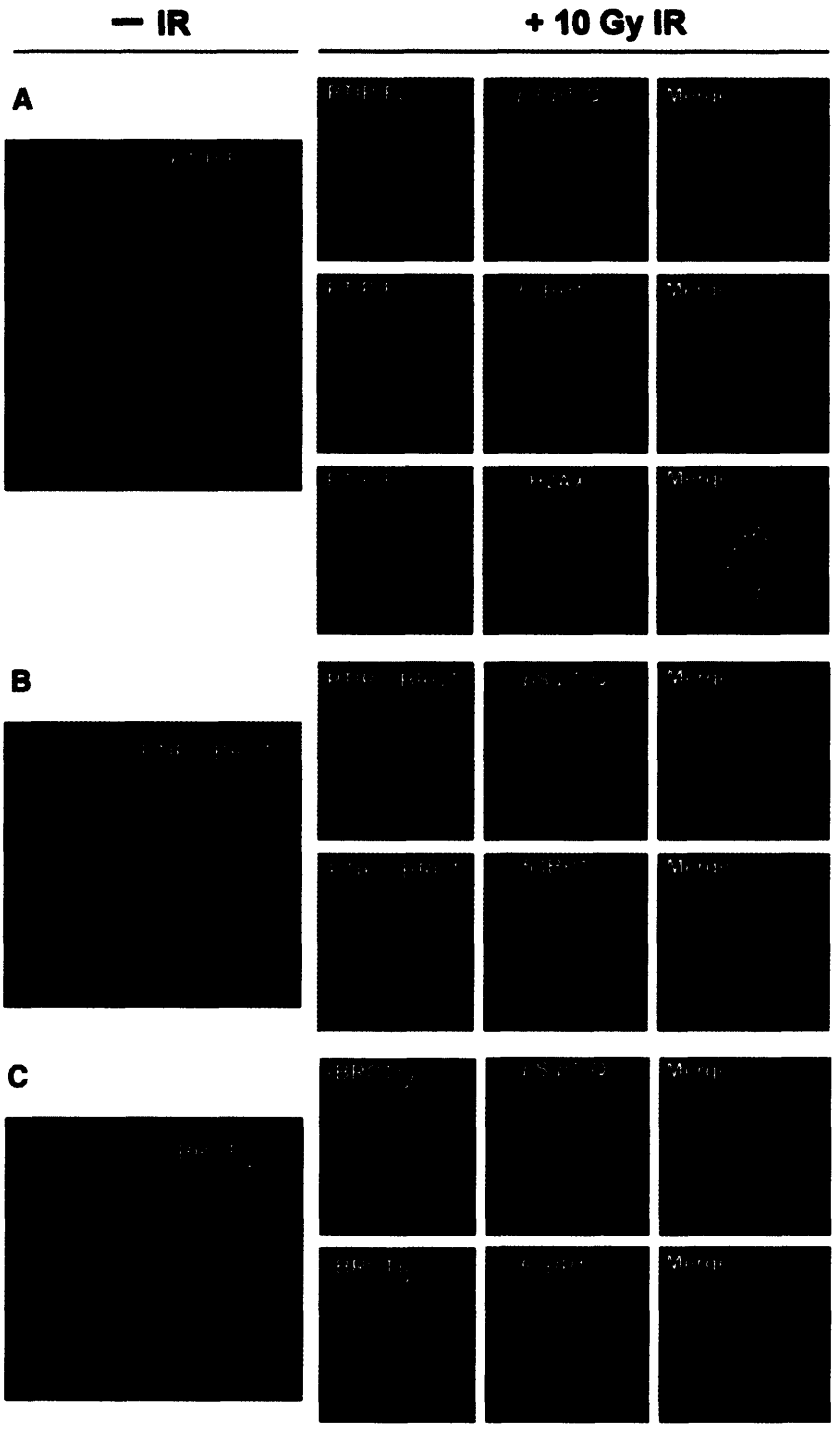

Fig. 4. Full-length PTIP forms DNA damage–induced foci and colocalizes with (pSer/pThr)-Gln proteins, 53BP1, and γ-H2AX. All cells shown were either treated with 10 Gy of γ-irradiation or mock-irradiated 24 hours after transfection, allowed to recover for 2 hours, stained, and analyzed by immunofluorescence microscopy. (**A**) U2OS cells were transfected with a full-length GFP-PTIP construct (PTIP-FL residues 1 to 757). (**B**) U2OS cells were transfected with a PTIP deletion construct in which the last two BRCT domains had been removed (PTIP-ΔBRCT, residues 1 to 549). (**C**) U2OS cells were transfected with a PTIP construct containing only the last two BRCT domains [$(BRCT)_2$, residues 550 to 757].

the use of a solid-phase array of immobilized phosphopeptides (fig. S1).

Isothermal titration calorimetry showed that the optimal pSer-containing peptide bound to the C-terminal $(BRCT)_2$ of PTIP with a dissociation constant of 280 nM, and to the $(BRCT)_2$ of BRCA1 with a dissociation constant of 400 nM (table S2). Substitution of pThr for pSer reduced the affinity of the peptide for PTIP-$(BRCT)_2$, although binding was still observed. Substitution of pTyr, Ser, or Thr for pSer abrogated binding, which confirmed that $(BRCT)_2$ modules are pSer- or pThr-specific (fig. S1).

After treatment of U2OS human osteosarcoma cells with 10 Gy of γ-irradiation, both PTIP-$(BRCT)_2$ and BRCA1-$(BRCT)_2$ bound distinct phosphoproteins, as detected by immunoblotting with a phospho-specific antibody to the (pSer/pThr)-Gln motif generated by ATM and ATR (Fig. 3, A, B, and D). Binding to $(BRCT)_2$ was inhibited by incubation with specific phosphopeptides but not by nonphosphorylated peptides. Pretreatment of the cells with caffeine to inhibit the activity of ATM and ATR before irradiation also largely eliminated binding (*14*).

In response to γ-irradiation, 53BP1 undergoes multisite phosphorylation by ATM and forms nuclear foci (*15–17*). We found that 53BP1 bound to the C-terminal PTIP-$(BRCT)_2$ only after irradiation, and in a phosphorylation-dependent manner (Fig. 3C). In addition, in vivo association of full-length FLAG-tagged PTIP with hemagglutinin (HA)–tagged 53BP1 increased after irradiation (*18*).

The binding of $(BRCT)_2$ domains to ATM- or ATR-phosphorylated substrates could localize PTIP to sites of DNA damage in vivo. In the absence of DNA damage, PTIP tagged with green fluorescent protein (GFP-PTIP) was diffusely nuclear with a small amount of cytosolic staining (Fig. 4). Two hours after irradiation, PTIP localized into discrete nuclear foci with (pSer/pThr)-Gln phosphoepitopes, 53BP1, and γ-H2AX (Fig. 4A). PTIP lacking the C-terminal $(BRCT)_2$ did not form foci (Fig. 4B). The isolated C-terminal $(BRCT)_2$ was diffusely nuclear in the absence of DNA damage, but relocalized into these nuclear foci after irradiation (Fig. 4C). Inhibition of ATM and ATR by caffeine before irradiation reduced the number and altered the appearance of full-length PTIP foci, and caused loss of colocalization with γ-H2AX (fig. S2). These findings strongly suggest that PTIP functions as a key component of the DNA damage response and may provide a molecular rationale for the early embryonic lethality of PTIP knockout mice with extensive unrepaired DNA ends (*10*).

$(BRCT)_2$ selection for aromatic and aliphatic residues in the (pSer/pThr) +3 positions exceeds their selection for Gln in the +1 position. Thus, only a subset of ATM- and ATR-phosphorylated substrates are likely to bind with high affinity, and other kinases might also generate $(BRCT)_2$-binding motifs. The important role for $(BRCT)_2$ domains as pSer- or pThr-binding modules is emphasized by the finding that ~80% of germline mutations in BRCA1 result in C-terminal truncations involving the BRCT region, predisposing women to breast and ovarian cancer (*12*). Interestingly, a BRCA1 cancer-associated mutation in the $(BRCT)_2$ module that ablates critical BRCA1 protein interactions (*19*), $Met^{1775} \rightarrow Arg$ (M1775R), fails to bind phosphopeptides (Fig. 2A), even though the M1775R crystal structure is nearly identical to that of the wild-type $(BRCT)_2$ (*20*). Agents that interfere with DNA damage signaling sensitize tumor cells to killing by radiation and chemotherapy. Thus, the phosphopeptide-binding pocket of $(BRCT)_2$ modules may constitute a target for anticancer drug development.

References and Notes

1. T. Pawson, P. Nash, *Science* **300**, 445 (2003).
2. B. B. Zhou, S. J. Elledge, *Nature* **408**, 433 (2000).
3. M. B. Yaffe, *Nature Rev. Mol. Cell Biol.* **3**, 177 (2002).
4. M. B. Yaffe, A. E. Elia, *Curr. Opin. Cell Biol.* **13**, 131 (2001).
5. A. E. H. Elia, L. C. Cantley, M. B. Yaffe, *Science* **299**, 1228 (2003).
6. R. T. Abraham, *Genes Dev.* **15**, 2177 (2001).
7. S. T. Kim, D. S. Lim, C. E. Canman, M. B. Kastan, *J. Biol. Chem.* **274**, 37538 (1999).
8. T. O'Neill *et al.*, *J. Biol. Chem.* **275**, 22719 (2000).
9. M. S. Lechner, I. Levitan, G. R. Dressler, *Nucleic Acids Res.* **28**, 2741 (2000).
10. E. A. Cho, M. J. Prindle, G. R. Dressler, *Mol. Cell. Biol.* **23**, 1666 (2003).
11. K. Shimizu, P. Y. Bourillot, S. J. Nielsen, A. M. Zorn, J. B. Gurdon, *Mol. Cell. Biol.* **21**, 3901 (2001).
12. T. Huyton, P. A. Bates, X. Zhang, M. J. Sternberg, P. S. Freemont, *Mutat. Res.* **460**, 319 (2000).
13. R. S. Williams, R. Green, J. N. Glover, *Nature Struct. Biol.* **8**, 838 (2001).
14. J. N. Sarkaria *et al.*, *Cancer Res.* **59**, 4375 (1999).
15. L. B. Schultz, N. H. Chehab, A. Malikzay, T. D. Halazonetis, *J. Cell Biol.* **151**, 1381 (2000).
16. I. Rappold, K. Iwabuchi, T. Date, J. Chen, *J. Cell Biol.* **153**, 613 (2001).
17. B. Wang, S. Matsuoka, P. B. Carpenter, S. J. Elledge, *Science* **298**, 1435 (2002).
18. I. A. Manke, D. M. Lowery, A. Nguyen, M. B. Yaffe, unpublished data.
19. R. Scully, D. M. Livingston, *Nature* **408**, 429 (2000).
20. R. S. Williams, J. N. Glover, *J. Biol. Chem.* **278**, 2630 (2003).
21. See supporting data on *Science* Online.
22. A. Bateman *et al.*, *Nucleic Acids Res.* **27**, 260 (1999).
23. M. B. Yaffe, L. C. Cantley, *Methods Enzymol.* **328**, 157 (2000).
24. A. Blasina, B. D. Price, G. A. Turenne, C. H. McGowan, *Curr. Biol.* **9**, 1135 (1999).

25. We thank K. Hoepker and A. Elia for participation at early stages in this work, T. Ho and S. Bissonnette for figure construction, D. Rubinson and J. Loureiro for assistance with microscopy, R. Grant for assistance with protein purification, J. Robbins for critical reading of the manuscript, R. T. Abraham for discussions, and J. Chen for sharing unpublished data. The MDC1, 53BP1, and Brca1 plasmids were gifts from S. J. Elledge, K. Iwabuchi, and D. Livingston, respectively. D.M.L. is a Howard Hughes Medical Institute predoctoral fellow. Supported by NIH grant GM60594 and a Burroughs-Wellcome Career Development Award (M.B.Y.).

Supporting Online Material

www.sciencemag.org/cgi/content/full/302/5645/636/DC1
Materials and Methods
Figs. S1 and S2
Tables S1 and S2
References

7 July 2003; accepted 10 September 2003

The BRCT Domain Is a Phospho-Protein Binding Domain

Xiaochun Yu,[1] Claudia Christiano Silva Chini,[1] Miao He,[2] Georges Mer,[3] Junjie Chen[1]*

The carboxyl-terminal domain (BRCT) of the Breast Cancer Gene 1 (BRCA1) protein is an evolutionarily conserved module that exists in a large number of proteins from prokaryotes to eukaryotes. Although most BRCT domain–containing proteins participate in DNA-damage checkpoint or DNA-repair pathways, or both, the function of the BRCT domain is not fully understood. We show that the BRCA1 BRCT domain directly interacts with phosphorylated BRCA1-Associated Carboxyl-terminal Helicase (BACH1). This specific interaction between BRCA1 and phosphorylated BACH1 is cell cycle regulated and is required for DNA damage–induced checkpoint control during the transition from G_2 to M phase of the cell cycle. Further, we show that two other BRCT domains interact with their respective physiological partners in a phosphorylation-dependent manner. Thirteen additional BRCT domains also preferentially bind phospho-peptides rather than nonphosphorylated control peptides. These data imply that the BRCT domain is a phospho-protein binding domain involved in cell cycle control.

The BRCT domain was first identified as ~100–amino acid tandem repeats at the C-terminus of the tumor-suppressor gene product BRCA1, in which the germline mutations lead to ~50% familial breast cancer. A large number of proteins also contain single or multiple BRCT motifs, and many of them appear to function in DNA-damage checkpoint control and DNA repair (*1*, *2*).

The BRCT domains are important for the tumor-suppressor function of BRCA1. Most *BRCA1* mutations cause truncated *BRCA1* gene